MISSIONE 4
ISTRUZIONE RICERCA

WP1 - *Experimental analysis for the characterization of faulty and normal operation of a typical AHU*

Finanziato dall'Unione europea NextGenerationEU
Ministero dell'Università e della Ricerca
Italiadomani
PIANO NAZIONALE DI RIPRESA E RESILIENZA

MISSIONE 4
ISTRUZIONE RICERCA

DELIVERABLE WP1_D1

LITERATURE REVIEW OF AHU EXPERIMENTAL STUDIES FOR FDD

EDIT BY UNICAMPANIA

PRIN 2022 - UTMOST FDD: AN AUTOMATED, OPEN, SCALABLE AND TRANSPARENT FAULT DETECTION AND DIAGNOSIS PROCESS FOR AIR-HANDLING UNITS BASED ON A HYBRID EXPERT AND ARTIFICIAL INTELLIGENCE APPROACH

Funded by the European Union - Next Generation EU within the "Piano Nazionale di Ripresa e Resilienza (PNRR), missione 4 componente 2 investimento 1.1 - fondo per il programma nazionale di ricerca e progetti di rilevante interesse nazionale (PRIN)"

Finanziato dall'Unione europea NextGenerationEU
Ministero dell'Università e della Ricerca
Italiadomani PIANO NAZIONALE DI RIPRESA E RESILIENZA

The UTMOST FDD Project is organised into the following 7 Work Packages (WPs):
WP0) PROJECT COORDINATION
WP1) EXPERIMENTAL ANALYSIS FOR THE CHARACTERIZATION OF FAULTY AND NORMAL OPERATION OF A TYPICAL AHU
WP2) KPIs IDENTIFICATION FOR ASSESSING FAULT IMPACT IN AHU OPERATION
WP3) AHU DIGITAL TWIN AND SIMULATION-BASED FAULT IMPACT SCENARIO ANALYSIS
WP4) DEFINITION OF HYBRID FDD STRATEGIES FOR AHUs
WP5) TRANSFERABILITY ANALYSIS OF THE FDD STRATEGIES
WP6) KNOWLEDGE TRANSFER AND DISSEMINATION

The WPs are organized into Tasks (T) ranging from 2 to 4 for each WP.

The WP1 aims at achieving the following main objectives: 1) categorize scientific studies on Automated Fault Detection and Diagnosis (AFDD) methods for Air-Handling Units (AHUs) based on experimental datasets, 2) create a reliable experimental dataset of a typical AHU covering a wide range of fault free and faulty scenarios.

This WP1 helps to a) better understand the current research gaps, b) address the lack of datasets for AFDD with verified ground truth information, c) support the development of, and benchmark the performance accuracy of AFDD methods, d) recognize fault patterns of AHUs and gain insights on AHUs performance.

The WP1 includes 2 tasks (WP1_T1, WP1_T2) with the following main activities:

- WP1_T1) this task provided a scientific written report (WP1_D1) focusing on a literature review of AHU experimental studies for AFDD.
- WP1_T2) this task will perform an extensive experimental campaign to assess the fault free and faulty performance of the typical fully instrumented single-duct dual-fan constant air volume AHU set-up for AFDD purposes at the "SENS i-Lab" of UNICAMPANIA while serving a 4x4x3.6 m^3 test room. Tests encompass different fault types and severities.

This deliverable WP1_D1 provides a detailed analysis of scientific studies that experimentally developed AFDD methods for AHUs to categorize them in terms of: AHU operating schemes; measured key-parameters; type and accuracy of sensors; measurement duration and frequency; range of operational, seasonal and weather conditions; fault types, fault severity and fault imposition methods; fault effects on AHUs performance

1. Introduction

It is well known that energy demand associated to the utilization of Heating, Ventilation and Air-Conditioning (HVAC) systems equipped with Air-Handling Units (AHUs) are significant [1,2] also due to the fact that, according to several studies [2-4], a relevant portion of AHUs operates under faulty conditions that are not timely and effectively detected and/or diagnosed. About 5%÷30% of the energy demand of HVAC units is wasted due to the occurrence of faults [2-4]. A fault is intended as an instance where one component and/or sensor performs in a way that is different from normal/expected behaviour and Automated Fault Detection and Diagnosis (AFDD) is an automated process for timely detecting and/or diagnosing the type and/or location of faults [2-5]. AFDD methods are gaining more and more interest in the scientific community [3,4]. The approaches used for developing AFDD analyses are generally classified as follows: (i) qualitative model-based, (ii) quantitative model-based, and (iii) data-driven [3,4]. With respect to both quantitative and qualitative methods, data-driven approach is based on the exploitation of operational data experimentally collected from AHUs running under fault free and faulted scenarios; this approach is recognized as easier to be developed thanks to the facts that (i) nowadays building-integrated systems are equipped with a number of sensors, (ii) several computer-aided techniques have been developed for data mining, (iii) it can be applied even in the case of the physics-based knowledge of the system is not wide enough, as well as (iv) it is potentially able to provide a higher accuracy in detecting and diagnosing typical faults [4,6-8]. A number of scientific researches [3,9,10] demonstrated that data-driven AFDD tools can effectively contribute in significantly reducing energy demand, operational costs and greenhouse gas emissions, as well as enhancing user comfort and equipment lifetime of AHUs.

Although data-driven AFDD methods are maturing, they are in the early stage of adoption stock-wide [7,11] mainly due to the facts that they (i) require labelled, affordable, reliable and scalable faulty data and (ii) cannot operate beyond the operational range of training data. Up to now a limited number of faulty datasets have been

Finanziato dall'Unione europea NextGenerationEU | Ministero dell'Università e della Ricerca | Italiadomani PIANO NAZIONALE DI RIPRESA E RESILIENZA

developed because they are generally difficult to be obtained taking into account that: (i) sensors in AHUs are generally not devoted to AFDD purposes and, thus, some significant parameters are usually not measured; (ii) data under faulty scenarios are challenging to be derived due to cost and time required for implementing faults into AHUs; (iii) AHUs are typically custom-designed and each one is unique in terms of operating scheme, components and/or control logic; (iv) available datasets generally refer to limited ranges of weather/load conditions; (v) in addition to single-fault scenarios, the effects of multiple faults occurring simultaneously should be investigated. Finally, it should be underlined that a very few examples of detailed datasets of AHUs with a verified ground truth information on specific tagged faults are publicly available. Even if a number of scientific studies regarding data-driven AFDD methods can be found in related literature, additional efforts have to be made in order to more effectively support the development of such tools [2,7,11]. Some reviews on AFDD algorithms have been already published. In 2005, Katipamula and Brambley [12] addressed applications related to the field of HVAC systems, discussing about the state of diagnostics in the building sector and the future of AFDD algorithms. Later, Yu et al. [3] provided (i) a systematic review of HVAC typical faults, (ii) an illustration of desirable characteristics of AFDD methods, as well as (iii) an analysis of existing AFDD tools for HVAC units. More recently, Mirnaghi and Haghighat [4] discussed (i) the classification of AFDD procedures, (ii) fault detection and diagnosis process, (iii) potential faults of HVAC systems and (iv) applications of AFDD tools in HVAC units. However, these reviews don't allow to clearly identify the AHU operating schemes, fault types, faults severities and climatic conditions requiring further studies. Therefore, it is required to continue publicly documenting the studies on data-driven AFDD technologies to provide a wider knowledge of what today's technology is delivering and how it can be improved upon.

The development of data-driven AFDD methods is based on the analysis of experimental data collected from AHUs operating under normal and faulty conditions. In this deliverable, the most significant 24 scientific papers [13-36] experimentally investigating AHUs with the aim of developing data-driven AFDD algorithms are systematically reviewed and categorized in terms of AHU operating schemes and served buildings (section 2.1), measured AHU operating parameters (section 2.2), accuracy of AHU measuring sensors, tests duration and measurement frequency (section 2.3), AHU fault types and severities (section 2.4), climatic conditions of experimental tests (section 2.5). This review has been performed with the main aim of supporting and guiding the future studies devoted to the development of new and accurate data-driven AFDD systems by highlighting: (i) the most poorly examined AHU operating scheme, (ii) the AHU operating parameters to be generally measured for AFDD purposes, (iii) measuring accuracy and frequency specifically required in collecting data for AFDD tools, (iv) fault types as well as fault severities to be additionally analyzed, and (v) climatic conditions under which further experimental datasets have to be obtained.

2. Results

In the following subsections the most important features of the reviewed 24 scientific papers [13-36], focusing on the experimental investigation of AHUs with the aim of developing data-driven AFDD algorithms, are clearly reported in order to highlight the aspects to be further investigated and analyzed.

2.1. AHU operating schemes and type of served buildings

HVAC systems including AHUs are used to control air temperature, air relative humidity, air velocity and air quality in enclosed spaces. AHUs contain a significant number of interconnected components (including supply and return air fans, cooling coil, heating coil, heating coil valve, cooling coil valve, return air damper, mixed air damper, exhaust air damper, fresh air damper, filters, etc.) and they can operate under different configurations. The analysis of the reviewed 24 papers [13-36] highlighted that the following 3 main AHU operating schemes have been analyzed:

- single-duct dual-fan constant air volume AHUs (Figure 1a). In this case, the supply air flowrate remains constant and the desired indoor conditions are obtained by regulating the air supply temperature. This AHU scheme has been investigated in two papers [13,27]; in addition, some studies [20,33-36] investigated a very similar AHU scheme with the addition of a humidifier; in [27] only one heat exchanger to be alternatively used for heating or cooling purposes is included in the AHU.
- single-duct dual-fan Variable Air Volume (VAV) AHUs (Figure 1b). Unlike the constant air volume AHU scheme reported in Figure 1a, this scheme allows to adjust the supply air flowrate depending on heating/cooling load while maintaining a constant supply air temperature. This AHU scheme has been investigated in 16 studies [13-15,17-19,22-26,28-32], even if in 4 works [18,22,26,32] it is without the heating coil.

Finanziato dall'Unione europea NextGenerationEU | Ministero dell'Università e della Ricerca | Italiadomani PIANO NAZIONALE DI RIPRESA E RESILIENZA

- dual-duct dual-fan variable air volume AHUs (Figure 1c). This scheme has separate ducts for hot and cold air, and served zone has a plenum where their airflows are mixed; the ratio of hot and cold airflows is set according to the desired temperature to be maintained in the zone. It has been investigated only in two papers [16,21].

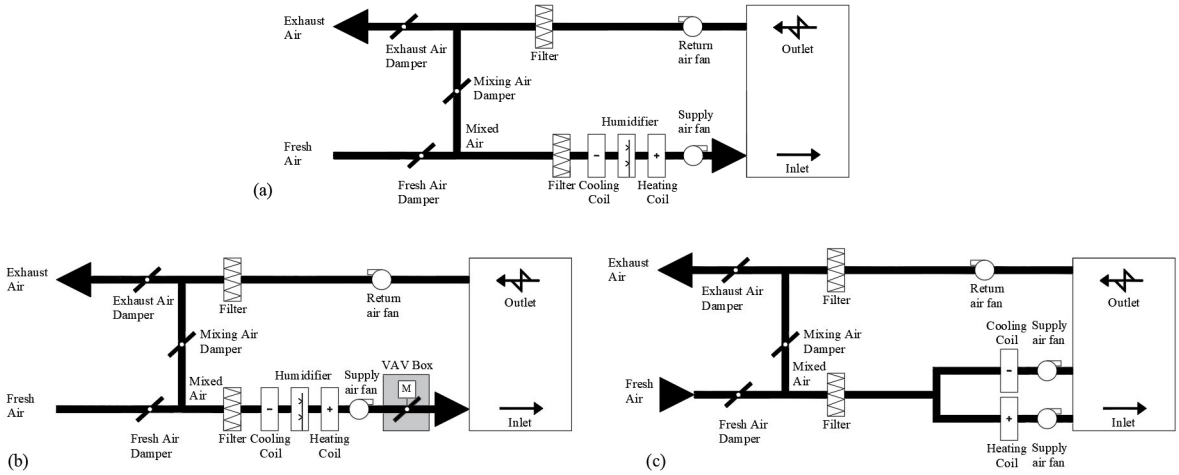

Fig. 1. (a) Scheme of single-duct dual-fan constant air volume AHUs, (b) Scheme of single-duct dual-fan variable air volume AHUs, (c) Scheme of dual-duct dual-fan variable air volume AHUs.

Table 1 indicates the type as well as the size of the building served by the AHUs analyzed in the reviewed papers [13-36], highlighting that (i) AHUs are generally installed inside university test facilities, and (ii) the floor area of served zones (where indicated) varies from a minimum of 16.0 m^2 up to a maximum of 38000 m^2.

Table 1. Type and size of buildings served by the AHUs in the reviewed papers.

Building type	Building size	References
Iowa Energy Center Energy Resource Station	27.6 m^2	[13-16,19,21,24]
Oak Ridge National Laboratory	359.12 m^2	[13,15]
Test room housed in a multi-purpose research and test facility	20.7 m^2	[17,23,25]
Office of Nanyang Technological University	240 m^3	[18,22,29,32]
University building	Not specified	[20]
University building	3360 m^2	[26]
South-facing rooms of a seven-story office building	Not specified	[27]
Shopping mall and hospital	Not specified	[28]
Research and Development Center of Tokyo Electric and Power Company	38000 m^2	[30]
Building of the campus of University of California	Not specified	[31]
Test room housed in a multi-purpose research and test facility	16.0 m^2	[33-36]

2.2 Measured AHU operating parameters

AFDD algorithms utilize the measured values of key operating parameters, the variation of which with respect to a "healthy" trend is considered as a symptom of faults. Determining the key measurements to be adopted as indicators for reflecting equipment operation/performance is a challenging task in the development of AFDD methods. Therefore, Table 2 lists the AHU operating parameters and specifies the corresponding scientific papers [13-36] where they have been measured. This table highlights those 10 parameters (return and supply air temperature, return and supply air relative humidity, return and supply air volumetric flowrate, mixed air temperature, outdoor air temperature, return and supply chilled water temperature) have been measured in more than 11 papers and, therefore, they should be considered as fundamental for AFDD purposes of AHUs. Some parameters (return air pressure [31], exhaust air volumetric flowrate [31], chilled water pressure [19], heat recovery air differential pressure [20], refrigerating system electric power [19], room CO_2 concentration [20], outdoor air pressure [31], mixed air relative humidity [29], exhaust air relative humidity [20], hot/chilled water differential pressure [27], filter air differential pressure [20], water pump electric power [19]) have been measured only in one paper, thus representing unessential measurements for AFDD tools associated to the operation of AHUs.

Table 2. Measured AHU parameters and corresponding reviewed papers.

Measured parameters	References	Measured parameters	References
supply air temperature	[13-36]	supply air relative humidity	[13,15,18-20,22,24,29,30,32-36]

Finanziato dall'Unione europea NextGenerationEU | Ministero dell'Università e della Ricerca | Italiadomani PIANO NAZIONALE DI RIPRESA E RESILIENZA

supply air volumetric flowrate	[13,14,15,17-20,22-32]	supply air pressure	[13,15,17,23-26,28,30,31]
supply air fan electric power	[13,15,19,24]	hot/cold deck supply air temperature	[16,21]
hot/cold deck supply air flowrate	[16,21]	hot/cold deck supply air relative humidity	[16,21]
hot/cold deck supply air pressure	[16,21]	hot/cold deck supply air fan electric power	[16,21]
supply air CO_2 concentration	[16,21]	return air temperature	[13-28,30-36]
return air relative humidity	[13-16,18-22,24,29,30,32-36]	return air volumetric flowrate	[13,15-17,19-21,23-25,28,31]
return air pressure	[31]	return air fan electric power	[13,15,16,19,21,24]
return air CO_2 concentration	[16,21,30]	room temperature	[17,20,23,25,30]
room relative humidity	[20,30]	room CO_2 concentration	[20]
outdoor air temperature	[13-15,17-20,22-36]	outdoor air relative humidity	[14,18,19,22,24,26,29,30,32]
outdoor air volumetric flowrate	[13,15,16,19,21,24,31]	outdoor air pressure	[31]
outdoor solar irradiance	[26,30]	outdoor CO_2 concentration	[16,21]
mixed air temperature	[13-17,19,21,23-29]	mixed air relative humidity	[29]
exhaust air temperature	[20,31]	exhaust air relative humidity	[20]
exhaust air volumetric flowrate	[31]	cooling coil outlet air temperature	[13,15,16,19,21,24,33-36]
heating coil outlet air temperature	[13,15,16,19,21,24]	supply chilled water temperature	[13,15,16,18,19,21,22,24,27-30,32]
return chilled water temperature	[13,15,16,18,19,21,22,24,27, 30,32]	chilled water volumetric flowrate	[13,15,16,18,19,21,22,24.30,32]
chilled water pressure	[19]	chilled water differential pressure	[27]
supply hot water temperature	[13,15,16,19,21,24,27,30]	return hot water temperature	[13,15,16,19-21,24,27,30]
hot water volumetric flowrate	[13-16,19,21,24,30]	hot water differential pressure	[27]
heat recovery air differential pressure	[20]	filter air differential pressure	[20]
refrigerating system electric power	[19]	water pump electric power	[19]

2.3 Characteristics of AHU measuring sensors and tests duration

Building energy management units include a number of sensors that could provide valuable information for the development of AFDD methods. An indication of measurements accuracy has to be provided in order to quantify the reliability of test data [37], also taking into account that AFDD process is substantially affected by the accuracy of sensors. Table 3 specifies the accuracy of sensors used in the reviewed papers (indicated only in 12 studies [13,15,19,22,25-27,32,33-36] out of 24). This table underlines that air temperature is measured with an accuracy between ±0.1 and ±0.8 °C, while the accuracy of water temperature sensors ranges from ±0.1 up to ±1.3 °C; the accuracy associated to the measurements of air relative humidity is in the range between ±0.8% and ±3%, while it is between ±0.25% and ±5% in the case of air volumetric flowrate sensors.

Given the time, cost and complexities of performing experiments in existing buildings, field assessments are generally limited in terms of duration. Table 4 indicates the duration of experimental tests as well as the frequency of measurements of the papers under analysis. According to this table, it can be derived that the measurements frequency is generally equal to 1 minute or 5 minutes, while only in 4 cases [18,22,29,32] it is lower than 1 minute; tests duration ranges from a minimum of 0.6 h up to a maximum of 8 weeks.

Table 3. Accuracy of AHU measuring sensors used in the reviewed papers.

Air temperature sensor accuracy	Water temperature sensor accuracy	Air relative humidity sensor accuracy	Air volumetric flowrate sensor accuracy	Water flowrate sensor accuracy	Power sensor accuracy	Air pressure sensor accuracy	References
±0.1 °C	Not specified	±0.8%	±0.25%, ±2%	Not specified	±0.5%	±0.08% of full scale	[13,15]
±0.14 °C, ±0.2 °C	±0.14 °C	±3%, ±1%	±2%	Not specified	±0.2%	±1% of full scale	[19]
±0.2 °C	±0.1 °C	±2%	±5%	±1%	Not measured	Not measured	[22,32]
±0.5 K, ±0.8 K	Not measured	Not measured	±1%, ±2%	Not measured	Not measured	±0.25%	[25]
±0.6 °F	Not measured	Not measured	Not specified	Not measured	Not measured	Not measured	[26]
±0.8 °C	±1.3 °C	Not measured	±3.1 Pa	Not measured	Not measured	Not measured	[27]
±0.8 K, ±0.75, ±0.5 K	Not measured	±3%	Not measured	Not measured	Not measured	Not measured	[33-35]
±0.8 K, ±0.75 K	Not measured	±3%	Not measured	Not measured	Not measured	Not measured	[36]

Table 4. Duration and measurement frequency of the experiments as a function of the reviewed papers.

Duration of experiments	Frequency of measurements	References	Duration of experiments	Frequency of measurements	References

Finanziato dall'Unione europea NextGenerationEU | Ministero dell'Università e della Ricerca | Italiadomani PIANO NAZIONALE DI RIPRESA E RESILIENZA

24 h	1 min	[13,15]	10 days	5 min	[26]
48-72 h	1 min	[14]	Not specified	5 min	[27]
24 h	1 min	[16,21]	10 h	5 min	[28]
90 min	Not specified	[17,23,25]	24 h	1 min	[30]
10 h	35 s	[18,29]	From 2 to 8 weeks	Not specified	[31]
24 h	1 min	[19,24]	From 15 to 34 h	35 s	[32]
From 2 to 34 h	35 s	[22]	From 0.6 h to 6.2 h	1 min	[33-36]

2.4 AHU fault types and severities

AHUs include a number of components and sensors at risk of fault, which may affect energy efficiency, greenhouse gas emissions, operating costs, user comfort and equipment lifetime. Yu et al. [3] distinguish AHU fault types into 3 main categories (faults of equipment, faults of sensors and controllers, and faults of actuators), with each fault type that could be characterized by different severities. The task W1_T1 highlighted that 42 different fault types have been investigated in the 24 reviewed papers [13-36]. Table 5 describes the fault of fans and pumps, Table 6 refers to the faults of sensors and controllers, Table 7 is focused on the faults of dampers and valves. Tables 5-7 clarify the severity levels as well as the scientific papers corresponding to each fault type investigated in the reviewed papers. These tables indicate that fresh air damper stuck (12 scientific papers) and cooling coil valve stuck (11 scientific papers) are the most analyzed fault types. The following fault types have been studied only in a single case and, thus, they require additional researches: slipping of supply air fan belt, heating/cooling pump stuck, fresh air temperature sensor failure, freezing of return/supply air temperature sensor, unstable control of fresh air damper, unstable control of heating coil valve, offset of fresh air temperature sensor, return/supply air differential pressure sensor failure, mixed air damper leakage. These tables also indicate that only a single severity level has been analyzed with reference to the following fault types: supply air fan stuck, cooling pump stuck, offset of supply air pressure sensor, humidifier valve stuck. In addition, it should be also highlighted that, even if it is common that multiple faults occur during AHU operation, the effects of multiple faults occurring simultaneously have been experimentally investigated only in 5 studies ([17,22,23,25,32]). Finally, more efforts have to be devoted in order to estimate fault prevalence in terms of energy consumption, greenhouse gas emissions, costs, thermal comfort and indoor air quality according to its severity [10,11]. This task should be performed by identifying novel weighted multi-criteria key performance indicators [10,11] capable to identify faults with most adverse impacts with the aim of making it possible to rank faults according to their impact under different operating scenarios, as well as evaluating a maintenance action prioritization scheme considering how the impact of a fault changes during AHU operation.

Table 5. Type and severity of AHU faults for fans and pumps.

Type of fault	**Fault severity**	**References**	**Type of fault**	**Fault severity**	**References**
supply air fan stuck	Not specified 20%	[17,23,25,31] [34-36]	supply air fan failure	-	[16,18-21]
slipping of supply air fan belt	Not specified	[19]	return air fan failure	-	[20,21,24,28]
return air fan stuck	20% 30% 80%	[24,34,35,36] [24,28] [24]	filter clogging	Not specified 10%, 25% 20%, 50%, 80%	[22] [24] [32]
air duct leakage	Not specified 20%, 50%, 100%	[18,22,24,29] [32]	insufficient/excessive supply hot/chilled water temperature	Not specified	[21,26,27]
heating pump stuck	0%, 100%	[20]	cooling pump stuck	100%	[20]

Table 6. Type and severity of AHU faults for sensors and controllers.

Type of fault	**Fault severity**	**References**	**Type of fault**	**Fault severity**	**References**
offset of supply air temperature sensor	3 °C, -3 °C 1.7 °C, 2.8 °C 5 °F 10%, 15%, 20% 20%	[21] [14] [16] [17,23] [25]	offset of supply air flowrate sensor	Not specified 10% 20%	[17] [23] [25]
offset of supply air pressure sensor	Not specified 147 Pa	[19] [16,21]	offset of return air temperature sensor	3 °C 10% 20%	[21] [23] [25]
offset of room temperature sensor	Not specified 2.2 °C, -2.2 °C	[30] [13,15]	offset of fresh air temperature sensor	3 °F, -3 °F	[24]

Finanziato dall'Unione europea NextGenerationEU
Ministero dell'Università e della Ricerca
Italiadomani PIANO NAZIONALE DI RIPRESA E RESILIENZA

fresh air temperature sensor failure	-	[31]	supply and return air differential pressure sensor failure	-	[20]
freezing of supply air temperature sensor	-20 °C, 150 °C	[20]	freezing of return air temperature sensor	-20 °C, 150 °C	[20]
unstable control of fresh air damper	Not specified	[21]	unstable control of mixed air damper	Not specified	[24,26]
unstable control of cooling coil valve	Not specified	[24,30]	unstable control of heating coil valve	Not specified	[30]
unstable control of supply air fan	Not specified	[19,26,29]	unstable control of heating and cooling mode	Not specified	[20,21,24]

Table 7. Type and severity of AHU faults for actuators (dampers and valves).

Type of fault	Fault severity	References	Type of fault	Fault severity	References
fresh air damper stuck	Not specified	[17,18,23,25,29]	fresh air damper leakage	45%, 52%, 55%, 62%	[24]
	0%	[20,24,28]			
	15%	[13,15]			
	20%	[21]			
	40%	[24]			
	45%	[27]			
	50%, 100%	[13,15,21,22,32]			
return air damper stuck	Not specified	[14]	supply air damper stuck	0%	[16,21,30,31]
	0%	[19,27]		50%	[21,22,30,32]
	50%	[22,32]		100%	[16,21,32]
	55%, 100%	[27]			
mixed air damper leakage	Not specified	[19]	exhaust air damper stuck	0%	[24,28]
				40%, 100%	[24]
cooling coil valve leakage	Not specified	[13,15,19]	cooling coil fouling	Not specified	[16,19,21,24,27]
				10%, 30%, 50%	[22,32]
cooling coil valve stuck	Not specified	[18,29]	heating coil valve leakage	Not specified	[13,15,19,27]
	0%	[13,15,20,24,28,34,35]		0.019 l/s, 0.032 l/s, 0.032 l/s	[14]
	15%	[24,28]			[24]
	20%, 65%	[24]		0.4 GPM, 1 GPM, 2 GPM	
	50%,100%	[13,15,20,24,27]			
heating coil fouling	Not specified	[21,24,27]	heating coil valve stuck	0%	[13,15,20,34,35]
				50%, 100%	[13,15,20]
humidifier valve stuck	0%	[34-36]			

2.5 Climatic conditions

Climatic conditions could significantly affect the performance of AHUs and, therefore, the effects of single/multiple faults. Table 8 classifies the 24 reviewed papers [13-36] in terms of both location and season of the experimental tests (if specified), highlighting that only 8 studies [13,14,15,19,24,27,34,36] have been performed during both winter and summer, with only 4 works [33-36] referring to Mediterranean climatic conditions.

Table 8. Location and season of experiments as a function of the reviewed papers.

Test location	Test season	References	Test location	Test season	References
Iowa and Tennessee (USA)	Winter, summer and spring	[13,15]	Stockholm (Sweden)	Whole year	[27]
Iowa (USA)	Winter and summer	[14]	Hefei (China)	Summer	[28]
Iowa (USA)	Summer, fall and spring	[16,21]	Kawasaki (Japan)	Summer	[30]
Singapore	Not specified	[18,22,29,32]	California (USA)	Summer and spring	[31]
Iowa (USA)	Winter, spring and summer	[19,24]	Aversa (Italy)	Spring and summer	[33]
Bustehrad (Czech Republic)	Not specified	[20]	Aversa (Italy)	Summer and winter	[34,36]
Not specified	Winter	[23,25]	Aversa (Italy)	Summer	[35]
New Mexico (USA)	Summer and fall	[26]			

3. Discussion and conclusions

In this deliverable the most significant 24 scientific papers [13-36] focusing on experimental analyses of AHUs aiming at the development of data-driven AFDD algorithms have been systematically reviewed and categorized. The review highlighted that: (i) dual-duct dual-fan variable air volume AHUs have been poorly investigated (only in two studies [16,21]); (ii) 10 parameters (return and supply air temperature and relative humidity, return and supply air volumetric flowrate, mixed air temperature, outdoor air temperature, return and supply chilled water temperature,) have been identified as fundamental for AFDD purposes of AHUs; (iii) the accuracy of measuring sensors has been indicated only in a few works; (iv) the accuracy of measuring sensors have to carefully selected in order to obtain the desired effectiveness of AFDD tools; (v) the following fault types have been analyzed only in a single scientific study and, thus, they require additional researches: slipping of supply air fan belt, heating and cooling pump stuck, outdoor air temperature sensor failure, freezing

Finanziato dall'Unione europea NextGenerationEU | Ministero dell'Università e della Ricerca | Italiadomani PIANO NAZIONALE DI RIPRESA E RESILIENZA

of supply and return air temperature sensor, unstable control of fresh air damper, offset of fresh air temperature sensor, supply and return air differential pressure sensor failure, unstable control of heating coil valve, mixed air damper leakage; (vi) only in 5 cases ([17,22,23,25,32]) the effects of multiple faults occurring simultaneously have been investigated and, therefore, additional efforts have to be paid to this point from an experimental point of view; (vii) AHU faulty operation under both summer and winter as well as Mediterranean climatic conditions has not been considered enough and requires further researches.

Moreover, it should be highlighted that only a few experimental databases [13-15,19,20,24] are publicly available; in the future, it would desirable that all measured data are uploaded in public repositories, allowing its utilization to AFDD developers, AFDD users and research organizations for institutional and research purposes with the aim of supporting AFDD applications.

An additional persistent challenge is represented by the lack of common datasets (covering a wide diversity of operating scenarios, AHU configurations and equipment) and test methods to assess the accuracy of AFDD tools [10,11]. Finally, it should be underlined that AFDD end-users must be aware about the costs and potential savings associated to AFDD algorithms in order to support technology investment; unfortunately, such kind of information is rarely available in the scientific literature [11] with reference to commercially available AFDD tools in real buildings and, therefore, additional efforts have to be performed with reference to this aspect.

4. References

[1] Cao, Xiaodong, Xilei Dai, and Junjie Liu. (2016) "Building energy-consumption status worldwide and the state-of-the-art technologies for zero-energy buildings during the past decade." *Energy and Buildings* 128.15 (2016): 198-213.

[2] Yun, Woo-Seung, Won-Hwa Hong, and HyunCheol Seo. (2021) "A data-driven fault detection and diagnosis scheme for air handling units in building HVAC systems considering undefined states." *Journal of Building Engineering* 35 (2021).

[3] Yu, Yuebin, Denchai Woradechjumroen, and Daihong Yu. (2014) "A review of fault detection and diagnosis methodologies on air-handling units." *Energy and Buildings* 82 (2014): 550-562.

[4] Mirnaghi, S. Maryam, and Fariborz Haghighat. (2020) "Fault detection and diagnosis of large-scale HVAC systems in buildings using data-driven methods: A comprehensive review." *Energy & Buildings* 229 (2020).

[5] Wang, Haitao, and Youming Chen. (2016) "A robust fault detection and diagnosis strategy for multiple faults of VAV air handling units." *Energy and Buildings* 127.1 (2016): 442-451.

[6] Piscitelli, S. Marco, Daniele M. Mazzarelli, and Alfonso Capozzoli. (2020) "Enhancing operational performance of AHUs through an advanced fault detection and diagnosis process based on temporal association and decision rules." *Energy and Building* 226.1 (2020).

[7] Granderson, Jessica, Guanjing Lin, Rupman Singla, Ebony Mayhorn, Paul Ehrlich, Draguna Vrabie, and Stephen Frank. (2021) "Commercial Fault Detection and Diagnostics Tools: What They Offer, How They Differ, and What's Still Needed." *Lawrence Berkeley National Laboratory* (2021).

[8] Casillas, Armando, Guanjing Lin, and Jessica Granderson. (2022) "Curation of Ground-Truth Validated Benchmarking Datasets for Fault Detection & Diagnostics Tools." *Lawrence Berkeley National Laboratory* (2022).

[9] Au-Yong, P. Cheong, Azlan S. Ali, and Faizah Ahmad. (2014) "Improving occupants' satisfaction with effective maintenance management of HVAC system in office buildings." *Automation Construction* 43 (2014): 31-37.

[10] Frank, Stephen, Guanjing Lin, Xin Jin, Rupam Singla, Amanda Farthing, and Jessica Granderson. (2019) "A performance evaluation framework for building fault detection and diagnosis algorithms" *Energy & Buildings* 192.1 (2019): 84-92.

[11] Lin, Guanjing, Hannah Kramer, and Jessica Granderson. (2020) "Building fault detection and diagnostics: Achieved savings, and methods to evaluate algorithm performance." *Building and Environment* 168.15 (2020).

[12] Katipamula, Srinivas and Michael R. Brambley. (2005) "Review Article: Methods for Fault Detection, Diagnostics, and Prognostics for Building Systems - A Review, Part II." *HVAC&R Research* 11.2 (2005): 169-187.

[13] Granderson, Jessica, Guanjing Lin, Ari Harding, Piljae Im, and Yan Chen. (2020). "Building fault detection data to aid diagnostic algorithm creation and performance testing." *Energy Technologies Area - Lawrence Berkeley National Laboratory* (2020).

[14] Castro, S. Natascha, Jeffrey Schein, Cheol Park, Michael A. Galler, Steven T. Bushby. (2003) "NISTIR 6964 Results from Simulation and Laboratory Testing of Air Handling Unit and Variable Air Volume Box Diagnostic Tools." *Scientific Data* (2003).

[15] Granderson, Jessica, Guanjing Lin, Ari Harding, Piljae Im, and Yan Chen. (2020) "Building fault detection data to aid diagnostic algorithm creation and performance testing." *Scientific Data* 65.7 (2020).

[16] Wen, Jin, Shokouh Pourarian, Xuebin Yang, and Xiwang Li. (2015) "Tools for Evaluating Fault Detection and Diagnostic Methods for HVAC Secondary Systems of a Net Zero Building. " *Scientific Data* (2015).

[17] Cho Sung H., Young J. Hong, Hooncheal Yang, Byung C. Ahan. (2004) "An Experimental Study on Multi-Fault Detection and Diagnosis Analysis of HVAC System." *Journal of ordnance equipment engineering* (2004): 932-941.

[18] Liao, Huanyue, Wenjian Cai, Fanyong Cheng, Swapnil Dubey and Pudupadi B. Rajesh. (2021) "An Online Data-Driven Fault Diagnosis Method for Air Handling Units by Rule and Convolutional Neural Networks." *Sensors* 21.13 (2021).

[19] Norford, K. Leslie, Jonathan Wright, Richard Buswell, Dong Luo, Curtis J. Klaassen, and Andy Suby. (2002) "Demonstration of Fault Detection and Diagnosis Methods for Air-Handling Units (ASHRAE 1020-RP)." *HVAC&R RESEARCH* 8.1 (2002).

[20] Nehasil, Ondrej, Lucie Dobiášová, Vojteˇch Mazanec, and Jan Široky. (2021) "Versatile AHU fault detection - Design, field validation and practical application." *Energy & Buildings* 237 (2021): 110781-110792

[21] Liu, Ran, Xiaohui Zhou, and Robert Milbrandt. (2015) "Experimental Study of Lab Controlled Faults in Dual-Duct VAV System." *ASHRAE Annual Conference - Papers* (2015).

[22] Wu Bingjie, Wenjian Cai, Haoran Chen, and Xin Zhang. (2021). "A hybrid data-driven simultaneous fault diagnosis model for air handling units." *Energy & Buildings* 245 (2021).

[23] Cho, H. Sung, Young J. Hong, Won T. Kim, and Mohammed Zaheer-uddin. (2005) "Multi fault detection and diagnosis of HVAC systems an experimental study." *International Journal of Energy Research* 29 (2005): 471-483.

[24] Wen, Jin, and Shun Li. (2011) "ASHRAE RP-1312-Tools for Evaluating Fault Detection and Diagnostic Methods for Air-Handling Units." *ASHRAE* (2012).

[25] Cho, H. Sung, Yang Hoon C., Mohammed Zaheer-uddin, and Byung C. Ahn. (2005) "Transient pattern analysis for fault detection and diagnosis of HVAC System." *Energy Conversion and Management* 46 (2005): 3103-3116.

Finanziato dall'Unione europea NextGenerationEU | Ministero dell'Università e della Ricerca | Italiadomani PIANO NAZIONALE DI RIPRESA E RESILIENZA

[26] Van Every, Philip M., Mykel Rodriguez, Birk C. Jones, Andrea A. Mammoli, and Manel Martínez-Ramón. (2017) "Advanced detection of HVAC faults using unsupervised SVM novelty detection and Gaussian process models." *Energy and Buildings* 149 (2017): 216-224.
[27] Carling, Par (2002) "Comparison of Three Fault Detection and Diagnosis Methods Based on Field Data of an Air Handling Unit" *ASHRAE Transactions* 108 (2002): 904-921.
[28] Feng, Bowei, Qizhen Zhou, Jianchun Xing, Qiliang Yang, Xia Qin, Yixin Mo, and Wenjie Chen. (2022) "A fully distributed voting strategy for AHU fault detection and diagnosis based on a decentralized structure." *Energy Reports* 8 (2022): 390-404.
[29] Cheng, Fanyong , Wenjian Cai, Xin Zhang, Huanyue Liao, and Can Cui. (2021) "Fault detection and diagnosis for Air Handling Unit based on multiscale convolutional neural networks." *Energy & Buildings* 236 (2021).
[30] Kumar, Sanjay, Sangeeta Sinha, Toshinori Kojima, and Harunori Yoshida. (2001) "Development of parameter based fault detection and diagnosis technique for energy efficient building management system." *Energy Conversion and Management* 42 (2001): 833-854.
[31] Siyu, Wu, and Jian Q. Sun. (2011) "Cross-level fault detection and diagnosis of building HVAC systems" *Building and Environment* 46 (2011): 1558-1566.
[32] Wu, Bingjie, Wenjian Cai, Fanyong Cheng, and Haoran Chen. (2022) "Simultaneous-fault diagnosis considering time series with a deep learning transformer architecture for air handling units." *Energy & Buildings* 257 (2022).
[33] Rosato, Antonio, Francesco Guarino, Vincenzo Filomena, Sergio Sibilio, and Luigi Maffei. (2020) "Experimental Calibration and Validation of a Simulation Model for Fault Detection of HVAC Systems and Application to a Case Study." *Energies* 13 (2020).
[34] Rosato, Antonio, Francesco Guarino, Sergio Sibilio, Evgueniy Entchev, Massimiliano Masullo, and Luigi Maffei. (2021) "Healthy and Faulty Experimental Performance of a Typical HVAC System under Italian Climatic Conditions: Artificial Neural Network-Based Model and Fault Impact Assessment" *Energies* 14 (2021).
[35] Rosato, Antonio, Sergio Sibilio, Francesco Guarino, Mohammad El Youssef, Evgueniy Entchev, and Luigi Maffei. (2022) "Field performance of HVAC system under healthy and faulty conditions during the summer: preliminary development of a simulation model based on artificial neural networks." *Smart Innovation, System and Technology* 263 (2022): 183-196
[36] Rosato, Antonio, Francesco Guarino, Mohammad El Youssef, Sergio Sibilio. (2021) "Preliminary symptoms assessment of typical faults related to the fans and humidifiers of HVAC systems based on experimental data collected during Italian summer and winter." IOP Conference Series: Earth and Environmental Science 897 (2021).
[37] Mastrullo, Rita, Antonio Rosato, Giuseppe P. Vanoli, and John R. Thome. (2008) "A methodology to select the experimental plant instrumentation based on an a priori analysis of measurement errors and instrumentation cost." *International Communications in Heat and Mass Transfer* 35 (2008): 689-695.

Finanziato dall'Unione europea NextGenerationEU
Ministero dell'Università e della Ricerca
Italiadomani PIANO NAZIONALE DI RIPRESA E RESILIENZA

DELIVERABLE WP1_D2

EXPERIMENTAL ANALYSIS OF A TYPICAL AHU UNDER FAULTY AND FAULT FREE SCENARIOS

EDIT BY UNICAMPANIA

PRIN 2022 - UTMOST FDD: AN AUTOMATED, OPEN, SCALABLE AND TRANSPARENT FAULT DETECTION AND DIAGNOSIS PROCESS FOR AIR-HANDLING UNITS BASED ON A HYBRID EXPERT AND ARTIFICIAL INTELLIGENCE APPROACH

Funded by the European Union - Next Generation EU within the "Piano Nazionale di Ripresa e Resilienza (PNRR), missione 4 componente 2 investimento 1.1 - fondo per il programma nazionale di ricerca e progetti di rilevante interesse nazionale (PRIN)"

The UTMOST FDD Project is organised into the following 7 Work Packages (WPs):
WP0) PROJECT COORDINATION
WP1) EXPERIMENTAL ANALYSIS FOR THE CHARACTERIZATION OF FAULTY AND NORMAL OPERATION OF A TYPICAL AHU
WP2) KPIs IDENTIFICATION FOR ASSESSING FAULT IMPACT IN AHU OPERATION
WP3) AHU DIGITAL TWIN AND SIMULATION-BASED FAULT IMPACT SCENARIO ANALYSIS
WP4) DEFINITION OF HYBRID FDD STRATEGIES FOR AHUs
WP5) TRANSFERABILITY ANALYSIS OF THE FDD STRATEGIES
WP6) KNOWLEDGE TRANSFER AND DISSEMINATION

The WPs are organized into Tasks (T) ranging from 2 to 4 for each WP.

The WP1 aims at achieving the following main objectives: 1) categorize scientific studies on Automated Fault Detection and Diagnosis (AFDD) methods for Air-Handling Units (AHUs) based on experimental datasets, 2) create a reliable experimental dataset of a typical AHU covering a wide range of fault free and faulty scenarios.

This WP1 helps to a) better understand the current research gaps, b) address the lack of datasets for AFDD with verified ground truth information, c) support the development of, and benchmark the performance accuracy of AFDD methods, d) recognize fault patterns of AHUs and gain insights on AHUs performance.

The WP1 includes 2 tasks (WP1_T1, WP1_T2) with the following main activities:

- WP1_T1): this task provided a scientific written report (deliverable WP1_D1) focusing on a literature review of AHU experimental studies for AFDD.
- WP1_T2): this task focuses on an extensive experimental campaign to evaluate the normal and faulty performance of a typical single-duct dual-fan constant air volume AHU setup for AFDD purposes. The experimental dataset, together with its detailed description, will be uploaded in a public repository as 2nd WP1 deliverable WP1_D2.

This deliverable WP1_D2 describes the above-mentioned extensive experimental campaign to assess the fault-free and faulty performance of the typical fully instrumented single-duct dual-fan constant air volume AHU installed at the "SENS i-Lab" (https://www.architettura.unicampania.it/images/ricerca/laboratori/EN/SENS-i_Lab_2025_EN.pdf) of UNICAMPANIA while serving a 4x4x3.6 m^3 test room. Tests encompass the following fault types: heating/cooling coil valve stuck; humidifier valve stuck; supply/return air fan stuck; positive/negative offset of return air temperature/relative humidity sensor; air filters clogging; outside/return/exhaust air damper stuck. Scenarios with different fault severities and different seasonal/weather/load conditions were experimentally investigated. One method of fault imposition is put in place: tests with static faults maintained at a constant level for the entire day, All AHU key-parameters (on both water- and air-side) are measured.

1. Description of the experimental set-up

This section presents a comprehensive description of the experimental set-up used to perform the experimental tests.

The HVAC system of the SENS i-Lab, located in the Department of Architecture and Industrial Design at the University of Campania Luigi Vanvitelli (Aversa, south of Italy), includes a single-duct dual-fan constant air volume air-handling unit allowing to guarantee thermal/hygrometric comfort inside a 57.6 m^3 test room [1]. The schematic of the HVAC system is shown in Fig. 1, while the main nominal characteristics of the main components of the HVAC unit are reported in Table 1.

Finanziato dall'Unione europea NextGenerationEU | Ministero dell'Università e della Ricerca | Italiadomani PIANO NAZIONALE DI RIPRESA E RESILIENZA

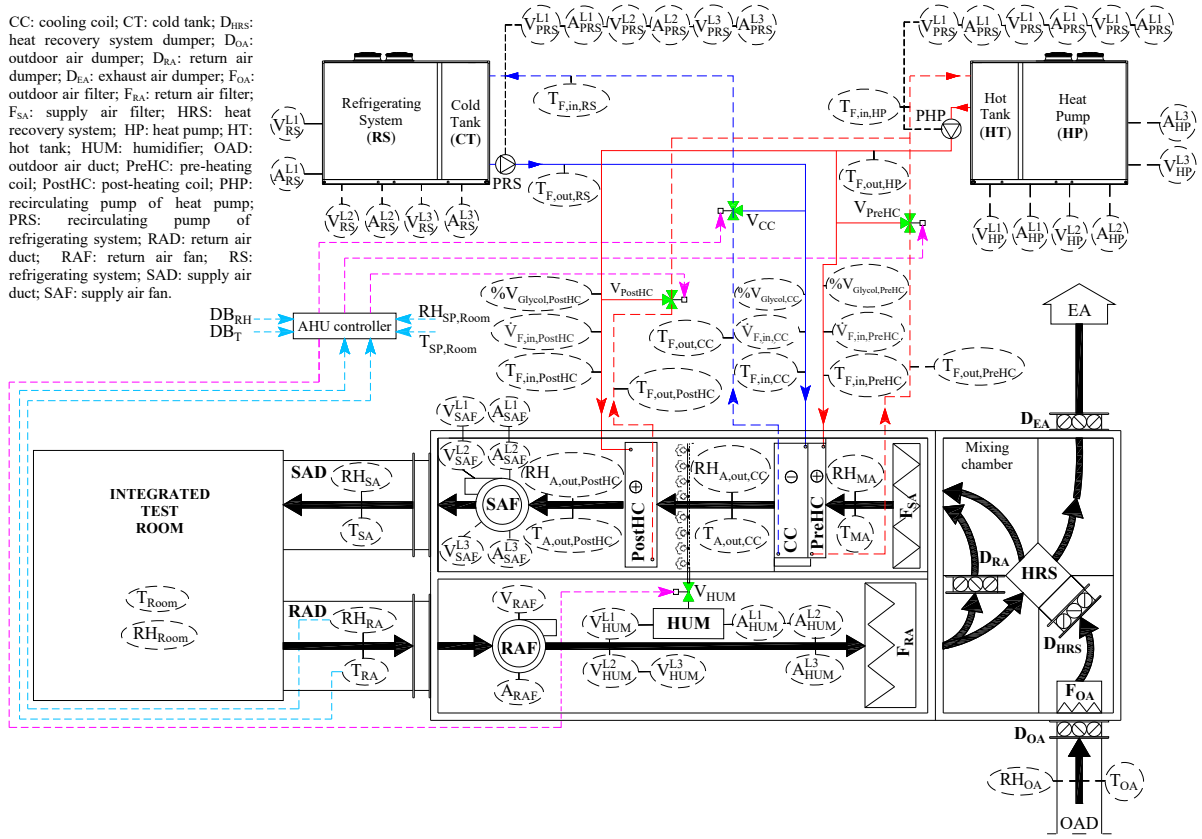

Figure 1. Operating scheme of the HVAC system [1].

Table 1. Nominal main characteristics of the HVAC system main components.

Supply air fan (SAF)	Nominal supply air flow rate (m^3/h)	600
	Nominal power (kW)	2.50
Return air fan (RAF)	Nominal return air flow rate (m^3/h)	600
	Nominal power (kW)	0.50
Cross flow heat recovery system (HRS)	Nominal efficiency (%)	74.7
	Recovery capacity (kW)	3.1
Pre-heating coil (PreHC)	Nominal heating capacity (kW)	4.1
	Nominal heat carrier fluid flow rate (m^3/h)	0.71
	Nominal air flow rate (m^3/h)	600
Cooling coil (CC)	Nominal cooling capacity (kW)	5.0
	Nominal heat carrier fluid flow rate (m^3/h)	0.86
	Nominal air flow rate (m^3/h)	600
Humidifier (HUM) [2]	Nominal steam capacity (kg/h)	5.0
	Nominal power (kW)	3.7
Post-heating coil (PostHC)	Nominal heating capacity (kW)	5.0
	Nominal heat carrier fluid flow rate (m^3/h)	0.86
	Nominal air flow rate (m^3/h)	600
Heat pump (HP) [3]	Nominal heating capacity (kW)	13.8
	Nominal input power (compressor + evaporator fan) (kW)	4.5
Refrigerating system (RS) [3]	Nominal cooling capacity (kW)	13.6
	Nominal input power (compressor + condenser fan) (kW)	4.2

The HVAC system described in Figure 1 is managed through a specific control logic, implemented and executed in the LabVIEW environment [4]. End-users have the ability to manually adjust and set the following parameters:

- set points of indoor air temperature $T_{SP,Room}$ and relative humidity $RH_{SP,Room}$ to be reached in the test room;

Finanziato dall'Unione europea NextGenerationEU
Ministero dell'Università e della Ricerca
Italiadomani PIANO NAZIONALE DI RIPRESA E RESILIENZA

- deadbands associated with $T_{SP,Room}$ and $RH_{SP,Room}$, that are named DB_T and DB_{RH}, respectively;
- return air fan and the supply air fan speed (i.e., OL_{RAF} and OL_{SAF}, respectively) in the range between 0% and 100% (those parameters are kept constant throughout all the tests considered in this study);
- opening percentages of the return air damper (OP_{DRA}), the outside air damper (OP_{DOA}) and the exhaust air damper (OP_{DEA}) in the range between 0% and 100%, where 0% indicates that the damper is completely closed (those parameters are kept constant throughout all the tests considered in this work);
- activation/deactivation of the heat-recovery system that is determined by adjusting the opening percentage (between 0% and 100%) of the heat-recovery system damper OP_{DHRS} (heat recovery system is inactive throughout all the tests considered in this research).

As the parameters mentioned above are defined, the operation mode of the HVAC system components (post-heating coil, cooling coil, humidifier, heat pump, and refrigerating system) is determined, regardless to the season, according to the control logics reported in Table 2 (the control logic of the pre-heating coil is omitted from the table as it is deliberately set to the off-mode during all the tests carried out in this study; thus, the demand for heating was only met by the operation of the post-heating coil).

Table 2. Conditions for activating/deactivating the AHU components.

	ON	OFF
Humidifier (HUM)	$RH_{RA} \leq (RH_{SP,Room} - DB_{RH})$	$RH_{RA} \geq (RH_{SP,Room} + DB_{RH})$
Cooling coil (CC)	$T_{RA} \geq (T_{SP,Room} + DB_T)$ OR $RH_{RA} \geq (RH_{SP,Room} + DB_{RH})$	$T_{RA} \leq (T_{SP,Room} - DB_T)$ AND $RH_{RA} \leq (RH_{SP,Room} - DB_{RH})$
Post-heating coil (PostHC)	$T_{RA} \leq (T_{SP,Room} - DB_T)$	$T_{RA} \geq (T_{SP,Room} + DB_T)$
Heat Pump (HP)	$T_{HT} < (T_{HT,set-point} - DB_{T,HT})$	$T_{HT} \geq (T_{HT,set-point} + DB_{T,HT})$
Refrigerating System (RS)	$T_{CT} > (T_{CT,set-point} + DB_{T,CT})$	$T_{CT} \leq (T_{CT,set-point} - DB_{T,CT})$

In particular, the Heat Pump (HP) is activated only when the temperature of the heat transfer fluid (T_{HT}) inside the hot tank (HT) is lower than the desired set-point temperature ($T_{HT,set-point}$) decreased by a specified deadband temperature ($DB_{T,HT}$); then it remains activated until the temperature of the heat transfer fluid becomes equal to $T_{HT,set-point} + DB_{T,HT}$. The heat transfer fluid is circulated by the pump PHP, which connects the HT and the PostHC/PreHC coils (only when one of the PostHC or PreHC coil valve is open). Regarding the Refrigerating System (RS), it is activated only when the temperature of the heat transfer fluid inside the cold tank (CT) exceeds the desired set-point temperature ($T_{CT,set-point}$) increased by the specified deadband temperature ($DB_{T,CT}$); then, it remains activated until the heat transfer fluid temperature becomes equal to $T_{CT,set-point} - DB_{T,CT}$. The pump PRS circulates the fluid between the CT and the cooling coil (CC) only when the CC valve is open. The heat transfer fluid is a mixture of water and ethylene glycol (about 6% by volume). PID (proportional-integral-derivative) controllers autonomously adjust the valve opening percentages for the post-heating coil (OP_{V_PostHC}), cooling coil (OP_{V_CC}), and humidifier (OP_{V_HUM}). These adjustments ensure that the return air temperature (T_{RA}) remains within the specified upper bound UDB_T ($UDB_T = T_{SP,Room} + DB_T$) and the lower bound LDB_T ($LDB_T = T_{SP,Room} - DB_T$) of the deadband of the return air temperature set-point ($T_{SP,Room}$), while the actual return air relative humidity (RH_{RA}) stays within the upper bound UDB_{RH} ($UDB_{RH} = RH_{SP,Room} + DB_{RH}$) and the lower bound LDB_{RH} ($LDB_{RH} = RH_{SP,Room} - DB_{RH}$) of the deadband of the return air relative humidity set-point ($RH_{SP,Room}$).

However, the user can override the control signals in order to customize the system operation and, therefore, artificially introduce specific faults (and corresponding intensities) related to specific components of the experimental set-up.

1.1. Sensors and measurement uncertainty

The HVAC system is fully equipped with a range of sensors that monitor, measure, record, and control crucial operating parameters that are acquired using a management system developed in the LabVIEW environment [4]. Table 3 reports both the measuring range and the accuracy of each sensor. It is important to note that all AHU's electrical components operate on three-phase power, except the return air fan (RAF) requiring single-phase power.

Table 3. Main characteristics of the sensors.

Measured parameter	Measuring range	Accuracy

Finanziato dall'Unione europea NextGenerationEU | Ministero dell'Università e della Ricerca | Italiadomani PIANO NAZIONALE DI RIPRESA E RESILIENZA

Temperature of return air T_{RA} [5], supply air T_{SA} [5], mixed air T_{MA} [5], air at cooling coil outlet $T_{A,out,CC}$ [5], and at post-heating coil outlet $T_{A,out,PostHC}$ [5]	0÷50 °C	0.8 °C (between 15 °C and 35 °C), ±1 °C (between 0 °C and 50 °C),
Temperature of outside air T_{OA} [6]	–40÷60 °C	±0.2 °C at T_{OA} = 20 °C, ±(–0.008333·T_{OA} + 0.366667) °C when T_{OA} < 20 °C, ±(0.00875·T_{OA} – 0.025) °C when T_{OA} > 20 °C
Air temperature inside the integrated test room T_{Room} [7]	–10÷60 °C	±0.5 °C at 25 °C + 0.03 °C/°C
Heat carrier fluid temperature at heat pump outlet $T_{F,out,HP}$ [8], heat pump inlet $T_{F,in,HP}$ [8], refrigerating system outlet $T_{F,out,RS}$ [8], and refrigerating system inlet $T_{F,in,RS}$ [8]	–10÷60 °C	±(0.03 + 0.0005·T_F) °C
Heat carrier fluid temperature at pre-heating coil outlet $T_{F,out,PreHC}$ [9], pre-heating coil inlet $T_{F,in,PreHC}$ [9], post-heating coil outlet $T_{F,out,PostHC}$ [9], post-heating coil inlet $T_{F,in,PostHC}$ [9], cooling coil outlet $T_{F,out,CC}$ [9], and cooling coil inlet $T_{F,in,CC}$ [9]	–10÷120 °C	±0.6 °C at 60 °C
Relative humidity of return air RH_{RA} [5], supply air RH_{SA} [5], mixed air RH_{MA} [5], air at cooling coil outlet $RH_{A,out,CC}$ [5], and air at post-heating coil outlet $RH_{A,out,PostHC}$ [5]	0÷100%	±3% (between 30% and 70%), ±5% (between 0% and 100%)
Relative humidity of outside air RH_{OA} [6]	0÷100%	± (2.3+0.008 of reading) %
Air relative humidity inside the integrated test room RH_{Room} [7]	0÷95%	±3% at 25 °C + 0.2 %/°C
Volumetric flow rate of heat carrier fluid flowing in pre-heating coil $\dot{V}_{F,in,PreHC}$ [9], cooling coil $\dot{V}_{F,in,CC}$ [9], and post-heating coil $\dot{V}_{F,in,PostHC}$ [9]	0.70÷2.34 m³/h	±2% at 20 °C with %V_{glycol} = 0 %
Heat pump single phase L1 voltage V_{HP}^{L1} [10], single phase L2 voltage V_{HP}^{L2} [10], and single phase L3 voltage V_{HP}^{L3} [10] Heat pump circulating pump single phase L1 voltage V_{PHP}^{L1} [10], single phase L2 voltage V_{PHP}^{L2} [10], and single phase L3 voltage V_{PHP}^{L3} [10] Refrigerating system circulating pump single phase L1 voltage V_{PRS}^{L1} [10], single phase L2 voltage V_{PRS}^{L2} [10], and single phase L3 voltage V_{PRS}^{L3} [10] Refrigerating system single phase L1 voltage V_{RS}^{L1} [10], single phase L2 voltage V_{RS}^{L2} [10], and single phase L3 voltage V_{RS}^{L3} [10] Supply air fan single phase L1 voltage V_{SAF}^{L1} [10], single phase L2 voltage V_{SAF}^{L2} [10], and single phase L3 voltage V_{SAF}^{L3} [10] Humidifier single phase L1 voltage V_{HUM}^{L1} [10], single phase L2 voltage V_{HUM}^{L2} [10], and single phase L3 voltage V_{HUM}^{L3} [10]	0÷425 V	±0.50% of full scale
Return air fan voltage V_{RAF} [10]	0÷280 V	±0.50% of full scale
Supply air fan single phase L1 current A_{SAF}^{L1} [10], single phase L2 current A_{SAF}^{L2} [10], and single phase L3 current A_{SAF}^{L3} [10]	0÷12.5 A	±0.50% of full scale

Finanziato dall'Unione europea NextGenerationEU
Ministero dell'Università e della Ricerca
Italiadomani PIANO NAZIONALE DI RIPRESA E RESILIENZA

Humidifier single phase L1 current A_{HUM}^{L1} [10], single phase L2 current A_{HUM}^{L2} [10], and single phase L3 current A_{HUM}^{L3} [10]		
Heat pump single phase L1 current A_{HP}^{L1} [10], single phase L2 current A_{HP}^{L2} [10], and single phase L3 current A_{HP}^{L3} [10]		
Heat pump circulating pump single phase L1 current A_{PHP}^{L1} [10], single phase L2 current A_{PHP}^{L2} [10], single phase L3 current A_{PHP}^{L3} [10]		
Refrigerating system circulating pump single phase L1 current A_{PRS}^{L1} [10], single phase L2 current A_{PRS}^{L2} [10], and single phase L3 current A_{PRS}^{L3} [10]	0÷50 A	±0.50% of full scale
Refrigerating system single phase L1 current A_{RS}^{L1} [10], single phase L2 current A_{RS}^{L2} [10], and single phase L3 current A_{RS}^{L3} [10]		
Return air fan current A_{RAF} [10]	0÷2.5 A	±0.50% of full scale

Electric power consumption of the supply air fan (EP_{SAF}), the return air fan (EP_{RAF}), the heat pump (EP_{HP}), the heat pump circulating pump (EP_{PHP}), the refrigerating system (EP_{RS}), the refrigerating system circulating pump (EP_{PRS}), as well as the humidifier (EP_{HUM}) are calculated through the following equations according to the measured values of voltage and current intensity:

$$EP_{SAF} = \frac{\left(V_{SAF}^{L1} \cdot A_{SAF}^{L1} + V_{SAF}^{L2} \cdot A_{SAF}^{L2} + V_{SAF}^{L3} \cdot A_{SAF}^{L3}\right) \cdot \cos\varphi_{SAF}}{\sqrt{3}} \quad (1)$$

$$EP_{RAF} = V_{RAF} \cdot A_{RAF} \cdot \cos\varphi_{RAF} \quad (2)$$

$$EP_{HP} = \left(V_{HP}^{L1} \cdot A_{HP}^{L1} + V_{HP}^{L2} \cdot A_{HP}^{L2} + V_{HP}^{L3} \cdot A_{HP}^{L3}\right) \cdot \cos\varphi_{HP} \quad (3)$$

$$EP_{PHP} = \left(V_{PHP}^{L1} \cdot A_{PHP}^{L1} + V_{PHP}^{L2} \cdot A_{PHP}^{L2} + V_{PHP}^{L3} \cdot A_{PHP}^{L3}\right) \cdot \cos\varphi_{PHP} \quad (4)$$

$$EP_{RS} = \left(V_{RS}^{L1} \cdot A_{RS}^{L1} + V_{RS}^{L2} \cdot A_{RS}^{L2} + V_{RS}^{L3} \cdot A_{RS}^{L3}\right) \cdot \cos\varphi_{RS} \quad (5)$$

$$EP_{PRS} = \left(V_{PRS}^{L1} \cdot A_{PRS}^{L1} + V_{PRS}^{L2} \cdot AP_{RS}^{L2} + V_{PRS}^{L3} \cdot A_{PRS}^{L3}\right) \cdot \cos\varphi_{PRS} \quad (6)$$

$$EP_{HUM} = \frac{\left(V_{HUM}^{L1} \cdot A_{HUM}^{L1} + V_{HUM}^{L2} \cdot A_{HUM}^{L2} + V_{HUM}^{L3} \cdot A_{HUM}^{L3}\right) \cdot \cos\varphi_{HUM}}{\sqrt{3}} \quad (7)$$

where $\cos\varphi_{SAF}$, $\cos\varphi_{RAF}$, $\cos\varphi_{HP}$, $\cos\varphi_{PHP}$, $\cos\varphi_{RS}$, $\cos\varphi_{PRS}$ and $\cos\varphi_{HUM}$ are the power factors of the SAF, the RAF, the HP, the PHP, the RS, the PRS and the HUM, respectively. The following values recommended by the manufacturers have been presumed for the power factors: $\cos\varphi_{SAF} = 0.95$, $\cos\varphi_{RAF} = 0.95$, $\cos\varphi_{HP} = 0.95$, $\cos\varphi_{PHP} = 0.95$, $\cos\varphi_{RS} = 0.95$, $\cos\varphi_{PRS} = 0.95$, and $\cos\varphi_{HUM} = 0.95$.

The absolute measurement errors $\delta(EP_{SAF})$, $\delta(EP_{RAF})$, $\delta(EP_{HP})$, $\delta(EP_{PHP})$, $\delta(EP_{RS})$, $\delta(EP_{PRS})$ and $\delta(EP_{HUM})$ related to the assessment of the electric power consumption of the supply air fan (Eq. 1), the return air fan (Eq. 2), the heat pump (Eq. 3), the circulating pump connected to the heat pump (Eq. 4), the refrigerating system (Eq. 5), the circulating pump connected to the refrigerating system (Eq. 6), and also the humidifier (Eq. 7), respectively, are calculated based on the single-sample uncertainty analysis [11] by using below equations:

Finanziato dall'Unione europea NextGenerationEU | Ministero dell'Università e della Ricerca | Italiadomani PIANO NAZIONALE DI RIPRESA E RESILIENZA

$$\delta(EP_{SAF}) = \left(\frac{\cos\varphi_{SAF}}{\sqrt{3}}\right) \cdot \sqrt{\begin{matrix}\left[A_{SAF}^{L1} \cdot \delta\left(V_{SAF}^{L1}\right)\right]^2 + \left[V_{SAF}^{L1} \cdot \delta\left(A_{SAF}^{L1}\right)\right]^2 + \left[A_{SAF}^{L2} \cdot \delta\left(V_{SAF}^{L2}\right)\right]^2 + \\ \left[V_{SAF}^{L2} \cdot \delta\left(A_{SAF}^{L2}\right)\right]^2 + \left[A_{SAF}^{L3} \cdot \delta\left(V_{SAF}^{L3}\right)\right]^2 + \left[V_{SAF}^{L2} \cdot \delta\left(A_{SAF}^{L3}\right)\right]^2\end{matrix}} \quad (8)$$

$$\delta(EP_{RAF}) = \left(\cos\varphi_{RAF}\right) \cdot \sqrt{\left[A_{RAF} \cdot \delta\left(V_{RAF}\right)\right]^2 + \left[V_{RAF} \cdot \delta\left(A_{RAF}\right)\right]^2} \quad (9)$$

$$\delta(EP_{HP}) = \left(\cos\varphi_{HP}\right) \cdot \sqrt{\begin{matrix}\left[A_{HP}^{L1} \cdot \delta\left(V_{HP}^{L1}\right)\right]^2 + \left[V_{HP}^{L1} \cdot \delta\left(A_{HP}^{L1}\right)\right]^2 + \left[A_{HP}^{L2} \cdot \delta\left(V_{HP}^{L2}\right)\right]^2 + \\ \left[V_{HP}^{L2} \cdot \delta\left(A_{HP}^{L2}\right)\right]^2 + \left[A_{HP}^{L3} \cdot \delta\left(V_{HP}^{L3}\right)\right]^2 + \left[V_{HP}^{L2} \cdot \delta\left(A_{HP}^{L3}\right)\right]^2\end{matrix}} \quad (10)$$

$$\delta(EP_{PHP}) = \left(\cos\varphi_{PHP}\right) \cdot \sqrt{\begin{matrix}\left[A_{PHP}^{L1} \cdot \delta\left(V_{PHP}^{L1}\right)\right]^2 + \left[V_{PHP}^{L1} \cdot \delta\left(A_{PHP}^{L1}\right)\right]^2 + \left[A_{PHP}^{L2} \cdot \delta\left(V_{PHP}^{L2}\right)\right]^2 + \\ \left[V_{PHP}^{L2} \cdot \delta\left(A_{PHP}^{L2}\right)\right]^2 + \left[A_{PHP}^{L3} \cdot \delta\left(V_{PHP}^{L3}\right)\right]^2 + \left[V_{PHP}^{L2} \cdot \delta\left(A_{PHP}^{L3}\right)\right]^2\end{matrix}} \quad (11)$$

$$\delta(EP_{RS}) = \left(\cos\varphi_{RS}\right) \cdot \sqrt{\begin{matrix}\left[A_{RS}^{L1} \cdot \delta\left(V_{RS}^{L1}\right)\right]^2 + \left[V_{RS}^{L1} \cdot \delta\left(A_{RS}^{L1}\right)\right]^2 + \left[A_{RS}^{L2} \cdot \delta\left(V_{RS}^{L2}\right)\right]^2 + \\ \left[V_{RS}^{L2} \cdot \delta\left(A_{RS}^{L2}\right)\right]^2 + \left[A_{RS}^{L3} \cdot \delta\left(V_{RS}^{L3}\right)\right]^2 + \left[V_{RS}^{L2} \cdot \delta\left(A_{RS}^{L3}\right)\right]^2\end{matrix}} \quad (12)$$

$$\delta(EP_{PRS}) = \left(\cos\varphi_{PRS}\right) \cdot \sqrt{\begin{matrix}\left[A_{PRS}^{L1} \cdot \delta\left(V_{PRS}^{L1}\right)\right]^2 + \left[V_{PRS}^{L1} \cdot \delta\left(A_{PRS}^{L1}\right)\right]^2 + \left[A_{PRS}^{L2} \cdot \delta\left(V_{PRS}^{L2}\right)\right]^2 + \\ \left[V_{PRS}^{L2} \cdot \delta\left(A_{PRS}^{L2}\right)\right]^2 + \left[A_{PRS}^{L3} \cdot \delta\left(V_{PRS}^{L3}\right)\right]^2 + \left[V_{PRS}^{L2} \cdot \delta\left(A_{PRS}^{L3}\right)\right]^2\end{matrix}} \quad (13)$$

$$\delta(EP_{HUM}) = \left(\frac{\cos\varphi_{HUM}}{\sqrt{3}}\right) \cdot \sqrt{\begin{matrix}\left[A_{HUM}^{L1} \cdot \delta\left(V_{HUM}^{L1}\right)\right]^2 + \left[V_{HUM}^{L1} \cdot \delta\left(A_{HUM}^{L1}\right)\right]^2 + \left[A_{HUM}^{L2} \cdot \delta\left(V_{HUM}^{L2}\right)\right]^2 + \\ \left[V_{HUM}^{L2} \cdot \delta\left(A_{HUM}^{L2}\right)\right]^2 + \left[A_{HUM}^{L3} \cdot \delta\left(V_{HUM}^{L3}\right)\right]^2 + \left[V_{HUM}^{L2} \cdot \delta\left(A_{HUM}^{L3}\right)\right]^2\end{matrix}} \quad (14)$$

where in $\delta(X)$ the above formulas denote the uncertainty of variable X, as listed in Table 3, related to the measured current and voltage values of the SAF, the RAF, the HP, the PHP, the RS, the PRS and the HUM.

2. Design of experiments

The AHU serving the test room of the SENS i-Lab has been operated under faulty and fault-free conditions. In particular, 113 experiments have been performed. The following subsections detail the faulty and fault-free conditions experimental tests that have been (subsection 2.1) and a brief description of the experimental dataset (subsection 2.2).

In the following, the tests are indicated by a specific ID including:

1) a first letter S or W to indicate weather it is a summer (S) or winter (W) test, respectively;
2) a second letter N or F to indicate whether it is a normal test (N) or a faulty test (F), respectively;
3) a number that in the case of faulty tests indicates both a specific type of fault and a specific level of severity; in the case of normal tests, the number simply indicates the time history.

In particular, the following 30 fault types/severities have been investigated during both summer and winter (related numbers are used in the IDs of the faulty tests):

- fault 1: post-heating coil valve stuck fully closed (stuck at 0%);
- fault 2: post-heating coil valve stuck fully open (stuck at 100%);
- fault 3: cooling coil valve stuck fully closed (stuck at 0%);
- fault 4: cooling coil valve stuck fully open (stuck at 100%);
- fault 5: humidifier valve stuck fully closed (stuck at 0%);
- fault 6: positive offset equal to +3.0 °C purposely added on the return air temperature sensor;
- fault 7: negative offset equal to −3.0 °C purposely subtracted from the values measured by return air temperature sensor;
- fault 8: positive offset of the return air relative humidity sensor kept equal to +15 %;
- fault 9: negative offset equal to −15% purposely subtracted from the values measured by the return air relative humidity sensor;
- fault 10: complete failure of the return air fan (stuck at 0%);

Finanziato dall'Unione europea NextGenerationEU | Ministero dell'Università e della Ricerca | Italiadomani PIANO NAZIONALE DI RIPRESA E RESILIENZA

- fault 11: complete failure of the supply air fan (stuck at 0%);
- fault 12: return air damper kept always closed (stuck at 0%);
- fault 13: fresh air damper kept always closed (stuck at 0%);
- fault 14: fresh air damper kept always open (stuck at 100%);
- fault 15: exhaust air damper kept always closed (stuck at 0%);
- fault 16: fresh air filter partially clogged at 50%;
- fault 17: supply air filter partially clogged at 50%;
- fault 18: return air filter partially clogged at 50%;
- fault 19: cooling coil valve stuck at 25%;
- fault 20: cooling coil valve stuck at 50%;
- fault 21: cooling coil valve stuck at 75%;
- fault 22: post-heating coil valve stuck at 25%;
- fault 23: post-heating coil valve stuck at 50%;
- fault 24: post-heating coil valve stuck at 75%
- fault 25: supply air fan stuck at 25%;
- fault 26: supply air fan stuck at 75%;
- fault 27: supply air fan stuck at 100%;
- fault 28: return air fan stuck at 25%;
- fault 29: return air fan stuck at 75%;
- fault 30: return air fan stuck at 100%.

2.1 Description of faulty and normal experiments performed

Tables 4 and 5 summarize the operating conditions for the normal (N) summer (S) tests and the normal (N) winter (W) tests, respectively, conducted.

Table 4. Operating conditions of the normal experiments conducted during summer.

ID	$T_{SP,Room}$ (°C)	$RH_{SP,Room}$ (%)	OL_{SAF} (%)	OL_{RAF} (%)	OP_{V_PostHC} (%)	OP_{V_CC} (%)	OP_{V_HUM} (%)	OP_{DRA} (%)	OP_{DOA} (%)	OP_{DEA} (%)
SN1	26	50	50	50	0÷100	0÷100	0÷100	100	20	20
SN2										
SN3										
SN4										
SN5										
SN6										
SN7										
SN8										
SN9										
SN10										
SN11										
SN12										
SN13										
SN14										
SN15										
SN16										
SN17										
SN18										

Table 5. Operating conditions of the normal experiments performed during winter.

ID	$T_{SP,Room}$ (°C)	$RH_{SP,Room}$ (%)	OL_{SAF} (%)	OL_{RAF} (%)	OP_{V_PostHC} (%)	OP_{V_CC} (%)	OP_{V_HUM} (%)	OP_{DRA} (%)	OP_{DOA} (%)	OP_{DEA} (%)
WN1	20	50	50	50	0÷100	0÷100	0÷100	100	20	20
WN2										
WN3										
WN4										
WN5										
WN6										
WN7										
WN8										
WN9										
WN10										

Finanziato dall'Unione europea NextGenerationEU | Ministero dell'Università e della Ricerca | Italiadomani PIANO NAZIONALE DI RIPRESA E RESILIENZA

WN11										
WN12										
WN13										
WN14										
WN15										
WN16										

Table 6 presents the operating conditions of the faulty (F) experiments conducted during summer. Similarly, Table 7 provides the operating conditions of the faulty tests performed during winter. In Tables 6 and 7, the highlighted cells indicate the settings that were artificially imposed to simulate system component malfunctions.

It should be noted that during each faulty test, a single fault type or severity was investigated.

Table 6. Operating conditions of the faulty tests SF1÷SF30 carried out during summer.

ID	$T_{SP,Room}$ (°C)	$RH_{SP,Room}$ (%)	Offset of T_{RA} sensor (°C)	Offset of RH_{RA} sensor (%)	OL_{SAF} (%)	OL_{RAF} (%)	OP_{V_PostHC} (%)	OP_{V_CC} (%)	OP_{V_HUM} (%)	OP_{DRA} (%)	OP_{DOA} (%)	OP_{DEA} (%)	OP_{FOA} (%)	OP_{FSA} (%)	OP_{FRA} (%)
SF1	26	50	0	0	50	50	0	0÷100	0÷100	100	20	20	100	100	100
SF2	26	50	0	0	50	50	100	0÷100	0÷100	100	20	20	100	100	100
SF3	26	50	0	0	50	50	0÷100	0	0÷100	100	20	20	100	100	100
SF4	26	50	0	0	50	50	0÷100	100	0÷100	100	20	20	100	100	100
SF5	26	50	0	0	50	50	0÷100	0÷100	0	100	20	20	100	100	100
SF6	26	50	+3	0	50	50	0÷100	0÷100	0÷100	100	20	20	100	100	100
SF7	26	50	−3	0	50	50	0÷100	0÷100	0÷100	100	20	20	100	100	100
SF8	26	50	0	+15	50	50	0÷100	0÷100	0÷100	100	20	20	100	100	100
SF9	26	50	0	−15	50	50	0÷100	0÷100	0÷100	100	20	20	100	100	100
SF10	26	50	0	0	50	0	0÷100	0÷100	0÷100	100	20	20	100	100	100
SF11	26	50	0	0	0	50	0÷100	0÷100	0÷100	100	20	20	100	100	100
SF12	26	50	0	0	50	50	0÷100	0÷100	0÷100	0	20	20	100	100	100
SF13	26	50	0	0	50	50	0÷100	0÷100	0÷100	100	0	20	100	100	100
SF14	26	50	0	0	50	50	0÷100	0÷100	0÷100	100	100	20	100	100	100
SF15	26	50	0	0	50	50	0÷100	0÷100	0÷100	100	20	0	100	100	100
SF16	26	50	0	0	50	50	0÷100	0÷100	0÷100	100	20	20	50	100	100
SF17	26	50	0	0	50	50	0÷100	0÷100	0÷100	100	20	20	100	50	100
SF18	26	50	0	0	50	50	0÷100	0÷100	0÷100	100	20	20	100	100	50
SF19	26	50	0	0	50	50	0÷100	25	0÷100	100	20	20	100	100	100
SF20	26	50	0	0	50	50	0÷100	50	0÷100	100	20	20	100	100	100
SF21	26	50	0	0	50	50	0÷100	75	0÷100	100	20	20	100	100	100
SF22	26	50	0	0	50	50	25	0÷100	0÷100	100	20	20	100	100	100
SF23	26	50	0	0	50	50	50	0÷100	0÷100	100	20	20	100	100	100
SF24	26	50	0	0	50	50	75	0÷100	0÷100	100	20	20	100	100	100
SF25	26	50	0	0	25	50	0÷100	0÷100	0÷100	100	20	20	100	100	100
SF26	26	50	0	0	75	50	0÷100	0÷100	0÷100	100	20	20	100	100	100
SF27	26	50	0	0	100	50	0÷100	0÷100	0÷100	100	20	20	100	100	100
SF28	26	50	0	0	50	25	0÷100	0÷100	0÷100	100	20	20	100	100	100
SF29	26	50	0	0	50	75	0÷100	0÷100	0÷100	100	20	20	100	100	100
SF30	26	50	0	0	50	100	0÷100	0÷100	0÷100	100	20	20	100	100	100

Table 7. Operating conditions of the faulty tests WF1÷WF30 carried out during winter.

ID	$T_{SP,Room}$ (°C)	$RH_{SP,Room}$ (%)	Offset of T_{RA} sensor (°C)	Offset of RH_{RA} sensor (%)	OL_{SAF} (%)	OL_{RAF} (%)	OP_{V_PostHC} (%)	OP_{V_CC} (%)	OP_{V_HUM} (%)	OP_{DRA} (%)	OP_{DOA} (%)	OP_{DEA} (%)	OP_{FOA} (%)	OP_{FSA} (%)	OP_{FRA} (%)
WF1	20	50	0	0	50	50	0	0÷100	0÷100	100	20	20	100	100	100
WF2	20	50	0	0	50	50	100	0÷100	0÷100	100	20	20	100	100	100

Finanziato dall'Unione europea NextGenerationEU
Ministero dell'Università e della Ricerca
Italiadomani PIANO NAZIONALE DI RIPRESA E RESILIENZA

WF3	20	50	0	0	50	50	0÷100	0	0÷100	100	20	20	100	100	100
WF4	20	50	0	0	50	50	0÷100	100	0÷100	100	20	20	100	100	100
WF5	20	50	0	0	50	50	0÷100	0÷100	0	100	20	20	100	100	100
WF6	20	50	+3	0	50	50	0÷100	0÷100	0÷100	100	20	20	100	100	100
WF7	20	50	−3	0	50	50	0÷100	0÷100	0÷100	100	20	20	100	100	100
WF8	20	50	0	+15	50	50	0÷100	0÷100	0÷100	100	20	20	100	100	100
WF9	20	50	0	−15	50	50	0÷100	0÷100	0÷100	100	20	20	100	100	100
WF10	20	50	0	0	50	0	0÷100	0÷100	0÷100	100	20	20	100	100	100
WF11	20	50	0	0	0	50	0÷100	0÷100	0÷100	100	20	20	100	100	100
WF12	20	50	0	0	50	50	0÷100	0÷100	0÷100	0	20	20	100	100	100
WF13	20	50	0	0	50	50	0÷100	0÷100	0÷100	100	0	20	100	100	100
WF14	20	50	0	0	50	50	0÷100	0÷100	0÷100	100	100	20	100	100	100
WF15	20	50	0	0	50	50	0÷100	0÷100	0÷100	100	20	0	100	100	100
WF16	20	50	0	0	50	50	0÷100	0÷100	0÷100	100	20	20	50	100	100
WF17	20	50	0	0	50	50	0÷100	0÷100	0÷100	100	20	20	100	50	100
WF18	20	50	0	0	50	50	0÷100	0÷100	0÷100	100	20	20	100	100	50
WF19	20	50	0	0	50	50	0÷100	25	0÷100	100	20	20	100	100	100
WF20	20	50	0	0	50	50	0÷100	50	0÷100	100	20	20	100	100	100
WF21	20	50	0	0	50	50	0÷100	75	0÷100	100	20	20	100	100	100
WF22	20	50	0	0	50	50	25	0÷100	0÷100	100	20	20	100	100	100
WF23	20	50	0	0	50	50	50	0÷100	0÷100	100	20	20	100	100	100
WF24	20	50	0	0	50	50	75	0÷100	0÷100	100	20	20	100	100	100
WF25	20	50	0	0	25	50	0÷100	0÷100	0÷100	100	20	20	100	100	100
WF26	20	50	0	0	75	50	0÷100	0÷100	0÷100	100	20	20	100	100	100
WF27	20	50	0	0	100	50	0÷100	0÷100	0÷100	100	20	20	100	100	100
WF28	20	50	0	0	50	25	0÷100	0÷100	0÷100	100	20	20	100	100	100
WF29	20	50	0	0	50	75	0÷100	0÷100	0÷100	100	20	20	100	100	100
WF30	20	50	0	0	50	100	0÷100	0÷100	0÷100	100	20	20	100	100	100

Table 8 reports the pairs of the tests (normal and faulty) that are comparable.

Table 8. List of comparable pair tests during summer and winter.

Summer	Winter
SF1 is comparable with SN4	WF1 is comparable with WN2
SF2 is comparable with SN5	WF2 is comparable with WN5
SF3 is comparable with SN5	WF3 is comparable with WN1
SF4 is comparable with SN4	WF4 is comparable with WN8
SF5 is comparable with SN2	WF5 is comparable with WN6
SF6 is comparable with SN1	WF6 is comparable with WN5
SF7 is comparable with SN4	WF7 is comparable with WN3
SF8 is comparable with SN2	WF8 is comparable with WN7
SF9 is comparable with SN3	WF9 is comparable with WN4
SF10 is comparable with SN5	WF10 is comparable with WN2
SF11 is comparable with SN6	WF11 is comparable with WN2
SF12 is comparable with SN9	WF12 is comparable with WN5
SF13 is comparable with SN7	WF13 is comparable with WN9
SF14 is comparable with SN11	WF14 is comparable with WN5
SF15 is comparable with SN10	WF15 is comparable with WN11
SF16 is comparable with SN8	WF16 is comparable with WN7
SF17 is comparable with SN11	WF17 is comparable with WN10

Finanziato dall'Unione europea NextGenerationEU | Ministero dell'Università e della Ricerca | Italiadomani PIANO NAZIONALE DI RIPRESA E RESILIENZA

SF18 is comparable with SN12	WF18 is comparable with WN7
SF19 is comparable with SN13	WF19 is comparable with WN12
SF20 is comparable with SN13	WF20 is comparable with WN12
SF21 is comparable with SN13	WF21 is comparable with WN15
SF22 is comparable with SN14	WF22 is comparable with WN13
SF23 is comparable with SN15	WF23 is comparable with WN14
SF24 is comparable with SN14	WF24 is comparable with WN13
SF25 is comparable with SN17	WF25 is comparable with WN12
SF26 is comparable with SN16	WF26 is comparable with WN13
SF27 is comparable with SN17	WF27 is comparable with WN12
SF28 is comparable with SN18	WF28 is comparable with WN15
SF29 is comparable with SN18	WF29 is comparable with WN15
SF30 is comparable with SN18	WF30 is comparable with WN16

2.2 Description of experimental dataset

The experimental dataset consists of 94 files with the .xlsx extension, each test is identified by a specific ID composed of:

1. a first letter, S or W, indicating whether the test refers to summer (S) or winter (W) boundary conditions;
2. a second letter, N or F, indicating whether the test is a normal (N) or faulty (F) condition;
3. a sequential number.

Each file is characterized by 10 columns, which report the experimental set-up measured operational parameters with 1-second timestep:

1. Column 1: Time (hh:mm:ss);
2. Column 2: Return Air Temperature T_{RA} (°C);
3. Column 3: Return Air Relative Humidity RH_{RA} (%);
4. Column 4: Supply Air Fan (SAF) Electric Power (EP) consumption EP_{SAF} (W);
5. Column 5: Return Air Fan (RAF) Electric Power (EP) consumption EP_{RAF} (W);
6. Column 6: Humidifier (HUM) Electric Power (EP) consumption EP_{HUM} (W);
7. Column 7: Refrigerating System (RS) Electric Power (EP) consumption EP_{RS} (W);
8. Column 8: Refrigerating System Recirculation Pump (PRS) Electric Power (EP) consumption EP_{PRS} (W);
9. Column 9: Heat Pump (HP) Electric Power (EP) consumption EP_{HP} (W);
10. Column 10: Heat Pump Recirculation Pump (HP) Electric Power (EP) consumption EP_{PHP} (W).

The experimental dataset named “PRIN22_UTMOST FDD_Deliverable WP1_D2” is available at the following link: https://www.dropbox.com/scl/fo/552f6iiy7f738bcpouln8/ANww0HaXcXHQrkVBaSmxL3k?rlkey=svw2ytl1ucdvg440a216iiopv&dl=0

3. References

[1] SENS i-Lab, Department of Architecture and Industrial Design, University of Campania Luigi Vanvitelli. Available online: https://www.architettura.unicampania.it/images/ricerca/laboratori/EN/SENS-i_Lab_2025_EN.pdf
[2] CAREL, Humidifiers Technical Datasheet. Available online: https://www.carel.com/documents/10191/0/2B030220621/92fca658-a251-49ee-9979-b8829fcba49f?version=1.0
[3] AERMEC, Reversible Air/Water Heat Pump Technical Datasheet. Available online: https://download.aermec.com/docs/schede/ANL-021-203-HP_Y_UN50_03.pdf?r=14395.
[4] National Instruments. LabVIEW (Version 2019 SP1). National Instruments. 2019. Available online: https://www.ni.com/
[5] SIEMENS, Duct Sensors Technical Datasheet. Available online: https://www.downloads.siemens.com/download-center/Download.aspx?pos=download&fct=getasset&id1=24897.
[6] E+E Elektronic, EE210 Outdoor Datasheet. Available online: https://www.epluse.com/fileadmin/data/product/ee210/datasheet_EE210_Outdoor.pdf.
[7] TSI, Q-TRAK Technical Datasheet. Available online: https://tsi.com/getmedia/d2a8d1d1-7551-47fe-8a0f-3c14b09b494b/7575_QTrak_A4_UK_5001356-web?ext=.pdf.
[8] MEASUREIT. Sensors. Available online: https://shop.measureit.eu/sensori.html..
[9] BELIMO, Energy Valve Technical Datasheet. Available online: https://www.belimoseoul.com/data/medium/9d020b80b518dcf144d3cc8db59f777e.pdf.
[10] MEASUREIT Voltage and Current Transducer Datasheet. Available online: https://www.measureit.it/var/import/Attachment/DS_Mit_VI.pdf
[11] Mastrullo, R.; Rosato, A.; Vanoli, G.P.; Thome, J.R. A Methodology to Select the Experimental Plant Instrumentation Based on an a Priori Analysis of Measurement Errors and Instrumentation Cost. Int. J. Heat Mass Transf. 2008, 35, 689–695.

Finanziato dall'Unione europea NextGenerationEU | Ministero dell'Università e della Ricerca | Italiadomani PIANO NAZIONALE DI RIPRESA E RESILIENZA

MISSIONE 4
ISTRUZIONE RICERCA

WP2 - *KPIs identification for assessing fault impact in AHU operation*

Finanziato dall'Unione europea NextGenerationEU
Ministero dell'Università e della Ricerca
Italiadomani
PIANO NAZIONALE DI RIPRESA E RESILIENZA

MISSIONE 4
ISTRUZIONE RICERCA

DELIVERABLE WP2_D1

DEFINITION OF WEIGHTED MULTI-CRITERIA KPI FOR COMPARING DIFFERENT FAULTS ACCORDING TO THEIR IMPACTS

EDIT BY POLITO

PRIN 2022 - UTMOST FDD: AN AUTOMATED, OPEN, SCALABLE AND TRANSPARENT FAULT DETECTION AND DIAGNOSIS PROCESS FOR AIR-HANDLING UNITS BASED ON A HYBRID EXPERT AND ARTIFICIAL INTELLIGENCE APPROACH

Funded by the European Union - Next Generation EU within the "Piano Nazionale di Ripresa e Resilienza (PNRR), missione 4 componente 2 investimento 1.1 - fondo per il programma nazionale di ricerca e progetti di rilevante interesse nazionale (PRIN)"

Finanziato dall'Unione europea NextGenerationEU
Ministero dell'Università e della Ricerca
Italiadomani PIANO NAZIONALE DI RIPRESA E RESILIENZA

The UTMOST FDD Project is organised into the following 7 Work Packages (WPs):
WP0) PROJECT COORDINATION
WP1) EXPERIMENTAL ANALYSIS FOR THE CHARACTERIZATION OF FAULTY AND NORMAL OPERATION OF A TYPICAL AHU
WP2) KPIs IDENTIFICATION FOR ASSESSING FAULT IMPACT IN AHU OPERATION
WP3) AHU DIGITAL TWIN AND SIMULATION-BASED FAULT IMPACT SCENARIO ANALYSIS
WP4) DEFINITION OF HYBRID FDD STRATEGIES FOR AHUs
WP5) TRANSFERABILITY ANALYSIS OF THE FDD STRATEGIES
WP6) KNOWLEDGE TRANSFER AND DISSEMINATION

The WPs are organized into Tasks (T) ranging from 2 to 4 for each WP.

The aim of the WP2 is the definition of KPIs to evaluate fault impacts in terms of energy consumption, energy cost, thermal comfort and indoor air quality. The assessment of fault impact based on these KPIs will be performed starting from the experimental/simulation data collected in the WP1 and WP3.

The WP2 will include the following 3 tasks (WP2_T1, WP2_T2, WP2_T3):

- WP2_T1) this task aims at selecting in the literature the single-criteria KPIs that well fit with the purpose of quantify the impact of specific faulty conditions on AHU operation. The objective is to identify faults with most adverse impacts and to rank them accordingly. The identified single-criteria KPIs will be then employed with reference to the datasets collected in WP1 and WP3.
- WP2_T2) this task aims to formulate new weighted multi-criteria KPIs, considering a trade-off between energy consumption, GHG emissions, cost, thermal comfort and ventilation impacts. The objective is to identify faults with most adverse impacts and to rank them accordingly. The identified weighted multi-criteria KPIs will be then employed with reference to the datasets collected in the WP1 and WP3. In the context of the WP2_T2, a written report (1st WP2 deliverable WP2_D1), including a detailed categorization of relevant scientific studies on fault impact assessment and the identified single- and multi-criteria KPIs, will be delivered.
- WP2_T3) this task will perform an impact analysis by comparing the results of faulty experiments with those of fault free tests carried out under the same boundary conditions during the WP1 based on the single- and multi-criteria KPIs identified in the WP2_T1 and WP2_T2. This will make it possible to rank faults according to their impact under different operating conditions based on a fault scenario analysis, as well as evaluate a maintenance action prioritization scheme considering how the impact of a fault changes during system operation. A scientific written report illustrating the symptoms on the AHU performance associated to the faults' occurrence will be provided as 2nd WP2 deliverable WP2_D2.

1. Introduction

In real building operations, HVAC systems are often exposed to a wide range of faults. These can occur at the level of individual components—such as HVAC equipment, sensors, or actuators—or affect the entire system, including control strategies, design, and operation **[1]**. Such faults can significantly reduce the overall performance of the building and may even cancel out the energy savings expected from using high-performance control sequences.

The impact of faults can vary widely, depending on the type, location, and duration of the issue. Some faults may lead to increased energy consumption, while others can affect indoor comfort, equipment lifespan, or system reliability. Understanding how different types of faults affect building performance is essential. This knowledge allows building operators and designers to evaluate the consequences of each fault and prioritize actions based on their impact, helping to set an effective hierarchy of responses according to specific goals, such as energy efficiency, occupant comfort, or maintenance costs [2].

For these reasons, being able to quantify the relative impact of different faults across multiple criteria - using well-defined and meaningful Key Performance Indicators (KPIs) - is fundamental.

2. Literature review on multiple KPIs for the quantification of fault impact during AHU operation

As highlighted in the literature, the application of Fault Detection and Diagnosis (FDD) techniques to Air Handling Units (AHUs) requires the definition of dedicated KPIs. These KPIs enable a quantitative evaluation of the system's operational performance by measuring the specific impact of individual faults. In doing so, they support more informed maintenance decisions and contribute to improving the overall efficiency and reliability of AHU operations.

Several studies in the literature have focused on evaluating and ranking the impact of HVAC system faults through different methodological approaches. Kim et al. [3] analyzed and prioritized common faults in HVAC systems by applying proprietary methods designed to estimate their effects from both energy consumption and financial cost perspectives. Li et al. [4] developed a comprehensive fault impact analysis framework based on large-scale simulations using EnergyPlus. Their methodology employed parametric sensitivity analysis to assess the criticality of faults and

Finanziato dall'Unione europea NextGenerationEU | Ministero dell'Università e della Ricerca | Italiadomani PIANO NAZIONALE DI RIPRESA E RESILIENZA

establish a ranking. In total, 129 different fault modes were simulated in a medium-sized office building model. These included a wide variety of faults, such as physical malfunctions in HVAC equipment and sensors, as well as operational issues like scheduling errors. Building on a similar simulation-based approach, Lu et al. [5] conducted an in-depth investigation into the impact of sensor errors in a demand-controlled ventilation HVAC system. Their study focused on identifying which sensors had the most significant influence on system performance, ultimately producing a ranked list of sensor importance.

From the literature, there are various single-criteria KPIs, and the most used ones are:

- Total site energy: $E_{tot} = E_{el} + E_{gas}$;
- Total operation cost: $C_{tot} = C_{el} + C_{gas}$;
- Total source energy: $E_{source,tot} = f_{el} \cdot E_{el} + f_{gas} \cdot E_{gas}$ (f_{el}, f_{gas} site-to-source ratios);
- Total GHG emissions: $e_{GHG} = f_{\frac{kgCO2}{kWh_{el}}} \cdot E_{el} + f_{\frac{kgCO2}{kWh_{gas}}} \cdot E_{gas}$ ($f_{\frac{kgCO2}{kWh_{el}}}$, $f_{\frac{kgCO2}{kWh_{gas}}}$ emission factors);
- Maximum zone air temperature deviation: $dT_{max} = \sum_i \max(s_i(t))$ (s deviation from the lower and upper temperature setpoint; i zone index for the set of zones);
- Total zone air temperature deviation: $dT_{tot} = \sum_i \sum_{t=0}^{n} s_i(t)$;
- Maximum zone air relative humidity deviation: $dRH_{max} = \sum_i \max(r_i(t))$ (r deviation from the lower and upper relative humidity setpoint; i zone index for the set of zones);
- Total zone air relative humidity deviation: $dRH_{tot} = \sum_i \sum_{t=0}^{n} r_i(t)$;
- Outdoor Air Ratio: $OAR(t_j) = \frac{V_{OA,actual}(t_j)}{V_{OA,required}(t_j)}$ (V_{OA} outdoor air flow rate);
- Power peak: $P_{max} = \max(P_{el}(t))$;

Since the previously described indicators have different units of measurement, to enable a meaningful comparison of the impact of each fault, the Fault Impact Ratio (FIR) is introduced. FIR represents how the performance has changed due to the fault in respect to the performance that is normally expected. The FIR is larger than zero for the negative impact while it is smaller than zero for the positive impact.

$$FIR = sgn(KPI) \cdot \frac{KPI_{faulted} - KPI_{unfaulted}}{KPI_{unfaulted}} \quad (1)$$

Where:

- FIR is defined for all equations except for Outdoor Air Ratio;
- $sgn(KPI)$ is always equal to +1 considering the KPIs defined before. In other cases, it could be -1.

3. Definition of weighted multi-criteria KPIs for comparing different faults according to their impact

After highlighting the importance of single-criterion KPIs and introducing the FIR as a normalization method to compare the fault effects on different KPIs, it becomes essential to expand the analysis toward a multi-criteria perspective. While single-criterion KPIs (e.g., energy consumption or thermal comfort alone) provide valuable insights into specific aspects of building performance, they may fall short in capturing the broader impact that faults can have across multiple dimensions. To address this limitation, multi-criteria KPIs are introduced. These indicators are specifically designed to evaluate fault impacts from various perspectives simultaneously, such as energy consumption, energy cost, greenhouse gas (GHG) emissions, thermal comfort, indoor air quality (IAQ), and power system reliability. Considering these diverse criteria allows for a more comprehensive and balanced assessment of how faults affect building operation and occupant well-being.

A well-established method for managing and analyzing such multi-dimensional data is the use of Multi-Criteria Decision Analysis (MCDA) techniques. MCDA provides a structured framework to compare and rank the impacts of different faults by accounting for the relative importance of each criterion. In this process, decision-makers can assign weights to each performance indicator based on their priorities—whether focused on sustainability, cost reduction, occupant comfort, or grid stability—and then evaluate how each fault performs across the selected criteria.

This approach enables a more informed and nuanced decision-making process, especially in complex environments where trade-offs between competing objectives are common. The integration of MCDA with normalized fault impact data (via FIR) ensures that comparisons are not only comprehensive but also equitable, regardless of the units or scales of the original indicators. An example of commonly used evaluation criteria is provided in the following Fig 1.

Finanziato dall'Unione europea NextGenerationEU | Ministero dell'Università e della Ricerca | Italiadomani PIANO NAZIONALE DI RIPRESA E RESILIENZA

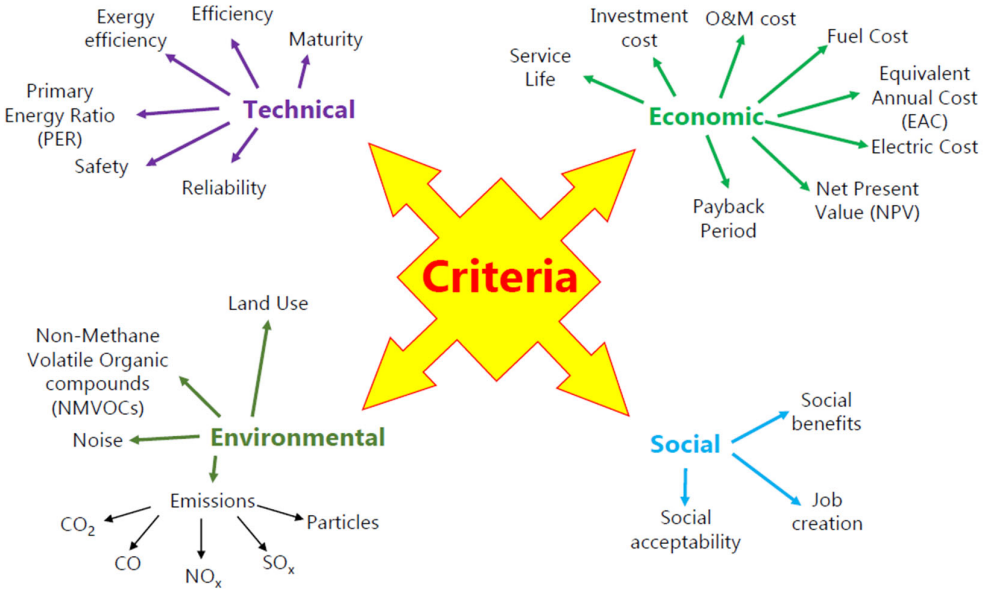

Figure 1. Example of different criteria for MCDA strategy.

The decision making (DM) process passes through different phases. In general, four phases can be identified:

1. Methods of selection criteria: define the criteria to be adopted in the analysis. The criteria system should be consistent and measurable, and they should not have inclusion relationships;
2. Weighting methods: decide the relative importance of each criterion. Generally, an equal weights method or a rank-order weighting method is used;
3. MCDA methods: rank the alternatives (fault types in this case study) after determining criteria weights. Several methods exist (Elementary methods, Unique synthesizing methods and Outranking methods);
4. Aggregation methods: compare among different MCDA methods. To compare results from different MCDA methods, some aggregation methods can be used to make the same decision. Some examples of aggregation methods are Voting methods and Mathematical methods,

In the analyzed case study, the monitored and available variables enable the evaluation of several KPIs. These include the electrical consumption of individual components (fans, humidifier, heat pump, and chiller), the total and maximum deviations of temperature and relative humidity from their respective ambient setpoints, and the peak power demand of the entire system. Overall, the assessment encompasses 5 KPIs for energy consumption criteria, 4 KPIs for thermo-hygrometric comfort criteria, and 1 KPI for grid performance criteria. By normalizing the 10 KPIs through FIR calculation, a comprehensive evaluation can be achieved, allowing for the simultaneous consideration of multiple aspects through an MCDA approach.

Criterion	*Associated KPIs*
Energy consumption	Electrical consumption of supply fan
	Electrical consumption of return fan
	Electrical consumption of humidifier
	Electrical consumption of heat pump
	Electrical consumption of chiller
Thermo-hygrometric comfort	Total temperature deviation from setpoint
	Maximum temperature deviation from setpoint
	Total relative humidity deviation from setpoint
	Maximum relative humidity deviation from setpoint
Grid reliability	Peak power demand of the entire HVAC system

Table 1. Selected criteria and KPIs for the analyzed case study.

Assuming equal weight is given to all three criteria, it is then possible to rank the faults based on their overall impact. An example is provided in Fig.2 below for the summer season only (analogous approach applies to the winter season).

Finanziato dall'Unione europea NextGenerationEU | Ministero dell'Università e della Ricerca | Italiadomani PIANO NAZIONALE DI RIPRESA E RESILIENZA

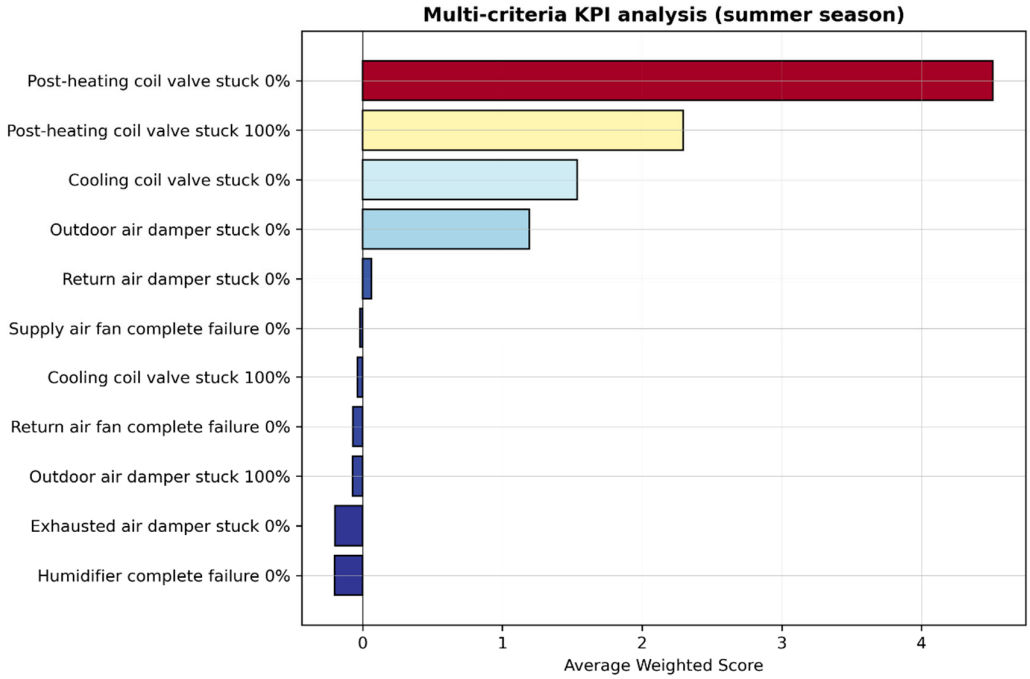

Figure 2. Ranking of analyzed fault based on multi-criteria impact.

4. References

[1] Kim, Woohyun; Katipamula, Srinivas: A review of fault detection and diagnostics methods for building systems. Sci. Technol. Built Environ., 24 (1) (2018), pp. 3-21.

[2] Lu, Xing et al.: A holistic fault impact analysis of the high-performance sequences of operation for HVAC systems: Modelica-based case study in a medium-office building. Energy and Buildings (2021).

[3] Kim, J.; Cai, J.; Braun, J.E.; Frank, S.M.: Common Faults and Their Prioritization in Small Commercial Buildings. (2018).

[4] Li, Yanfei; O'Neill, Zheng: An innovative fault impact analysis framework for enhancing building operations. Energy and Buildings, 199 (2019), pp. 311–331.

[5] Lu, Xing; O'Neill, Zheng; Li, Yanfei; Niu, Fuxin: A novel simulation-based framework for sensor error impact analysis in smart building systems: A case study for a demand-controlled ventilation system. Applied Energy, 263 (2020), p. 114638.

Finanziato dall'Unione europea NextGenerationEU
Ministero dell'Università e della Ricerca
Italiadomani PIANO NAZIONALE DI RIPRESA E RESILIENZA

DELIVERABLE WP2_D2

IMPACT ANALYSIS PERFORMED ON FAULTY EXPERIMENTAL DATA THOUGHT THE IDENTIFIED KPIs

EDIT BY UNICAMPANIA

PRIN 2022 - UTMOST FDD: AN AUTOMATED, OPEN, SCALABLE AND TRANSPARENT FAULT DETECTION AND DIAGNOSIS PROCESS FOR AIR-HANDLING UNITS BASED ON A HYBRID EXPERT AND ARTIFICIAL INTELLIGENCE APPROACH

Funded by the European Union - Next Generation EU within the "Piano Nazionale di Ripresa e Resilienza (PNRR), missione 4 componente 2 investimento 1.1 - fondo per il programma nazionale di ricerca e progetti di rilevante interesse nazionale (PRIN)"

Finanziato dall'Unione europea NextGenerationEU

Ministero dell'Università e della Ricerca

Italiadomani PIANO NAZIONALE DI RIPRESA E RESILIENZA

The UTMOST FDD Project is organised into the following 7 Work Packages (WPs):
WP0) PROJECT COORDINATION
WP1) EXPERIMENTAL ANALYSIS FOR THE CHARACTERIZATION OF FAULTY AND NORMAL OPERATION OF A TYPICAL AHU
WP2) KPIs IDENTIFICATION FOR ASSESSING FAULT IMPACT IN AHU OPERATION
WP3) AHU DIGITAL TWIN AND SIMULATION-BASED FAULT IMPACT SCENARIO ANALYSIS
WP4) DEFINITION OF HYBRID FDD STRATEGIES FOR AHUs
WP5) TRANSFERABILITY ANALYSIS OF THE FDD STRATEGIES
WP6) KNOWLEDGE TRANSFER AND DISSEMINATION

The WPs are organized into Tasks (T) ranging from 2 to 4 for each WP.

The aim of the WP2 is the definition of KPIs to evaluate fault impacts in terms of energy consumption, energy cost, thermal comfort and indoor air quality. The assessment of fault impact based on these KPIs will be performed starting from the experimental/simulation data collected in the WP1 and WP3.

The WP2 includes the following 3 tasks (WP2_T1, WP2_T2, WP2_T3) with the following main activities:
- WP2_T1) this task aims at selecting in the literature the single-criteria KPIs that well fit with the purpose of quantify the impact of specific faulty conditions on AHU operation. The objective is to identify faults with most adverse impacts and to rank them accordingly. The identified single-criteria KPIs will be then employed with reference to the datasets collected in WP1 and WP3;
- WP2_T2) this task aims to formulate new weighted multi-criteria KPIs, considering a trade-off between energy consumption, GHG emissions, cost, thermal comfort and ventilation impacts. The objective is to identify faults with most adverse impacts and to rank them accordingly. The identified weighted multi-criteria KPIs will be then employed with reference to the datasets collected in the WP1 and WP3. In the context of the WP2_T2, a written report (1st WP2 deliverable WP2_D1), including a detailed categorization of relevant scientific studies on fault impact assessment and the identified single- and multi-criteria KPIs, will be delivered;
- WP2_T3) this task performs an impact analysis by comparing the results of faulty experiments with those of fault free tests carried out under the same boundary conditions during the WP1 based on the single- and multi-criteria KPIs identified in the WP2_T1 and WP2_T2. This will make it possible to rank faults according to their impact under different operating conditions based on a fault scenario analysis, as well as evaluate a maintenance action prioritization scheme considering how the impact of a fault changes during system operation.

This deliverable WP2_D2 illustrates the symptoms on the AHU performance associated to the faults' occurrence, described in the deliverable WP1_D2, in terms of the KPIs defined in the WP2_T2.

In the next sections, the faults' impacts in terms of indoor thermo-hygrometric conditions (Section 1), electrical power (Section 2) electric energy demand (Section 3), operational costs (Section 4), global equivalent CO_2 emissions (Section 5) as well as operating times of AHU components (Section 6) are described.

1. Indoor thermo-hygrometric conditions

In this section the impacts of the investigated faults on indoor air temperature and relative humidity are analysed. In greater detail, the percentages of time during which indoor air temperature (TMR) or indoor air relative humidity (RHMR) is maintained within the specified deadbands for each normal and corresponding faulty test are calculated via the following formulas based on the measured data:

$$TMR = \frac{N_{in,DBT}}{N} \cdot 100 \quad (1)$$

$$RHMR = \frac{N_{in,DBRH}}{N} \cdot 100 \quad (2)$$

where:
- $N_{in,DBT}$ represents the number of experimental data points throughout the test duration when T_{RA} falls within its corresponding deadbands;

Finanziato dall'Unione europea NextGenerationEU | Ministero dell'Università e della Ricerca | Italiadomani PIANO NAZIONALE DI RIPRESA E RESILIENZA

- $N_{in,DBRH}$ represents the number of experimental data points throughout the test duration when RH_{RA} falls within its corresponding deadbands;
- N denotes the total number of recorded data points per test (considering a 1-second sampling rate and a daily operating period from 9:00 a.m. to 6:00 p.m., this leads to have 32400 experimental data points).

Additionally, the relevance of deviations from desired indoor air temperatures $\left|\bar{\varepsilon}_{T,D}\right|$ and the relevance of deviations from desired indoor air relative humidity $\left|\bar{\varepsilon}_{RH,D}\right|$ are defined based on the experimental data as follows:

$$\left|\bar{\varepsilon}_{T,D}\right| = \frac{1}{N_{out,DBT}} \cdot \left(\sum_{i=1}^{N} \left|\Delta T_{out,DBT,i}\right| \quad | \quad T_{RA,i} \notin [LDB_T, UDB_T] \right) \tag{3}$$

$$\left|\bar{\varepsilon}_{RH,D}\right| = \frac{1}{N_{out,DBRH}} \cdot \left(\sum_{i=1}^{N} \left|\Delta RH_{out,DBRH,i}\right| \quad | \quad RH_{RA,i} \notin [LDB_{RH}, UDB_{RH}] \right) \tag{4}$$

where:

- $\Delta T_{out,DBT}$ is the deviation of actual return air temperature from the desired temperature boundaries; it's only computed when actual T_{RA} falls outside the upper deadband (UDB_T) or the lower deadband (LDB_T) of $T_{SP,Room}$;
- $\Delta RH_{out,DBRH}$ is the deviation from the desired relative humidity range of actual return air relative humidity; it's only computed when actual RH_{RA} falls outside the upper deadband (UDB_{RH}) or the lower deadband (LDB_{RH}) of $RH_{SP,Room}$;
- $N_{out,DBT}$ represents the total number of data points during which return air tempera-ture is outside the acceptable range;
- $N_{out,DBRH}$ represents the total number of data points during which return air relative humidity is outside the acceptable range.

Tables 1a and 1b report the values of parameters calculated via Eqs. (1-4), during summer and winter, respectively.

Table 1a. Daily indoor air temperature/relative humidity met ratios together with relevance of deviations from desired indoor air temperature/relative humidity, during summer.

Test ID	TMR (%)	RHMR (%)	$\left\|\bar{\varepsilon}_{T,D}\right\|$ (°C)	$\left\|\bar{\varepsilon}_{RH,D}\right\|$ (%)
SF1	2.6	57.8	3.8	2.5
SN4	74.8	91.8	0.3	2.0
SF2	0.0	90.1	2.5	0.9
SN5	69.4	86.2	0.3	3.1
SF3	1.9	76.2	2.0	5.4
SN5	69.4	86.2	0.3	3.1
SF4	73.7	94.1	0.2	0.7
SN4	74.8	91.8	0.3	2.0
SF5	67.8	96.1	0.2	1.1
SN2	71.6	92.2	0.4	1.8
SF6	2.5	59.4	1.9	2.4
SN1	68.8	83.5	0.3	3.4
SF7	0.0	75.4	2.1	1.8
SN4	74.8	91.8	0.3	2.0
SF8	76.0	25.4	0.1	2.2
SN2	71.6	92.2	0.4	1.8
SF9	88.1	0.6	0.4	11.9
SN3	76.0	89.9	0.4	2.5
SF10	70.5	86.0	0.3	3.4

Finanziato dall'Unione europea NextGenerationEU | Ministero dell'Università e della Ricerca | Italiadomani PIANO NAZIONALE DI RIPRESA E RESILIENZA

Test ID	TMR (%)	RHMR (%)	$\lvert\bar{\varepsilon}_{T,D}\rvert$ (°C)	$\lvert\bar{\varepsilon}_{RH,D}\rvert$ (%)
SN5	69.4	86.2	0.3	3.1
SF11	58.7	31.3	0.2	1.2
SN6	77.3	93.3	0.2	3.8
SF12	70.2	93.0	0.5	0.9
SN9	69.6	93.7	0.5	0.6
SF13	71.5	84.7	0.4	2.3
SN7	71.9	94.2	0.2	0.4
SF14	68.5	90.6	0.5	1.0
SN11	68.0	90.0	0.5	1.0
SF15	70.7	92.8	0.4	0.8
SN10	70.8	94.0	0.2	0.4
SF16	67.3	92.2	0.5	0.9
SN8	71.5	93.2	0.4	0.8
SF17	68.0	91.5	0.5	0.9
SN11	68.0	90.0	0.5	1.0
SF18	67.5	90.8	0.4	1.5
SN12	67.6	92.9	0.4	1.0
SN13	71.0	95.5	0.3	1.4
SF19	70.5	95.5	0.2	1.5
SN13	71.0	96.4	0.2	2.0
SF20	70.5	95.5	0.2	1.5
SN13	72.4	94.9	0.2	2.2
SF21	70.5	95.5	0.2	1.5
SN14	0.0	95.0	3.1	3.6
SF22	71.6	97.3	0.2	0.3
SN15	0.0	95.8	4.1	0.5
SF23	71.4	95.7	0.2	0.7
SN14	0.0	95.2	3.9	0.2
SF24	71.6	97.3	0.2	0.3
SF25	90.8	64.1	0.7	0.8
SN17	73.3	94.3	0.2	2.1
SF26	63.6	94.0	0.2	1.4
SN16	71.4	96.4	0.2	0.7
SF27	57.9	98.3	0.3	0.3
SN17	73.3	94.3	0.2	2.1
SF28	75.1	93.0	0.2	1.2
SN18	72.3	96.1	0.2	1.2
SF29	71.5	88.2	0.2	0.6
SN18	72.3	96.1	0.2	1.2
SF30	74.4	69.0	0.2	1.2
SN18	72.3	96.1	0.2	1.2

Table 1b. Daily indoor air temperature/relative humidity met ratios together with relevance of deviations from desired indoor air temperature/relative humidity, during winter.

Finanziato dall'Unione europea NextGenerationEU | Ministero dell'Università e della Ricerca | Italiadomani PIANO NAZIONALE DI RIPRESA E RESILIENZA

Test ID	TMR (%)	RHMR (%)	$\lvert\bar{\varepsilon}_{T,D}\rvert$ (°C)	$\lvert\bar{\varepsilon}_{RH,D}\rvert$ (%)
WF1	0.0	0.0	3.0	2.9
WN2	75.8	96.8	0.2	1.2
WF2	5.5	88.5	3.9	0.7
WN5	78.2	92.5	0.5	0.6
WF3	18.5	97.7	0.6	2.5
WN1	76.9	97.1	0.2	2.0
WF4	74.0	87.7	0.3	1.3
WN8	73.7	90.8	0.3	1.3
WF5	80.5	18.4	0.3	2.6
WN6	77.2	90.9	0.5	0.9
WF6	0.0	95.8	1.6	0.7
WN5	78.2	92.5	0.5	0.6
WF7	8.2	86.8	1.9	1.2
WN3	75.2	95.3	0.2	1.5
WF8	76.4	96.3	0.3	1.8
WN7	76.3	95.3	0.3	1.5
WF9	72.0	0.0	0.5	8.7
WN4	78.0	90.9	0.2	1.4
WF10	76.3	89.6	0.3	2.5
WN2	75.8	96.8	0.2	1.2
WF11	74.8	98.1	0.2	1.2
WN2	75.8	96.8	0.2	1.2
WF12	76.0	88.2	0.3	1.3
WN5	78.2	92.5	0.5	0.7
WF13	75.3	97.7	0.3	0.6
WN9	70.9	89.2	0.5	1.3
WF14	73.2	94.8	0.3	2.0
WN5	78.2	92.5	0.5	0.7
WF15	73.7	56.6	0.3	1.4
WN11	80.9	86.0	0.3	0.7
WF16	74.0	99.0	0.3	0.8
WN7	76.3	95.3	0.3	1.5
WF17	75.4	4.4	0.3	2.9
WN10	75.7	4.0	0.3	2.8
WF18	74.1	91.2	0.3	0.8
WN7	76.3	95.3	0.3	1.5
WN12	75.4	97.3	0.3	3.1
W519	74.3	98.4	0.3	2.9
WN12	71.1	89.2	0.3	2.1
WF20	74.3	98.4	0.3	2.9
WN15	71.9	34.7	0.3	2.2
WF21	72.5	76.5	0.3	0.8
WN13	3.9	90.7	4.4	1.5
WF22	72.3	78.2	0.3	1.0
WN14	3.6	90.9	4.7	1.0

Finanziato dall'Unione europea NextGenerationEU | Ministero dell'Università e della Ricerca | Italiadomani PIANO NAZIONALE DI RIPRESA E RESILIENZA

Test ID	TMR (%)	RHMR (%)	$\left\|\bar{\varepsilon}_{T,D}\right\|$ (°C)	$\left\|\bar{\varepsilon}_{RH,D}\right\|$ (%)
WF23	72.3	54.1	0.3	1.6
WN13	2.6	93.1	5.2	1.3
WF24	72.3	78.2	0.3	1.0
WF25	92.3	93.7	0.2	2.8
WN12	74.3	98.4	0.3	2.9
WF26	60.6	90.8	0.4	1.3
WN13	72.3	78.2	0.3	1.0
WF27	55.3	89.4	0.5	1.0
WN12	74.3	98.4	0.3	2.9
WF28	69.5	93.7	0.3	1.1
WN15	72.5	76.5	0.3	0.8
WF29	76.2	50.5	0.3	1.5
WN15	72.5	76.5	0.3	0.8
WF30	74.4	69.0	0.2	1.2
WN16	72.3	96.1	0.2	1.2

The following key performance indexes (KPIs): (i) the absolute maximum indoor air temperature deviation (dT_{max}) calculated as the largest absolute deviation between actual return air temperature T_{RA} and the upper or lower $T_{SP,Room}$ deadband; (ii) the absolute total indoor air temperature deviation (dT_{tot}) defined by adding all indoor air temperature absolute deviations over the entire test period; (iii) the absolute maximum indoor air relative humidity deviation (dRH_{max}) calculated as the largest absolute deviation between actual return air relative humidity RH_{RA} and the upper or lower $RH_{SP,Room}$ deadband; (iv) the absolute total indoor air relative humidity deviation (dRH_{tot}) defined by adding all indoor air relative humidity absolute deviations, over the entire duration of the test, are calculated for both normal and faulty tests according to the following equations:

$$dT_{max} = \max\left|\Delta T_{out,DBRH,i}\right| \quad | \quad T_{RA,i} \notin [LDB_T, UDB_T] \tag{5}$$

$$dT_{tot} = \sum_{i=1}^{N}\left|\Delta T_{out,DBT,i}\right| \quad | \quad T_{RA,i} \notin [LDB_T, UDB_T] \tag{6}$$

$$dRH_{max} = \max\left|\Delta RH_{out,DBRH,i}\right| \quad | \quad RH_{RA,i} \notin [LDB_{RH}, UDB_{RH}] \tag{7}$$

$$dRH_{tot} = \sum_{i=1}^{N}\left|\Delta RH_{out,DBRH,i}\right| \quad | \quad RH_{RA,i} \notin [LDB_{RH}, UDB_{RH}] \tag{8}$$

The percentage difference of the previous parameters between faulty and normal tests is also calculated as follows:

$$\%d = \frac{\left(d_{Faulty} - d_{Baseline}\right)}{d_{Baseline}} \cdot 100 \tag{9}$$

where:

- d_{Faulty} are the values of dT_{max}, dT_{tot}, dRH_{max}, and dRH_{tot} associated to the corresponding faulty experiments;
- $d_{Baseline}$ represents the values of dT_{max}, dT_{tot}, dRH_{max}, and dRH_{tot} corresponding to the normal tests.

A positive %d indicates that the value of the corresponding metric during the normal test is lower than that one observed in the related faulty test, which means that during the faulty experiment the AHU is able to control in a worse way the associated indoor parameter in comparison to the normal experiment.

Tables 2a and b report the values of %d (calculated via Eq. 9) of the KPIs defined by Eqs. (5-8) for each pair of tests under comparison during summer and winter, respectively. The cells displaying the values of %d in Tables 2a and b are color-coded according to the legend reported at the end of this table (cells are in yellow if %d is included in the range ±10%, in red if %d is greater than 20% or lower than –20%, in orange in all other cases).

Finanziato dall'Unione europea NextGenerationEU | Ministero dell'Università e della Ricerca | Italiadomani PIANO NAZIONALE DI RIPRESA E RESILIENZA

Table 2a. Values of %d (calculated via Eq. 9) for dT_{max}, dT_{tot}, dRH_{max}, and dRH_{tot} for the corresponding faulty and normal tests, during summer.

	dT_{max} (° C)	dT_{tot} (° C)	dRH_{max} (%)	dRH_{tot} (%)
SN4	1.1	2486.7	7.0	5269.6
SF1	5.5	121334.1	6.9	34473.3
$\%d_{SF1\ vs.\ SN4}$ (%)	409.3	4779.3	–1.0	554.2
SN5	1.3	3214.9	8.0	13759.9
SF2	3.3	80458.4	5.2	2768.9
$\%d_{SF2\ vs.\ SN5}$ (%)	148.9	2402.7	–34.4	–79.9
SN5	1.3	3214.9	8.0	13759.9
SF3	3.6	64192.2	9.6	41809.6
$\%d_{SF3\ vs.\ SN5}$ (%)	169.2	1896.7	20.9	203.9
SN4	1.1	2486.7	7.0	5269.6
SF4	1.4	1933.8	4.3	1355.1
$\%d_{SF4\ vs.\ SN4}$ (%)	33.6	–22.2	–38.2	–74.3
SN2	1.3	3318.7	6.3	4551.2
SF5	1.2	2313.6	5.5	1409.9
$\%d_{SF5\ vs.\ SN2}$ (%)	–1.6	–30.3	–12.5	–69.0
SN1	1.1	3033.7	12.6	18152.1
SF6	3.1	58986.3	7.1	31561.6
$\%d_{SF6\ vs.\ SN1}$ (%)	168.8	1844.4	–43.7	73.9
SN4	1.1	2486.7	7.0	5269.6
SF7	3.3	69292.1	6.0	14489.9
$\%d_{SF7\ vs.\ SN4}$ (%)	203.7	2686.5	–14.0	175.0
SN2	1.3	3318.7	6.3	4551.2
SF8	1.1	1023.2	4.9	53182.3
$\%d_{SF8\ vs.\ SN2}$ (%)	–10.3	–69.2	–23.1	1068.5
SN3	1.1	2865.3	6.9	8211.8
SF9	1.2	1371.9	20.7	381609.1
$\%d_{SF9\ vs.\ SN3}$ (%)	6.3	–52.1	200.0	4547.1
SN5	1.3	3214.9	8.0	13759.9
SF10	1.2	2764.6	12.4	15195.7
$\%d_{SF10\ vs.\ SN5}$ (%)	–12.8	–14.0	55.4	10.4
SN6	1.5	1194.5	8.0	8320.7
SF11	1.2	3112.1	5.8	27395.4
$\%d_{SF11\ vs.\ SN6}$ (%)	–20.7	160.5	–27.6	229.2
SF12	1.3	4453.4	2.4	1189.7
SN9	1.1	4352.5	4.1	2019.0
$\%d_{SF12\ vs.\ SN9}$ (%)	–11.0	–2.3	73.8	69.7
SF13	1.0	1585.7	3.9	796.3
SN7	1.1	3480.0	8.4	11515.9
$\%d_{SF13\ vs.\ SN7}$ (%)	10.7	119.5	115.7	1346.1

Finanziato dall'Unione europea NextGenerationEU | Ministero dell'Università e della Ricerca | Italiadomani PIANO NAZIONALE DI RIPRESA E RESILIENZA

	dT_{max} (° C)	dT_{tot} (° C)	dRH_{max} (%)	dRH_{tot} (%)
SF14	1.4	4821.6	10.2	2994.7
SN11	1.2	5044.4	6.5	2898.3
%d$_{SF14\ vs.\ SN11}$ (%)	–12.1	4.6	–35.9	–3.2
SF15	1.4	3908.3	5.9	1897.8
SN10	1.3	2215.6	1.5	770.4
%d$_{SF15\ vs.\ SN10}$ (%)	–8.0	–43.3	–74.2	–59.4
SF16	1.4	3270.4	6.1	1776.2
SN8	1.4	4759.4	8.1	2307.0
%d$_{SF16\ vs.\ SN8}$ (%)	3.7	45.5	33.3	29.9
SF17	1.4	4821.6	10.2	2994.7
SN11	1.4	5093.2	8.0	2590.2
%d$_{SF17\ vs.\ SN11}$ (%)	2.1	5.6	–21.0	–13.5
SF18	1.2	4206.1	5.1	2326.6
SN12	1.0	4173.0	5.9	4436.6
%d$_{SF18\ vs.\ SN12}$ (%)	–15.6	–0.8	15.6	90.7
SN13	1.6	2114.6	4.2	2217.7
SF19	1.5	2389.7	3.1	2010.1
%d$_{SF19\ vs.\ SN13}$ (%)	–5.6	13.0	–25.2	–9.4
SN13	1.6	2114.6	4.2	2217.7
SF20	1.1	1895.0	5.0	2390.5
%d$_{SF20\ vs.\ SN13}$ (%)	–34.4	–10.4	19.8	7.8
SN13	1.6	2114.6	4.2	2217.7
SF21	1.2	1475.7	4.7	3576.6
%d$_{SF21\ vs.\ SN13}$ (%)	–23.8	–30.2	12.6	61.3
SN14	1.6	1990.5	1.1	271.5
SF22	4.7	101612.1	435.7	5898.7
%d$_{SF22\ vs.\ SN14}$ (%)	191.9	5004.8	39507.3	2072.7
SN15	1.4	1972.6	5.8	950.3
SF23	5.6	133126.7	3.5	637.1
%d$_{SF23\ vs.\ SN15}$ (%)	291.0	6648.7	–40.8	–33.0
SN14	1.6	1990.5	1.1	271.5
SF24	5.5	127147.3	0.6	351.2
%d$_{SF24\ vs.\ SN14}$ (%)	240.6	6287.6	–46.4	29.3
SN17	1.2	1522.9	6.9	3780.0
SF25	1.5	2167.2	7.9	8760.6
%d$_{SF25\ vs.\ SN17}$ (%)	27.0	42.3	13.4	131.8
SN16	1.3	1967.7	2.8	778.2
SF26	1.2	2855.6	7.5	2668.9
%d$_{SF26\ vs.\ SN16}$ (%)	–7.7	45.1	170.1	243.0
SN17	1.2	1522.9	6.9	3780.0
SF27	1.5	3803.0	2.3	160.7

Finanziato dall'Unione europea NextGenerationEU | Ministero dell'Università e della Ricerca | Italiadomani PIANO NAZIONALE DI RIPRESA E RESILIENZA

	dT_{max} (° C)	dT_{tot} (° C)	dRH_{max} (%)	dRH_{tot} (%)
%d$_{SF27\ vs.\ SN17}$ (%)	33.0	149.7	–66.9	–95.7
SN18	1.3	1605.7	4.7	1513.2
SF28	1.1	1560.8	6.2	2794.4
%d$_{SF28\ vs.\ SN18}$ (%)	–14.5	–2.8	31.2	84.7
SN18	1.3	1605.7	4.7	1513.2
SF29	1.3	1648.2	2.0	2328.7
%d$_{SF29\ vs.\ SN18}$ (%)	0.0	2.6	–57.3	53.9
SN18	1.3	1605.7	4.7	1513.2
SF30	1.3	1309.3	3.5	12496.4
%d$_{SF30\ vs.\ SN18}$ (%)	–3.8	–18.5	–26.1	725.8
Legend				
	–10% ≤ %d ≤ +10%			
	+10% < %d ≤ +20% OR –20% ≤ %d < –10%			
	%d > +20% OR %d < –20%			

Table 2b. Values of %d (calculated via Eq. 9) for dTmax, dTtot, dRHmax, and dRHtot for the corresponding faulty and normal tests, during winter.

	dT_{max} (° C)	dT_{tot} (° C)	dRH_{max} (%)	dRH_{tot} (%)
WN2	0.9	1336.7	3.5	1259.0
WF1	4.3	98518.6	4.3	93765.9
%d$_{WF1\ vs.\ WN2}$ (%)	376.7	7270.1	22.1	7347.4
WN5	1.3	3717.0	2.5	1576.4
WF2	5.9	118150.0	3.8	2562.0
%d$_{WF2\ vs.\ WN5}$ (%)	360.6	3078.7	49.6	62.5
WN1	1.1	1381.1	4.4	1925.0
WF3	1.1	16083.4	5.3	1882.5
%d$_{WF3\ vs.\ WN1}$ (%)	–3.6	1064.6	21.6	–2.2
WN8	1.0	2424.3	4.7	3733.6
WF4	1.1	2782.8	7.6	5123.3
%d$_{WF4\ vs.\ WN8}$ (%)	4.9	14.8	63.3	37.2
WN6	1.2	3960.0	4.2	2593.6
WF5	1.1	2038.1	6.5	67510.3
%d$_{WF5\ vs.\ WN6}$ (%)	–9.4	–48.5	54.8	2503.0
WN5	1.3	3717.0	2.5	1576.4
WF6	2.2	53062.6	3.5	974.0
%d$_{WF6\ vs.\ WN5}$ (%)	74.8	1327.6	39.4	–38.2
WN3	1.0	1434.5	5.6	2232.4
WF7	3.4	57910.2	4.9	5115.5
%d$_{WF7\ vs.\ WN3}$ (%)	252.6	3936.9	–13.1	129.1
WN7	0.9	1956.9	6.1	2276.4
WF8	1.0	1970.3	6.4	2190.3

Finanziato dall'Unione europea NextGenerationEU | Ministero dell'Università e della Ricerca | Italiadomani PIANO NAZIONALE DI RIPRESA E RESILIENZA

	dT_{max} (° C)	dT_{tot} (° C)	dRH_{max} (%)	dRH_{tot} (%)
%d$_{WF8\ vs.\ WN7}$ (%)	4.2	0.7	4.6	–3.8
WN4	1.0	1325.1	4.8	4200.5
WF9	1.0	4192.4	18.2	281629.5
%d$_{WF9\ vs.\ WN4}$ (%)	4.0	216.4	284.0	6604.7
WN2	0.9	1336.7	3.5	1259.0
WF10	0.9	2111.5	9.0	8600.3
%d$_{WF10\ vs.\ WN2}$ (%)	2.2	58.0	159.8	583.1
WN2	0.9	1336.7	3.5	1259.0
WF11	1.0	1238.6	2.5	729.1
%d$_{WF11\ vs.\ WN2}$ (%)	11.1	–7.3	–29.6	–42.1
WF12	1.3	3687.9	2.5	1596.1
WN5	1.0	1909.1	6.1	4934.7
%d$_{WF12\ vs.\ WN5}$ (%)	–22.8	–48.2	138.6	209.2
WF13	1.2	4465.7	8.0	4669.8
WN9	1.2	2241.4	1.5	458.5
%d$_{WF13\ vs.\ WN9}$ (%)	–6.5	–49.8	–81.1	–90.2
WF14	1.3	3687.9	2.5	1596.1
WN5	0.9	2263.7	10.5	3430.3
%d$_{WF14\ vs.\ WN5}$ (%)	–28.3	–38.6	311.8	114.9
WF15	0.9	1664.7	3.4	3217.5
WN11	1.0	2277.7	3.5	19060.4
%d$_{WF15\ vs.\ WN11}$ (%)	11.1	36.8	4.4	492.4
WF16	0.9	1956.9	6.1	2276.4
WN7	1.0	2434.2	1.5	255.9
%d$_{WF16\ vs.\ WN10}$ (%)	5.3	24.4	–75.5	–88.8
WF17	1.0	2211.3	7.2	86247.9
WN10	0.9	2075.0	9.5	88487.5
%d$_{WF17\ vs.\ WN10}$ (%)	–3.1	–6.2	33.3	2.6
WF18	0.9	1956.9	6.1	2276.4
WN7	1.0	2460.7	3.0	2385.9
%d$_{WF18\ vs.\ WN7}$ (%)	8.4	25.7	–51.6	4.8
WN12	1.0	2158.4	5.0	1553.7
WF19	0.9	2223.0	7.1	2771.0
%d$_{WF19\ vs.\ WN12}$ (%)	–6.1	3.0	42.9	78.3
WN12	1.0	2158.4	5.0	1553.7
WF20	1.1	2398.9	10.1	7218.8
%d$_{WF20\ vs.\ WN12}$ (%)	13.1	11.1	103.2	364.6
WN15	0.9	2343.9	3.5	5809.0
WF21	0.9	2455.0	8.5	46145.8
%d$_{WF21\ vs.\ WN15}$ (%)	3.3	4.7	139.5	694.4
WN13	0.9	2679.7	9.7	6982.3

Finanziato dall'Unione europea NextGenerationEU
Ministero dell'Università e della Ricerca
Italiadomani PIANO NAZIONALE DI RIPRESA E RESILIENZA

	dT_{max} (° C)	dT_{tot} (° C)	dRH_{max} (%)	dRH_{tot} (%)
WF22	6.8	135200.3	8.7	4561.1
%d$_{WF22\ vs.\ WN13}$ (%)	640.2	4945.3	–9.8	–34.7
WN14	1.0	2829.6	4.4	24288.4
WF23	7.1	146752.2	5.0	2913.5
%d$_{WF23\ vs.\ WN14}$ (%)	642.7	5086.3	13.6	–88.0
WN13	0.9	2679.7	9.7	6982.3
WF24	7.7	164018.5	7.6	2917.3
%d$_{WF24\ vs.\ WN13}$ (%)	740.2	6020.7	–22.1	–58.2
WN12	1.0	2158.4	5.0	1553.7
WF25	1.0	406.7	7.0	5799.1
%d$_{WF25\ vs.\ WN12}$ (%)	–2.0	–81.2	40.3	273.2
WN13	0.9	2679.7	9.7	6982.3
WF26	0.9	4652.3	8.0	3918.9
%d$_{WF26\ vs.\ WN13}$ (%)	2.2	73.6	–17.3	–43.9
WN12	1.0	2158.4	5.0	1553.7
WF27	1.5	7857.3	6.0	3487.7
%d$_{WF27\ vs.\ WN12}$ (%)	55.6	264.0	21.2	124.5
WN15	0.9	2343.9	3.5	5809.0
WF28	1.0	2596.7	3.7	2261.5
%d$_{WF28\ vs.\ WN15}$ (%)	5.4	10.8	4.8	–61.1
WN15	0.9	2343.9	3.5	5809.0
WF29	1.1	2054.5	3.5	23604.1
%d$_{WF29\ vs.\ WN15}$ (%)	14.1	–12.3	–2.0	306.3
WN16	1.0	2929.2	2.7	782.1
WF30	1.1	2296.7	3.1	2557.8
%d$_{WF30\ vs.\ WN16}$ (%)	11.3	–21.6	13.7	227.1
Legend				
	$-10\% \leq \%d \leq +10\%$			
	$+10\% < \%d \leq +20\%$ OR $-20\% \leq \%d < -10\%$			
	$\%d > +20\%$ OR $\%d < -20\%$			

2. Effects of faults on electrical power demand of AHU components

In this section the effects of the tested faults in terms of power demand are presented. For each normal/faulty experiment as well as AHU components, Tables 3a and b report the parameters $\%\mu_{el}$ and $\%\sigma_{el}$ defined as follows upon varying both the pair of tests under comparison as well as the AHU component:

$$\%\mu_{el} = \frac{\left(\mu_{el,Faulty} - \mu_{el,Baseline}\right)}{\mu_{el,Baseline}} \cdot 100 \quad (10)$$

$$\%\sigma_{el} = \frac{\left(\sigma_{el,Faulty} - \sigma_{el,Baseline}\right)}{\sigma_{el,Baseline}} \cdot 100 \quad (11)$$

where $\mu_{el,Faulty}$ and $\mu_{el,Baseline}$ are, respectively, the arithmetic mean μ_{el} of electric power consumption P_{el} during faulty and baseline tests, while $\sigma_{el,Faulty}$ and $\sigma_{el,Baseline}$ are, respectively, the standard deviation σ_{el} of electric power consumption P_{el} during faulty and baseline tests.

Finanziato dall'Unione europea NextGenerationEU | Ministero dell'Università e della Ricerca | Italiadomani PIANO NAZIONALE DI RIPRESA E RESILIENZA

In Tables 3a and b the cells reporting the values of $\%\mu_{el}$ and $\%\sigma_{el}$ are filled in yellow if $\%\mu_{el}$ or $\%\sigma_{el}$ is included in the range ±10%, in red if $\%\mu_{el}$ or $\%\sigma_{el}$ is greater than 20% or lower than –20%, in orange in other cases (the symbol N.A. (not applicable) denotes that the AHU component has not been activated during both tests and the calculation of $\%\mu_{el}$ or $\%\sigma_{el}$ cannot be performed, while the symbol '∞' indicates that the AHU component has not been activated only during the normal test).

Table 3a. Values of $\%\mu_{el}$ (calculated via Eq. 10) and $\%\sigma_{el}$ (calculated via Eq. 11) upon varying both the pair of tests under comparison as well as the AHU component, during summer.

	SAF		RAF		RS		HP		HUM	
	μ_{el} (W)	σ_{el} (W)	μ_{el} (W)	σ_{el} (W)	μ_{el} (W)	σ_{el} (W)	μ_{el} (W)	σ_{el} (W)	μ_{el} (W)	σ_{el} (W)
EP of SN4 (W)	341.4	13.8	73.3	2.6	4836.8	547.5	5411.8	560.6	3233.5	885.2
EP of SF1 (W)	352.7	13.8	73.8	2.5	4833.9	438.9	0.0	0.0	0.0	0.0
$\%EP_{SF1\ vs.\ SN4}$ (%)	3.3	–0.1	0.8	–3.1	–0.1	–19.8	–100.0	–100.0	–100.0	–100.0
EP of SN5 (W)	344.5	14.2	73.7	2.6	4766.5	670.7	5377.8	534.7	3244.7	864.6
EP of SF2 (W)	341.2	12.9	73.2	2.6	4821.7	381.6	5376.5	521.0	3425.1	591.0
$\%EP_{SF2\ vs.\ SN5}$ (%)	–1.0	–9.5	–0.8	–0.5	1.2	–43.1	0.0	–2.6	5.6	–31.6
EP of SN5 (W)	344.5	14.2	73.7	2.6	4766.5	670.7	5377.8	534.7	3244.7	864.6
EP of SF3 (W)	340.9	13.3	73.1	2.6	4900.7	496.0	0.0	0.0	3075.5	1197.9
$\%EP_{SF3\ vs.\ SN5}$ (%)	–1.1	–6.4	–0.9	2.9	2.8	–26.0	–100.0	–100.0	–5.2	38.6
EP of SN4 (W)	341.4	13.8	73.3	2.6	4836.8	547.5	5411.8	560.6	3233.5	885.2
EP of SF4 (W)	345.1	14.0	73.6	2.5	4824.1	392.5	5359.4	593.6	3281.0	827.4
$\%EP_{SF4\ vs.\ SN4}$ (%)	1.1	1.1	0.5	–3.8	–0.3	–28.3	–1.0	5.9	1.5	–6.5
EP of SN2 (W)	337.3	8.3	74.0	1.3	3824.8	1573.9	3659.4	1801.3	3081.2	995.7
EP of SF5 (W)	344.4	14.0	73.6	2.6	4918.7	962.6	5433.5	545.5	0.0	0.0
$\%EP_{SF5\ vs.\ SN2}$ (%)	2.1	68.8	–0.4	96.4	28.6	–38.8	48.5	–69.7	–100.0	–100.0
EP of SN1 (W)	343.7	8.4	74.6	3.0	3406.5	1533.2	3571.9	1797.7	3151.5	911.3
EP of SF6 (W)	346.4	13.9	73.7	2.6	4812.2	461.3	5442.9	590.0	0.0	0.0
$\%EP_{SF6\ vs.\ SN1}$ (%)	0.8	65.3	–1.2	–14.8	41.3	–69.9	52.4	–67.2	–100.0	–100.0
EP of SN4 (W)	341.4	13.8	73.3	2.6	4836.8	547.5	5411.8	560.6	3233.5	885.2
EP of SF7 (W)	337.1	14.0	73.2	2.9	4823.3	539.7	5372.0	535.9	3235.3	868.2
$\%EP_{SF7\ vs.\ SN4}$ (%)	–1.3	1.4	0.0	10.9	–0.3	–1.4	–0.7	–4.4	0.1	–1.9
EP of SN2 (W)	337.3	8.3	74.0	1.3	3824.8	1573.9	3659.4	1801.3	3081.2	995.7
EP of SF8 (W)	336.1	8.0	73.9	1.3	3781.9	1568.1	3645.6	1790.1	0.0	0.0
$\%EP_{SF8\ vs.\ SN2}$ (%)	–0.4	–3.7	–0.1	–4.0	–1.1	–0.4	–0.4	–0.6	–100.0	–100.0
EP of SN3 (W)	338.5	10.3	73.8	1.9	4479.1	1403.4	4354.2	1657.9	3151.6	936.3
EP of SF9 (W)	333.6	13.7	73.7	2.6	5139.0	429.5	5351.8	508.3	3461.2	484.4
$\%EP_{SF9\ vs.\ SN3}$ (%)	–1.4	32.7	–0.2	36.8	14.7	–69.4	22.9	–69.3	9.8	–48.3
EP of SN5 (W)	344.5	14.2	73.7	2.6	4766.5	670.7	5377.8	534.7	3244.7	864.6
EP of SF10 (W)	333.2	15.8	16.9	0.0	4829.6	444.9	5331.4	551.6	3278.1	830.4
$\%EP_{SF10\ vs.\ SN5}$ (%)	–3.3	11.3	–77.1	–98.3	1.3	–33.7	–0.9	3.2	1.0	–4.0
EP of SN6 (W)	337.7	13.3	73.5	2.6	4774.3	437.5	5347.3	551.5	0.0	0.0
EP of SF11 (W)	92.8	4.4	70.9	3.1	4814.8	474.4	5560.5	461.2	0.0	0.0
$\%EP_{SF11\ vs.\ SN6}$ (%)	–72.5	–67.2	–3.6	22.4	0.9	8.4	4.0	–16.4	N.A.	N.A.
EP of SN9 (W)	352.6	14.0	72.1	2.4	5581.4	473.0	6080.4	653.7	3565.4	1212.0

Finanziato dall'Unione europea NextGenerationEU | Ministero dell'Università e della Ricerca | Italiadomani PIANO NAZIONALE DI RIPRESA E RESILIENZA

	SAF		RAF		RS		HP		HUM	
	μ_{el} (W)	σ_{el} (W)	μ_{el} (W)	σ_{el} (W)	μ_{el} (W)	σ_{el} (W)	μ_{el} (W)	σ_{el} (W)	μ_{el} (W)	σ_{el} (W)
EP of SF12 (W)	343.7	13.6	70.0	2.4	5653.2	474.4	6105.5	627.6	3306.6	793.3
%$EP_{SF12\ vs.\ SN9}$ (%)	–2.5	–2.6	–3.0	–2.1	1.3	0.3	0.4	–4.0	–7.3	–34.5
EP of SN7 (W)	341.9	13.8	72.0	2.6	5121.7	406.4	5763.8	599.3	3216.9	892.7
EP of SF13 (W)	346.3	13.6	72.4	2.5	5625.1	434.3	6116.4	660.9	3243.2	880.1
%$EP_{SF13\ vs.\ SN7}$ (%)	1.3	–1.1	0.5	–4.7	9.8	6.9	6.1	10.3	0.8	–1.4
EP of SN11 (W)	333.9	13.5	71.9	2.6	5004.6	415.1	5811.2	644.5	3255.9	829.7
EP of SF14 (W)	339.8	13.7	72.3	2.6	5050.0	428.8	5855.1	592.8	3256.4	832.6
%$EP_{SF14\ vs.\ SN11}$ (%)	–1.7	1.1	0.5	–0.8	0.9	3.3	0.8	–8.0	0.0	0.4
EP of SN10 (W)	341.6	13.5	72.0	2.6	5068.1	360.6	5723.9	619.0	3307.9	752.0
EP of SF15 (W)	344.8	14.1	70.8	2.6	5140.3	393.5	5731.9	595.0	3228.1	883.8
%$EP_{SF15\ vs.\ SN10}$ (%)	0.9	3.9	–1.7	0.8	1.4	9.1	0.1	–3.9	–2.4	14.9
EP of SN8 (W)	354.3	14.1	72.5	2.5	5510.6	444.8	6167.4	625.6	3246.0	885.0
EP of SF16 (W)	339.7	13.9	72.3	2.6	5005.5	404.9	5780.8	606.8	3257.5	834.5
%$EP_{SF16\ vs.\ SN8}$ (%)	–4.1	–1.6	–0.3	2.4	–9.2	–9.0	–6.3	–3.0	0.4	–5.7
EP of SN11 (W)	333.9	13.5	71.9	2.6	5004.6	415.1	5811.2	644.5	3255.9	829.7
EP of SF17 (W)	339.0	13.6	72.6	2.5	5015.1	423.1	5819.3	643.6	3291.6	804.9
%$EP_{SF17\ vs.\ SN11}$ (%)	1.5	0.2	0.9	–3.9	0.2	1.9	0.1	–0.1	1.1	–2.3
EP of SN12 (W)	341.3	14.3	72.8	2.6	4722.2	462.1	5820.5	625.0	3319.5	772.8
EP of SF18 (W)	339.1	14.1	72.0	2.6	4876.8	466.2	5779.6	626.1	3318.7	779.3
%$EP_{SF18\ vs.\ SN12}$ (%)	–0.6	–1.3	–1.0	2.0	3.3	0.9	–0.7	0.2	0.0	0.8
EP of SN13 (W)	335.6	13.9	73.9	2.6	5080.1	365.8	5764.4	619.4	116.3	615.7
EP of SF19 (W)	333.8	12.7	73.3	2.7	5029.1	450.7	5826.2	618.6	0.0	0.0
%$EP_{SF19\ vs.\ SN13}$ (%)	–0.6	–8.7	–0.9	3.1	–1.0	23.2	1.1	–0.1	–100.0	–100.0
EP of SN13 (W)	335.6	13.9	73.9	2.6	5080.1	365.8	5764.4	619.4	116.3	615.7
EP of SF20 (W)	328.7	13.5	71.8	2.5	4993.8	368.0	5780.8	593.4	13.0	0.1
%$EP_{SF20\ vs.\ SN13}$ (%)	–2.1	–2.7	–2.9	–2.8	–1.7	0.6	0.3	–4.2	–88.9	–100.0
EP of SN13 (W)	335.6	13.9	73.9	2.6	5080.1	365.8	5764.4	619.4	116.3	615.7
EP of SF21 (W)	338.5	13.2	73.4	2.7	5152.7	391.5	5788.8	595.6	66.0	427.4
%$EP_{SF21\ vs.\ SN13}$ (%)	0.9	–5.0	–0.7	3.0	1.4	7.0	0.4	–3.8	–43.3	–30.6
EP of SN14 (W)	328.7	13.0	72.6	2.6	4435.1	405.7	5534.8	580.1	348.7	1070.3
EP of SF22 (W)	333.1	12.5	71.7	2.5	4793.6	399.2	5762.8	614.5	1569.9	1829.0
%$EPSF_{22\ vs.\ SN14}$ (%)	1.3	–3.7	–1.2	–0.9	8.1	–1.6	4.1	5.9	350.3	70.9
EP of SN15 (W)	322.6	12.9	72.2	2.5	4483.2	404.3	5426.9	588.2	387.7	1106.8
EP of SF23 (W)	318.3	11.6	71.8	2.6	4506.2	334.9	5445.6	539.5	2089.4	1763.3
%$EP_{SF23\ vs.\ SN15}$ (%)	–1.3	–9.9	–0.5	5.2	0.5	–17.2	0.3	–8.3	439.0	59.3
EP of SN14 (W)	328.7	13.0	72.6	2.6	4435.1	405.7	5534.8	580.1	348.7	1070.3
EP of SF24 (W)	321.2	11.6	72.2	2.5	4433.5	376.6	5384.5	561.1	2065.3	1763.8
%$EP_{SF24\ vs.\ SN14}$ (%)	–2.3	–10.5	–0.4	–1.2	0.0	–7.2	–2.7	–3.3	492.3	64.8
EP of SN17 (W)	341.4	13.3	72.8	2.5	4717.5	421.3	5702.0	630.8	221.6	868.5
EP of SF25 (W)	135.4	7.3	71.3	2.6	4865.5	486.6	5813.2	919.2	0.0	0.0

Finanziato dall'Unione europea NextGenerationEU | Ministero dell'Università e della Ricerca | Italiadomani PIANO NAZIONALE DI RIPRESA E RESILIENZA

	SAF		RAF		RS		HP		HUM	
	μ_{el} (W)	σ_{el} (W)	μ_{el} (W)	σ_{el} (W)	μ_{el} (W)	σ_{el} (W)	μ_{el} (W)	σ_{el} (W)	μ_{el} (W)	σ_{el} (W)
%EP$_{SF25\ vs.\ SN17}$ (%)	–60.3	–45.2	–2.0	6.5	3.1	15.5	2.0	45.7	–100.0	–100.0
EP of SN16 (W)	348.7	13.3	72.4	2.4	3902.1	2269.5	6129.2	637.2	293.8	1023.1
EP of SF26 (W)	802.4	38.9	74.4	2.8	4915.1	351.4	5675.1	596.1	332.2	1062.7
%EP$_{SF26\ vs.\ SN16}$ (%)	130.1	192.6	2.8	15.3	26.0	–84.5	–7.4	–6.4	13.1	3.9
EP of SN17 (W)	341.4	13.3	72.8	2.5	4717.5	421.3	5702.0	630.9	221.6	868.5
EP of SF27 (W)	1817.3	95.5	76.8	3.2	4932.3	289.2	5634.8	582.8	140.3	703.9
%EP$_{SF27\ vs.\ SN17}$ (%)	432.3	617.4	5.6	29.7	4.6	–31.4	–1.2	–7.6	–36.7	–18.9
EP of SN18 (W)	340.7	13.3	73.0	2.4	4675.2	445.3	5762.5	618.0	222.9	880.1
EP of SF28 (W)	335.8	14.2	26.6	1.3	4626.9	417.2	5736.4	615.2	411.4	1168.9
%EP$_{SF28\ vs.\ SN18}$ (%)	–1.4	6.9	–63.6	–47.4	–1.0	–6.3	–0.5	–0.5	84.6	32.8
EP of SN18 (W)	340.7	13.3	73.0	2.4	4675.2	445.3	5762.6	618.0	222.9	880.1
EP of SF29 (W)	340.4	14.8	216.9	10.0	4706.1	407.9	5756.4	587.4	0.0	0.0
%EP$_{SF29\ vs.\ SN18}$ (%)	–0.1	11.6	197.0	309.4	0.7	–8.4	–0.1	–5.0	–100.0	–100.0
EP of SN18 (W)	340.7	13.3	73.0	2.4	4675.2	445.3	5762.6	617.9	222.9	880.1
EP of SF30 (W)	350.4	15.9	483.4	24.5	4566.2	398.2	5736.5	606.2	0.0	0.0
%EP$_{SF30\ vs.\ SN18}$ (%)	2.8	19.9	562.0	905.4	–2.3	–10.6	–0.5	–1.9	–100.0	–100.0
Legend										
	$-10\% \leq \%\mu_{el}, \%\sigma_{el} \leq +10\%$									
	$+10\% < \%\mu_{el}, \%\sigma_{el} \leq +20\%$ OR $-20\% \leq \%\mu_{el}, \%\sigma_{el} < -10\%$									
	$\%\mu_{el}, \%\sigma_{el} > +20\%$ OR $\%\mu_{el}, \%\sigma_{el} < -20\%$									

Table 3b. Values of $\%\mu_{el}$ (calculated via Eq. 10) and $\%\sigma_{el}$ (calculated via Eq. 11) upon varying both the pair of tests under comparison as well as the AHU component, during winter.

	SAF		RAF		RS		HP		HUM	
	μ_{el} (W)	σ_{el} (W)	μ_{el} (W)	σ_{el} (W)	μ_{el} (W)	σ_{el} (W)	μ_{el} (W)	σ_{el} (W)	μ_{el} (W)	σ_{el} (W)
EP of WN2 (W)	349.1	16.3	75.6	3.3	4180.4	394.3	5283.8	800.4	2879.5	1374.5
EP of WF1 (W)	357.7	13.6	76.3	2.7	4153.6	365.3	5379.7	618.2	0.0	0.0
%EP$_{WF1\ vs.\ WN2}$ (%)	2.4	–16.4	0.8	–16.3	–0.6	–7.4	1.8	–22.8	–100.0	–100.0
EP of WN5 (W)	354.6	15.4	75.9	8.5	4113.7	385.0	5589.8	703.6	3212.2	884.0
EP of WF2 (W)	339.0	13.8	75.4	3.7	4118.8	368.4	5249.3	820.9	3354.0	715.0
%EP$_{WF2\ vs.\ WN5}$ (%)	–4.4	–10.6	–0.7	–56.0	0.1	–4.3	–6.1	16.7	4.4	–19.1
EP of WN1 (W)	342.7	14.4	75.1	2.7	4080.4	380.5	5265.9	926.6	0.0	0.0
EP of WF3 (W)	348.5	3.9	73.3	2.6	4099.2	358.7	5252.9	971.6	0.0	0.0
%EP$_{WF3\ vs.\ WN1}$ (%)	1.7	–73.1	–2.4	–1.9	0.5	–5.7	–0.2	4.9	N.A.	N.A.
EP of WN8 (W)	358.6	15.6	75.3	2.7	4636.1	435.7	5965.4	648.0	3143.2	976.4
EP of WF4 (W)	357.2	15.4	75.4	2.6	5231.2	485.1	5948.8	887.0	3172.3	939.2
%EP$_{WF4\ vs.\ WN8}$ (%)	–0.4	–1.4	0.1	–5.1	12.8	11.4	–0.3	36.9	0.9	–3.8
EP of WN6 (W)	353.1	14.9	75.6	3.3	4153.7	378.2	5552.0	801.2	3239.6	879.8
EP of WF5 (W)	352.8	14.8	75.8	2.7	4160.6	378.6	5549.0	786.9	0.0	0.0
%EP$_{WF5\ vs.\ WN6}$ (%)	–0.1	–0.3	0.3	–18.5	0.2	0.1	–0.1	–1.8	–100.0	–100.0

Finanziato dall'Unione europea NextGenerationEU | Ministero dell'Università e della Ricerca | Italiadomani PIANO NAZIONALE DI RIPRESA E RESILIENZA

EP of WN5 (W)	354.6	15.4	75.9	8.5	4113.7	385.0	5589.8	703.6	3212.2	884.0
EP of WF6 (W)	357.5	10.5	76.1	2.7	4141.7	354.6	5620.6	680.1	3040.0	1076.1
%EP$_{WF6\ vs.\ WN5}$ (%)	0.8	–32.1	0.2	–68.8	0.7	–7.9	0.6	–3.3	–5.4	21.7
EP of WN3 (W)	350.3	15.0	75.6	4.5	4020.0	388.5	5257.3	876.2	3059.2	1073.5
EP of WF7 (W)	346.7	14.1	75.6	2.6	4030.2	354.2	5268.8	832.2	3250.3	845.7
%EP$_{WF7\ vs.\ WN3}$ (%)	–1.0	–5.6	0.0	–41.8	0.3	–8.8	0.2	–5.0	6.2	–21.2
EP of WN7 (W)	358.6	15.9	75.8	2.8	4691.0	437.1	5955.5	826.2	0.0	0.0
EP of WF8 (W)	358.6	15.2	75.6	2.8	4704.9	439.2	6006.9	752.4	0.0	0.0
%EP$_{WF8\ vs.\ WN7}$ (%)	0.0	–3.9	–0.2	–0.9	0.3	0.5	0.9	–8.9	N.A.	N.A.
EP of WN4 (W)	346.5	14.2	75.6	2.7	4322.1	384.2	5343.1	762.4	0.0	0.0
EP of WF9 (W)	345.6	14.4	74.7	2.7	4277.7	410.3	5356.4	664.6	3263.2	830.3
%EP$_{WF9\ vs.\ WN4}$ (%)	–0.2	1.1	–1.2	3.7	–1.0	6.8	0.2	–12.8	∞	∞
EP of WN2 (W)	349.1	16.3	75.6	3.3	4180.4	394.3	5283.8	800.4	2879.5	1374.5
EP of WF10 (W)	341.0	16.8	16.9	0.1	4176.0	354.6	5283.4	848.8	3236.3	886.2
%EP$_{WF10\ vs.\ WN2}$ (%)	–2.3	3.0	–77.6	–97.9	–0.1	–10.1	0.0	6.0	12.4	–35.5
EP of WN2 (W)	349.1	16.3	75.6	3.3	4180.4	394.3	5283.8	800.4	2879.5	1374.5
EP of WF11 (W)	87.9	1.6	73.4	3.6	4219.7	389.9	5360.7	628.9	0.0	0.0
%EP$_{WF11\ vs.\ WN2}$ (%)	–74.8	–90.0	–2.9	8.9	0.9	–1.1	1.5	–21.4	–100.0	–100.0
EP of WN5 (W)	354.6	15.4	75.9	8.5	4129.1	385.0	5591.8	703.3	3210.9	884.0
EP of WF12 (W)	342.2	14.4	72.1	2.5	4340.1	395.7	5761.8	800.5	3171.1	967.1
%EP$_{WF12\ vs.\ WN5}$ (%)	–3.5	–6.7	–5.1	71.0	5.1	2.8	3.0	13.8	–1.2	9.4
EP of WN9 (W)	360.0	15.5	75.5	2.6	4190.2	375.4	5650.7	620.9	3292.3	816.1
EP of WF13 (W)	327.2	13.8	75.3	7.2	4646.3	415.9	5963.1	813.8	3279.1	796.7
%EP$_{WF13\ vs.\ WN9}$ (%)	–9.1	–11.5	–0.3	181.3	10.9	10.8	5.5	31.1	–0.4	–2.4
EP of WN5 (W)	354.6	15.4	75.9	8.5	4129.1	385.0	5591.8	703.3	3210.9	884.0
EP of WF14 (W)	352.8	14.9	75.4	2.6	4083.4	382.2	5670.7	828.8	0.0	0.0
%EP$_{WF14\ vs.\ WN5}$ (%)	–0.5	–3.1	–0.8	–69.3	–1.1	–0.8	1.4	17.9	–100.0	–100.0
EP of WN11(W)	354.9	15.3	75.1	2.7	4310.9	406.5	5715.8	785.3	0.0	0.0
EP of WF15 (W)	357.7	15.6	74.5	2.7	4475.1	468.9	5849.5	749.8	0.0	0.0
%EP$_{WF15\ vs.\ WN11}$ (%)	0.8	1.8	–0.1	–1.9	3.8	15.4	2.3	–4.5	N.A.	N.A.
EP of WN7 (W)	358.6	15.9	75.8	2.8	4707.3	437.1	5967.9	815.3	0.0	0.0
EP of WF16 (W)	328.2	14.1	75.4	2.7	4234.5	407.0	5693.2	735.0	0.0	0.0
%EP$_{WF16\ vs.\ WN7}$ (%)	–8.5	–11.0	–0.5	–5.0	–10.0	–6.9	–4.6	–9.8	N.A.	N.A.
EP of WN10 (W)	347.1	15.2	74.6	2.7	4379.9	410.3	5820.8	596.2	0.0	0.0
EP of WF17 (W)	354.8	15.1	75.2	2.6	4581.4	421.7	6008.5	641.9	0.0	0.0
%EP$_{WF17\ vs.\ WN10}$ (%)	0.0	–0.5	0.8	–3.0	4.6	2.8	3.2	7.7	N.A.	N.A.
EP of WN7 (W)	358.6	15.9	75.8	2.8	4707.3	437.1	6619.4	847.8	0.0	0.0
EP of WF18 (W)	357.8	16.2	74.3	2.6	4552.8	437.1	5935.2	809.7	0.0	0.0
%EP$_{WF18\ vs.\ WN7}$ (%)	–0.2	–2.1	–2.0	–7.4	–3.3	0.0	–10.3	–4.5	N.A.	N.A.
EP of WN12 (W)	358.2	15.8	74.9	2.7	3223.0	2105.5	6043.1	829.6	0.0	0.0
EP of W519 (W)	359.4	15.5	74.8	2.6	3261.5	2136.0	6102.6	764.9	0.0	0.0
%EP$_{WF19\ vs.\ WN12}$ (%)	0.3	–1.3	–0.2	–3.0	1.2	1.4	1.0	–7.8	N.A.	N.A.

Finanziato dall'Unione europea NextGenerationEU | Ministero dell'Università e della Ricerca | Italiadomani PIANO NAZIONALE DI RIPRESA E RESILIENZA

EP of WN12 (W)	358.2	15.8	74.9	2.7	3222.9	2105.4	6043.1	829.6	0.0	0.0
EP of WF20 (W)	357.4	15.1	75.0	2.7	3204.9	2102.3	6079.4	800.3	127.5	654.8
%EP$_{WF20\ vs.\ WN12}$ (%)	–0.2	–4.1	0.1	–0.6	–0.6	–0.1	0.6	–3.5	∞	∞
EP of WN15 (W)	350.9	15.0	74.8	2.6	3244.4	2121.9	6104.3	637.9	0.0	0.0
EP of WF21 (W)	350.2	14.6	74.3	2.6	3276.1	2132.0	6135.4	694.2	0.0	0.0
%EP$_{WF21\ vs.\ WN15}$ (%)	–0.2	–2.9	–0.7	–1.2	1.0	0.5	0.5	8.8	N.A.	N.A.
EP of WN13 (W)	354.2	14.8	74.5	2.6	3201.3	2091.2	6027.1	807.3	0.0	0.0
EP of WF22 (W)	346.7	13.7	74.4	2.5	3155.2	2045.7	6014.4	706.5	967.4	1655.8
%EP$_{WF22\ vs.\ WN13}$ (%)	–2.1	–7.0	–0.1	–3.5	–1.4	–2.2	–0.2	–12.5	∞	∞
EP of WN14 (W)	347.8	14.8	73.5	2.7	3282.9	2142.3	6082.3	676.1	0.0	0.0
EP of WF23 (W)	339.7	13.1	73.0	2.6	3286.2	2148.9	6113.9	625.1	961.0	1657.8
%EP$_{WF23\ vs.\ WN14}$ (%)	–2.4	–11.5	–0.8	–3.8	0.1	0.3	0.5	–7.5	∞	∞
EP of WN13 (W)	354.2	14.8	74.5	2.6	3201.1	2091.2	6027.2	807.3	0.0	0.0
EP of WF24 (W)	346.0	13.8	74.6	2.6	3169.8	2094.3	5985.6	718.5	1347.6	1819.8
%EP$_{WF24\ vs.\ WN13}$ (%)	–2.3	–6.8	0.2	–0.2	–1.0	0.1	–0.7	–11.0	∞	∞
EP of WN12 (W)	358.2	15.8	74.9	2.7	3222.8	2105.5	6043.0	829.6	0.0	0.0
EP of WF25 (W)	131.2	4.1	74.1	2.8	3151.6	2112.9	6093.9	941.8	0.0	0.0
%EP$_{WF25\ vs.\ WN12}$ (%)	–63.4	–73.9	–1.2	5.7	–2.2	0.3	0.8	13.5	N.A.	N.A.
EP of WN13 (W)	354.2	14.8	74.5	2.6	3201.2	2091.2	6027.2	807.3	0.0	0.0
EP of WF26 (W)	839.1	41.5	77.2	2.9	3187.2	2099.5	6058.9	738.6	634.0	1422.1
%EP$_{WF26\ vs.\ WN13}$ (%)	136.9	181.1	3.6	12.0	–0.4	0.4	0.5	–8.5	∞	∞
EP of WN12 (W)	358.2	15.8	74.9	2.7	3222.9	2105.5	6043.0	829.6	0.0	0.0
EP of WF27 (W)	1871.6	99.6	79.2	3.6	3219.5	2112.4	6086.9	717.6	1706.3	1904.8
%EP$_{WF27\ vs.\ WN12}$ (%)	422.5	531.9	5.7	34.0	–0.1	0.3	0.7	–13.5	∞	∞
EP of WN15 (W)	350.9	15.0	74.8	2.6	3244.5	2121.8	6104.4	637.9	0.0	0.0
EP of WF28 (W)	348.8	15.0	26.7	1.1	3270.3	2128.5	6110.8	703.0	0.0	0.0
%EP$_{WF28\ vs.\ WN15}$ (%)	–0.6	–0.3	–64.3	–57.2	0.8	0.3	0.1	10.2	N.A.	N.A.
EP of WN15 (W)	350.9	15.0	74.8	2.6	3244.5	2121.8	6104.3	637.9	0.0	0.0
EP of WF29 (W)	352.1	15.8	221.7	10.3	3240.7	2118.8	6071.1	663.4	0.0	0.0
%EP$_{WF29\ vs.\ WN15}$ (%)	0.3	5.3	196.2	295.6	–0.1	–0.1	–0.5	4.0	N.A.	N.A.
EP of WN16 (W)	356.7	14.9	74.7	2.6	3282.1	2149.3	6114.7	648.4	72.7	463.6
EP of WF30 (W)	360.9	17.2	475.9	23.5	3249.5	2125.2	6062.3	836.7	0.0	0.0
%EP$_{WF30\ vs.\ WN16}$ (%)	1.2	15.4	537.5	804.5	–1.0	–1.1	–0.9	29.0	–100.0	–100.0

Legend	
	$-10\% \le \%\mu_{el}, \%\sigma_{el} \le +10\%$
	$+10\% < \%\mu_{el}, \%\sigma_{el} \le +20\%$ OR $-20\% \le \%\mu_{el}, \%\sigma_{el} < -10\%$
	$\%\mu_{el}, \%\sigma_{el} > +20\%$ OR $\%\mu_{el}, \%\sigma_{el} < -20\%$

3. Effects of faults on daily electrical energy consumption

In this section the effects of the selected faults in terms of daily electric energy consumption are analysed. Tables 4a and b report the percentage difference %EE calculated as follows:

$$\%EE = \frac{\left(EE_{Faulty} - EE_{Baseline}\right)}{EE_{Baseline}} \cdot 100 \qquad (12)$$

Finanziato dall'Unione europea NextGenerationEU | Ministero dell'Università e della Ricerca | Italiadomani PIANO NAZIONALE DI RIPRESA E RESILIENZA

where EE_{Faulty} and $EE_{Baseline}$ are, respectively, the daily electric energy consumption during faulty and corresponding normal experiment. The cells in Tables 4a and b are filled in yellow if %EE is included in the range ±10%, in red if %Eel is greater than 20% or lower than –20%, in orange in other cases (the symbol N.A. denotes that the AHU component has not been activated during both tests and the calculation of $\%E_{el}$ is not applicable, while the symbol '∞' indicates that the AHU component has not been activated only during the normal test).

Table 4a. Values of %EE (calculated via Eq. 12) as function of both normal/faulty test and AHU component, during summer.

	SAF	RAF	RS + PRS	HP + PHP	HUM	TOTAL
EE of SN4 (kWh)	3.1	0.7	26.0	10.1	4.3	44.1
EE of SF1 (kWh)	3.2	0.7	26.3	0.0	0.0	30.2
%EE$_{SF1\ vs.\ SN4}$ (%)	3.3	0.8	1.3	–100.0	–100.0	–31.6
EE of SN5 (kWh)	3.1	0.7	23.7	8.6	5.7	41.8
EE of SF2 (kWh)	3.1	0.7	28.8	16.0	19.6	68.2
%EE$_{SF2\ vs.\ SN5}$ (%)	–1.0	–0.8	21.6	86.5	244.1	63.3
EE of SN5 (kWh)	3.1	0.7	23.7	8.6	5.7	41.8
EE of SF3 (kWh)	3.1	0.7	3.8	0.0	0.6	8.1
%EE$_{SF3\ vs.\ SN5}$ (%)	–1.1	–0.9	–84.1	–100.0	–88.7	–80.5
EE of SN4 (kWh)	3.1	0.7	26.0	10.1	4.3	44.1
EE of SF4 (kWh)	3.1	0.7	28.6	9.4	6.0	47.7
%EE$_{SF4\ vs.\ SN4}$ (%)	1.1	0.5	10.0	–7.7	40.3	8.1
EE of SN2 (kWh)	3.0	0.7	28.5	9.3	5.1	46.6
EE of SF5 (kWh)	3.1	0.7	20.5	7.9	0.0	32.2
%EE$_{SF5\ vs.\ SN2}$ (%)	2.1	–0.4	–28.0	–14.9	–100.0	–30.9
EE of SN1 (kWh)	3.1	0.7	22.4	9.6	5.3	41.0
EE of SF6 (kWh)	3.1	0.7	25.9	4.9	0.0	34.6
%EE$_{SF6\ vs.\ SN1}$ (%)	0.8	–1.2	16.0	–49.0	–100.0	–15.7
EE of SN4 (kWh)	3.1	0.7	26.0	10.1	4.3	44.1
EE of SF7 (kWh)	3.0	0.7	22.6	13.2	10.3	49.8
%EE$_{SF7\ vs.\ SN4}$ (%)	–1.3	0.0	–12.9	30.6	140.3	12.9
EE of SN2 (kWh)	3.0	0.7	28.5	9.3	5.1	46.6
EE of SF8 (kWh)	3.0	0.7	29.6	10.5	0.0	43.8
%EE$_{SF8\ vs.\ SN2}$ (%)	–0.4	–0.1	4.0	13.2	–100.0	–5.8
EE of SN3 (kWh)	3.0	0.7	28.5	10.3	4.4	46.9
EE of SF9 (kWh)	3.0	0.7	29.7	3.2	25.2	61.8
%EE$_{SF9\ vs.\ SN3}$ (%)	–1.4	–0.2	4.0	–68.7	471.6	31.6
EE of SN5 (kWh)	3.1	0.7	23.7	8.6	5.7	41.8
EE of SF10 (kWh)	3.0	0.2	22.1	9.6	5.5	40.3
%EE$_{SF10\ vs.\ SN5}$ (%)	–3.3	–77.1	–6.8	11.5	–3.6	–3.5
EE of SN6 (kWh)	3.0	0.7	24.8	10.6	0.0	39.0
EE of SF11 (kWh)	0.8	0.6	13.9	0.2	0.0	15.6
%EE$_{SF11\ vs.\ SN6}$ (%)	–72.5	–3.6	–43.8	–98.2	N.A.	–60.1
EE of SN9 (kWh)	3.2	0.7	30.0	10.7	6.7	51.8
EE of SF12 (kWh)	3.1	0.6	29.1	9.5	5.7	48.4
%EE$_{SF12\ vs.\ SN9}$ (%)	–2.5	–3.1	–4.5	–20.2	–15.7	–7.5
EE of SN7 (kWh)	3.1	0.7	32.2	10.5	4.5	51.2
EE of SF13 (kWh)	3.1	0.7	30.4	11.5	4.4	50.5

Finanziato dall'Unione europea NextGenerationEU | Ministero dell'Università e della Ricerca | Italiadomani PIANO NAZIONALE DI RIPRESA E RESILIENZA

	SAF	RAF	RS + PRS	HP + PHP	HUM	TOTAL
%EE$_{SF13\ vs.\ SN7}$ (%)	1.3	0.0	–13.8	15.8	–3.1	–1.4
EE of SN11 (kWh)	3.0	0.7	26.5	9.6	6.2	46.3
EE of SF14 (kWh)	3.1	0.7	27.0	9.8	5.8	46.6
%EE$_{SF14\ vs.\ SN11}$ (%)	1.7	0.0	2.9	3.9	–7.6	0.6
EE of SN10 (kWh)	3.1	0.7	31.7	9.8	5.5	50.9
EE of SF15 (kWh)	3.1	0.6	32.1	9.6	5.0	50.7
%EE$_{SF15\ vs.\ SN10}$ (%)	1.0	–1.5	5.1	–3.7	–8.7	–0.4
EE of SN8 (kWh)	3.2	0.7	30.2	11.4	4.9	50.8
EE of SF16 (kWh)	3.1	0.7	28.1	9.6	6.2	47.9
%EE$_{SF16\ vs.\ SN8}$ (%)	–4.1	0.0	–11.6	–28.2	25.4	–5.6
EE of SN11 (kWh)	3.0	0.7	26.5	9.6	6.2	46.3
EE of SF17 (kWh)	3.1	0.7	27.2	9.5	6.4	47.1
%EE$_{SF17\ vs.\ SN11}$ (%)	1.3	0.0	5.3	–0.1	2.6	1.8
EE of SN12 (kWh)	3.1	0.7	20.0	12.7	7.1	43.8
EE of SF18 (kWh)	3.1	0.7	21.4	13.1	7.0	45.4
%EE$_{SF18\ vs.\ SN12}$ (%)	–0.7	–1.5	8.5	9.2	–1.4	3.8
EE of SN13 (kWh)	3.0	0.7	33.5	9.9	1.0	48.1
EE of SF19 (kWh)	3.0	0.7	28.3	8.5	0.0	40.4
%EE$_{SF19\ vs.\ SN13}$ (%)	–0.6	–0.9	–15.7	–13.9	–100.0	–16.0
EE of SN13 (kWh)	3.0	0.7	33.5	9.9	1.0	48.1
EE of SF20 (kWh)	3.0	0.6	31.0	10.0	0.1	44.7
%EE$_{SF20\ vs.\ SN13}$ (%)	–2.1	–2.9	–7.5	1.5	–88.9	–7.0
EE of SN13 (kWh)	3.0	0.7	33.5	9.9	1.0	48.1
EE of SF21 (kWh)	3.0	0.7	33.2	11.1	0.6	48.6
%EE$_{SF21\ vs.\ SN13}$ (%)	0.9	–0.7	–1.0	12.0	–43.3	0.9
EE of SN14 (kWh)	3.0	0.7	23.9	10.3	3.1	41.0
EE of SF22 (kWh)	3.0	0.6	27.2	20.9	14.1	65.8
%EE$_{SF22\ vs.\ SN14}$ (%)	1.3	–1.2	13.6	102.6	351.0	60.7
EE of SN15 (kWh)	2.9	0.6	25.9	9.7	3.5	42.6
EE of SF23 (kWh)	2.9	0.6	28.4	19.3	18.8	70.0
%EE$_{SF23\ vs.\ SN15}$ (%)	–1.3	–0.5	9.9	98.0	439.4	64.2
EE of SN14 (kWh)	3.0	0.7	23.9	10.3	3.1	41.0
EE of SF24 (kWh)	2.9	0.7	27.1	19.4	18.6	68.6
%EE$_{SF24\ vs.\ SN14}$ (%)	–2.3	–0.4	13.5	87.8	493.3	67.6
EE of SN17 (kWh)	3.1	0.7	25.9	12.6	2.0	44.3
EE of SF25 (kWh)	1.2	0.6	18.2	0.2	0.0	20.3
%EE$_{SF25\ vs.\ SN17}$ (%)	–60.3	–2.0	–29.9	–98.1	–100.0	–54.2
EE of SN16 (kWh)	3.1	0.7	29.4	10.9	2.6	46.7
EE of SF26 (kWh)	7.2	0.7	33.2	17.0	3.0	61.1
%EE$_{SF26\ vs.\ SN16}$ (%)	130.1	2.8	12.9	56.8	13.1	30.9
EE of SN17 (kWh)	3.1	0.7	25.9	12.6	2.0	44.3
EE of SF27 (kWh)	16.4	0.7	39.8	17.1	1.3	75.2
%EE$_{SF27\ vs.\ SN17}$ (%)	432.3	5.6	53.3	35.7	–36.7	69.8
EE of SN18 (kWh)	3.1	0.7	25.3	12.7	2.0	43.8
EE of SF28 (kWh)	3.0	0.2	25.1	13.2	3.7	45.2
%EE$_{SF28\ vs.\ SN18}$ (%)	–1.4	–63.6	–1.1	3.9	84.6	3.3

Finanziato dall'Unione europea NextGenerationEU
Ministero dell'Università e della Ricerca
Italiadomani PIANO NAZIONALE DI RIPRESA E RESILIENZA

	SAF	RAF	RS + PRS	HP + PHP	HUM	TOTAL
EE of SN18 (kWh)	3.1	0.7	25.3	12.7	2.0	43.8
EE of SF29 (kWh)	3.1	2.0	26.7	11.3	0.0	43.0
%EE$_{SF29\ vs.\ SN18}$ (%)	–0.1	197.0	5.3	–11.4	–100.0	–1.9
EE of SN18 (kWh)	3.1	0.7	25.3	12.7	2.0	43.8
EE of SF30 (kWh)	3.2	4.4	26.0	12.6	0.0	46.1
%EE$_{SF30\ vs.\ SN18}$ (%)	2.8	562.0	2.5	–1.2	–100.0	5.2
Legend						
	–10% ≤ %EE ≤ +10%					
	+10% < %EE ≤ +20% OR –20% ≤ % EE < –10%					
	% EE > +20% OR % EE < –20%					

Table 4b. Values of %EE (calculated via Eq. 12) as function of both normal/faulty test and AHU component, during winter.

	SAF	RAF	RS + PRS	HP + PHP	HUM	TOTAL
EE of WN2 (kWh)	3.1	0.7	14.4	10.0	0.4	28.7
EE of WF1 (kWh)	3.2	0.7	13.4	0.6	0.0	17.9
%EE$_{WF1\ vs.\ WN2}$ (%)	2.4	0.8	–7.3	–94.5	–100.0	–37.8
EE of WN5 (kWh)	3.2	0.7	13.3	7.2	3.5	27.9
EE of WF2 (kWh)	3.1	0.7	15.5	21.3	10.5	51.0
%EE$_{WF2\ vs.\ WN5}$ (%)	–4.4	–0.7	16.9	194.9	196.7	82.8
EE of WN1 (kWh)	3.1	0.7	12.9	13.6	0.0	30.2
EE of WF3 (kWh)	3.1	0.7	1.5	2.6	0.0	8.0
%EE$_{WF3\ vs.\ WN1}$ (%)	1.7	–2.4	–88.0	–80.7	N.A.	–73.6
EE of WN8 (kWh)	3.2	0.7	15.1	14.2	2.7	35.9
EE of WF4 (kWh)	3.2	0.7	15.2	15.1	3.6	37.8
%EE$_{WF4\ vs.\ WN8}$ (%)	–0.4	0.1	0.3	6.8	33.9	5.3
EE of WN6 (kWh)	3.2	0.7	13.1	6.9	4.1	28.0
EE of WF5 (kWh)	3.2	0.7	13.0	6.7	0.0	23.6
%EE$_{WF5\ vs.\ WN6}$ (%)	–0.1	0.3	–0.4	–3.1	–100.0	–15.6
EE of WN5 (kWh)	3.2	0.7	13.3	7.2	3.5	27.9
EE of WF6 (kWh)	3.2	0.7	14.6	1.4	1.6	21.5
%EE$_{WF6\ vs.\ WN5}$ (%)	0.8	0.2	9.8	–80.1	–54.5	–22.9
EE of WN3 (kWh)	3.2	0.7	13.0	12.5	1.6	31.0
EE of WF7 (kWh)	3.1	0.7	11.7	17.7	5.1	38.3
%EE$_{WF7\ vs.\ WN3}$ (%)	–1.0	0.0	–9.8	41.1	212.0	23.7
EE of WN7 (kWh)	3.2	0.7	15.4	12.8	0.0	32.2
EE of WF8 (kWh)	3.2	0.7	15.7	13.4	0.0	33.0
%EE$_{WF8\ vs.\ WN7}$ (%)	0.0	–0.2	1.7	4.2	N.A.	2.5
EE of WN4 (kWh)	3.1	0.7	16.0	10.9	0.0	30.7
EE of WF9 (kWh)	3.1	0.7	14.8	7.4	8.9	34.8
%EE$_{WF9\ vs.\ WN4}$ (%)	–0.2	–1.2	–7.9	–32.3	∞	13.2
EE of WN2 (kWh)	3.1	0.7	14.4	10.0	0.4	28.7
EE of WF10 (kWh)	3.1	0.2	11.9	12.3	3.5	30.9
%EE$_{WF10\ vs.\ WN2}$ (%)	–2.3	–77.6	–17.6	23.0	732.3	7.9
EE of WN2 (kWh)	3.1	0.7	14.4	10.0	0.4	28.7
EE of WF11 (kWh)	0.8	0.7	10.2	8.0	0.0	19.6

Finanziato dall'Unione europea NextGenerationEU
Ministero dell'Università e della Ricerca
Italiadomani PIANO NAZIONALE DI RIPRESA E RESILIENZA

	SAF	RAF	RS + PRS	HP + PHP	HUM	TOTAL
%EE$_{WF11\ vs.\ WN2}$ (%)	–74.8	–2.9	–29.3	–20.1	–100.0	–31.5
EE of WN5 (kWh)	3.2	0.7	13.2	7.2	3.5	28.0
EE of WF12 (kWh)	3.1	0.7	12.4	13.0	2.5	31.8
%EE$_{WF12\ vs.\ WN5}$ (%)	–3.5	–4.4	–12.0	191.0	–28.4	13.6
EE of WN9 (kWh)	3.2	0.7	14.2	13.6	5.3	37.5
EE of WF13 (kWh)	2.9	0.7	14.6	13.6	0.5	32.5
%EE$_{WF13\ vs.\ WN9}$ (%)	–9.3	0.0	7.0	3.4	–90.9	–13.3
EE of WN5 (kWh)	3.2	0.7	13.2	7.2	3.5	28.0
EE of WF14 (kWh)	3.2	0.7	13.2	13.5	0.0	30.8
%EE$_{WF14\ vs.\ WN5}$ (%)	–0.3	0.0	0.8	195.8	–100.0	9.9
EE of WN11(kWh)	3.2	0.7	14.5	9.7	0.0	28.3
EE of WF15 (kWh)	3.2	0.7	15.3	12.5	0.0	31.9
%EE$_{WF15\ vs.\ WN11}$ (%)	0.9	–1.5	9.8	55.1	N.A.	12.6
EE of WN7 (kWh)	3.2	0.7	15.3	12.8	0.0	32.3
EE of WF16 (kWh)	3.0	0.7	14.8	12.7	0.0	31.3
%EE$_{WF16\ vs.\ WN7}$ (%)	–8.7	0.0	–6.8	0.0	N.A.	–3.1
EE of WN10 (kWh)	3.1	0.7	14.6	11.3	0.0	29.9
EE of WF17 (kWh)	3.2	0.7	14.6	12.7	0.0	31.4
%EE$_{WF17\ vs.\ WN10}$ (%)	2.2	1.5	0.1	24.2	N.A.	4.9
EE of WN7 (kWh)	3.2	0.7	15.3	12.8	0.0	32.3
EE of WF18 (kWh)	3.2	0.7	15.7	12.7	0.0	32.5
%EE$_{WF18\ vs.\ WN7}$ (%)	0.3	–1.5	3.8	–0.7	N.A.	0.6
EE of WN12 (kWh)	3.2	0.7	16.0	12.2	0.0	32.0
EE of W519 (kWh)	3.2	0.7	15.9	11.6	0.0	31.4
%EE$_{WF19\ vs.\ WN12}$ (%)	0.3	–0.2	–0.5	–4.7	N.A.	–2.0
EE of WN12 (kWh)	3.2	0.7	16.0	12.2	0.0	32.0
EE of WF20 (kWh)	3.2	0.7	15.7	13.6	1.1	34.3
%EE$_{WF20\ vs.\ WN12}$ (%)	–0.2	0.1	–1.7	11.5	∞	7.1
EE of WN15 (kWh)	3.2	0.7	16.5	12.8	0.0	33.1
EE of WF21 (kWh)	3.2	0.7	16.7	13.1	0.0	33.6
%EE$_{WF21\ vs.\ WN15}$ (%)	–0.2	–0.7	1.1	2.2	N.A.	1.4
EE of WN13 (kWh)	3.2	0.7	15.9	11.3	0.0	31.0
EE of WF22 (kWh)	3.1	0.7	17.4	25.4	8.7	55.4
%EE$_{WF22\ vs.\ WN13}$ (%)	–2.1	–0.1	9.6	125.8	∞	78.5
EE of WN14 (kWh)	3.1	0.7	18.0	10.5	0.0	32.2
EE of WF23 (kWh)	3.1	0.7	19.4	24.9	8.6	56.6
%EE$_{WF23\ vs.\ WN14}$ (%)	–2.4	–0.8	7.9	137.5	∞	75.7
EE of WN13 (kWh)	3.2	0.7	15.9	11.3	0.0	31.0
EE of WF24 (kWh)	3.1	0.7	18.5	26.2	12.1	60.6
%EE$_{WF24\ vs.\ WN13}$ (%)	–2.3	0.2	16.3	132.8	∞	95.4
EE of WN12 (kWh)	3.2	0.7	16.0	12.2	0.0	32.0
EP of WF25 (kWh)	1.2	0.7	12.1	7.1	0.0	21.1
%EE$_{WF25\ vs.\ WN12}$ (%)	–63.4	–1.2	–24.0	–41.3	N.A.	–34.0
EE of WN13 (kWh)	3.2	0.7	15.9	11.3	0.0	31.0
EE of WF26 (kWh)	7.6	0.7	18.3	16.9	5.7	49.1
%EE$_{WF26\ vs.\ WN13}$ (%)	136.9	3.6	14.8	49.9	∞	58.3

Finanziato dall'Unione europea NextGenerationEU
Ministero dell'Università e della Ricerca
Italiadomani PIANO NAZIONALE DI RIPRESA E RESILIENZA

	SAF	RAF	RS + PRS	HP + PHP	HUM	TOTAL
EE of WN12 (kWh)	3.2	0.7	16.0	12.2	0.0	32.0
EE of WF27 (kWh)	16.8	0.7	21.1	13.9	15.4	67.9
%EE$_{WF27\ vs.\ WN12}$ (%)	422.5	5.7	32.0	14.4	∞	112.0
EE of WN15 (kWh)	3.2	0.7	16.5	12.8	0.0	33.1
EE of WF28 (kWh)	3.1	0.2	15.1	14.0	0.0	32.5
%EE$_{WF28\ vs.\ WN15}$ (%)	–0.6	–64.3	–8.5	9.5	N.A.	–1.9
EE of WN15 (kWh)	3.2	0.7	16.5	12.8	0.0	33.1
EE of WF29 (kWh)	3.2	2.0	17.1	10.1	0.0	32.4
%EE$_{WF29\ vs.\ WN15}$ (%)	0.3	196.2	3.9	–20.9	N.A.	–2.1
EE of WN16 (kWh)	3.2	0.7	17.1	12.1	0.7	33.7
EE of WF30 (kWh)	3.2	4.3	17.5	12.6	0.0	37.6
%EE$_{WF30\ vs.\ WN16}$ (%)	1.2	537.5	2.3	3.9	–100.0	11.4

Legend	
	–10% ≤ %EE ≤ +10%
	+10% < %EE ≤ +20% OR –20% ≤ % EE < –10%
	% EE > +20% OR % EE < –20%

4. Effects of faults on operational costs

In this section the effects of the selected faults in terms of daily operating costs are discussed. The percentage difference %OC between faulty and corresponding normal tests in terms of operating costs is calculated as follows:

$$\%OC = \frac{\left(OC_{Faulty} - OC_{Baseline}\right)}{OC_{Baseline}} \cdot 100 = \frac{\sum_i UC_{el,i} \cdot P_{el,Faulty,i} \cdot ETS - \sum_i UC_{el,i} \cdot P_{el,Baseline,i} \cdot ETS}{\sum_i UC_{el,i} \cdot P_{el,Baseline,i} \cdot ETS} \cdot 100 \quad (13)$$

where OC_{Faulty} and $OC_{Baseline}$ are, respectively, the operational costs during the faulty test and the corresponding normal experiment, $P_{el,Faulty,i}$ and $P_{el,Baseline,i}$ are, respectively, the electric power demand in the case of the faulty test and the corresponding normal test at the i-th time step, $UC_{el,i}$ is the unit cost of electricity purchased from the grid at the same i-th time step, and ETS is the experimental data acquisition time step (equal to 1 second).

Tables 5a and b report the values of %OC upon varying both the pair of tests under comparison and AHU component during cooling and heating seasons, respectively. The cells in Tables 5a and b are filled in yellow if %OC is included in the range ±10%, in red if %OC is greater than 20% or lower than –20%, in orange in other cases (the symbol N.A. denotes that the AHU component has not been activated during both tests and the calculation of %OC is not possible, while the symbol '∞' indicates that the AHU component has not been activated only during the normal test).

Table 5a. Values of %OC (calculated via Eq. 13) as a function of both pairs of tests under comparison and AHU component, during summer.

	SAF	RAF	RS + PRS	HP + PHP	HUM	TOTAL
OC of SN4 (€)	0.4	0.1	3.4	1.3	0.6	5.8
OC of SF1 (€)	0.4	0.1	3.5	0.0	0.0	4.0
%OC$_{SF1\ vs.\ SN4}$ (%)	3.4	0.7	1.5	–100.0	–100.0	–31.6
OC of SN5 (€)	0.4	0.1	3.1	1.1	0.8	5.5
OC of SF2 (€)	0.4	0.1	3.8	2.1	2.6	9.0
%OC$_{SF2\ vs.\ SN5}$ (%)	–1.0	–0.7	21.4	86.9	241.3	62.8
OC of SN5 (€)	0.4	0.1	3.1	1.1	0.7	5.4
OC of SF3 (€)	0.4	0.1	0.5	0.0	0.1	1.0
%OC$_{SF3\ vs.\ SN5}$ (%)	–1.0	–0.8	–84.2	–100.0	–89.7	–80.7

Finanziato dall'Unione europea NextGenerationEU | Ministero dell'Università e della Ricerca | Italiadomani PIANO NAZIONALE DI RIPRESA E RESILIENZA

	SAF	RAF	RS + PRS	HP + PHP	HUM	TOTAL
OC of SN4 (€)	0.3	0.1	2.8	1.1	0.5	4.8
OC of SF4 (€)	0.3	0.1	3.1	1.0	0.6	5.2
%$OC_{SF4\ vs.\ SN4}$ (%)	1.1	0.5	10.2	–8.2	38.6	7.9
OC of SN2 (€)	0.4	0.1	3.4	1.1	0.6	5.6
OC of SF5 (€)	0.4	0.1	2.5	1.0	0.0	3.9
%$OC_{SF5\ vs.\ SN2}$ (%)	2.1	–0.4	–27.8	–14.5	–100.0	–30.7
OC of SN1 (€)	0.3	0.1	2.4	1.0	0.6	4.5
OC of SF6 (€)	0.3	0.1	2.8	0.5	0.0	3.8
%$OC_{SF6\ vs.\ SN1}$ (%)	0.8	–1.2	16.3	–50.3	–100.0	–15.7
OC of SN4 (€)	0.4	0.1	3.0	1.2	0.5	5.0
OC of SF7 (€)	0.3	0.1	2.6	1.5	1.2	5.7
%$OC_{SF7\ vs.\ SN4}$ (%)	–1.3	0.0	–12.8	30.5	140.3	13.0
OC of SN2 (€)	0.3	0.1	3.0	1.0	0.5	4.9
OC of SF8 (€)	0.3	0.1	3.1	1.1	0.0	4.6
%$OC_{SF8\ vs.\ SN2}$ (%)	–0.4	–0.1	4.0	13.1	–100.0	–5.9
OC of SN3 (€)	0.4	0.1	3.3	1.2	0.5	5.5
OC of SF9 (€)	0.4	0.1	3.5	0.4	3.0	7.2
%$OC_{SF9\ vs.\ SN3}$ (%)	–1.5	–0.2	4.2	–68.9	465.0	31.7
OC of SN5 (€)	0.4	0.1	3.3	1.2	0.8	5.8
OC of SF10 (€)	0.4	0.0	3.0	1.3	0.8	5.6
%$OC_{SF10\ vs.\ SN5}$ (%)	–3.3	–77.1	–7.2	11.5	–2.7	–3.6
OC of SN6 (€)	0.4	0.1	3.5	1.5	0.0	5.4
OC of SF11 (€)	0.1	0.1	1.9	0.0	0.0	2.2
%$OC_{SF11\ vs.\ SN6}$ (%)	–72.5	–3.6	–43.7	–98.1	N.A.	–60.0
OC of SF12 (€)	1.6	0.3	15.5	3549.1	3.5	3570.0
OC of SN9 (€)	1.6	0.3	15.1	3163.3	2.9	3183.2
%$OC_{SF12\ vs.\ SN9}$ (%)	–2.5	–3.0	–2.7	–10.9	–15.5	–10.8
OC of SF13 (€)	1.3	0.3	13.8	4106.7	1.9	4124.1
OC of SN7 (€)	1.3	0.3	13.1	4486.2	1.8	4502.8
%$OC_{SF13\ vs.\ SN7}$ (%)	1.3	0.5	–5.4	9.2	–4.1	9.2
OC of SF14 (€)	2.4	0.5	20.8	3702.5	4.9	3731.0
OC of SN11 (€)	2.4	0.5	21.2	3753.0	4.5	3781.6
%$OC_{SF14\ vs.\ SN11}$ (%)	1.8	0.5	1.9	1.4	–8.0	1.4
OC of SF15 (€)	1.8	0.4	18.2	3960.0	3.2	3983.5
OC of SN10 (€)	1.8	0.4	18.4	3911.5	2.9	3934.9
%$OC_{SF15\ vs.\ SN10}$ (%)	0.9	–1.7	1.1	–1.2	–9.2	–1.2
OC of SF16 (€)	1.5	0.3	14.3	4301.5	2.3	4319.9
OC of SN8 (€)	1.5	0.3	13.4	3620.5	2.9	3638.6
%$OC_{SF16\ vs.\ SN8}$ (%)	–4.1	–0.3	–6.4	–15.8	25.4	–15.8
OC of SF17 (€)	1.7	0.4	14.6	3617.5	3.4	3637.4
OC of SN11 (€)	1.7	0.4	14.9	3586.2	3.5	3606.7
%$OC_{SF17\ vs.\ SN11}$ (%)	1.5	0.9	2.7	–0.9	2.6	–0.8
OC of SF18 (€)	1.1	0.2	7.4	4109.7	2.5	4121.0

Finanziato dall'Unione europea NextGenerationEU
Ministero dell'Università e della Ricerca
Italiadomani PIANO NAZIONALE DI RIPRESA E RESILIENZA

	SAF	RAF	RS + PRS	HP + PHP	HUM	TOTAL
OC of SN12 (€)	1.1	0.2	7.8	4202.0	2.5	4213.7
%OC$_{SF18\ vs.\ SN12}$ (%)	–0.7	–0.9	5.9	2.2	–0.4	2.2
OC of SN13 (€)	0.3	0.1	0.1	3.7	1.1	5.3
OC of SF19 (€)	0.3	0.1	0.0	3.1	0.9	4.5
%OC$_{SF19\ vs.\ SN13}$ (%)	–0.6	–0.8	–100.0	–15.6	–13.9	–15.7
OC of SN13 (€)	0.3	0.1	0.1	3.9	1.1	5.6
OC of SF20 (€)	0.3	0.1	0.0	3.6	1.2	5.2
%OC$_{SF20\ vs.\ SN13}$ (%)	–2.1	–2.8	–88.9	–7.5	1.6	–7.0
OC of SN13 (€)	0.3	0.1	0.1	3.6	1.1	5.2
OC of SF21 (€)	0.3	0.1	0.1	3.6	1.2	5.3
%OC$_{SF21\ vs.\ SN13}$ (%)	0.8	–0.7	–47.3	–1.1	12.2	0.7
OC of SN14 (€)	0.3	0.1	0.3	2.4	1.0	4.1
OC of SF22 (€)	0.3	0.1	1.4	2.7	2.1	6.6
%OC$_{SF22\ vs.\ SN14}$ (%)	1.2	–1.1	361.2	13.4	104.4	60.4
OC of SN15 (€)	0.3	0.1	0.4	2.8	1.1	4.6
OC of SF23 (€)	0.3	0.1	2.0	3.1	2.1	7.5
%OC$_{SF23\ vs.\ SN15}$ (%)	–1.4	–0.4	454.9	9.6	98.4	63.9
OC of SN14 (€)	0.3	0.1	0.3	2.3	1.0	4.0
OC of SF24 (€)	0.3	0.1	1.8	2.6	1.9	6.7
%OC$_{SF24\ vs.\ SN14}$ (%)	–2.3	–0.5	510.0	12.9	89.9	67.3
OC of SN17 (€)	0.4	0.1	0.2	3.4	1.7	5.9
OC of SF25 (€)	0.2	0.1	0.0	2.4	0.0	2.7
%OC$_{SF25\ vs.\ SN17}$ (%)	–60.5	–2.1	–100.0	–29.6	–97.7	–53.8
OC of SN16 (€)	0.4	0.1	0.3	3.3	1.2	5.2
OC of SF26 (€)	0.8	0.1	0.3	3.7	2.0	6.9
%OC$_{SF26\ vs.\ SN16}$ (%)	129.9	2.9	17.7	12.3	57.1	31.1
OC of SN17 (€)	0.4	0.1	0.2	3.6	1.8	6.2
OC of SF27 (€)	2.3	0.1	0.2	5.5	2.5	10.6
%OCS$_{F27\ vs.\ SN17}$ (%)	431.6	5.6	–10.8	51.8	35.3	70.7
OC of SN18 (€)	0.5	0.1	0.3	4.0	2.0	6.9
OC of SF28 (€)	0.5	0.0	0.6	4.0	2.1	7.2
%OC$_{SF28\ vs.\ SN18}$ (%)	–1.5	–63.7	95.0	–1.0	3.6	3.5
OC of SN18 (€)	0.4	0.1	0.3	3.6	1.9	6.3
OC of SF29 (€)	0.4	0.3	0.0	3.8	1.7	6.2
%OCS$_{F29\ vs.\ SN18}$ (%)	0.0	197.1	–100.0	5.4	–11.5	–1.6
OC of SN18 (€)	0.4	0.1	0.2	3.5	1.8	6.1
OC of SF30 (€)	0.4	0.6	0.0	3.6	1.8	6.5
%OC$_{SF30\ vs.\ SN18}$ (%)	2.9	562.1	–100.0	3.0	–1.9	6.0
Legend						
	–10% ≤ %OC ≤ +10%					
	+10% < %OC ≤ +20% OR –20% ≤ %OC < –10%					
	%OC > +20% OR %OC < –20%					

Table 5b. Values of %OC (calculated via Eq. 13) as a function of both pairs of tests under comparison and AHU component, during summer.

Finanziato dall'Unione europea NextGenerationEU | Ministero dell'Università e della Ricerca | Italiadomani PIANO NAZIONALE DI RIPRESA E RESILIENZA

	SAF	RAF	RS + PRS	HP + PHP	HUM	TOTAL
OC of WN2 (€)	1.2	0.3	5.7	3.9	0.2	11.3
OC of WF1 (€)	1.3	0.3	5.3	0.2	0.0	7.0
%$OC_{WF1\ vs.\ WN2}$ (%)	2.4	0.8	–7.3	–94.4	–100.0	–37.9
OC of WN5 (€)	1.0	0.2	4.3	2.4	1.1	9.1
OC of WF2 (€)	1.0	0.2	5.1	7.0	3.4	16.6
%$OC_{WF2\ vs.\ WN5}$ (%)	–4.4	–0.7	16.6	192.3	193.8	82.0
OC of WN1 (€)	0.8	0.2	3.2	3.4	0.0	7.5
OC of WF3 (€)	0.8	0.2	0.4	0.7	0.0	2.0
%$OC_{WF3\ vs.\ WN1}$ (%)	1.7	–2.4	–87.9	–80.4	N.A.	–73.5
OC of WN8 (€)	1.5	0.3	6.8	6.5	1.2	16.3
OC of WF4 (€)	1.5	0.3	6.9	7.0	1.6	17.2
%$OC_{WF4\ vs.\ WN8}$ (%)	–0.4	0.1	0.3	7.3	34.3	5.5
OC of WN6 (€)	0.7	0.2	2.9	1.6	0.9	6.2
OC of WF5 (€)	0.7	0.2	2.9	1.5	0.0	5.3
%$OC_{WF5\ vs.\ WN6}$ (%)	–0.1	0.3	–0.6	–2.6	–100.0	–15.3
OC of WN5 (€)	0.7	0.2	3.0	1.7	0.8	6.3
OC of WF6 (€)	0.7	0.2	3.3	0.3	0.3	4.8
%$OC_{WF6\ vs.\ WN5}$ (%)	0.9	0.1	9.4	–80.0	–57.7	–23.8
OC of WN3 (€)	1.5	0.3	6.1	6.0	0.8	14.7
OC of WF7 (€)	1.5	0.3	5.5	8.4	2.4	18.2
%$OC_{WF7\ vs.\ WN4}$ (%)	–1.0	0.0	–9.7	40.8	210.5	23.6
OC of WN7 (€)	0.8	0.2	3.6	3.2	0.0	7.7
OC of WF8 (€)	0.8	0.2	3.7	3.3	0.0	8.0
%$OC_{WF8\ vs.\ WN7}$ (%)	0.0	–0.3	2.9	4.2	N.A.	3.1
OC of WN4 (€)	0.8	0.2	3.9	2.7	0.0	7.5
OC of WF9 (€)	0.8	0.2	3.6	1.8	2.1	8.4
%$OC_{WF9\ vs.\ WN4}$ (%)	–0.2	–1.2	–8.1	–32.9	∞	12.7
OC of WN2 (€)	1.3	0.3	5.8	4.0	0.2	11.5
OC of WF10 (€)	1.2	0.1	4.7	4.9	1.4	12.4
%$OC_{WF10\ vs.\ WN2}$ (%)	–2.3	–77.6	–17.8	23.5	665.1	7.9
OC of WN2 (€)	1.2	0.3	5.3	3.7	0.2	10.6
OC of WF11 (€)	0.3	0.2	3.8	3.0	0.0	7.3
%$OC_{WF11\ vs.\ WN2}$ (%)	–74.8	–2.9	–29.3	–19.5	–100.0	–31.3
OC of WF12 (€)	0.7	0.1	2.7	2415.5	0.7	2419.6
OC of WN5 (€)	0.6	0.1	2.5	4353.0	0.5	4356.8
%$OC_{WF12\ vs.\ WN5}$ (%)	–3.4	–5.1	–6.6	80.2	–29.6	80.1
OC of WF13 (€)	0.6	0.1	2.5	4877.4	0.9	4881.6
OC of WN9 (€)	0.5	0.1	2.6	4910.0	0.1	4913.3
%$OC_{WF13\ vs.\ WN9}$ (%)	–9.1	–0.3	2.7	0.7	–92.1	0.7
OC of WF14 (€)	0.6	0.1	2.5	2903.0	0.7	2906.8
OC of WN5 (€)	0.6	0.1	2.5	5421.7	0.0	5424.9
%$OC_{WF14\ vs.\ WN5}$ (%)	–0.5	–0.8	0.1	86.8	–100.0	86.6
OC of WF15 (€)	0.6	0.1	2.6	3121.5	0.0	3124.8
OC of WN11 (€)	0.6	0.1	2.8	4049.3	0.0	4052.8

Finanziato dall'Unione europea NextGenerationEU | Ministero dell'Università e della Ricerca | Italiadomani PIANO NAZIONALE DI RIPRESA E RESILIENZA

	SAF	RAF	RS + PRS	HP + PHP	HUM	TOTAL
%OC$_{WF15\ vs.\ WN11}$ (%)	0.8	–0.9	4.9	29.7	N.A.	29.7
OC of WF16 (€)	0.5	0.1	2.5	3971.8	0.0	3974.9
OC of WN7 (€)	0.5	0.1	2.4	3931.8	0.0	3934.8
%OC$_{WF16\ vs.\ WN10}$ (%)	–8.5	–0.5	–3.1	–1.0	N.A.	–1.0
OC of WF17 (€)	0.5	0.1	2.3	3986.5	0.0	3989.5
OC of WN10 (€)	0.5	0.1	2.3	4448.7	0.0	4451.7
%OC$_{WF17\ vs.\ WN10}$ (%)	2.2	0.8	0.4	11.6	N.A.	11.6
OC of WF18 (€)	0.6	0.1	2.6	4499.0	0.0	4502.2
OC of WN7 (€)	0.6	0.1	2.6	4544.8	0.0	4548.1
%OC$_{WF18\ vs.\ WN7}$ (%)	0.0	–2.0	2.6	1.0	N.A.	1.0
OC of WN12 (€)	0.4	0.1	0.0	1.8	1.4	3.6
OC of WF19 (€)	0.4	0.1	0.0	1.8	1.3	3.6
%OC$_{WF19\ vs.\ WN12}$ (%)	0.4	–0.2	N.A.	–0.1	–4.6	–1.8
OC of WN12 (€)	0.5	0.1	0.0	2.2	1.7	4.5
OC of WF20 (€)	0.5	0.1	0.2	2.2	1.9	4.9
%OC$_{WF20\ vs.\ WN12}$ (%)	–0.2	0.1	N.A.	–1.4	11.9	7.6
OC of WN15 (€)	0.4	0.1	0.0	1.9	1.5	3.8
OC of WF21 (€)	0.4	0.1	0.0	1.9	1.5	3.9
%OC$_{WF21\ vs.\ WN15}$ (%)	–0.2	–0.7	N.A.	1.0	2.2	1.2
OC of WN13 (€)	0.3	0.1	0.0	1.7	1.3	3.4
OC of WF22 (€)	0.3	0.1	0.9	1.9	2.8	6.0
%OC$_{WF22\ vs.\ WN13}$ (%)	–2.1	–0.1	∞	9.4	121.9	74.8
OC of WN14 (€)	0.3	0.1	0.0	1.8	1.1	3.3
OC of WF23 (€)	0.3	0.1	0.8	2.0	2.5	5.7
%OC$_{WF23\ vs.\ WN14}$ (%)	–2.3	–0.7	∞	7.5	134.4	72.5
OC of WN13 (€)	0.3	0.1	0.0	1.7	1.2	3.3
OC of WF24 (€)	0.3	0.1	1.2	1.9	2.8	6.3
%OC$_{WF24\ vs.\ WN13}$ (%)	–2.3	0.2	∞	15.4	130.0	91.8
OC of WN12 (€)	0.3	0.1	0.0	1.6	1.2	3.2
OC of WF25 (€)	0.1	0.1	0.0	1.2	0.8	2.2
%OC$_{WF25\ vs.\ WN12}$ (%)	–63.4	–1.2	N.A.	–23.8	–37.0	–32.1
OC of WN13 (€)	0.3	0.1	0.0	1.6	1.2	3.2
OC of WF26 (€)	0.8	0.1	0.6	1.9	1.8	5.1
%OC$_{WF26\ vs.\ WN13}$ (%)	136.8	3.6	∞	14.1	50.1	58.1
OC of WN12 (€)	0.3	0.1	0.0	1.6	1.3	3.3
OC of WF27 (€)	1.7	0.1	1.6	2.1	1.5	6.9
%OC$_{WF27\ vs.\ WN12}$ (%)	423.8	5.7	∞	30.8	14.8	110.0
OC of WN15 (€)	0.3	0.1	0.0	1.3	1.0	2.7
OC of WF28 (€)	0.3	0.0	0.0	1.2	1.1	2.6
%OC$_{WF28\ vs.\ WN15}$ (%)	–0.6	–64.2	N.A.	–8.5	9.3	–1.9
OC of WN15 (€)	0.3	0.1	0.0	1.6	1.3	3.3
OC of WF29 (€)	0.3	0.2	0.0	1.7	1.0	3.2
%OC$_{WF29\ vs.\ WN15}$ (%)	0.3	196.2	N.A.	3.4	–20.1	–2.2
OC of WN16 (€)	0.3	0.1	0.1	1.4	1.1	2.9
OC of WF30 (€)	0.3	0.4	0.0	1.5	1.1	3.3

Finanziato dall'Unione europea NextGenerationEU
Ministero dell'Università e della Ricerca
Italiadomani PIANO NAZIONALE DI RIPRESA E RESILIENZA

	SAF	RAF	RS + PRS	HP + PHP	HUM	TOTAL
$\%OC_{WF30\ vs.\ WN16}$ (%)	1.1	537.3	–100.0	2.4	4.2	11.9

Legend	
	$-10\% \leq \%OC \leq +10\%$
	$+10\% < \%OC \leq +20\%$ OR $-20\% \leq \%OC < -10\%$
	$\%OC > +20\%$ OR $\%OC < -20\%$

5. Effects of faults on global equivalent CO2 emissions

In this section the effects of the selected faults in terms of daily global equivalent CO_2 emissions are reported. The mass m_x of a given pollutant x while generating the energy output E can be calculated as:

$$m_x = U_x \cdot E \tag{14}$$

where U_x is the energy output-based emission factor, that is the specific emission of equivalent global pollutant x per unit of E. The percentage difference $\%CO_2$ between faulty and normal tests in terms of global equivalent CO_2 emissions is calculated as follows:

$$\%CO_2 = \frac{mCO_{2,Faulty} - mCO_{2,Baseline}}{mCO_{2,Baseline}} \cdot 100 = \frac{\sum_i U^{el}_{CO_2,i} \cdot P_{el,Faulty,i} \cdot ETS - \sum_i U^{el}_{CO_2,i} \cdot P_{el,Baseline,i} \cdot ETS}{\sum_i U^{el}_{CO_2,i} \cdot P_{el,Baseline,i} \cdot ETS} \cdot 100 \tag{15}$$

where $mCO_{2,Faulty}$ and $mCO_{2,Baseline}$ are, respectively, the mass of global equivalent CO_2 emissions of AHU during faulty and corresponding normal test.

Tables 6a and b reports the values of $\%CO_2$, during summer and winter, respectively. The cells of Tables 6a and b are filled in yellow if $\%CO_2$ is included in the range ±10%, in red if $\%CO_2$ is greater than 20% or lower than –20%, in orange in other cases (the symbol N.A. denotes that the AHU component has not been activated during both tests and calculating $\%CO_2$ is not applicable, while the symbol '∞' indicates that the AHU component has not been activated only during the normal test).

Table 6a. Values of $\%CO_2$ (calculated via Eq. 15) as a function of both pairs of tests under comparison and AHU component, during summer.

	SAF	RAF	RS + PRS	HP + PHP	HUM	TOTAL
mCO_2 of SN4 (gCO_2)	978.5	209.9	8296.1	3214.6	1356.9	14056.0
mCO_2 of SF1 (gCO_2)	1009.8	211.5	8362.4	0.0	0.0	9583.7
$\%CO_{2,SF1\ vs.\ SN4}$ (%)	3.2	0.8	0.8	–100.0	–100.0	–31.8
mCO_2 of SN5 (gCO_2)	844.5	180.7	6472.5	2348.8	1554.5	11401.1
mCO_2 of SF2 (gCO_2)	835.7	179.3	7891.7	4356.6	5452.8	18716.0
$\%CO_{2,SF3\ vs.\ SN5}$ (%)	–1.0	–0.8	21.9	85.5	250.8	64.2
mCO_2 of SN5 (gCO_2)	787.4	168.5	6030.1	2189.8	1450.1	10625.9
mCO_2 of SF3 (gCO_2)	778.5	166.8	962.4	0.0	156.1	2063.8
$\%CO_{2,SF3\ vs.\ SN5}$ (%)	–1.1	–1.0	–84.0	–100.0	–89.2	–80.6
mCO_2 of SN4 (gCO_2)	955.4	204.9	8114.6	3131.5	1334.7	13741.1
mCO_2 of SF4 (gCO_2)	964.9	206.0	8905.4	2936.2	1929.3	14941.7
$\%CO_{2,SF4\ vs.\ SN4}$ (%)	1.0	0.5	9.7	–6.2	44.5	8.7
mCO_2 of SN2 (gCO_2)	951.8	208.7	8919.0	2910.1	1579.2	14568.9
mCO_2 of SF5 (gCO_2)	972.1	207.8	6435.5	2487.9	0.0	10103.2
$\%CO_{2,SF5\ vs.\ SN2}$ (%)	2.1	–0.4	–27.8	–14.5	–100.0	–30.7
mCO_2 of SN1 (gCO_2)	660.7	143.4	4777.8	2068.4	1174.3	8824.6
mCO_2 of SF6 (gCO_2)	666.2	141.8	5528.5	1096.2	0.0	7432.7
$\%CO_{2,SF6\ vs.\ SN1}$ (%)	0.8	–1.1	15.7	–47.0	–100.0	–15.8

Finanziato dall'Unione europea NextGenerationEU | Ministero dell'Università e della Ricerca | Italiadomani PIANO NAZIONALE DI RIPRESA E RESILIENZA

	SAF	RAF	RS + PRS	HP + PHP	HUM	TOTAL
mCO_2 of SN4 (gCO_2)	941.2	201.8	7977.6	3094.6	1312.7	13527.9
mCO_2 of SF7 (gCO_2)	929.5	201.8	6892.9	4050.6	3139.4	15214.3
$\%CO_{2,SF7\ vs.\ SN4}$ (%)	–1.2	0.0	–13.6	30.9	139.2	12.5
mCO_2 of SN2 (gCO_2)	878.3	192.6	8235.3	2700.7	1454.7	13461.7
mCO_2 of SF8 (gCO_2)	874.8	192.4	8540.7	3064.6	0.0	12672.6
$\%CO_{2,SF8\ vs.\ SN2}$ (%)	–0.4	–0.1	3.7	13.5	–100.0	–5.9
mCO_2 of SN3 (gCO_2)	1121.1	244.4	10484.5	3767.7	1647.4	17265.1
mCO_2 of SF9 (gCO_2)	1103.5	243.9	10923.5	1178.1	9296.6	22745.5
$\%CO_{2,SF9\ vs.\ SN3}$ (%)	–1.6	–0.2	4.2	–68.7	464.3	31.7
mCO_2 of SN5 (gCO_2)	1021.3	218.6	7825.2	2837.6	1876.8	13779.5
mCO_2 of SF10 (gCO_2)	987.9	50.1	7353.3	3198.3	1740.9	13330.5
$\%CO_{2,SF10\ vs.\ SN5}$ (%)	–3.3	–77.1	–6.0	12.7	–7.2	–3.3
mCO_2 of SN6 (gCO_2)	1053.0	229.3	8597.9	3652.4	0.0	13532.6
mCO_2 of SF11 (gCO_2)	290.4	221.0	4836.4	59.2	0.0	5407.1
$\%CO_{2,SF11\ vs.\ SN6}$ (%)	–72.4	–3.6	–43.7	–98.4	N.A.	–60.0
mCO_2 of SF12 (gCO_2)	1053.7	215.7	9952.9	3549.1	2215.9	16987.2
mCO_2 of SN9 (gCO_2)	1027.2	209.2	9680.6	3163.3	1856.0	15936.3
$\%CO_{2,SF12\ vs.\ SN9}$ (%)	–2.5	–3.0	–2.7	–10.9	–16.2	–6.2
mCO_2 of SF13 (gCO_2)	1202.9	253.5	12607.1	4106.7	1761.6	19931.8
mCO_2 of SN7 (gCO_2)	1218.7	254.9	11864.1	4486.2	1747.5	19571.4
$\%CO_{2,SF13\ vs.\ SN7}$ (%)	1.3	0.6	–5.9	9.2	–0.8	–1.8
mCO_2 of SF14 (gCO_2)	1154.8	248.8	10177.1	3702.5	2413.1	17696.3
mCO_2 of SN11 (gCO_2)	1175.1	250.0	10396.1	3753.0	2211.8	17786.1
$\%CO_{2,SF14\ vs.\ SN11}$ (%)	1.8	0.5	2.2	1.4	–8.3	0.5
mCO_2 of SF15 (gCO_2)	1253.8	264.4	12940.8	3960.0	2255.2	20674.2
mCO_2 of SN10 (gCO_2)	1265.9	260.0	13081.0	3911.5	2057.7	20576.1
$\%CO_{2,SF15\ vs.\ SN10}$ (%)	1.0	–1.7	1.1	–1.2	–8.8	–0.5
mCO_2 of SF16 (gCO_2)	1203.0	246.4	11378.5	4301.5	1854.9	18984.2
mCO_2 of SN8 (gCO_2)	1153.3	245.5	10582.8	3620.5	2336.2	17938.3
$\%CO_{2,SF16\ vs.\ SN8}$ (%)	–4.1	–0.3	–7.0	–15.8	25.9	–5.5
mCO_2 of SF17 (gCO_2)	1124.5	242.3	9890.0	3617.5	2347.3	17221.4
mCO_2 of SN11 (gCO_2)	1142.0	244.6	10220.5	3586.2	2417.9	17611.2
$\%CO_{2,SF17\ vs.\ SN11}$ (%)	1.6	1.0	3.3	–0.9	3.0	2.3
mCO_2 of SF18 (gCO_2)	992.9	211.8	6408.0	4109.7	2307.5	14030.0
mCO_2 of SN12 (gCO_2)	986.4	209.6	6895.6	4202.0	2270.1	14563.7
$\%CO_{2.SF18\ vs.\ SN12}$ (%)	–0.6	–1.0	7.6	2.2	–1.6	3.8
mCO_2 of SN13 (gCO2)	808.8	178.1	287.7	8980.4	2632.7	12887.6
mCO_2 of SF19 (gCO2)	804.1	176.6	0.0	7563.8	2281.3	10857.2
$\%CO_{2,FS5\ vs.\ SN13}$ (%)	–0.6	–0.9	–100.0	–15.8	–13.3	–15.8
mCO_2 of SN13 (gCO2)	970.8	213.8	352.2	10799.0	3162.2	15498.0
mCO_2 of SF20 (gCO2)	950.6	207.7	37.5	9949.7	3200.5	14346.0
$\%CO_{2,SF20\ vs.\ SN13}$ (%)	–2.1	–2.8	–89.4	–7.9	1.2	–7.4
mCO_2 of SN13 (gCO2)	931.6	205.2	334.5	10375.9	3030.2	14877.4

Finanziato dall'Unione europea NextGenerationEU | Ministero dell'Università e della Ricerca | Italiadomani PIANO NAZIONALE DI RIPRESA E RESILIENZA

	SAF	RAF	RS + PRS	HP + PHP	HUM	TOTAL
mCO_2 of SF21 (gCO_2)	939.2	203.7	190.6	10247.7	3394.7	14975.9
$\%CO_{2,SF21\ vs.\ SN13}$ (%)	0.8	–0.7	–43.0	–1.2	12.0	0.7
mCO_2 of SN14 (gCO_2)	443.4	98.0	517.9	3593.4	1554.4	6207.2
mCO_2 of SF22 (gCO_2)	450.5	96.8	2292.8	4090.5	3126.9	10057.5
$\%CO_{2,SF22\ vs.\ SN14}$ (%)	1.6	–1.2	342.7	13.8	101.2	62.0
mCO_2 of SN15 (gCO_2)	648.0	145.3	785.3	5791.3	2198.1	9568.0
mCO_2 of SF23 (gCO_2)	640.0	144.4	4382.7	6423.8	4301.8	15892.8
$\%CO_{2,SF23\ vs.\ SN15}$ (%)	–1.2	–0.6	458.1	10.9	95.7	66.1
mCO_2 of SN14 (gCO_2)	640.9	141.6	738.0	5194.2	2237.8	8952.5
mCO_2 of SF24 (gCO_2)	626.4	141.1	4189.9	5940.7	4182.1	15080.1
$\%CO_{2,SF24\ vs.\ SN14}$ (%)	–2.3	–0.4	467.8	14.4	86.9	68.4
mCO_2 of SN17 (gCO_2)	891.2	190.0	631.0	7560.8	3641.8	12914.8
mCO_2 of SF25 (gCO_2)	354.9	186.2	0.0	5283.3	62.0	5903.4
$\%CO_{2,SF25\ vs.\ SN17}$ (%)	–60.2	–2.0	–100.0	–30.1	–98.3	–54.3
mCO_2 of SN16 (gCO_2)	712.6	148.0	719.1	6661.5	2450.0	10691.3
mCO_2 of SF26 (gCO_2)	1638.5	151.9	712.1	7602.8	3844.5	13949.8
$\%CO_{2,SF26\ vs.\ SN16}$ (%)	129.9	2.6	–1.0	14.1	56.9	30.5
mCO_2 of SN17 (gCO_2)	880.3	187.7	633.4	7473.2	3592.8	12767.3
mCO_2 of SF27 (gCO_2)	4688.1	198.1	303.0	11477.1	4875.3	21541.5
$\%CO_{2,SF27\ vs.\ SN17}$ (%)	432.6	5.5	–52.2	53.6	35.7	68.7
mCO_2 of SN18 (gCO_2)	834.1	178.7	589.7	6912.0	3451.7	11966.2
mCO_2 of SF28 (gCO_2)	821.3	65.0	1043.5	6822.5	3587.9	12340.1
$\%CO_{2,SF28\ vs.\ SN18}$ (%)	–1.5	–63.6	77.0	–1.3	3.9	3.1
mCO_2 of SN18 (gCO_2)	862.6	184.8	620.2	7174.9	3558.7	12401.2
mCO_2 of SF29 (gCO_2)	861.9	548.8	0.0	7548.9	3169.4	12145.5
$\%CO_{2,SF29\ vs.\ SN18}$ (%)	–0.1	196.9	–100.0	5.2	–10.9	–2.1
mCO_2 of SN18 (gCO_2)	879.6	188.4	629.0	7302.0	3634.6	12633.8
mCO_2 of SF30 (gCO_2)	904.1	1247.4	0.0	7487.7	3590.8	13246.7
$\%CO_{2,SF30\ vs.\ SN18}$ (%)	2.8	561.9	–100.0	2.5	–1.2	4.9
Legend						
	$-10\% \leq \%CO_2 \leq +10\%$					
	$+10\% < \%CO_2 \leq +20\%$ OR $-20\% \leq \%CO_2 < -10\%$					
	$\%CO_2 > +20\%$ OR $\%CO_2 < -20\%$					

Table 6b. Values of $\%CO_2$ (calculated via Eq. 15) as a function of both pairs of tests under comparison and AHU component, during winter.

	SAF	RAF	RS + PRS	HP + PHP	HUM	TOTAL
mCO_2 of WN2 (gCO_2)	1094.6	237.2	5023.0	3473.5	150.8	9979.1
mCO_2 of WF1 (gCO_2)	1121.4	239.1	4659.3	193.8	0.0	6213.6
$\%CO_{2,WF1\ vs.\ WN2}$ (%)	2.4	0.8	–7.2	–94.4	–100.0	–37.7
mCO_2 of WN5 (gCO_2)	907.6	194.2	3763.1	2038.8	1018.8	7922.4
mCO_2 of WF2 (gCO_2)	866.6	192.8	4430.5	6049.9	3122.1	14661.9
$\%CO_{2,WF2\ vs.\ WN5}$ (%)	–4.5	–0.7	17.7	196.7	206.5	85.1

Finanziato dall'Unione europea NextGenerationEU | Ministero dell'Università e della Ricerca | Italiadomani PIANO NAZIONALE DI RIPRESA E RESILIENZA

	SAF	RAF	RS + PRS	HP + PHP	HUM	TOTAL
mCO_2 of WN1 (gCO_2)	939.6	205.8	3912.3	4161.3	0.0	9219.0
mCO_2 of WF3 (gCO_2)	955.4	200.9	470.8	809.4	0.0	2436.6
$\%CO_{2,WF3\ vs.\ WN1}$ (%)	1.7	–2.4	–88.0	–80.5	N.A.	–73.6
mCO_2 of WN8 (gCO_2)	1160.4	243.7	5425.7	5122.9	978.4	12931.2
mCO_2 of WF4 (gCO_2)	1155.8	243.9	5437.0	5462.9	1289.2	13588.7
$\%CO_{2,WF4\ vs.\ WN8}$ (%)	–0.4	0.1	0.2	6.6	31.8	5.1
mCO_2 of WN6 (gCO_2)	1180.1	252.6	4835.2	2547.8	1544.6	10360.4
mCO_2 of WF5 (gCO_2)	1179.0	253.2	4806.4	2439.4	0.0	8678.0
$\%CO_{2,WF5\ vs.\ WN6}$ (%)	–0.1	0.2	–0.6	–4.3	–100.0	–16.2
mCO_2 of WN5 (gCO_2)	1029.9	220.4	4260.0	2341.0	1150.3	9001.6
mCO_2 of WF6 (gCO_2)	1037.7	220.8	4722.9	469.9	558.9	7010.2
$\%CO_{2,WF6\ vs.\ WN5}$ (%)	0.8	0.2	10.9	–79.9	–51.4	–22.1
mCO_2 of WN3 (gCO_2)	1365.2	294.7	5615.8	5395.9	728.8	13400.3
mCO_2 of WF7 (gCO_2)	1351.6	294.7	5052.1	7610.1	2249.2	16557.8
$\%CO_{2,WF7\ vs.\ WN3}$ (%)	–1.0	0.0	–10.0	41.0	208.6	23.6
mCO_2 of WN7 (gCO_2)	1245.0	263.1	5945.0	4936.2	0.0	12389.3
mCO_2 of WF8 (gCO_2)	1244.9	262.5	6045.5	5140.9	0.0	12693.8
$\%CO_{2,WF8\ vs.\ WN7}$ (%)	0.0	–0.3	1.7	4.1	N.A.	2.5
mCO_2 of WN4 (gCO_2)	1066.1	232.5	5476.7	3657.1	0.0	10432.5
mCO_2 of WF9 (gCO_2)	1063.6	229.9	5052.3	2510.2	2993.3	11849.2
$\%CO_{2,WF9\ vs.\ WN4}$ (%)	–0.2	–1.1	–7.7	–31.4	∞	13.6
mCO_2 of WN2 (gCO_2)	957.0	207.4	4372.6	3058.2	147.4	8742.5
mCO_2 of WF10 (gCO_2)	935.0	46.4	3605.1	3767.2	1068.3	9422.1
$\%CO_{2,WF10\ vs.\ WN2}$ (%)	–2.3	–77.6	–17.6	23.2	624.8	7.8
mCO_2 of WN2 (gCO_2)	992.1	215.0	4541.3	3156.6	152.0	9057.1
mCO_2 of WF11 (gCO_2)	249.6	208.6	3221.5	2383.3	0.0	6063.0
$\%CO_{2,WF11\ vs.\ WN2}$ (%)	–74.8	–2.9	–29.1	–24.5	–100.0	–33.1
mCO_2 of WN5 (gCO_2)	1075.0	230.0	4406.2	2415.5	1209.6	9336.1
mCO_2 of WF12 (gCO_2)	1037.2	218.2	4149.2	4353.0	863.4	10621.0
$\%CO_{2,WF12\ vs.\ WN5}$ (%)	–3.5	–5.1	–5.8	80.2	–28.6	13.8
mCO_2 of WN9 (gCO_2)	1180.9	247.5	5173.2	4877.4	1935.7	13414.7
mCO_2 of WF13 (gCO_2)	1073.2	246.7	5317.1	4910.0	202.6	11749.5
$\%CO_{2,WF13\ vs.\ WN9}$ (%)	–9.1	–0.3	2.8	0.7	–89.5	–12.4
mCO_2 of WN5 (gCO_2)	1279.1	273.9	5264.6	2903.0	1421.4	11141.9
mCO_2 of WF14 (gCO_2)	1272.4	271.8	5284.9	5421.7	0.0	12250.8
$\%CO_{2,WF14\ vs.\ WN5}$ (%)	–0.5	–0.8	0.4	86.8	–100.0	10.0
mCO_2 of WN11 (gCO_2)	1032.7	218.6	4691.9	3121.5	0.0	9064.7
mCO_2 of WF15 (gCO_2)	1040.5	216.7	4931.9	4049.3	0.0	10238.5
$\%CO_{2,WF15\ vs.\ WN11}$ (%)	0.8	–0.8	5.1	29.7	N.A.	12.9
mCO_2 of WN7 (gCO_2)	1009.4	213.3	4786.8	3971.8	0.0	9981.3
mCO_2 of WF16 (gCO_2)	923.2	212.3	4606.8	3931.8	0.0	9674.1
$\%CO_{2,WF16\ vs.\ WN7}$ (%)	–8.5	–0.5	–3.8	–1.0	N.A.	–3.1
mCO_2 of WN10 (gCO_2)	1105.4	237.1	5176.3	3986.5	0.0	10505.4

Finanziato dall'Unione europea NextGenerationEU | Ministero dell'Università e della Ricerca | Italiadomani PIANO NAZIONALE DI RIPRESA E RESILIENZA

	SAF	RAF	RS + PRS	HP + PHP	HUM	TOTAL
mCO_2 of WF17 (gCO_2)	1128.7	239.1	5165.6	4448.7	0.0	10982.1
$\%CO_{2,WF17\ vs.\ WN10}$ (%)	2.1	0.8	–0.2	11.6	N.A.	4.5
mCO_2 of WN7 (gCO_2)	1158.6	244.8	5516.7	4499.0	0.0	11419.0
mCO_2 of WF18 (gCO_2)	1155.2	239.8	5614.4	4544.8	0.0	11554.1
$\%CO_{2,WF18\ vs.\ WN7}$ (%)	–0.3	–2.0	1.8	1.0	N.A.	1.2
mCO_2 of WN12 (gCO_2)	948.7	198.2	0.0	4649.8	3617.5	9431.9
mCO_2 of WF19 (gCO_2)	951.8	197.7	0.0	4640.0	3407.0	9214.3
$\%CO_{2,WF19\ vs.\ WN12}$ (%)	0.3	–0.2	N.A.	–0.2	–5.8	–2.3
mCO_2 of WN12 (gCO_2)	1194.4	249.6	0.0	5850.6	4548.0	11864.9
mCO_2 of WF20 (gCO_2)	1190.8	249.8	496.0	5788.1	5002.0	12726.7
$\%CO_{2,WF20\ vs.\ WN12}$ (%)	–0.3	0.1	∞	–1.1	10.0	7.3
mCO_2 of WN15 (gCO_2)	1284.9	273.9	0.0	6696.5	5218.7	13523.0
mCO_2 of WF21 (gCO_2)	1282.2	272.0	0.0	6764.9	5311.8	13659.5
$\%CO_{2,WF21vs.\ WN15}$ (%)	–0.2	–0.7	N.A.	1.0	1.8	1.0
mCO_2 of WN13 (gCO_2)	1203.6	253.1	0.0	5991.5	4268.8	11739.7
mCO_2 of WF22 (gCO_2)	1178.2	252.9	3270.5	6572.4	9609.1	20883.2
$\%CO_{2,WF22vs.\ WN13}$ (%)	–2.1	–0.1	∞	9.7	125.1	77.9
mCO_2 of WN14 (gCO_2)	1145.2	241.9	0.0	6559.1	3803.3	11793.5
mCO_2 of WF23 (gCO_2)	1117.4	240.0	3356.0	7127.2	9084.7	20925.2
$\%CO_{2,WF23\ vs.\ WN14}$ (%)	–2.4	–0.8	∞	8.7	138.9	77.4
mCO_2 of WN13 (gCO_2)	1224.7	257.5	0.0	6092.8	4332.5	11930.6
mCO_2 of WF24 (gCO_2)	1196.5	258.0	4748.3	7122.0	10066.9	23391.6
$\%CO_{2,WF24vs.\ WN13}$ (%)	–2.3	0.2	∞	16.9	132.4	96.1
mCO_2 of WN12 (gCO_2)	1293.2	270.5	0.0	6422.4	4870.1	12880.4
mCO_2 of WF25 (gCO_2)	473.1	267.1	0.0	4856.1	2857.6	8502.2
$\%CO_{2,WF25\ vs.\ WN12}$ (%)	–63.4	–1.3	N.A.	–24.4	–41.3	–34.0
mCO_2 of WN13 (gCO_2)	1051.7	221.1	0.0	5197.4	3726.9	10217.0
mCO_2 of WF26 (gCO_2)	2492.7	229.0	1824.2	5981.8	5588.5	16116.2
$\%CO_{2,WF26\ vs.\ WN13}$ (%)	137.0	3.6	∞	15.1	50.0	57.7
mCO_2 of WN12 (gCO_2)	1226.3	256.2	0.0	6031.8	4640.7	12177.8
mCO_2 of WF27 (gCO_2)	6400.2	270.7	5970.3	7999.1	5248.5	25888.8
$\%CO_{2,WF27\ vs.\ WN12}$ (%)	421.9	5.7	∞	32.6	13.1	112.6
mCO_2 of WN15 (gCO_2)	1255.5	267.6	0.0	6541.4	5101.9	13214.4
mCO_2 of WF28 (gCO_2)	1247.4	95.4	0.0	5988.9	5558.2	12937.9
$\%CO_{2,WF28\ vs.\ WN15}$ (%)	–0.6	–64.3	N.A.	–8.4	8.9	–2.1
mCO_2 of WN15 (gCO_2)	1054.9	224.7	0.0	5486.0	4283.9	11089.8
mCO_2 of WF29 (gCO_2)	1058.5	665.7	0.0	5713.4	3401.6	10879.3
$\%CO_{2,WF29\ vs.\ WN15}$ (%)	0.3	196.2	N.A.	4.1	–20.6	–1.9
mCO_2 of WN16 (gCO_2)	1003.9	210.0	239.4	5317.5	3804.6	10575.4
mCO_2 of WF30 (gCO_2)	1016.0	1339.0	0.0	5446.8	3911.0	11750.4
$\%CO_{2,WF30\ vs.\ WN16}$ (%)	1.2	537.6	–100.0	2.4	2.8	11.1

Legend

	$-10\% \leq \%CO_2 \leq +10\%$

Finanziato dall'Unione europea NextGenerationEU
Ministero dell'Università e della Ricerca
Italiadomani PIANO NAZIONALE DI RIPRESA E RESILIENZA

	SAF	RAF	RS + PRS	HP + PHP	HUM	TOTAL
	$+10\% < \%CO_2 \leq +20\%$ OR $-20\% \leq \%CO_2 < -10\%$					
	$\%CO_2 > +20\%$ OR $\%CO_2 < -20\%$					

6. Effects of faults on operation time of AHU components

In this section the effects of the selected faults in terms of daily operation time of AHU components are described. Tables 7a and b report the percentage of difference %OT between faulty and corresponding normal tests in terms of operation time during summer and winter, respectively. The values of %OT are calculated as follows:

$$\%OT = \frac{\left(OT_{Faulty} - OT_{Baseline}\right)}{OT_{Baseline}} \cdot 100 \tag{16}$$

where OT_{Faulty} and $OT_{Baseline}$ are, respectively, the operating time during faulty and corresponding normal test. The cells of Tables 7a and b are filled in yellow if %OT is included in the range ±10%, in red if %OT is greater than 20% or lower than –20%, in orange in other cases (the symbol N.A. denotes that the AHU component has not been activated during both tests, while the symbol '∞' indicates that the AHU component has not been activated only during the normal test).

Table 7a. Values of %OT (calculated via Eq. 16) as a function of pairs of tests under comparison and AHU component, during summer.

	SAF	RAF	RS	HP	HUM	PRS	PHP
OT of SN4 (min)	538.7	539.6	241.9	64.2	79.2	488.4	330.2
OT of SF1 (min)	538.7	539.6	238.3	0.0	0.0	538.4	0.0
%$OT_{SF1\ vs.\ SN4}$ (%)	0.0	0.0	–1.5	–100.0	–100.0	10.2	–100.0
OT of SN5 (min)	538.7	539.5	224.9	54.1	105.2	440.8	285.1
OT of SF2 (min)	538.7	539.6	269.9	99.3	343.0	538.7	540.0
%$OT_{SF2\ vs.\ SN5}$ (%)	0.0	0.0	20.0	83.8	226.0	22.2	89.4
OT of SN5 (min)	538.7	539.5	224.9	54.1	105.2	440.8	285.1
OT of SF3 (min)	538.7	539.6	46.1	0.0	12.5	0.0	0.0
%$OT_{SF3\ vs.\ SN5}$ (%)	0.0	0.0	–79.5	–100.0	–88.1	–100.0	–100.0
OT of SN4 (min)	538.7	539.6	241.9	64.2	79.2	488.4	330.2
OT of SF4 (min)	538.7	539.5	266.8	60.3	109.5	540.0	302.5
%$OT_{SF4\ vs.\ SN4}$ (%)	0.0	0.0	10.3	–6.1	38.3	10.6	–8.4
OT of SN2 (min)	540.0	540.0	345.3	83.1	98.7	484.2	319.2
OT of SF5 (min)	538.8	539.6	197.6	45.7	0.0	325.9	285.4
%$OT_{SF5\ vs.\ SN2}$ (%)	–0.2	–0.1	–42.8	–45.0	–100.0	–32.7	–10.6
OT of SN1 (min)	540.0	539.4	293.1	89.0	101.6	433.2	324.2
OT of SF5 (min)	538.7	539.6	234.3	32.2	0.0	538.7	148.6
%$OT_{SF5\ vs.\ SN1}$ (%)	–0.2	0.0	–20.1	–63.9	–100.0	24.3	–54.2
OT of SN4 (min)	538.7	539.6	241.9	64.2	79.2	488.4	330.2
OT of SF7 (min)	538.5	539.4	220.4	80.5	190.2	371.4	460.1
%$OT_{SF7\ vs.\ SN4}$ (%)	0.0	0.0	–8.9	25.4	140.2	–24.0	39.3
OT of SN2 (min)	540.0	540.0	345.3	83.1	98.7	484.2	319.2
OT of SF8 (min)	540.0	540.0	355.4	97.9	0.0	540.0	347.2
%$OT_{SF8\ vs.\ SN2}$ (%)	0.0	0.0	2.9	17.9	–100.0	11.5	8.8
OT of SN3 (min)	539.5	539.8	299.3	76.6	83.9	465.7	363.1
OT of SF9 (min)	538.7	539.5	274.4	17.6	436.8	464.9	126.6
%$OT_{SF9\ vs.\ SN3}$ (%)	–0.1	–0.1	–8.3	–77.0	420.5	–0.2	–65.1

Finanziato dall'Unione europea NextGenerationEU | Ministero dell'Università e della Ricerca | Italiadomani PIANO NAZIONALE DI RIPRESA E RESILIENZA

	SAF	RAF	RS	HP	HUM	PRS	PHP
OT of SN5 (min)	538.7	539.5	224.9	54.1	105.2	440.8	285.1
OT of SF10 (min)	538.7	0.0	200.8	60.2	100.4	448.1	322.2
%OT$_{SF10\ vs.\ SN5}$ (%)	0.0	–100.0	–10.7	11.4	–4.6	1.7	13.0
OT of SN6 (min)	538.7	539.6	221.5	70.2	0.0	538.5	327.9
OT of SF11 (min)	0.2	539.6	84.3	2.0	0.0	538.7	0.0
%OT$_{SF11\ vs.\ SN6}$ (%)	–100.0	0.0	–62.0	–97.2	N.A.	0.0	–100.0
OT of SN9 (min)	538.9	539.0	253.8	70.2	113.0	489.6	273.9
OT of SF12 (min)	539.2	539.1	242.1	60.1	102.7	484.1	256.8
%OT$_{SF12\ vs.\ SN9}$ (%)	0.0	0.0	–4.6	–14.4	–9.1	–1.1	–6.2
OT of SN7 (min)	538.7	539.5	296.5	72.1	83.9	530.3	274.7
OT of SF13 (min)	540.0	539.5	258.1	77.4	80.6	480.2	279.8
%OT$_{SF13\ vs.\ SN7}$ (%)	0.2	0.0	–13.0	7.3	–3.9	–9.4	1.9
OT of SN11 (min)	538.7	539.6	245.3	66.2	114.6	464.9	244.3
OT of SF14 (min)	538.7	539.6	248.5	66.8	105.9	468.0	249.9
%OT$_{SF14\ vs.\ SN11}$ (%)	0.0	0.0	1.3	1.0	–7.6	0.7	2.3
OT of SN10 (min)	538.7	539.6	297.8	66.2	99.6	504.5	263.7
OT of SF15 (min)	538.7	539.6	293.6	66.5	93.1	530.9	254.3
%OT$_{SF15\ vs.\ SN10}$ (%)	0.0	0.0	–1.4	0.5	–6.5	5.2	–3.6
OT of SN8 (min)	538.7	539.6	256.6	76.1	90.9	506.1	276.2
OT of SF16 (min)	538.7	539.5	261.0	66.2	113.7	486.4	249.5
%OT$_{SF16\ vs.\ SN8}$ (%)	0.0	0.0	1.7	–13.0	25.1	–3.9	–9.7
OT of SN11 (min)	538.7	539.6	245.3	66.2	114.6	464.9	244.3
OT of SF17 (min)	538.7	539.6	251.7	64.4	116.3	476.0	251.2
%OT$_{SF17\ vs.\ SN11}$ (%)	0.0	0.0	2.6	2.8	1.5	2.4	2.8
OT of SN12 (min)	538.7	539.5	179.2	92.8	128.1	450.9	281.7
OT of SF18 (min)	538.8	539.6	192.9	94.4	126.1	438.3	304.3
%OT$_{SF18\ vs.\ SN12}$ (%)	0.0	0.0	7.7	1.8	–1.5	–2.8	8.0
OT of SN13. (min)	538.7	539.5	311.6	68.0	15.2	538.8	258.8
OT of SF19 (min)	540.0	539.6	251.7	58.1	0.0	538.8	220.6
%OT$_{SF19\ vs.\ SN13}$ (%)	0.2	0.0	–19.2	–14.6	–100.0	0.0	–14.8
OT of SN13 (min)	538.7	539.5	311.6	68.0	15.2	538.8	258.8
OT of SF20 (min)	538.7	539.5	286.6	69.0	324.0	538.8	261.0
%OT$_{SF20\ vs.\ SN13}$ (%)	0.0	0.0	–8.0	1.3	2034.0	0.0	0.9
OT of SN13 (min)	538.7	539.5	311.6	68.0	15.2	538.8	258.8
OT of SF21 (min)	538.9	539.5	303.4	76.1	9.3	538.8	286.5
%OT$_{SF21\ vs.\ SN13}$ (%)	0.0	0.0	–2.6	11.9	–38.5	0.0	10.7
OT of SN14 (min)	539.2	539.5	227.2	78.2	50.9	538.7	249.8
OT of SF22 (min)	538.8	539.6	250.6	144.3	229.9	538.6	538.4
%OT$_{SF22\ vs.\ SN14}$ (%)	–0.1	0.0	10.3	84.5	351.4	0.0	115.5
OT of SN15 (min)	539.6	539.5	251.0	74.2	58.9	538.7	247.9
OT of SF23 (min)	539.1	539.5	283.8	139.0	316.9	538.4	538.4
%OT$_{SF23\ vs.\ SN15}$ (%)	–0.1	0.0	13.0	87.4	437.9	0.0	117.2
OT of SN14 (min)	539.2	539.5	227.2	78.2	50.9	538.7	249.8
OT of SF24 (min)	538.7	539.6	271.0	142.2	313.3	538.6	538.5
%OT$_{SF24\ vs.\ SN14}$ (%)	–0.1	0.0	19.3	81.9	515.1	0.0	115.5
OT of SN17 (min)	539.8	539.5	239.2	92.3	32.3	538.8	298.4

Finanziato dall'Unione europea NextGenerationEU
Ministero dell'Università e della Ricerca
Italiadomani PIANO NAZIONALE DI RIPRESA E RESILIENZA

	SAF	RAF	RS	HP	HUM	PRS	PHP
OT of SF25 (min)	538.8	539.5	136.1	2.1	0.0	538.8	3.1
%OT$_{SF25\ vs.\ SN17}$ (%)	–0.2	0.0	–43.1	–97.7	–100.0	0.0	–99.0
OT of SN16 (min)	540.0	539.5	342.5	74.2	39.9	538.8	247.6
OT of SF26 (min)	538.9	539.6	318.2	136.4	47.4	538.8	317.3
%OT$_{SF26\ vs.\ SN16}$ (%)	–0.2	0.0	–7.1	83.9	18.8	0.0	28.2
OT of SN17 (min)	539.8	539.5	239.2	92.3	32.3	538.8	298.4
OT of SF27 (min)	539.1	539.7	397.1	142.4	19.2	538.9	289.1
%OT$_{SF27\ vs.\ SN17}$ (%)	–0.1	0.0	66.0	54.3	–40.4	0.0	–3.1
OT of SN18 (min)	540.0	539.6	233.3	92.2	32.1	538.8	295.5
OT of SF28 (min)	538.7	539.5	232.1	95.5	59.6	538.8	314.3
%OT$_{SF28\ vs.\ SN18}$ (%)	–0.2	0.0	–0.5	3.6	85.8	0.0	6.4
OT of SN18 (min)	540.0	539.6	233.3	92.2	32.1	538.8	295.5
OT of SF29 (min)	538.7	539.6	248.9	82.0	0.0	538.8	261.3
%OT$_{SF29\ vs.\ SN18}$ (%)	–0.2	0.0	6.7	–11.0	–100.0	0.0	–11.6
OT of SN18 (min)	540.0	539.6	233.3	92.2	32.1	538.8	295.5
OT of SF30 (min)	538.8	539.6	247.7	94.1	0.0	538.8	275.0
%OT$_{SF30\ vs.\ SN18}$ (%)	–0.2	0.0	6.2	2.1	–100.0	0.0	–6.9
Legend							
	–10% ≤ %OT ≤ +10%						
	+10% < %OT ≤ +20% OR –20% ≤ %OT < –10%						
	%OT > +20% OR %OT < –20%						

Table 7b. Values of %OT (calculated via Eq. 16) as a function of pairs of tests under comparison and AHU component, during winter.

	SAF	RAF	RS	HP	HUM	PRS	PHP
OT of WN2 (min)	538.7	539.5	104.6	79.5	8.8	538.8	226.6
OT of WF1 (min)	538.7	539.5	90.2	6.2	0.0	538.3	0.0
%OT$_{WF1\ vs.\ WN2}$ (%)	0.0	0.0	–13.8	–92.2	–100.0	–0.1	–100.0
OT of WN5 (min)	538.7	539.5	96.7	62.5	65.8	501.3	107.9
OT of WF2 (min)	538.7	539.5	122.2	163.3	187.1	538.8	540.0
%OT$_{WF2\ vs.\ WN5}$ (%)	0.0	0.0	26.4	161.4	184.2	7.5	400.4
OT of WN1 (min)	538.7	539.5	84.1	111.1	0.0	538.6	294.1
OT of WF3 (min)	540.0	539.5	22.7	26.2	0.0	0.0	25.2
%OT$_{WF3\ vs.\ WN1}$ (%)	0.2	0.0	–73.0	–76.5	N.A.	–100.0	–91.4
OT of WN8 (min)	538.6	539.5	103.5	110.1	51.3	535.7	244.6
OT of WF4 (min)	538.7	539.5	92.4	118.4	68.0	538.6	256.2
%OT$_{WF4\ vs.\ WN8}$ (%)	0.0	0.0	–10.7	7.6	32.6	0.5	4.8
OT of WN6 (min)	538.7	539.5	96.2	56.3	75.8	482.5	130.6
OT of WF5 (min)	538.7	539.5	97.6	54.5	0.0	469.8	127.0
%OT$_{WF5\ vs.\ WN6}$ (%)	0.0	0.0	1.5	–3.2	–100.0	–2.6	–2.7
OT of WN5 (min)	538.7	539.5	96.7	62.5	65.8	501.3	107.9
OT of WF6 (min)	539.3	539.5	108.2	15.4	31.7	538.3	0.0
%OT$_{WF6\ vs.\ WN5}$ (%)	0.1	0.0	11.9	–75.4	–51.9	7.4	–100.0
OT of WN3 (min)	538.7	539.5	86.6	103.4	32.3	538.2	267.3
OT of WF7 (min)	538.7	539.5	86.1	140.6	94.8	443.6	409.3
%OT$_{WF7\ vs.\ WN3}$ (%)	0.0	0.0	–0.6	36.0	193.6	–17.6	53.1

Finanziato dall'Unione europea NextGenerationEU | Ministero dell'Università e della Ricerca | Italiadomani PIANO NAZIONALE DI RIPRESA E RESILIENZA

	SAF	RAF	RS	HP	HUM	PRS	PHP
OT of WN7 (min)	538.7	539.5	106.1	99.9	0.0	538.3	221.5
OT of WF8 (min)	538.7	539.5	109.2	103.2	0.0	538.4	231.5
%OT$_{WF8\ vs.\ WN7}$ (%)	0.0	0.0	2.9	3.3	N.A.	0.0	4.5
OT of WN4 (min)	538.7	539.5	123.5	82.9	0.0	538.7	266.7
OT of WF9 (min)	538.7	539.5	126.3	54.3	163.0	436.9	191.5
%OT$_{WF9\ vs.\ WN4}$ (%)	0.0	0.0	2.2	–34.5	∞	–18.9	–28.2
OT of WN2 (min)	538.7	539.5	104.6	79.5	8.8	538.8	226.6
OT of WF10 (min)	538.7	0.0	74.0	96.2	65.4	508.6	289.3
%OT$_{WF10\ vs.\ WN2}$ (%)	0.0	–100.0	–29.3	20.9	640.6	–5.6	27.7
OT of WN2 (min)	538.7	539.5	104.6	79.5	8.8	538.8	226.6
OT of WF11 (min)	0.0	539.3	43.4	36.4	0.0	538.4	359.8
%OT$_{WF11\ vs.\ WN2}$ (%)	–100.0	0.0	–58.5	–54.2	–100.0	–0.1	58.8
OT of WN5 (min)	540.0	540.0	96.7	62.7	65.8	501.3	107.9
OT of WF12 (min)	540.0	540.0	74.2	104.0	47.7	538.8	237.8
%OT$_{WF12\ vs.\ WN5}$ (%)	0.0	0.0	23.3	65.8	27.6	7.5	120.3
OT of WN9 (min)	540.0	540.0	100.7	106.6	96.4	491.3	235.5
OT of WF13 (min)	540.0	540.0	108.8	110.0	8.7	538.8	248.2
%OT$_{WF13\ vs.\ WN9}$ (%)	0.0	0.0	8.0	3.1	–91.0	9.7	5.4
OT of WN5 (min)	540.0	540.0	96.7	62.7	65.8	501.3	107.9
OT of WF14 (min)	540.0	540.0	91.2	113.4	0.0	538.8	231.3
%OT$_{WF14\ vs.\ WN5}$ (%)	0.0	0.0	–5.7	80.7	–100.0	7.5	114.4
OT of WN11 (min)	540.0	540.0	104.9	79.0	0.0	538.8	170.1
OT of WF15 (min)	540.0	540.0	110.8	99.8	0.0	538.8	213.1
%OT$_{WF15\ vs.\ WN11}$ (%)	0.0	0.0	5.7	26.4	N.A.	0.0	25.3
OT of WN7 (min)	540.0	540.0	106.1	100.0	0.0	538.3	221.5
OT of WF16 (min)	540.0	540.0	110.0	103.4	0.0	538.8	225.5
%OT$_{SF16\ vs.\ SN7}$ (%)	0.0	0.0	3.6	3.4	N.A.	0.1	1.8
OT of WN10 (min)	540.0	540.0	104.2	90.3	0.0	538.7	196.8
OT of WF17 (min)	540.0	540.0	99.7	98.3	0.0	538.8	219.6
%OT$_{WF17\ vs.\ WN10}$ (%)	0.0	0.0	–4.3	8.9	N.A.	0.0	11.6
OT of WN7 (min)	540.0	540.0	106.1	100.0	0.0	538.3	221.5
OT of WF18 (min)	540.0	540.0	113.9	99.0	0.0	538.8	223.0
%OT$_{WF18\ vs.\ WN7}$ (%)	0.0	0.0	7.4	–0.9	N.A.	0.1	0.7
OT of WN12 (min)	538.7	539.5	164.0	94.6	0.0	538.8	199.5
OT of WF19 (min)	538.7	539.5	160.4	89.4	0.0	538.8	189.1
%OT$_{WF19\ vs.\ WN12}$ (%)	0.0	0.0	–2.2	–5.5	N.A.	0.0	–5.2
OT of WN12 (min)	538.7	539.5	164.0	94.6	0.0	538.8	199.5
OT of WF20 (min)	538.7	539.5	160.1	104.7	16.6	538.8	223.2
%OT$_{WF20\ vs.\ WN12}$ (%)	0.0	0.0	–2.4	10.7	∞	0.0	11.9
OT of WN15 (min)	538.7	539.5	172.9	97.6	0.0	538.8	217.2
OT of WF21 (min)	538.7	539.6	175.0	98.5	0.0	537.1	228.1
%OTW$_{F21\ vs.\ WN15}$ (%)	0.0	0.0	1.2	0.9	N.A.	–0.3	5.0
OT of WN13 (min)	538.7	539.5	163.7	87.6	0.0	538.8	186.4
OT of WF22 (min)	538.8	539.6	195.2	182.8	135.9	538.8	538.5
%OT$_{WF22\ vs.\ WN13}$ (%)	0.0	0.0	19.2	108.6	∞	0.0	188.9
OT of WN14 (min)	538.7	539.6	197.7	79.4	0.0	538.8	183.5

Finanziato dall'Unione europea NextGenerationEU | Ministero dell'Università e della Ricerca | Italiadomani PIANO NAZIONALE DI RIPRESA E RESILIENZA

	SAF	RAF	RS	HP	HUM	PRS	PHP
OT of WF23 (min)	538.8	539.6	223.7	174.2	135.1	538.8	538.7
%OT$_{WF23\ vs.\ WN14}$ (%)	0.0	0.0	13.2	119.5	∞	0.0	193.6
OT of WN13 (min)	538.7	539.5	163.7	87.6	0.0	538.8	186.4
OT of WF24 (min)	538.7	539.5	215.1	191.6	190.6	536.5	538.7
%OT$_{WF24\ vs.\ WN13}$ (%)	0.0	0.0	31.4	118.7	∞	–0.4	189.0
OT of WN12 (min)	538.7	539.5	164.0	94.6	0.0	538.8	199.5
OT of WF25 (min)	538.7	539.6	94.8	48.8	0.0	538.8	165.9
%OT$_{WF25\ vs.\ WN12}$ (%)	0.0	0.0	–42.2	–48.4	N.A.	0.0	–16.8
OT of WN13 (min)	538.7	539.5	163.7	87.6	0.0	538.8	186.4
OT of WF26 (min)	538.7	539.5	209.2	138.8	87.5	538.7	218.0
%OT$_{WF26\ vs.\ WN13}$ (%)	0.0	0.0	27.8	58.3	∞	0.0	16.9
OT of WN12 (min)	538.7	539.5	164.0	94.6	0.0	538.8	199.5
OT of WF27 (min)	538.7	539.5	266.8	116.9	240.6	508.9	156.0
%OT$_{WF27\ vs.\ WN12}$ (%)	0.0	0.0	62.7	23.6	∞	–5.5	–21.8
OT of WN15 (min)	538.7	539.5	172.9	97.6	0.0	538.8	217.2
OT of WF28 (min)	538.7	539.5	145.8	106.8	0.0	538.8	237.8
%OT$_{WF28\ vs.\ WN15}$ (%)	0.0	0.0	–15.7	9.4	N.A.	0.0	9.5
OT of WN15 (min)	538.7	539.5	172.9	97.6	0.0	538.8	217.2
OT of WF29 (min)	538.7	539.5	184.7	78.0	0.0	538.8	169.2
%OT$_{WF29\ vs.\ WN15}$ (%)	0.0	0.0	6.8	–20.1	N.A.	0.0	–22.1
OT of WN16 (min)	538.7	539.5	181.9	92.0	9.9	538.8	205.3
OT of WF30 (min)	538.7	539.5	190.8	97.1	0.0	538.8	209.1
%OT$_{WF30\ vs.\ WN16}$ (%)	0.0	0.0	4.9	5.5	–100.0	0.0	1.8

Legend	
	$-10\% \leq \%OT \leq +10\%$
	$+10\% < \%OT \leq +20\%$ OR $-20\% \leq \%OT < -10\%$
	$\%OT > +20\%$ OR $\%OT < -20\%$

Finanziato dall'Unione europea NextGenerationEU
Ministero dell'Università e della Ricerca
Italiadomani PIANO NAZIONALE DI RIPRESA E RESILIENZA

MISSIONE 4
ISTRUZIONE RICERCA

WP3 - *AHU digital twin and simulation-based faults impact scenario analysis*

Finanziato dall'Unione europea NextGenerationEU
Ministero dell'Università e della Ricerca
Italiadomani
PIANO NAZIONALE DI RIPRESA E RESILIENZA

MISSIONE 4
ISTRUZIONE RICERCA

DELIVERABLE WP3_D1

LITERATURE REVIEW OF AHU SIMULATION STUDIES FOR FDD

EDIT BY UNICAMPANIA

PRIN 2022 - UTMOST FDD: AN AUTOMATED, OPEN, SCALABLE AND TRANSPARENT FAULT DETECTION AND DIAGNOSIS PROCESS FOR AIR-HANDLING UNITS BASED ON A HYBRID EXPERT AND ARTIFICIAL INTELLIGENCE APPROACH

Funded by the European Union - Next Generation EU within the "Piano Nazionale di Ripresa e Resilienza (PNRR), missione 4 componente 2 investimento 1.1 - fondo per il programma nazionale di ricerca e progetti di rilevante interesse nazionale (PRIN)"

Finanziato dall'Unione europea NextGenerationEU
Ministero dell'Università e della Ricerca
Italiadomani PIANO NAZIONALE DI RIPRESA E RESILIENZA

The UTMOST FDD Project is organised into the following 7 Work Packages (WPs):
WP0) PROJECT COORDINATION
WP1) EXPERIMENTAL ANALYSIS FOR THE CHARACTERIZATION OF FAULTY AND NORMAL OPERATION OF A TYPICAL AHU
WP2) KPIs IDENTIFICATION FOR ASSESSING FAULT IMPACT IN AHU OPERATION
WP3) AHU DIGITAL TWIN AND SIMULATION-BASED FAULT IMPACT SCENARIO ANALYSIS
WP4) DEFINITION OF HYBRID FDD STRATEGIES FOR AHUs
WP5) TRANSFERABILITY ANALYSIS OF THE FDD STRATEGIES
WP6) KNOWLEDGE TRANSFER AND DISSEMINATION

The WPs are organized into Tasks (T) ranging from 2 to 4 for each WP.

The WP3 aims at achieving the following main objectives: 1) analyse and categorize the scientific studies on digital twins of Air-Handling Units (AHUs) for Automated Fault Detection and Diagnosis (AFDD) purposes, 2) publicly provide a detailed digital twin of a typical AHU validated against measured data, 3) publicly provide labelled simulation data accurately representing the performance of a typical AHU under a wide range of fault free and faulty conditions, 4) perform an impact scenario analysis associated to faults' occurrence based on simulation results.

This WP3 will help in a) better understanding the current research gaps, b) address the lack of simulation tools of AHUs for impact scenario analyses, c) support the development of, and benchmark the performance accuracy of AFDD methods, d) recognize fault patterns of AHUs and rank the faults with most adverse impacts, e) assess the gap between AHU faulty operation and design expectations.

The WP3 will include the following 4 tasks (WP3_T1, WP3_T2, WP3_T3, WP3_T4):

- WP3_T1) this task provided a scientific written report (1st WP3 deliverable WP3_D1) carrying out a literature review of Air-Handling Unit (AHU) simulation studies for Automated Fault Detection and Diagnosis (AFDD).
- WP3_T2) this task will develop a simulation model able to accurately predict the performance of the typical AHU set-up for AFDD purposes at the "SENS i-Lab". The digital twin will be developed by means of the commercial software "Transient System Simulation Tool (TRNSYS) 18" (https://www.trnsys.com/), worldwide used and well-established in the scientific community. A specific model of each system component will be conceived and characterized to capture its dynamic performance; dedicated features allowing to model the desired faults will be included. The digital twin will be calibrated and validated against the data measured in the WP1. The TRNSYS files of the digital twin, together with the related documentation, will be uploaded in a public repository as 2nd WP3 deliverable WP3_D2.
- WP3_T3) this task will run the validated AHU digital twin with reference to a working week by assuming a 1-minute simulation time-step to obtain a huge simulation dataset representing the performance of the AHU under a wide range of fault free and single/multiple faulty scenarios. The simulations will extend the experimental dataset obtained in the WP1 by considering the same faults' types with additional faults' intensities, faults' durations, operational/seasonal/weather conditions (at least one city for each Italian climatic zone will be analysed). The derived simulation dataset, together with its detailed description, will be uploaded in a public repository as 3rd WP3 deliverable WP3_D3.
- WP3_T4) this task will perform an impact scenario analysis by comparing the simulation outputs related to faulty scenarios with those associated to fault free conditions obtained under the same boundary conditions (simulation period/time-step, climatic zone, location, AHU configuration and control logics) by means of the KPIs selected in the WP2. A scientific written report illustrating the faults' symptoms on AHU performance derived from the simulation dataset will be uploaded in a public repository as 4th WP3 deliverable WP3_D4.

This deliverable WP3_D1 includes a detailed categorization of the scientific studies that developed digital twins of AHUs for AFDD purposes in terms of: AHU operating schemes; simulation environments; simulation models; range of simulated operational, seasonal and weather conditions; duration and time-step of simulations; fault types, fault severity and methods of fault modelling/simulation; faults' symptoms on AHU performance.

Finanziato dall'Unione europea NextGenerationEU | Ministero dell'Università e della Ricerca | Italiadomani PIANO NAZIONALE DI RIPRESA E RESILIENZA

1. Introduction

The building sector represents the largest worldwide consumer of primary energy with a significant corresponding environmental impact (such as ozone layer depletion and global warming) [1]. Heating, Ventilation and Air-Conditioning (HVAC) systems based on the utilization of Air-Handling Units (AHUs) substantially contribute to the overall energy demand and related emissions of the building sector [2]. According to [3, 4], around 20%/30% of the overall energy consumption in buildings is attributable to incorrect system configurations and inappropriate operating procedures. The interest of the scientific community in exploring solutions aiming at improving energy efficiency in buildings by adopting advanced energy management strategies based on data analytics is significantly increasing [3,5,6]. Automated Fault Detection and Diagnosis (AFDD) represents a number of methods aiming at, on one hand, automatically recognizing a fault occurrence, and, on the other hand, identifying the causes and/or the location of the fault [3,5,6]. It has been demonstrated that the adoption of AFDD tools in the case of AHUs can lead to relevant potential energy savings of about 30% [5,7].

Several AFDD methods have been developed during the last years (categorized as quantitative model-based, qualitative model-based and data-driven) [3,5,6]; while qualitative approaches are still the norm in the reference market, vendors are beginning to use data-driven methodologies for addressing AFDD tasks [8] also thanks to (i) their applicability even in the case of the physics-based knowledge of the system is not wide enough as well as (ii) the advancements of statistical and computer-aided data mining techniques. However, the adoption of data-driven AFDD models for AHUs is mainly based on the capability of extracting patterns from performance data. With reference to this point, there are three categories for the research-oriented studies aiming at obtaining such data: (i) lab experiments and field tests, (ii) modelling and simulation activities, and (iii) combination of modelling/simulation and testing. Data from lab experiments and field tests reflect the AHU operation in reality (and they often are used as the ground truth for simulation model validation), but they are difficult to be derived because of a number of reasons to [3; 5-9]: a) several significant key operating parameters of AHUs are generally not measured taking into account that related sensors are usually not designed for developing AFDD tools; b) obtaining experimental data is labour-intensive as well as time- and cost-consuming, also considering that both single and multiple faulty scenarios should be investigated; c) field data can be generally obtained only with reference to limited ranges of weather/load scenarios. In addition, it should be underlined that there is a significant lack of generalizability of data-driven AFDD models due to the fact such tools cannot extrapolate beyond the boundary conditions of training data. The development of accurate simulation models of AHUs could represent one of the most promising options to address and overtake some of the above-mentioned barriers slowing down the fully penetration of data-driven AFDD methods. In fact, in comparison to experimental/field data, such models allow to: (i) monitor and control all the key operating parameters of AHUs; (ii) obtain a huge amount of data with reduced time and costs of investigation; (iii) explore wider range of weather/load scenarios, (iv) more easily investigate the occurrence of multiple faults; (v) more deeply test and assess the robustness and accuracy of AFDD tools versus simulation-based bulk data containing a variety of faulty scenarios under different boundary conditions; (vi) perform wide fault impact scenario analyses allowing to bring more insights on how single or multiple faults can affect building energy consumption, occupants' thermal comfort, etc.; (vii) assess the transferability of AFDD tools with reference to different AHU configurations/sizes/control logics.

Therefore, accurate digital twins of AHUs can lead to (i) a better understanding of AHUs operation by quantifying the effects of faults on building-integrated systems performance, (ii) support decision making about timely fault corrections by providing accurate estimates for potential energy/cost/emission savings that could be obtained by adopting AFDD tools, as well as (iii) help in improving existing tools or developing new simulation models able to accurately take into account the considerable discrepancy between AHU faulty operation performance and nominal expectations (the majority of the AHU energy software assumes the systems are in normal operations without any failures points). There exist some studies on the fault simulation and related fault impact assessment of AHUs demonstrating how much active is the AFDD research field; however, Zhang and Hong [10] highlighted that simulation research on the effects of AHU operational faults is still poor due to the fact that most simulation fault-related studies have been focused on single-component performance rather than the whole-building performance, without considering simultaneous faults occurrence. Moreover, the analyses have been usually devoted to specific AHUs serving particular buildings and, therefore, provided results that could be applied with significant difficulty to other AHU types/configurations. Lu et al. [11] also indicated that: (i) common combinations of multiple faults have to be more deeply investigated; (ii) annual fault simulations should be performed (instead of considering less significant smaller periods); (iii) an extension of climate zones including more load scenarios is necessary.

Finanziato dall'Unione europea NextGenerationEU | Ministero dell'Università e della Ricerca | Italiadomani PIANO NAZIONALE DI RIPRESA E RESILIENZA

This deliverable represents an innovative contribution in the field taking into account that the most significant 31 scientific papers [10, 12-41] focusing on AHU simulation tools to be used for the development of data-driven AFDD systems are systematically reviewed and categorized in terms of AHU operating scheme (section 2.1), modelling and simulation platforms (section 2.2), faults' type and severity level (section 2.3), as well as weather and simulation conditions (section 2.4). This deliverable aims at (i) highlighting the main research gaps to be covered in the field of modelling and simulation of AHUs for the development of AFDD methods, (ii) guiding the future development of new and accurate data-driven AFDD algorithms based on the utilization of AHU digital twins, (iii) increasing awareness of the HVAC research and development community to the body of AFDD.

2. Results

In the following subsections the most important characteristics of the above-mentioned reviewed 31 scientific papers are clearly stated and clarified in order to emphasize the aspects to be further investigated and analysed.

2.1 AHU operating schemes

HVAC systems including AHUs are used to control indoor air temperature, relative humidity, velocity and quality; they are quite sophisticated systems with several interconnected components that may present complex coupling effects. The following three main common AHU operating schemes/configurations are modelled/simulated in the 31 reviewed papers:

- single-duct dual-fan constant air volume AHU. It includes the following main components: supply air fan, return air fan, heating coil (supplied by hot water), cooling coil (supplied by cold water), return air damper, exhaust air damper, fresh air damper, mixing air damper, heating coil valve, cooling coil valve, filters. In this case, the supply air flow rate is constant and the desired indoor conditions are reached by adjusting the air supply temperature. This AHU scheme has been investigated in [34-41]; a very similar AHU scheme with the addition of a humidifier has been analysed in [38-40]; only one coil, operating alternatively as heating or cooling coil, is included in the AHU investigated in [36]; in [37] only the cooling coil is included in the AHU scheme, while only the heating coil is used in [41];
- single-duct dual-fan variable air volume AHU. Unlike the constant air volume AHU scheme, this configuration allows to adjust the supply air flow rate depending on thermal/cooling loads, while maintaining a constant supply air temperature. This scheme has been analysed in [10, 12-25; 27, 28, 30-33];
- dual-duct dual-fan variable air volume AHU. This scheme is characterized by separate ducts for hot and cold air, while served zone includes a plenum where airflows are mixed; the ratio of hot and cold air depends on the desired temperature to be maintained in the zone. This AHU configuration has been modelled and simulated only in [26; 29].

Table 1 indicates the type as well as the floor area of buildings served by the AHUs (where indicated by the authors) together with the corresponding papers.

Table 1. Type and floor area of buildings served by the AHUs in the reviewed papers.

Building type	Floor area (m^2)	References	Building type	Floor area (m^2)	References
Office building	450	[10]	Conference room	240.1	[34]
Office building	Not specified	[23]	Not specified	13500	[36]
Office building	168	[28]	Not specified	25	[37]
Commercial building	Not specified	[16]	Office building	4982.2	[21]
Academic building	Not specified	[17]	Test room of a university lab	16	[38-40]
School building	Not specified	[25]	Single floor in office building	200	[18]
Commercial office building	46321.5	[15]	Commercial building	1166	[27]
Commercial office building	9290.3	[33]	Office building	Not specified	[12, 13]
Iowa Energy Center Energy Resource Station	27.6	[20, 22, 24, 26, 30-33, 35]	Single floor in commercial office building	Not specified	[14]
			Federal Building	130064.26	[29]
Oak Ridge National Laboratory	359.12	[35]	Commercial office building	297	[19]

Finanziato dall'Unione europea NextGenerationEU | Ministero dell'Università e della Ricerca | Italiadomani PIANO NAZIONALE DI RIPRESA E RESILIENZA

2.2 AHU modelling and simulation environments

Whole-building performance simulation programs can be a powerful tool in addressing the barriers currently limiting a wider application of AFDD tools. Developing fault models of AHU is challenging due to the inherent complexity of such systems. Such models can be categorized into three groups [42]: white-box models (applying the first principles to build the detailed models of the actual system), black-box models (statistically created using data from buildings), and grey-box models (corresponding to a combination of white-box models and black-box models). According to the scientific literature, it remains a big research gap on how to model the faults in AHUs, including fault models for all components and fault occurrence probability. There are more than 170 building energy modelling and simulation programs/tools listed on the BEST Directory of the International Building Performance Simulation Association (IBPSA)-USA website [43]. The most important environments that can provide a solid support for AHU modelling and simulation are the following: Engineering equation solver (EES) [44] EnergyPlus [45], HVACSIM+ [46], Matlab [47], Modelica [48], Spark [49], TRNSYS [50], IDA_ICE [51], Ansys [52], Hourly Analysis Program (HAP) [53], IESVE [54]. They represent robust tools supporting scientists, building professionals and engineers in optimizing building design and performance. However, currently only a very limited number of these tools includes fault modelling capability with a limited fault library (e.g., EnergyPlus, TRNSYS, Modelica, and HVACSIM+), and some of them (e.g., TRNSYS, Modelica, and HVACSIM+) need users to create fault models based on physics and domain knowledge [42]. Table 2 highlights the modelling/simulation platforms adopted in the reviewed 31 papers. This table indicates that the most used platform is EnergyPlus [45] (10 cases), while HVACSIM+ [46] is used in 8 studies. Pourarian [26] selected the HVACSIM+ platform [46] based on a detailed review of different modelling/simulation environments (HVACSIM+ [46], TRNSYS [50], EnergyPlus [45], Spark, and Modelica [48]) for evaluating AFDD algorithms through generating faulty data using fault models. According to [42], EnergyPlus [45] is leading the trend in fault simulation thanks to more capabilities for fault modelling, while Modelica [48] seems to be promising for developing physics-based dynamic fault models with control-related faults. The simulation environment is not clearly specified in [17, 37, 41].

Table 2. Simulation platform as a function of the reviewed papers.

Software environment	References
Engineering Equation Solver (EES) [44]	[36]
EnergyPlus [45]	[10, 12, 15, 16, 19, 21, 22, 25, 35]
HVACSIM+ [46]	[13, 14, 20, 24, 26, 29, 32, 35]
Matlab [47]	[25, 28-30, 34, 39, 40]
Modelica [48]	[16, 23, 31, 35]
Spark [49]	[33]
TRNSYS [50]	[18, 27, 28, 36, 38-40]
Ansys [52]	[34]

Simulation models could provide a rapid alternative for the lab/field tests problem, but they should be firstly validated in contrast with accurate measured data. The comparison should be performed not only with reference to fault free performance, but also in contrast with faulty measurements taking into account that AHU faults may lead to a considerable discrepancy between field and design expectations. According to Huang et al. [55], only very limited discussions can be found in the scientific literature on how to assess the accuracy of simulation faulty datasets and almost no information on how to figure out the effects of simulation datasets' quality on data-driven AFDD methods' performance and scalability. With reference to the 31 studies reviewed in this WP task, an experimentally validation of the developed simulation AHU models has been performed only in a few papers [14, 16, 20, 24, 26, 30-33, 35, 38-41]; moreover, it should be underlined that the results of the related experimental validation process are reported only in [20, 26, 32, 35, 38-40].

2.3 AHU faults' type and severity

A fault is intended as an instance where one system or piece of equipment or component performs in a way that is different from normal/expected behaviour. Each type of AHU includes a number of components and each component could be a potential failure point and worth studying as a fault model. Each fault type can occur at different severity levels and a fault occurring at a certain level can affect the performance of many other interconnected components, and, therefore, make it difficult to understand the relationship between effects and causes and, therefore, to assess the overall impact on whole-building performance. Currently there

Finanziato dall'Unione europea NextGenerationEU | Ministero dell'Università e della Ricerca | Italiadomani PIANO NAZIONALE DI RIPRESA E RESILIENZA

is a lack of a comprehensive fault list covering major common faults for AHU in buildings [42]; this fault list could be important for fault modelling and fault impact analysis and it could be also used as a reference to study what faults are the most common ones. In the 31 reviewed papers, 50 different types of faults have been modelled and simulated. For each type of fault, Tables 3, 4, 5 and 6 clarify the scientific papers where the fault type has been investigated as well as its severities (where indicated by the authors). Table 3 corresponds to the faults of actuator, Table 4 highlights the results associated to the faults of sensors, Table 5 describes the faults of controllers, and Table 6 relates to the faults of fans and pumps. These Tables underline that the most investigated fault types are the following ones: fresh air damper stuck (10 papers [13,14,17,20,23,22,30,32,35,38]) in the case of the actuators' faults (Table 3), offset of supply air temperature sensor (11 papers [13,14,16,18,20,23,25, 26, 30-32]) in the case of the sensors' faults (Table 4), unstable control of supply air dumper (2 papers [23,27]) in the case of the faults of controllers (Table 5), and decreased supply air fan motor efficiency (4 papers [15,19,21,23]) in the case of the faults of fans and pumps (Table 6). The following fault types are the most analyzed ones in terms of number of fault severity levels: in the case of the faults of fans and pumps (Table 6), cooling coil valve and fresh air damper stuck (9 severities, i.e., 9 different positions [13,14,16,17,20,22,23,30,32,35,37,38]) in the case of the actuators' faults (Table 3), offset of supply and room air temperature sensor (13 severities, i.e., 13 different temperature bias [12-14,16,18-20,23, 26, 25,28, 30-32]) in the case of the sensors' faults (Table 4), unstable control of supply air damper (3 severities, i.e., 3 different proportional gains P of PID controllers [23,27]) in the case of the faults of controllers (Table 5) and reduced supply air fan flowrate and decreased supply air fan motor efficiency (4 severities, i.e., by 4 different percentages [33,37]).It should be also highlighted that only four studies [18, 21, 25, 34] investigated the effects of multiple faults occurring simultaneously. In addition to the 4 fault types described in Tables 3-6, it must be noted that other fault types have been analyzed in the 31 reviewed papers, such as the fouling of cooling coil/heating coil/filter/duct/pipe [10, 23,12,19,26, 28,36,37], the poor pipe insulation [23], and the duct leakage [19, 23, 35].

Table 3. Type and severity of AHU faults for actuator.

Type of fault	Fault severity	References	Type of fault	Fault severity	References
Mixing air damper stuck	25%	[34]	Supply air damper stuck	0%, 100%	[26]
Fresh air damper stuck	Not specified	[21]	Fresh air damper leakage	Not specified	[17]
	0%	[13, 14, 20, 23, 30, 32, 38]		10	[12]
				0.1%,1%	[23]
	5%, 65%	[23]		10%, 25%, 40%	[13]
	15%	[35, 23]	Return air damper leakage	10%	[13, 14]
	40%	[13, 35]		25%	[13]
	45%,50%	[35]		40%	[13, 14]
	100%	[13, 17, 23]		from 0% to 30 %	[19]
Return air damper stuck	Not specified	[24, 36, 37]	VAV box damper stuck	Not specified	[21, 31]
	0%	[13, 14, 20, 32, 33, 38]		0%,100%	[13, 14]
	30%, 35%, 40%	[36]		50%	[27]
	50%	[29]		80%	[28]
	100%	[13, 20, 32]	VAV reheat valve stuck	0%, 100%	[13; 14]
Economizer air damper stuck	from 0% to 100%	[19]	Return air damper hysteresis	-	[27]
Cooling coil valve stuck	Not specified	[37, 24]	Cooling coil valve leakage	Not specified	[30]
	0%	[13, 14, 16, 35, 23]		0.1%, 1%	[23]
	5%	[23]		10%,25%,40%	[13, 14]
	15%,65%	[23, 35]		20%	[29]
	25%,50%,75%	[16]		1.8 GPM	[20,32]
	100%	[16, 23, 35]			
Heating coil valve leakage	Not specified	[23, 35]	Heating coil valve stuck	Not specified	[41]
	10%, 25%, 40%	[13, 14]		0%	[13, 14, 23]
	1.0 GPM	[20, 32]		5%, 15%, 65%, 100%	[23]
Return air damper sticking	-	[27]			

Table 4. Type and severity of AHU faults for sensors.

Type of fault	Fault severity	References	Type of fault	Fault severity	References
Offset of supply air temperature sensor	Not specified	[30]	Offset of air room temperature sensor	Not specified	[12, 24]

Finanziato dall'Unione europea NextGenerationEU | Ministero dell'Università e della Ricerca | Italiadomani PIANO NAZIONALE DI RIPRESA E RESILIENZA

Type of fault	Fault severity	References	Type of fault	Fault severity	References
	±1 K, ±2 K	[23]		-3 K to +3 K	[19]
	10 °C, 10%	[25]		±1 K, ±2 K	[23]
	from 0 °C to ±4 °C	[13, 14]		10 °C, 10%	[25]
	+1.7 °C, +2.8	[20; 32)		±1 °C	[10]
	+2.8 °C	[31]		1 °C,2 °C	[28]
	±1° C, ±2° C,	[16]		0.3 °C/h, 0.5 °C/h, 0.7 °C/h, 3 °C, 7 °C	[18]
	0.5 °C/h	[18]			
	+5 °F	[26]			
Offset of supply air static pressure sensor	Not specified	[27]	Offset of supply and room CO_2 sensor	±100 ppm, ±200 ppm	[22]
	±15 Pa, ±25	[23]			
	149.3 Pa	[26]			
Offset of supply air flowrate sensor	Not specified	[24, 27]	Offset of return air temperature sensor	Not specified	[36]
	±15%, ±30%	[23]		from –3 K to +3 K	[19]
	±10%, ±20%	[22]		±1 K, ±2 K	[23]
				from 0 °C to ±4 °C	[13, 14]
				±2 °C	[38]
Offset of return air relative humidity sensor	±10%	[38]	Offset of mixed air temperature sensor	±1 K, ±2 K	[23]
	from –10% to +10%	[19]		from 0 °C to ±4 °C	[13, 14]
				from –3 K to +3 K	[19]
Offset of fresh air temperature sensor	from –3 K to	[19]	Offset of fresh air flowrate sensor	15%, 30%	[23]
	–2 °C, –4 °C	[10]			
	±1 °C, ±2 °C,	[35]		±10%, ±20%	[22]
	from 0 °C to ±4 °C	[13, 14]			
	±1 °C, ±2 °C,	[16]			
	±3 °F	[20, 32]			
Offset of fresh air relative humidity sensor	from -10% to +10%	[19]	Freezing of supply air flowrate sensor	0.22 kg/s, 0.5 kg/s	[27]
Freezing of air room temperature sensor	24 °C	[27]	Offset of return chilled water temperature sensor	+4 °C	[18]
Offset of supply hot water temperature sensor	±2 K, ±4 K	[23]	Offset of supply chilled water temperature sensor	±1 K, ±2 K	[23]
	10%, 10 °C	[25]		10%, 10 °C	[25]
				4 °C ,5 °C, 0.9 °C/h	[18]
Offset of chilled water differential pressure sensor	±5000 Pa, ±10000 Pa	[23]	Supply and exhaust air temperature sensors inversed	-	[34]
Offset of chilled water flow sensor	0.1 kg/s, 50%	[25]	Offset of hot water flow sensor	0.1 kg/s, 50%	[25]

Table 5. Type and severity of AHU faults for controllers.

Type of fault	Fault severity	References	Type of fault	Fault severity	References
Unstable control of heating coil valve	Not specified	[34]	Unstable control of supply air temperature PID	proportional gain equal to 0.001 and 0.1	[23]
Unstable control of supply air damper PID	Not specified	[27]	Deviation to minimum/maximum of supply air flowrate sensor	-	[27]
	proportional gain equal to 0.05 and 5	[23]			
Unstable control of supply air fan PID	proportional gain equal to 0.01 and 10	[23]	Unstable control of supply air flow	-	[34]
Delay of supply air fan speed	1 s	[23]	Delay of supply chilled water pump speed control	1 s	[23]
Unstable control of supply chilled water pump	Not specified	[23]	Poor tuning of supply air static pressure control loop	-	[27]

Table 6: Type and severity of AHU faults for fans and pumps

Finanziato dall'Unione europea NextGenerationEU
Ministero dell'Università e della Ricerca
Italiadomani PIANO NAZIONALE DI RIPRESA E RESILIENZA

Fault Type	Fault Severity	References	Fault Type	Fault Severity	References
Decreased supply air fan motor efficiency	Not specified	[15, 21]	Slipping of supply air fan belt	Not specified	[20, 32]
	By 0%-30%	[19]	Limited supply air fan speed	Maximum 25%	[24]
	By 15% and 30%	[23]	Supply air fan stuck	Not specified	[24]
Decreased supply chilled water motor pump efficiency	By 15% and 30%	[23]	Reduced supply air fan flowrate	By 10%, 12.5% and 15%	[36]
				By 14%	[33]
Reduced chilled water flowrate	By 15%, 20% and 25%	[36]	Limited return air fan speed	Maximum 35%	[24]

2.4 Weather conditions, simulation duration and time-step

Weather conditions affect the operation of AHUs; as a consequence, AHU faults may present diverse impacts depending on the season; therefore, a fault analysis assessment upon varying the period of the year should be performed and considering multiple climate regions could allow to assess the effects of faults under different load conditions and, thus, it would strengthen the significance of results. In addition, it should be highlighted that one particular fault may present different operational characteristics; it can be (1) a static fault (if it is constant over the analysis period), or (2) an abrupt fault (if it arises suddenly during the analysis period and stays at a constant level after occurrence) or (3) a degradation fault (if it gradually drifts over time). As a consequence, the duration of faulty scenarios could also affect the results of fault impact analyses. Table 7 classifies the 31 reviewed papers in terms of location, season, duration of simulation, and simulation time-step (if specified), highlighting that: (i) Mediterranean climatic conditions have been considered only in [38-40]; both summer and winter scenarios have been investigated only in 15 studies [10, 14-16, 19-23, 26; 30, 32, 35, 38; 39]. The adopted simulation time-step has been varied from a minimum of 2 seconds [27] up to a maximum of 15 minutes [19, 10], with a simulation duration ranging from 0.6 hours up to 2 years.

Table 7. Location, season, duration and simulation time-step in the reviewed papers.

Location	Season	Simulation duration	Simulation time-step	References
Miami, Houston, San Francesco, Seattle, Chicago (USA)	Whole year	1 year	15 min	[10]
Chicago (USA)	Whole year	7 days	1 min	[23]
Seoul (Korea)	Not specified	Not specified	Not specified	[36]
Not specified	Summer	10 hours	Not specified	[37]
Denver (USA)	Spring	2 days	1 min	[25]
Chicago (USA)	Whole year	2 years	Not specified	[15]
Boston (USA)	Winter	1 month	5 min	[17]
Iowa (USA)	Whole year	5 days	6 min	[30]
Not specified	Winter	6 weeks	1 min	[41]
Iowa, Tennessee (USA)	Whole year	1÷7 days	1 min	[35]
Washington (USA)	Whole year	14 days	Not specified	[14]
Iowa (USA)	Whole year	24 hours	Not specified	[20, 26, 32]
Iowa (USA)	Not specified	24 hours	30 s, 60 s	[24]
San Francisco (USA)	Not specified	12 hours	5 s	[29]
Shanghai (China)	Summer	24 hours	36 s	[28]
Iowa (USA)	Summer	24 hours	Not specified	[31]
San Francisco, Iowa (USA)	Not specified	2÷8 hours	Not specified	[33]
Chicago (USA)	Whole year	1 day, 7 days	Not specified	[16]
Naples (Italy)	Whole year	1 year	1 min	[38]
Aversa (Italy)	Summer and winter	From 0.6 hours to 6.2 hours	1 min	[39]
Aversa (Italy)	Summer	From 1.4 hours to 5.1 hours	1 min	[40]
Doha (Qatar)	Summer	3 months	1 min	[18]
Hong Kong (China)	Not specified	Not specified	2 s	[27]
Chicago, Atlanta (USA)	Not specified	Not specified	Not specified	[12]
Not specified	Not specified	Not specified	10 s	[13]
Not specified	Fall	1 week	5 min	[34]
Knoxville, Tennessee (USA)	Whole year	Whole year	15 min	[19]
Chicago (USA)	Whole year	Whole year	5 min	[22]
Atlanta, Miami, Chicago, San Francisco (USA)	Whole year	250 hours	5 min	[21]

Finanziato dall'Unione europea NextGenerationEU | Ministero dell'Università e della Ricerca | Italiadomani PIANO NAZIONALE DI RIPRESA E RESILIENZA

2.5 Effects of faults

Tables 8-11 indicate the effects of actuator faults (Table 8), faults of sensors' (Table 9), controllers' faults (Table 10), and fans and pumps faults (Table 11) investigated in the 31 reviewed papers [10, 12-41] in terms of thermal comfort, cooling/heating energy demand, and electric energy consumption. Tables 8-11 report the AHU fault impacts only in the case of the corresponding effect is significant, i.e., the fault causes a variation larger than 10% or lower than –10% with respect to the baseline case without faults (otherwise it is assumed as negligible). Fault impact is clearly reported in 10 papers only [10, 12, 16, 17, 22, 28, 23, 35, 38, 39] out of 31; these 10 papers discussed the effects associated to 20 fault types only (corresponding to the lines of the first column of Tables 8-11) at different levels of severity (indicated in the second column of Tables 8-11). With respect to the faults' impacts, it can be clearly noticed that: (i) thermal comfort time is significantly affected in the following fault types/severities: outdoor air damper stuck (at 0% and 5%) [23], VAV damper stuck at 80% [28], offset of room air temperature sensor (+1 °C) [28], offset of return air temperature sensor (±2 °C) [38], offset of return air relative humidity (±10%) [38], cooling coil valve stuck (at 0%, 15%, 65%) [23], heating coil valve stuck at 0% [39], and supply air fan stuck at 20% [39]; (ii) electric energy demand is reduced or increased in a relevant way in the following cases: offset of return air relative humidity sensor (10%) [38], cooling coil valve stuck at 0% [16,39], supply air fan stuck at 20% [39], humidifier valve stuck at 0% [39], and heating coil valve stuck at 0% [39]; (iii) heating energy demand significantly decreases or increases in the cases of the following fault types/severities: mixed air damper stuck at 18% [35], inversion of supply and exhaust air temperature sensors [35], cooling coil valve stuck (0%, 25%, 50%, 75%, 100%) [16, 23]; (iv) the most adverse fault with regard to heating and cooling energy demand is the offset of room air temperature sensor (–1 °C) [10]; (v) the most adverse fault with regard to overall electric demand is the heating coil valve stuck at 0% [39]. According to Tables 8-11, the most adverse faults' types and severities can be summarized as follows: (i) the most adverse fault type with regard to comfort time is the VAV damper stuck at 80% [28]; (ii) the most adverse fault with regard to heating energy demand is the cooling coil valve stuck at 100% [16]; (iii) the most adverse fault with regard to heating and cooling energy demand is the offset of room air temperature sensor (–1 °C) [10]; (iv) the most adverse fault with regard to overall electric demand is the heating coil valve stuck at 0% [38]; (v) the most adverse fault with regard to fan energy use is the unstable control of supply air flowrate [35]; (vi) humidifier valve stuck at 0% has been studied only in a single case [39], highlighting the effectiveness of this fault on overall electric energy demand; (vii) supply air fan stuck at 20% has been analyzed only in a single paper [39], demonstrating its relevancy with regard to thermal comfort time and overall electric energy demand. Tables 8-11 show that similar fault impacts can be obtained by different fault types and/or fault intensities. They also indicate that a single fault can cause single or multiple impacts based on the fault's type and its corresponding intensity.

Table 8. Most relevant effects of actuators' faults on thermal comfort and energy demands.

Type	Severity	Significant effect
Outdoor air damper leakage	20%	Cooling energy use increased by 12.5% [12]
Outdoor air damper stuck	0%	Thermal comfort time and electric energy use reduced by 87.8% and 31%, respectively [23]
	5%	Thermal comfort time and electric energy demand reduced by 89.1%, and 26.7%, respectively [23]
	65%	Electric energy demand increased by 16.6% [23]
	100%	Electric energy demand increased by 18% [17] and 25.2% [23]
Mixed air damper stuck	18%	Heating energy demand decreased by 95.6% [35]
VAV damper stuck	80%	Thermal comfort time decreased by 100% and fan energy demand increased by 21% [28]
Cooling coil valve stuck	0%	Thermal comfort time reduced by 98.8% in [23] and 70% in [39], heating energy use decreased by 70% [16], electric energy use decreased by 50% in [16] and 57% in [39]
	5%	Thermal comfort time decreased by 98.4% and electric energy use increased by 20.7% [23]
	15%	Thermal comfort time decreased by 98.2% and electric energy demand increased by 24.3% [23]
	65%	Thermal comfort time decreased by 74.2% and electric energy demand increased by 30.2% [23]
	25%, 50%, 75%	Heating energy demand increased by 150%, 240% and 280%, respectively, at 25%, 50% and 75% [16]
	100%	Electric energy demand increased by 35% [9], heating energy demand increased by 300% [16]
Heating coil valve stuck	0%	Thermal comfort time and electric energy demand decreased by 63% and 81%, respectively [39]

Finanziato dall'Unione europea NextGenerationEU | Ministero dell'Università e della Ricerca | Italiadomani PIANO NAZIONALE DI RIPRESA E RESILIENZA

Type	Severity	Significant effect
	0%, 5%, 15%	Electric energy demand increased by 46.2%, 27.6%, and 23.9%, respectively, at 0%, 5%, 15% [23]
Humidifier valve stuck	0%	Thermal comfort time and electric energy use reduced by 28% and 56%, respectively [39]

Table 9. Most relevant effects of sensors' faults on thermal comfort and energy demands.

Type	Severity	Significant effect
Offset of outdoor air temperature sensor	–4 °C	Cooling energy demand increased by 14.6% [10]
Offset of outdoor airflow sensor	20%	Electric energy demand decreased by 13.9% [22]
Offset of supply air temperature sensor	±1 °C, ±2 °C, ±4 °C	Heating energy demand decreased by 55%, 80%, and 20% at –4 °C, –2 °C, –1 °C, respectively, and increased by 50%, 130%, and 110% at 1 °C, 2 °C, 4 °C, respectively [16]
Offset of room air temperature sensor	±0.5 K	Heating energy demand decreased by 15% [12]
	2 K	Thermal comfort time decreased by 13.1% [23]
	–1 °C	Thermal comfort time decreased by 24.3%, and cooling and heating energy demand increased by 34.24% [10]
	+1 °C	Thermal comfort time decreased by 100% [26], cooling and heating energy demand reduced by 28.9% [10]
Offset of return air temperature sensor	2 °C	Thermal comfort time and electric energy demand reduced by 74.9% and 26.5%, respectively [38]
	–2 °C	Thermal comfort time reduced by 79.9% and electric energy demand increased by 18.1% [38]
Offset of return air relative humidity sensor	10%	Thermal comfort time reduced by 55.9% and electric energy demand decreased by 42.5% [38]
	–10%	Thermal comfort time reduced by 20.9%, and electric energy demand increased by 25.4% [38]

Table 10. Most relevant effects of controllers' faults on thermal comfort and energy demands.

Type	Severity	Significant effect
Chilled water supply temperature setpoint falsely set to maximum	-	Electric energy use increased by 21.9% [23]
Unstable control of heating coil valve	-	Heating energy use increased by 17.4% [35]
Inversion of supply and exhaust air temperature sensors	-	Heating energy use reduced by 54% [35]
Unstable control of supply fan air flowrate	-	Decreased fan energy use and heating energy use by 47% and 20%, respectively [35]
Unstable PID control of supply air temperature	P=0.001	Thermal comfort time decreased by 20% and electric energy use increased by 20% [23]
Unstable PID control of room air cooling	P=0.1	Thermal comfort time decreased by 15.8% [23]

Table 11. Most relevant effects of fans' and pumps' faults on thermal comfort and energy demands.

Type	Severity	Significant effect
Supply air fan stuck	20%	Thermal comfort time and electric energy demand decreased by 66% and 42%, respectively [39]

3. Discussion and conclusion

Scientific literature on data-driven AFDD algorithms mostly focuses on simulation faulty datasets due to the difficulties of obtaining lab/field data. In this deliverable the most significant scientific studies focusing on the development of digital twins of air-handling units for fault detection and diagnosis purposes have been systematically reviewed and categorized. The review highlighted that: (i) dual-duct dual-fan variable air volume AHUs have been poorly modelled and simulated; (ii) the most used software platform for modelling and simulating AHU operation is EnergyPlus [45]; (iii) the more frequently investigated fault types in the reviewed papers are: return air damper stuck, offset of supply air temperature sensor, fresh air damper stuck, cooling coil valve stuck, offset of room temperature sensor and offset of fresh air temperature sensor; (iv) the effects associated to the simultaneous occurrence of multiple faults have to be additionally analyzed; (v) most of the simulations have been performed under USA climatic conditions, while the performance of AHUs under Mediterranean climates requires further researches; (vi) whole year conditions have been investigated in a limited number of studies; (vii) most of the simulation researches have been performed with a time-step equal to 1 minute; (viii) the most adverse fault type with reference to comfort time is the VAV damper stuck at 80%

Finanziato dall'Unione europea NextGenerationEU | Ministero dell'Università e della Ricerca | Italiadomani PIANO NAZIONALE DI RIPRESA E RESILIENZA

[28]; (ix) the most adverse fault with reference to heating energy demand is the cooling coil valve stuck at 100% [16]; (x) the most adverse fault with reference to heating and cooling energy demand is the offset of room air temperature sensor (–1 °C) [10]; (xi) the most adverse fault with reference to overall electric demand is the heating coil valve stuck at 0% [39]; (xii) the development of future energy models for existing buildings should consider the occurrence of faults (instead of considering nominal/healthy operation only) to improve their accuracy and transparency; (xiii) next works should focus on the development of new category of fault-modelling features in the most used simulation and modelling platforms. It should be also underlined that AFDD strategies that are only tested based on simulation datasets might experience problems in the case of they are applied to real buildings mainly due to (a) sensors' accuracy and noise, as well as (b) typical differences between real data and simulated outputs (taking into account that simulation models cannot perfectly and/or completely predict the real building systems' operation). Finally, according to the scientific literature, there is a significant lack of assessment of both performance and scalability of data-driven AFDD approaches using simulated data in comparison to real building data.

4. References

[1] Cao, X, Dai, X, Liu, J, 2016. Building energy-consumption status worldwide and the state-of-the-art technologies for zero-energy buildings during the past decade. *Energy and Buildings*, *128*, 198–213.

[2] Yun, W. S, Hong, W. H, Seo, H, 2021. A data-driven fault detection and diagnosis scheme for air handling units in building HVAC systems considering undefined states. *Journal of Building Engineering*, *35*, 102111.

[3] Kim, J, Frank, S, Braun, J. E, Goldwasser, D, 2019. Representing Small Commercial Building Faults in EnergyPlus, Part I: Model Development. *Buildings*, *9*(11), 1–23.

[4] Au-Yong, C. P, Ali, A. S, Ahmad, F, 2014. Improving occupants' satisfaction with effective maintenance management of HVAC system in office buildings. *Automation in Construction*, *43*, 31–37.

[5] Yu, Y, Woradechjumroen, D, Yu, D, 2014. A review of fault detection and diagnosis methodologies on air-handling units. *Energy and Buildings*, *82*, 550–562.

[6] Mirnaghi, M. S, Haghighat, F, 2020. Fault detection and diagnosis of large-scale HVAC systems in buildings using data-driven methods: A comprehensive review. *Energy and Buildings*, *229*, 110492.

[7] Frank, S, Lin, G, Jin, X, Singla, R, Farthing, A, Granderson, J, 2019. A performance evaluation framework for building fault detection and diagnosis algorithms. *Energy and Buildings*, *192*, 84–92.

[8] Granderson, J, Lin, G, Singla, R, Mayhorn, E, Ehrlich, P, Vrabie, D, 2021. Commercial Fault Detection and Diagnostics Tools: What They Offer, How They Differ, and What's Still Needed. In *Lawrence Berkeley National Laboratory*.

[9] Rosato, A, Guarino, F, Youssef, M. El, Sibilio, S, Maffei, L, 2021a. Preliminary symptoms assessment of typical faults related to the fans and humidifiers of HVAC systems based on experimental data collected during Italian summer and winter. *IOP Conference Series: Earth and Environmental Science*, *897*(1).

[10] Zhang, R, Hong, T, 2017. Modeling of HVAC operational faults in building performance simulation. *Applied Energy*, *202*, 178–188.

[11] Lu, X., Adetola, V., & O'Neill, Z. 2021. What are the impacts on the HVAC system when it provides frequency regulation?–A comprehensive case study with a Multi-Zone variable air volume (VAV) system. *Energy and Buildings*, *243*, 110995.

[12] Basarkar, M, Pang, X, Wang, L, Haves, P, Hong, A, 2011. MODELING AND SIMULATION OF HVAC FAULTS IN ENERGYPLUS. *IBPSA Building Simulation 2011*, 2897–2903.

[13] Bushby, S. T, Castro, N, Park, M. A, Cheol, G, 2001. Using the Virtual Cybernetic Building Testbed and FDD Test Shell for FDD Tool Development NISTIR 6818 Using the Virtual Cybernetic Building Testbed and FDD Test Shell for FDD Tool Development. In *NIST Interagency/Internal Report NISTIR 6818*.

[14] Castro, N. S, Schein, J, Park, C, Galler, M. A, Bushby, S. T, House, J. M, 2003. Results from Simulation and Laboratory Testing of Air Handling Unit and Variable Air Volume Box Diagnostic Tools. In *NIST Interagency/Internal Report (NISTIR 6964)* (Issue July 2016).

[15] Chakraborty, D, Elzarka, H, 2019. Early detection of faults in HVAC systems using an XGBoost model with a dynamic threshold. *Energy and Buildings*, *185*, 326–344.

[16] Chen, Y, Huang, S, Vrabie, D, 2018. A SIMULATION BASED APPROACH FOR IMPACT ASSESSMENT OF PHYSICAL FAULTS : LARGE COMMERCIAL BUILDING HVAC CASE STUDY Yan Chen, Sen Huang, and Draguna Vrabie Pacific Northwest National Laboratory , Richland , WA. *ASHRAE Building Performance Modeling Conference And*, *2016*, 823–830.

[17] Deshmukh, S, Samouhos, S, Glicksman, L, Norford, L, 2019. Fault detection in commercial building VAV AHU: A case study of an academic building. *Energy and Buildings*, *201*, 163–173.

[18] Elnour, M, Meskin, N, Al-Naemi, M, 2020. Sensor data validation and fault diagnosis using Auto-Associative Neural Network for HVAC systems. *Journal of Building Engineering*, *27*, 100935.

[19] Kim, W, Katipamula, S, 2018. A review of fault detection and diagnostics methods for building systems. *Science and Technology for the Built Environment*, *24*(1), 3–21.

[20] Li, S, 2009. A Model-Based Fault Detection and Diagnostic Methodology for Secondary HVAC Systems. *Drexel University*.

[21] Li, Y, O'Neill, Z, 2019. An innovative fault impact analysis framework for enhancing building operations. *Energy and Buildings*, *199*, 311–331.

[22] Lu, X, Fu, Y, O'Neill, Z, Wen, J, 2021. A holistic fault impact analysis of the high-performance sequences of operation for HVAC systems: Modelica-based case study in a medium-office building. *Energy and Buildings*, *252*, 111448.

[23] Lu, X, O'Neill, Z, Li, Y, Niu, F, 2020. A novel simulation-based framework for sensor error impact analysis in smart building systems: A case study for a demand-controlled ventilation system. *Applied Energy*, *263*, 114638.

[24] Montazeri, A, Kargar, S. M, 2020. Fault detection and diagnosis in air handling using data-driven methods. *Journal of Building Engineering*, *31*, 101388.

[25] Papadopoulos, P. M, Lymperopoulos, G, Polycarpou, M. M, Ioannou, P, 2022. Distributed Diagnosis of Sensor and Actuator Faults in Air Handling Units in Multi-Zone Buildings: A Model-Based Approach. *Energy and Buildings*, *256*, 111709.

[26] Pourarian, S, 2015. *Tools for Evaluating Fault Detection and Diagnostic Methods for HVAC Secondary Systems* (Issue July) [PhD Thesis, Drexel University, USA]. http://marketingdatabase.tat.or.th/download/article/research/1201finalreport.pdf

[27] Qin, J, Wang, S, 2005. A fault detection and diagnosis strategy of VAV air-conditioning systems for improved energy and control performances. *Energy and Buildings*, *37*(10), 1035–1048.

[28] Qiu, A, Yan, Z, Deng, Q, Liu, J, Shang, L, Wu, J, 2020. Modeling of HVAC Systems for Fault Diagnosis. *IEEE Access*, *8*, 146248–146262.

[29] Salsbury, T. I, Diamond, R. C, 2001. Fault detection in HVAC systems using model-based feedforward control. *Energy and Buildings*, *33*(4), 403–415.
[30] Schiendorfer, A, Zimmermann, G, Lu, Y, Lo, G, 2012. FAULT DIAGNOSIS IN HVAC SYSTEMS BASED ON THE HEAT FLOW MODEL 1. *Siemens Corporation, Corporate Research and Technology, Princeton, NJ 2 Informatik, University of Kaiserslautern, Germany*. 440–447.
[31] Shahnazari, H, Mhaskar, P, House, J. M, Salsbury, T. I, 2019. Modeling and fault diagnosis design for HVAC systems using recurrent neural networks. *Computers and Chemical Engineering*, *126*, 189–203.
[32] Wen, J, Li, S, 2011. ASHRAE 1312-RP Tools for Evaluating Fault Detection and Diagnostic Methods for Air-Handling Units. In *Review of 3D printing and potential red meat applications*.
[33] Xu, P, Haves, P, 2002. Field testing of component-level model-based fault detection methods for mixing boxes and VAV fan systems. *Aceee 2002*, *50678*(50678), 1–11.
[34] Ginestet, S, Marchio, D, Morisot, O, 2008. Evaluation of faults impacts on energy consumption and indoor air quality on an air handling unit. *Energy and Buildings*, *40*(1), 51–57.
[35] Granderson, J, Lin, G, Harding, A, Im, P, Chen, Y, 2020. Building fault detection data to aid diagnostic algorithm creation and performance testing. *Scientific Data*, *7*(1), 1–14.
[36] Han, D. W, Chang, Y. S, Kim, S. Y, Kim, Y, 2010. *Fault Detection and Diagnosis Simulation for CAV AHU System*. 687–696.
[37] Liang, J, Du, R, 2007. Model-based Fault Detection and Diagnosis of HVAC systems using Support Vector Machine method. *International Journal of Refrigeration*, *30*(6), 1104–1114
[38] Rosato, A, Guarino, F, Filomena, V, Sibilio, S, Maffei, L, 2020. Experimental calibration and validation of a simulation model for fault detection of HVAC systems and application to a case study. *Energies*, *13*(15).
[39] Rosato, A, Guarino, F, Sibilio, S, Entchev, E, Masullo, M, Maffei, L, 2021b. Healthy and faulty experimental performance of a typical HVAC system under italian climatic conditions: Artificial neural network-based model and fault impact assessment. *Energies,* 14(17).
[40] Rosato, A, Sibilio, S, Guarino, F, El Youssef, M, Entchev, E, Maffei, L, 2022. Field Performance of HVAC System Under Healthy and Faulty Conditions During the Summer: Preliminary Development of a Simulation Model Based on Artificial Neural Networks. *Sustainability in Energy and Buildings 2021 - Smart Innovation, Systems and Technologies, 263*, 183–196.
[41] Verbert, K, Babuška, R, De Schutter, B, 2017. Combining knowledge and historical data for system-level fault diagnosis of HVAC systems. *Engineering Applications of Artificial Intelligence*, *59*, 260–273.
[42] Li, Y, O'Neill, Z, 2018. A critical review of fault modeling of HVAC systems in buildings. *Building Simulation*, *11*(5), 953–975.
[43] IBPSA, Building Energy Software Tools. BEST Directory, 2022, https://www.ibpsa.us/best-directory-list/
[44] F-Chart software, 2022. Engineering Equation Solver. https://fchartsoftware.com/ees
[45] EnergyPlus, 2022. Energy Simulation Software for Buildings. https://energyplus.net/
[46] HVACSIM+, 2022. https://www.nist.gov/publications/hvacsim-users-guide-update
[47] MatLab, Simulation and Model-Based Design, 2022. https://it.mathworks.com/products/matlab.html
[48] OpenModelica, 2022. https://www.openmodelica.org/
[49] Spark, 2022. https://spark.apache.org/
[50] TRNSYS, Transient energy system simulation tool, 2022. http://www.trnsys.com
[51] IDA_ICE, 2022. https://www.equa.se/en/ida-ice
[52] Ansys, 2022. https://www.ansys.com/
[53] HAP, Hourly Analysis Program, 2022. https://www.carrier.com/commercial/en/us/software/hvac-system-design/hourly-analysis-program/
[54] IESVE, 2022. https://www.iesve.com/software/virtual-environment
[55] Huang, J, Wen, J, Yoon, H, Pradhan, O, Wu, T, O'Neill, Z, Selcuk Candan, K, 2022. Real vs. simulated: Questions on the capability of simulated datasets on building fault detection for energy efficiency from a data-driven perspective. Energy and Buildings, 259, 111872.

Finanziato dall'Unione europea NextGenerationEU | Ministero dell'Università e della Ricerca | Italiadomani PIANO NAZIONALE DI RIPRESA E RESILIENZA

DELIVERABLE WP3_D2

EXPERIMENTAL CALIBRATION AND VALIDATION OF AHU DIGITAL TWIN

EDIT BY UNICAMPANIA

PRIN 2022 - UTMOST FDD: AN AUTOMATED, OPEN, SCALABLE AND TRANSPARENT FAULT DETECTION AND DIAGNOSIS PROCESS FOR AIR-HANDLING UNITS BASED ON A HYBRID EXPERT AND ARTIFICIAL INTELLIGENCE APPROACH

Funded by the European Union - Next Generation EU within the "Piano Nazionale di Ripresa e Resilienza (PNRR), missione 4 componente 2 investimento 1.1 - fondo per il programma nazionale di ricerca e progetti di rilevante interesse nazionale (PRIN)"

Finanziato dall'Unione europea NextGenerationEU

Ministero dell'Università e della Ricerca

Italiadomani PIANO NAZIONALE DI RIPRESA E RESILIENZA

The UTMOST FDD Project is organised into the following 7 Work Packages (WPs):
WP0) PROJECT COORDINATION
WP1) EXPERIMENTAL ANALYSIS FOR THE CHARACTERIZATION OF FAULTY AND NORMAL OPERATION OF A TYPICAL AHU
WP2) KPIs IDENTIFICATION FOR ASSESSING FAULT IMPACT IN AHU OPERATION
WP3) AHU DIGITAL TWIN AND SIMULATION-BASED FAULT IMPACT SCENARIO ANALYSIS
WP4) DEFINITION OF HYBRID FDD STRATEGIES FOR AHUs
WP5) TRANSFERABILITY ANALYSIS OF THE FDD STRATEGIES
WP6) KNOWLEDGE TRANSFER AND DISSEMINATION

The WPs are organized into Tasks (T) ranging from 2 to 4 for each WP.

The WP3 aims at achieving the following main objectives: 1) analyse and categorize the scientific studies on digital twins of Air-Handling Units (AHUs) for Automated Fault Detection and Diagnosis (AFDD) purposes, 2) publicly provide a detailed digital twin of a typical AHU validated against measured data, 3) publicly provide labelled simulation data accurately representing the performance of a typical AHU under a wide range of fault free and faulty conditions, 4) perform an impact scenario analysis associated to faults' occurrence based on simulation results.

This WP3 will help in a) better understanding the current research gaps, b) address the lack of simulation tools of AHUs for impact scenario analyses, c) support the development of, and benchmark the performance accuracy of AFDD methods, d) recognize fault patterns of AHUs and rank the faults with most adverse impacts, e) assess the gap between AHU faulty operation and design expectations.

The WP3 will include the following 4 tasks (WP3_T1, WP3_T2, WP3_T3, WP3_T4):

- WP3_T1) this task provided a scientific written report (1st WP3 deliverable WP3_D1) carrying out a literature review of Air-Handling Unit (AHU) simulation studies for Automated Fault Detection and Diagnosis (AFDD).
- WP3_T2) this task develops a simulation model able to accurately predict the performance of the typical AHU set-up for AFDD purposes at the "SENS i-Lab". The digital twin will be developed by means of the commercial software "Transient System Simulation Tool (TRNSYS) 18" (https://www.trnsys.com/), worldwide used and well-established in the scientific community. A specific model of each system component will be conceived and characterized to capture its dynamic performance; dedicated features allowing to model the desired faults will be included. The digital twin will be calibrated and validated against the data measured in the WP1. The TRNSYS files of the digital twin, together with the related documentation, will be uploaded in a public repository as 2nd WP3 deliverable WP3_D2.
- WP3_T3) this task will run the validated AHU digital twin with reference to a working week by assuming a 1-minute simulation time-step to obtain a huge simulation dataset representing the performance of the AHU under a wide range of fault free and single/multiple faulty scenarios. The simulations will extend the experimental dataset obtained in the WP1 by considering the same faults' types with additional faults' intensities, faults' durations, operational/seasonal/weather conditions (at least one city for each Italian climatic zone will be analysed). The derived simulation dataset, together with its detailed description, will be uploaded in a public repository as 3rd WP3 deliverable WP3_D3.
- WP3_T4) this task will perform an impact scenario analysis by comparing the simulation outputs related to faulty scenarios with those associated to fault free conditions obtained under the same boundary conditions (simulation period/time-step, climatic zone, location, AHU configuration and control logics) by means of the KPIs selected in the WP2. A scientific written report illustrating the faults' symptoms on AHU performance derived from the simulation dataset will be uploaded in a public repository as 4th WP3 deliverable WP3_D4.

This deliverable WP3_D2 describes the developed TRNSYS model used to calibrated and validate the TRNSYS models of each AHU component.

1. Description of TRNSYS AHU model

Fig.1 reports a schematic of the AHU as modelled in TRNSYS. In this scheme, all the components of the AHU set-up modelled in TRNSYS are illustrated, along with all the experimental data used to calibrate and validate the simulation model.

Finanziato dall'Unione europea NextGenerationEU | Ministero dell'Università e della Ricerca | Italiadomani PIANO NAZIONALE DI RIPRESA E RESILIENZA

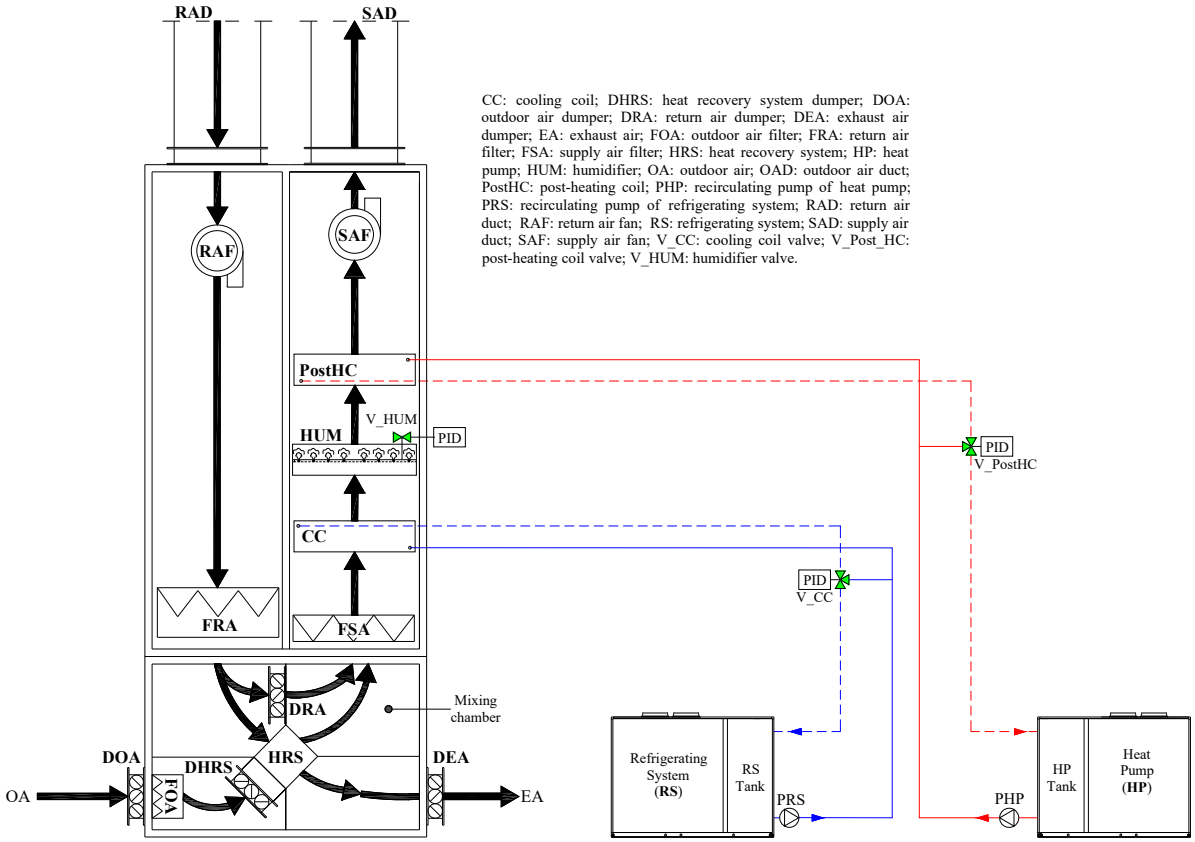

Figure 1. AHU TRNSYS model scheme.

Table 1 reports the TRNSYS Types used to model each AHU component.

Table 1. TRNSYS Model Types.

LIST OF TYPES	EXPERIMENTAL SET-UP COMPONENT
607a	Return Air Fan Duct (RAD)
Calculator	Return Air Fan (RAF)
Calculator	Return Air Filter (FRA)
Calculator	Exhaust and Return Air Dampers (DEA, DRA)
Calculator	Outdoor Air Damper (DOA)
Calculator	Outdoor Air Filter (FOA)
Type 667b	Heat Recovery System (HRS)
Type 648	Mixing Chamber
Calculator	Supply Air Filter (FSA)
Type 941	Refrigerating System (RS)
Type 1534	Refrigerating System Tank (RS Tank)
Type 742	Refrigerating System Recirculation Pump (Pump RS)
Type 31	Pipe Refrigerating System to Cooling Coil (RS to CC)
Type 647	Three-way flow diverter valve Cooling Coil (CC)
Type 508c	Cooling Coil (CC)
Type 649	Three-way mixing valve Cooling Coil to Refrigerating System (CC to RS)

Finanziato dall'Unione europea NextGenerationEU
Ministero dell'Università e della Ricerca
Italiadomani

Type 31	Pipe Cooling Coil to Refrigerating System (CC to RS)
Type 941	Heat Pump (HP)
Type 1534	Heat Pump Tank (HP Tank)
Type 742	Heat Pump Recirculation Pump (Pump HP)
Type 31	Pipe Heat Pump to Post-Heating Coil (HP to PostHC)
Type 647	Three-way flow diverter valve Post-Heating Coil (PostHC)
Type 753b	Post-Heating Coil (CC)
Type 649	Three-way mixing valve Post-Heating Coil to Heat Pump (PostHC to HP)
Type 31	Pipe Post-Heating Coil to Heat Pump (PostHC to HP)
Calculator	Humidifier (HUM)
Calculator	Supply Air Fan (SAF)
Type 607a	External Supply Air Fan Duct (External SAD)
Type 607a	Internal Supply Air Fan Duct (Internal SAD)
Type 2	Controller Ctrl_RS
Type 2	Controller Ctrl_HP
Type 2	Controller Ctrl_HUM
Type 2	Controller Ctrl_Dehum
Type 2	Controller Ctrl_CC_Temp
Type 2	Controller Ctrl_PostHC_Temp
Type 23	PID Controller CC_Temp
Type 23	PID Controller CC_Dehum
Type 23	PID Controller PostHC
Type 23	PID Controller Humidifier
Type 33e	Psychrometrics
Type 25c	Printer
Type 65d	Online plotter

In the following subsections, the above-mentioned TRNSYS Types, used to model each AHU component, are detailed.

1.1 Return Air Fan Duct (RAD) - Type 607a

The return Air Fan Duct (RAD) is modelled by the Type 607a. The parameters of the Return Air Fan Duct (RAD) type are reported in Fig. 2.

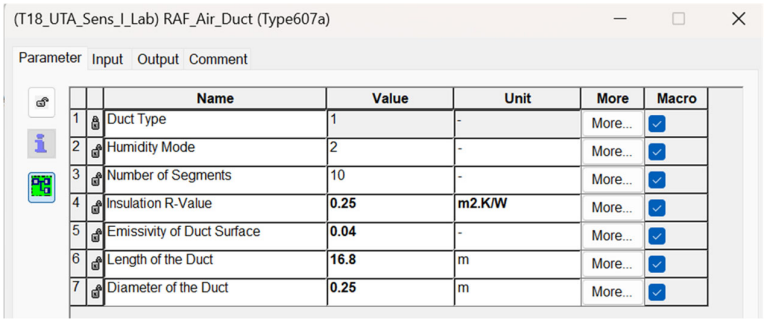

Figure 2. Parameters of RAD Types.

Finanziato dall'Unione europea NextGenerationEU
Ministero dell'Università e della Ricerca
Italiadomani PIANO NAZIONALE DI RIPRESA E RESILIENZA

Tables 2a and b illustrate the inputs and outputs of return air fan duct, respectively.

Table 2a. Inputs of RAD Type.

INPUTS	
LIST OF INPUTS	INPUTS USED
Inlet Air Temperature	Experimental Return Air Temperature - T_RA
Inlet Air Humidity Ratio	-
Inlet Air % Relative Humidity	Experimental Return Air Relative Humidity - RH_RA
Air Flowrate	Experimental Return Air mass flowrate - m_RA
Inlet Air Pressure	1 atm (constant value) - p_RA
Environment Temperature	Experimental Outdoor Air Temperature - T_OA
Wind Velocity	Outdoor Air Velocity (output Type 15-3)

Table 2b. Outputs of RAD Type.

OUTPUTS	
LIST OF OUTPUTS	OUTPUTS USED
Outlet Air Temperature	Experimental Return Air Temperature - T_RA
Outlet Air % Relative Humidity	Experimental Return Air Relative Humidity - RH_RA
Outlet Air Flowrate	Experimental Return Air mass flowrate - m_RA
Outlet Air Pressure	1 atm (constant value) - p_RA

The return air mass flowrate is defined according to Eq. 1 defined based on experimental data:

$$\begin{aligned} m\_RA = {} & (751.04*Density\_RA\_kg\_m3)*(eql(Set\_OL\_SAF,5)*eql(Set\_OL\_RAF,5)) \\ & +((611.43*Density\_SA\_kg\_m3+0*Density\_EA\_kg\_m3)- \\ & 252.69*Density\_OA\_kg\_m3)*(eql(Set\_OL\_SAF,5)*eql(Set\_OL\_RAF,0)) \\ & +(311.90*Density\_RA\_kg\_m3)*(eql(Set\_OL\_SAF,0)*eql(Set\_OL\_RAF,5)) \\ & +(682.12*Density\_RA\_kg\_m3)*(eql(Set\_OL\_SAF,10)*eql(Set\_OL\_RAF,5)) \\ & +(1149.68*Density\_RA\_kg\_m3)*(eql(Set\_OL\_SAF,5)*eql(Set\_OL\_RAF,10)) \end{aligned} \quad (1)$$

Where:

- The constant value 751.04 is the experimental return air volumetric flowrate, when the return air fan velocity and the supply air fan velocity is equal to 50% (fault-free scenario);
- Density_RA_kh_m3 is the return air density, calculated via the psychometric Type33e;
- Set_OL_SAF is the experimental supply air fan velocity;
- Set_OL_RAF is the experimental return air fan velocity;
- The constant value 611.43 is the experimental supply air volumetric flowrate when the return air fan velocity is equal to 0% (faulty scenario) and the supply air fan velocity is equal to 50% (fault-free scenario);
- Density_SA_kg_m3 is the supply air density, calculated via the psychometric Type33e;
- The constant value 0 is the experimental exhaust volumetric air flowrate when the return air fan velocity is equal to 0% (faulty scenario) and the supply air fan velocity is equal to 50% (fault-free scenario);
- Density_EA_kg_m3 is the exhaust air density, calculated via the psychometric Type33e;
- The constant value 252.69 is the experimental outdoor air volumetric flowrate when the return air fan velocity is equal to 0% (faulty scenario) and the supply air fan velocity is equal to 50% (fault-free scenario);
- Density_OA_kg_m3 is the outdoor air density, calculated via the psychometric Type33e;

Finanziato dall'Unione europea NextGenerationEU | Ministero dell'Università e della Ricerca | Italiadomani PIANO NAZIONALE DI RIPRESA E RESILIENZA

- The constant value 311.90 is the experimental return air volumetric flowrate, when the return air fan velocity is equal to 50% (fault-free scenario) and the supply air fan velocity is equal to 0% (faulty scenario);
- The constant value 682.12 is the experimental return air volumetric flowrate, when the return air fan velocity is equal to 50% (fault-free scenario) and the supply air fan velocity is equal to 100% (faulty scenario);
- The constant value 1149.68 is the experimental return air volumetric flowrate, when the return air fan velocity is equal to 100% (faulty scenario) and the supply air fan velocity is equal to 50% (fault-free scenario).

Outdoor Air Velocity are derived from the Type 15-3 taking into account the Energy+ weather data of Naples city.

1.2 Return Air Fan (RAF) - Calculator

The Return Air Fan (RAF) is modelled by using a calculator and not a specific type. Tables 3a and b illustrate the inputs and outputs of return air fan calculator, respectively.

Table 3a. Inputs of RAF Calculator.

INPUTS	
LIST OF INPUTS	INPUTS USED
Inlet Air Temperature	Experimental Return Air Temperature - T_RA
Inlet Air % Relative Humidity	Experimental Return Air Relative Humidity - RH_RA
Air Flowrate	Experimental Return Air mass flowrate - m_RA
Inlet Air Pressure	1 atm (constant value) - p_A_in_RAF

Table 3b. Outputs of RAF Calculator.

OUTPUTS	
LIST OF OUTPUTS	OUTPUTS USED
Outlet Air Temperature	Experimental Return Air Temperature - T_RA
Outlet Air % Relative Humidity	Experimental Return Air Relative Humidity - RH_RA
Outlet Air Flowrate	Experimental Return Air mass flowrate - m_RA
Outlet Air Pressure	1 atm (constant value) - p_A_out_RAF
	Electric power EP_RAF

The Electric power EP_{RAF} is defined according to Eq. 2. The equation is derived by interpolating the electrical power consumed by the return air fan as a function of its velocity.

$$EP\_RAF = (-0.0142*Set\_OL\_RAF^5+0.2882*Set\_OL\_RAF^4- 1.3779*Set\_OL\_RAF^3+4.0138*Set\_OL\_RAF^2-1.5187*Set\_OL\_RAF+17.101)/1000 \quad (2)$$

Where:

- Set_OL_RAF is the experimental return air fan velocity.

1.3 Return Air Filter (FRA) - Calculator

The Return Air Filter (FRA) is modelled by using a calculator and not a specific type. Tables 4a and 4b illustrates the inputs and outputs of return air filter calculator, respectively.

Table 4a. Inputs of FRA Calculator.

INPUTS	
LIST OF INPUTS	INPUTS USED

Finanziato dall'Unione europea NextGenerationEU | Ministero dell'Università e della Ricerca | Italiadomani PIANO NAZIONALE DI RIPRESA E RESILIENZA

Inlet Air Temperature	Experimental Return Air Temperature - T_RA
Inlet Air % Relative Humidity	Experimental Return Air Relative Humidity - RH_RA
Air Flowrate	Experimental Return Air mass flowrate - m_RA
Inlet Air Pressure	1 atm (constant value) - p_A_in_FRA

Table 4b. Outputs of FRA Calculator.

OUTPUTS	
LIST OF OUTPUTS	OUTPUTS USED
Outlet Air Temperature	Experimental Return Air Temperature - T_RA
Outlet Air % Relative Humidity	Experimental Return Air Relative Humidity - RH_RA
Outlet Air Flowrate	Experimental Return Air mass flowrate - m_RA
Outlet Air Pressure	1 atm (constant value) - p_A_out_FRA
Outlet Air Pressure Drop	Return air pressure difference outlet the FRA - Dp_A_FRA

Return air pressure difference outlet the FRA (Dp_A_FRA) is obtained according to the manufacturer's datashet, while the p_A_out_FRA is calculated as the difference between p_A_in_FRA and Dp_A_FRA.

1.4 Exhaust and Return Air Dampers (DEA, DRA) - Calculator

The Exhaust and Return Air Dampers (DEA, DRA) are modelled by using a calculator and not a specific type. Tables 4a and b illustrate the inputs and outputs of exhaust and return air dampers calculator, respectively.

Table 5a. Inputs of DEA and DRA Calculator.

INPUTS	
LIST OF INPUTS	INPUTS USED
Inlet Air Temperature	Experimental Return Air Temperature - T_RA
Inlet Air % Relative Humidity	Experimental Return Air Relative Humidity - RH_RA
Inlet Air Pressure	1 atm (constant value) - p_A_in_DRA
Air Density	Exhaust Air Density (output Type 33e)

Table 5b. Outputs of DEA and DRA Calculator.

OUTPUTS	
LIST OF OUTPUTS	OUTPUTS USED
Outlet Air Temperature	Experimental Return Air Temperature - T_RA
Outlet Air % Relative Humidity	Experimental Return Air Relative Humidity - RH_RA
Outlet Air Flowrate -1	Experimental Exhaust Air mass flowrate - m_EA
Outlet Air Pressure	1 atm (constant value) - p_A_out_DRA
Outlet Air Pressure Drop	Return air pressure difference outlet the DRA - Dp_A_DRA
Outlet Air Flowrate -2	Experimental Recirculation Air mass flowrate - m_Recirc

The input Exhaust air density is calculated via the psychometric Type33e.
Return air pressure difference outlet the DRA (Dp_DRA) is obtained according to the manufacturer's datashet, while the p_A_out_DRA is calculated as the difference between p_A_in_DRA and Dp_A_DRA.

Exhaust Air mass flowrate (m_EA) is defined according to Eq. 3, based on experimental data:

Finanziato dall'Unione europea NextGenerationEU | Ministero dell'Università e della Ricerca | Italiadomani PIANO NAZIONALE DI RIPRESA E RESILIENZA

$$\begin{aligned} m\_EA = &(155.70*Density\_EA\_kg\_m3)*(eql(Set\_OL\_SAF,5)*eql(Set\_OL\_RAF,5)) \\ &+(0*Density\_EA\_kg\_m3)*(eql(Set\_OL\_SAF,5)*eql(Set\_OL\_RAF,0)) \\ &+((311.90*Density\_RA\_kg\_m3+252.69*Density\_OA\_kg\_m3)- \\ &107.80*Density\_SA\_kg\_m3)*(eql(Set\_OL\_SAF,0)*eql(Set\_OL\_RAF,5)) \\ &+(18.20*Density\_EA\_kg\_m3)*(eql(Set\_OL\_SAF,10)*eql(Set\_OL\_RAF,5)) \\ &+((1149.68*Density\_RA\_kg\_m3+0*Density\_OA\_kg\_m3)- \\ &673.28*Density\_SA\_kg\_m3)*(eql(Set\_OL\_SAF,5)*eql(Set\_OL\_RAF,10)) \end{aligned} \quad (3)$$

Where:

- The constant value 155.70 is the experimental exhaust air volumetric flowrate, when the return air fan velocity and the supply air fan velocity is equal to 50% (fault-free scenario);
- Density_EA_kg_m3 is the exhaust air density, calculated via the psychometric Type33e;
- Set_OL_SAF is the experimental supply air fan velocity;
- Set_OL_RAF is the experimental return air fan velocity;
- The constant value 0 is the experimental exhaust air volumetric flowrate when the return air fan velocity is equal to 0% (faulty scenario) and the supply air fan velocity is equal to 50% (fault-free scenario);
- The constant value 311.90 is the experimental return air volumetric flowrate when the return air fan velocity is equal to 50% (fault-free scenario) and the supply air fan velocity is equal to 0% (faulty scenario);
- Density_RA_kh_m3 is the return air density, calculated via the psychometric Type33e;
- The constant value 252.69 is the experimental outdoor air volumetric flowrate when the return air fan velocity is equal to 50% (fault-free scenario) and the supply air fan velocity is equal to 0% (faulty scenario);
- Density_OA_kg_m3 is the outdoor air density, calculated via the psychometric Type33e;
- The constant value 107.80 is the experimental supply air volumetric flowrate when the return air fan velocity is equal to 50% (fault-free scenario) and the supply air fan velocity is equal to 0% (faulty scenario);
- Density_SA_kg_m3 is the supply air density, calculated via the psychometric Type33e;
- The constant value 18.20 is the experimental exhaust air volumetric flowrate when the return air fan velocity is equal to 50% (fault-free scenario) and the supply air fan velocity is equal to 100% (faulty scenario);
- The constant value 1149.68 is the experimental return air volumetric flowrate when the return air fan velocity is equal to 100% (faulty scenario) and the supply air fan velocity is equal to 50% (fault-free scenario);
- The constant value 0 is the experimental outdoor air volumetric flowrate when the return air fan velocity is equal to 100% (faulty scenario) and the supply air fan velocity is equal to 50% (fault-free scenario);
- The constant value 673.28 is the experimental supply air volumetric flowrate when the return air fan velocity is equal to 100% (faulty scenario) and the supply air fan velocity is equal to 50% (fault-free scenario).

The Recirculation Air mass flowrate (m_Recirc) is calculated as the difference between m_RA and m_EA.

1.5 Outdoor Air Damper (DOA) - Calculator

Outdoor Air Damper (DOA) is modelled by using a calculator and not a specific type. Tables 6a and b illustrate the inputs and outputs of outdoor air damper calculator, respectively.

Table 6a. Inputs of DOA Calculator.

INPUTS	
LIST OF INPUTS	INPUTS USED
Inlet Air Temperature	Experimental Outdoor Air Temperature - T_OA
Inlet Air % Relative Humidity	Experimental Outdoor Air Relative Humidity - RH_OA
Inlet Flowrate	Experimental Outdoor Air mass flowrate - m_OA
Inlet Air Pressure	Outdoor Air Pressure inlet the DOA - p_A_in_DOA

Finanziato dall'Unione europea NextGenerationEU | Ministero dell'Università e della Ricerca | Italiadomani PIANO NAZIONALE DI RIPRESA E RESILIENZA

Air Density	Outdoor Air Density (output Type 33e)

Table 6b. Outputs of DOA Calculator.

OUTPUTS	
LIST OF OUTPUTS	OUTPUTS USED
Outlet Air Temperature	Experimental Outdoor Air Temperature - T_OA
Outlet Air % Relative Humidity	Experimental Outdoor Air Relative Humidity - RH_OA
Outlet Air Flowrate	Experimental Outdoor Air mass flowrate - m_OA
Outlet Air Pressure	Outdoor Air Pressure outlet the DOA - p_A_out_DOA
Outlet Air Pressure Drop	Outdoor air pressure difference outlet the DOA - Dp_A_DOA

The input Outdoor Air Density is calculated via the psychometric Type33e.

The Outdoor Air mass flowrate (m_OA) is defined according to Eq. 4, based on experimental data.

$$\begin{aligned} m\_OA = &((645.01*Density\_SA\_kg\_m3+155.70*Density\_EA\_kg\_m3)– \\ &751.04*Density\_RA\_kg\_m3)*(eql(Set\_OL\_SAF,5)*eql(Set\_OL\_RAF,5)) \\ &+(252.69*Density\_OA\_kg\_m3)*(eql(Set\_OL\_SAF,5)*eql(Set\_OL\_RAF,0)) \\ &+(0*Density\_OA\_kg\_m3)*(eql(Set\_OL\_SAF,0)*eql(Set\_OL\_RAF,5)) \\ &+((1546.25*Density\_SA\_kg\_m3+18.20*Density\_EA\_kg\_m3)– \\ &682.12*Density\_RA\_kg\_m3)*(eql(Set\_OL\_SAF,10)*eql(Set\_OL\_RAF,5)) \\ &+(0*Density\_OA\_kg\_m3)*(eql(Set\_OL\_SAF,5)*eql(Set\_OL\_RAF,10)) \end{aligned} \quad (4)$$

Where:

- The constant value 645.01 is the experimental supply air volumetric flowrate, when the return air fan velocity and the supply air fan velocity is equal to 50% (fault-free scenario);
- Density_SA_kg_m3 is the supply air density, calculated via the psychometric Type33e;
- The constant value 155.70is the experimental exhaust air volumetric flowrate, when the return air fan velocity and the supply air fan velocity is equal to 50% (fault-free scenario);
- Density_EA_kg_m3 is the exhaust air density, calculated via the psychometric Type33e;
- The constant value 751.04 is the experimental return air volumetric flowrate, when the return air fan velocity and the supply air fan velocity is equal to 50% (fault-free scenario);
- Density_RA_kh_m3 is the return air density, calculated via the psychometric Type33e;
- Set_OL_SAF is the experimental supply air fan velocity;
- Set_OL_RAF is the experimental return air fan velocity;
- The constant value 252.69 is the experimental outdoor air volumetric flowrate when the return air fan velocity is equal to 0% (faulty scenario) and the supply air fan velocity is equal to 50% (fault-free scenario);
- Density_OA_kg_m3 is the outdoor air density, calculated via the psychometric Type33e;
- The constant value 0 is the experimental outdoor air volumetric flowrate when the return air fan velocity is equal to 50% (fault-free scenario) and the supply air fan velocity is equal to 0% (faulty scenario);
- The constant value 1546.25 is the experimental supply air volumetric flowrate when the return air fan velocity is equal to 50% (fault-free scenario) and the supply air fan velocity is equal to 100% (faulty scenario);
- The constant value 18.20 is the experimental exhaust air volumetric flowrate when the return air fan velocity is equal to 50% (fault-free scenario) and the supply air fan velocity is equal to 100% (faulty scenario);
- The constant value 682.12 is the experimental return air volumetric flowrate when the return air fan velocity is equal to 50% (fault-free scenario) and the supply air fan velocity is equal to 100% (faulty scenario);

Finanziato dall'Unione europea NextGenerationEU | Ministero dell'Università e della Ricerca | Italiadomani PIANO NAZIONALE DI RIPRESA E RESILIENZA

- The constant value 0 is the experimental outdoor air volumetric flowrate when the return air fan velocity is equal to 100% (faulty scenario) and the supply air fan velocity is equal to 50% (fault-free scenario).

The Outdoor air pressure difference outlet the DOA (Dp_DOA) is obtained according to the manufacturer's datashet, while Outdoor air pressure outlet the Outdoor air damper p_DOA_out_atm is calculated as the difference between p_A_in_DOA and Dp_A_DOA.

1.6 Outdoor Air Filter (FOA) - Calculator

Outdoor Air Filter (FOA) is modelled by using a calculator and not a specific type. Tables 7a and b illustrate the inputs and outputs of outdoor ai filter calculator, respectively.

Table 7a. Inputs of FOA Calculator.

INPUTS	
LIST OF INPUTS	INPUTS USED
Inlet Air Temperature	Experimental Outdoor Air Temperature - T_OA
Inlet Air % Relative Humidity	Experimental Outdoor Air Relative Humidity - RH_OA
Inlet Flowrate	Experimental Outdoor Air mass flowrate - m_OA
Inlet Air Pressure	Outdoor Air Pressure inlet the FOA - p_A_in_FOA

Table 7b. Outputs of FOA Calculator.

OUTPUTS	
LIST OF OUTPUTS	OUTPUTS USED
Outlet Air Temperature	Experimental Outdoor Air Temperature - T_OA
Outlet Air % Relative Humidity	Experimental Outdoor Air Relative Humidity - RH_OA
Outlet Air Flowrate	Experimental Outdoor Air mass flowrate - m_OA
Outlet Air Pressure	Outdoor Air Pressure outlet the FOA - p_A_out_FOA
Outlet Air Pressure Drop	Outdoor air pressure difference outlet the FOA - Dp_A_FOA

The Outdoor air pressure difference outlet the FOA (Dp_A_FOA) is obtained according to the manufacturer's datashet, while the Outdoor Air Pressure outlet the FOA (p_A_out_FOA) is calculated as the difference between p_A_in_FOA and Dp_A_FOA.

1.7 Heat Recovery System (HRS) - Type 667b

The Heat Recovery System (HRS) is modelled by the Type 667b. Fig. 3 reports the HRS parameters.

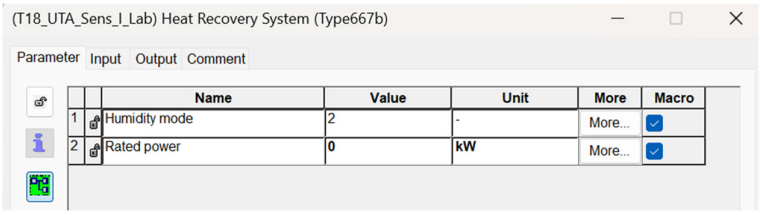

Figure 3. Parameters of HRS Type.

This component is disabled, therefore the Rated power parameter is set equal to 0.
Table 8a and b illustrate the inputs and outputs of heat recovery system type, respectively.

Table 8a. Inputs of HRS Type.

INPUTS	
LIST OF INPUTS	INPUTS USED

Finanziato dall'Unione europea NextGenerationEU
Ministero dell'Università e della Ricerca
Italiadomani PIANO NAZIONALE DI RIPRESA E RESILIENZA

Exhaust air temperature	Experimental Return Air Temperature - T_RA
Exhaust Air Humidity Ratio	-
Exhaust air %RH	Experimental Return Air Relative Humidity - RH_RA
Exhaust air flow rate	Experimental Return Air mass flowrate - m_RA
Exhaust air pressure	1 atm (constant value) - p_A_out_FRA
Exhaust air pressure drop	0.000474 (constant value)
Fresh air temperature	Experimental Outdoor Air Temperature - T_OA
Fresh Air Humidity Ratio	-
Fresh air %RH	Experimental Outdoor Air Relative Humidity - RH_OA
Fresh air flow rate	Experimental Outdoor Air mass flowrate - m_OA
Fresh air pressure	Outdoor Air Pressure outlet the FOA - p_A_out_FOA
Fresh air pressure drop	0.000464 (constant value)
Sensible effectiveness	0.7481 (constant value)
Latent effectiveness	0.794 (constant value)
On/Off Control Signal	Opening percentage of HRS damper - Set_OP_DHRS

Table 8b. Outputs of HRS Type.

OUTPUTS	
LIST OF OUTPUTS	OUTPUTS USED
Fresh air temperature	Experimental Outdoor Air Temperature - T_OA
Fresh air %RH	Experimental Outdoor Air Relative Humidity - RH_OA
Fresh air flow rate	Experimental Outdoor Air mass flowrate - m_OA
Fresh air pressure	Outdoor Air Pressure outlet the FOA - p_A_out_FOA

1.8 Mixing Chamber - Type 648

The mixing chamber is modelled by the Type 648. Fig. 4 illustrates the mixing chamber parameters.

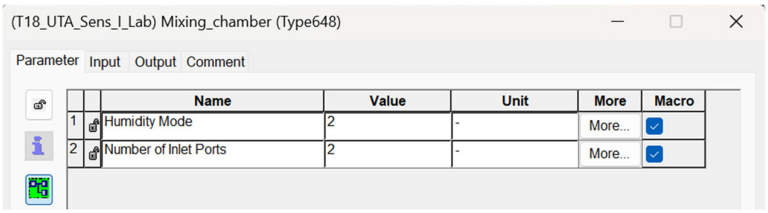

Figure 4. Parameters of Mixing Chamber Type.

Tables 9a and b illustrate the inputs and outputs of mixing chamber type, respectively.

Table 9a. Inputs of Mixing Chamber Type.

INPUTS	
LIST OF INPUTS	INPUTS USED
Inlet Air Temperature-1	Experimental Outdoor Air Temperature - T_OA
Inlet Air Humidity Ratio-1	-
Inlet Air % Relative Humidity-1	Experimental Outdoor Air Relative Humidity - RH_OA
Inlet Air Flowrate-1	Experimental Outdoor Air mass flowrate - m_OA
Inlet Air Pressure-1	Outdoor air pressure outlet the FOA - p_A_out_FOA
Inlet Air Temperature-2	Experimental Return Air Temperature - T_RA

Finanziato dall'Unione europea NextGenerationEU
Ministero dell'Università e della Ricerca
Italiadomani PIANO NAZIONALE DI RIPRESA E RESILIENZA

Inlet Air Humidity Ratio-2	-
Inlet Air % Relative Humidity-2	Experimental Return Air Relative Humidity - RH_RA
Inlet Air Flowrate-2	Experimental Return Air mass flowrate - m_RA
Inlet Air Pressure-2	1 atm (constant value) - p_A_out_FRA
Air-Side Pressure Drop	0 atm (constant value)

Table 9b. Outputs of Mixing Chamber Type.

OUTPUTS	
LIST OF OUTPUTS	OUTPUTS USED
Outlet Air Temperature	Mixed Air Temperature - T_MA
Outlet Air % Relative Humidity	Mixed Air Relative Humidity - RH_MA
Outlet Air Flowrate	Mixed Air mass flowrate - m_MA
Outlet Air Pressure	Mixed air pressure - p_A_out_MA

1.9 Supply Air Filter (FSA) - Calculator

The Supply Air Filter (FSA) is modelled by using a calculator and not a specific type. Tables 10a and b illustrate the inputs and outputs of supply air filter calculator, respectively.

Table 10a. Inputs of FSA Calculator.

INPUTS	
LIST OF INPUTS	INPUTS USED
Inlet Air Temperature	Mixed Air Temperature - T_MA (output Type 648)
Inlet Air % Relative Humidity	Mixed Air Relative Humidity - RH_MA (output Type 648)
Inlet Air Flowrate	Mixed Air mass flowrate - m_MA (output Type 648)
Inlet Air Pressure	Mixed air pressure - p_A_in_FSA (output Type 648)

Table 10b. Outputs of FSA Calculator.

OUTPUTS	
LIST OF OUTPUTS	OUTPUTS USED
Outlet Air Temperature	Mixed Air Temperature - T_MA
Outlet Air % Relative Humidity	Mixed Air Relative Humidity - RH_MA
Outlet Air Flowrate	Mixed Air mass flowrate - m_MA
Outlet Air Pressure	Mixed air pressure - p_A_out_FSA
Outlet Air Pressure Drop	Mixed air pressure difference outlet the FSA - Dp_A_FSA

The Mixed air pressure difference outlet the FSA (Dp_A_FSA) is obtained according to the manufacturer's datashet, while the Mixed air pressure (p_A_out_FSA) is calculated as the difference between p_A_in_FSA and Dp_A_FSA.

1.10 Refrigerating System (RS) - Type 941

The Refrigerating System (RS) is modelled by using the Type 941. Fig. 5 reports parameters of refrigerating system type.

Finanziato dall'Unione europea NextGenerationEU | Ministero dell'Università e della Ricerca | Italiadomani PIANO NAZIONALE DI RIPRESA E RESILIENZA

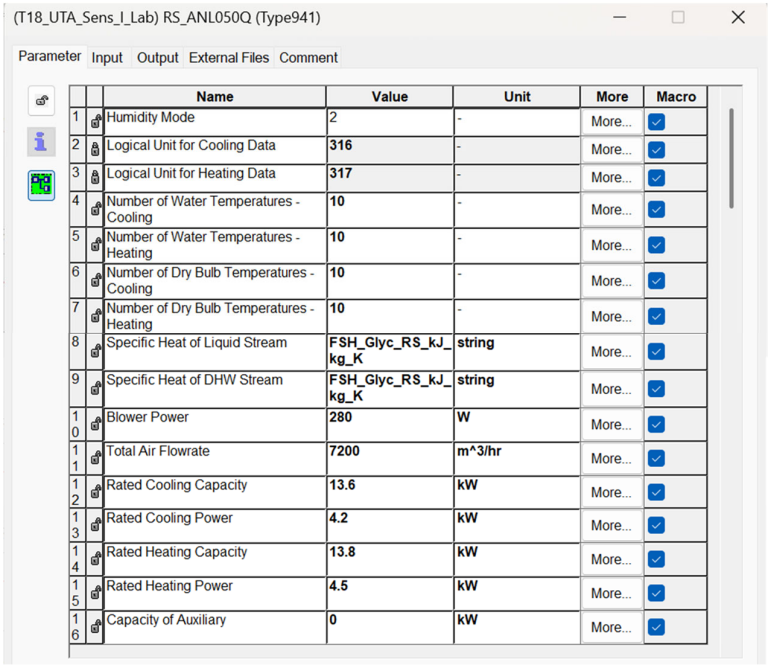

	Name	Value	Unit	More	Macro
1	Humidity Mode	2	-	More...	☑
2	Logical Unit for Cooling Data	316	-	More...	☑
3	Logical Unit for Heating Data	317	-	More...	☑
4	Number of Water Temperatures - Cooling	10	-	More...	☑
5	Number of Water Temperatures - Heating	10	-	More...	☑
6	Number of Dry Bulb Temperatures - Cooling	10	-	More...	☑
7	Number of Dry Bulb Temperatures - Heating	10	-	More...	☑
8	Specific Heat of Liquid Stream	FSH_Glyc_RS_kJ_kg_K	string	More...	☑
9	Specific Heat of DHW Stream	FSH_Glyc_RS_kJ_kg_K	string	More...	☑
10	Blower Power	280	W	More...	☑
11	Total Air Flowrate	7200	m^3/hr	More...	☑
12	Rated Cooling Capacity	13.6	kW	More...	☑
13	Rated Cooling Power	4.2	kW	More...	☑
14	Rated Heating Capacity	13.8	kW	More...	☑
15	Rated Heating Power	4.5	kW	More...	☑
16	Capacity of Auxiliary	0	kW	More...	☑

Figure 5 . Parameters of RS Type.

Tables 11a and b illustrate the inputs and outputs of refrigerating system type, respectively.

Table 11a. Inputs of RS Type.

INPUTS	
LIST OF INPUTS	INPUTS USED
Inlet Liquid Temperature	Experimental Inlet Fluid Temperature - T_F_in_RS
Inlet Liquid Flowrate	Experimental Fluid mass flowrate - m_PRS
Inlet Air Temperature	Experimental Outdoor Air Temperature - T_OA
Inlet Air Humidity Ratio	-
Inlet Air % Relative Humidity	Experimental Outdoor Air Relative Humidity - RH_OA
Inlet Air Pressure	Outdoor air pressure (output Type 15-3)
Air pressure rise across heat pump	2 atm (constant value)
Cooling Control Signal	1 - Ctrl_RS_sign_ON_OFF (output Ctrl_RS Calculator)
Heating Control Signal	0 (constant value)
Auxiliary Signal	0 (constant value)
Inlet DHW Temperature	20 °C (constant value)
DHW Flowrate	0 kJ/h (constant value)
Desuperheater Temperature - Cooling Mode	20 °C (constant value)
Desuperheater Temperature - Heating Mode	20 °C (constant value)
Desuperheater UA - Cooling Mode	0 kJ/hK (constant value)
Desuperheater UA - Heating Mode	0 kJ/hK (constant value)
Compressor Loss Fraction	0.1 (constant value)

Table 11b. Outputs of RS Type.

OUTPUTS	
LIST OF OUTPUTS	OUTPUTS USED

Finanziato dall'Unione europea NextGenerationEU
Ministero dell'Università e della Ricerca
Italiadomani PIANO NAZIONALE DI RIPRESA E RESILIENZA

Exiting Fluid Temperature	Experimental Outlet Fluid Temperature - T_F_out_RS
Exiting Fluid Flowrate	Experimental Fluid mass flowrate - m_PRS
Heat Pump Power	Electric Power EP_RS

Outdoor Air pressure is derived from the Type 15-3 taking into account the Energy+ weather data of Naples city.
This type required as an external file the performance map of the refrigerating systems. This map, derived from the manufacturers' manual, has been changed according to the real performance of the experimental set-up.

1.11 Refrigerating System Tank (RS Tank) - Type 1534

The Refrigerating System Tank (RS Tank) is modelled by using the Type 1534. Fig. 6 reports the parameters of RS Tank type defined in the required external file.

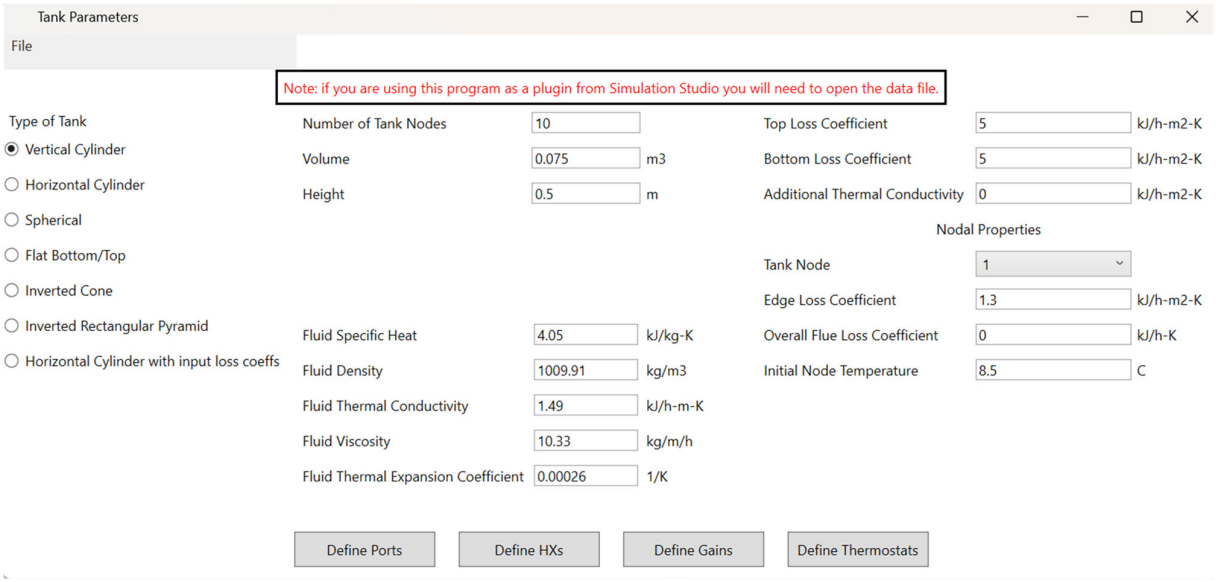

Figure 6 . RS Tank parameters.

Table 12a and b illustrate the inputs and outputs of refrigerating system's tank type, respectively.

Table 12a. Inputs of RS Tank Type.

INPUTS	
LIST OF INPUTS	INPUTS USED
Inlet Temperature for Port	Experimental Outlet Fluid Temperature - T_F_out_RS
Inlet Flowrate for Port	Experimental Fluid mass flowrate - m_PRS
Top Loss Temperature	Experimental Outdoor Air Temperature - T_OA
Edge Loss Temperature for Node-1	Experimental Outdoor Air Temperature - T_OA
Edge Loss Temperature for Node-2	Experimental Outdoor Air Temperature - T_OA
Edge Loss Temperature for Node-3	Experimental Outdoor Air Temperature - T_OA
Edge Loss Temperature for Node-4	Experimental Outdoor Air Temperature - T_OA
Edge Loss Temperature for Node-5	Experimental Outdoor Air Temperature - T_OA
Edge Loss Temperature for Node-6	Experimental Outdoor Air Temperature - T_OA
Edge Loss Temperature for Node-7	Experimental Outdoor Air Temperature - T_OA
Edge Loss Temperature for Node-8	Experimental Outdoor Air Temperature - T_OA
Edge Loss Temperature for Node-9	Experimental Outdoor Air Temperature - T_OA
Edge Loss Temperature for Node-10	Experimental Outdoor Air Temperature - T_OA

Finanziato dall'Unione europea NextGenerationEU | Ministero dell'Università e della Ricerca | Italiadomani PIANO NAZIONALE DI RIPRESA E RESILIENZA

Bottom Loss Temperature	Experimental Outdoor Air Temperature - T_OA
Gas Flue Temperature	20 °C (constant value)
Inversion Mixing Flowrate	-100 kJ/hK (constant value)
Auxiliary Heat Input for Node-1	0 kJ/h (constant value)
Auxiliary Heat Input for Node-2	0 kJ/h (constant value)
Auxiliary Heat Input for Node-3	0 kJ/h (constant value)
Auxiliary Heat Input for Node-4	0 kJ/h (constant value)
Auxiliary Heat Input for Node-5	0 kJ/h (constant value)
Auxiliary Heat Input for Node-6	0 kJ/h (constant value)
Auxiliary Heat Input for Node-7	0 kJ/h (constant value)
Auxiliary Heat Input for Node-8	0 kJ/h (constant value)
Auxiliary Heat Input for Node-9	0 kJ/h (constant value)
Auxiliary Heat Input for Node-10	0 kJ/h (constant value)

Table 12b. Outputs of RS Tank Type.

OUTPUTS	
LIST OF OUTPUTS	OUTPUTS USED
Temperature at Outlet	Experimental Outlet Fluid Temperature - T_F_out_RS
Flowrate at Outlet	Experimental Fluid mass flowrate - m_PRS

1.12 Refrigerating System Recirculation Pump (Pump RS) - Type 742

The Refrigerating System Recirculation Pump (Pump RS) is modelled by using the Type 742. Fig. 7 reports the parameters of Pump RS type.

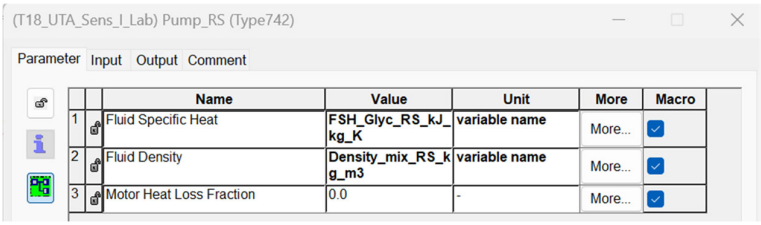

Figure 7. Parameters of Pump RS Type.

The fluid specific heat and the fluid density are parameters recalled from the calculator named "Water_Glycol_Properties" where are defined the fluid specific heat and the fluid density of the glycol mixture according to the manufacturers' data.

Tables 13a and b illustrate the inputs and outputs of refrigerating system's recirculation pump type, respectively.

Table 13a. Inputs of Pump RS Type.

INPUTS	
LIST OF INPUTS	INPUTS USED
Inlet Fluid Temperature	Inlet Fluid Temperature (output Type 31)
Inlet Fluid Flowrate	Experimental Fluid mass flowrate - m_PRS
Overall Pump Efficiency	0.0277 (constant value)
Motor Efficiency	1 (constant value)
Pressure Drop	10 kPa (constant value)

Finanziato dall'Unione europea NextGenerationEU | Ministero dell'Università e della Ricerca | Italiadomani PIANO NAZIONALE DI RIPRESA E RESILIENZA

Table 13b. Outputs of Pump RS Type.

OUTPUTS	
LIST OF OUTPUTS	OUTPUTS USED
Outlet Fluid Flowrate	Experimental Fluid mass flowrate - m_PRS

The inlet fluid temperature input of the Pump RS is the output of a pipe modelled by the Type 31, that connect the three-way mixing valve at the outlet of the CC to the RS.
The electric power consumption of the recirculation pump is equal to 0.780 kW defined according to the experimental data.

1.13 Pipe Refrigerating System to Cooling Coil (RS to CC) - Type 31

The Pipe RS to CC is modelled by using the Type 31. Fig. 8 reports parameters of pipe type.

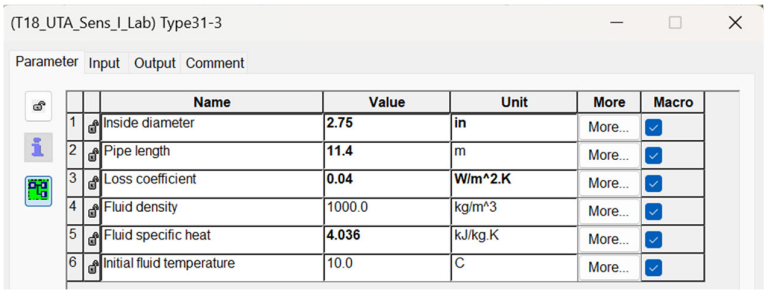

Figure 8. Parameters of Pipe RS to CC.

Table 14a and b illustrate the inputs and outputs of the pipe type, respectively.

Table 14a. Inputs of Pipe RS to CC Type.

INPUTS	
LIST OF INPUTS	INPUTS USED
Inlet temperature	Inlet Fluid Temperature - T_F_out_RS
Inlet flow rate	Experimental Fluid mass flowrate - m_PRS
Environment temperature	Experimental Outdoor Air Temperature - T_OA

Table 14b. Outputs of Pipe RS to CC Type.

OUTPUTS	
LIST OF OUTPUTS	OUTPUTS USED
Outlet temperature	Outlet Fluid Temperature - T_F_out_RS
Outlet flow rate	Experimental Fluid mass flowrate - m_PRS

1.14 Three-way flow diverter valve Cooling Coil (CC) - Type 647

The three-way flow diverter valve CC is modelled by the Type 647. Fig. 9 reports the parameters of the three-way valve type.

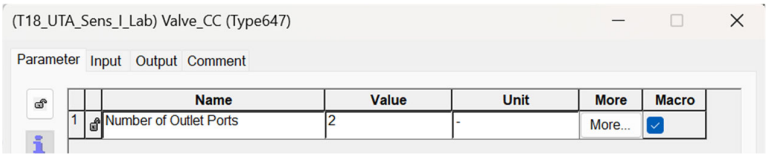

Figure 9. Three-way flow diverter valve CC parameters.

Table 15a and b illustrate the inputs and outputs of the three-way flow diverter valve CC type.

Finanziato dall'Unione europea NextGenerationEU
Ministero dell'Università e della Ricerca
Italiadomani PIANO NAZIONALE DI RIPRESA E RESILIENZA

Table 15a. Inputs of Three-way flow diverter valve CC Type.

INPUTS	
LIST OF INPUTS	INPUTS USED
Inlet Temperature	Experimental Fluid Temperature - T_F_in_CC
Inlet Flowrate	Experimental Fluid mass flowrate - m_F_in_CC
Fraction of Flow to Outlet -1	Fraction of Flow to CC (output CC_Operation Calculator)
Fraction of Flow to Outlet -2_CC	Fraction of Flow to RS (output CC_Operation Calculator)

Table 15b. Outputs of Three-way flow diverter valve CC Type.

OUTPUTS	
LIST OF OUTPUTS	OUTPUTS USED
Outlet Temperature-1	Experimental Fluid Temperature - T_F_in_CC
Outlet Flowrate-1	Experimental Fluid mass flowrate - m_F_in_CC
Outlet Temperature-2	Outlet Fluid Temperature to RS
Outlet Flowrate-2	Outlet Fluid mass flowrate to RS

The inputs Fraction of Flow to CC and Fraction of Flow to RS are defined as function of the opening percentage of Cooling coil valve, in the calculator named "CC_Operation".

1.15 Cooling Coil (CC) - Type 508c

The Cooling Coil CC is modelled by the Type 508c. Fig. 10 reports the parameters of cooling coil type.

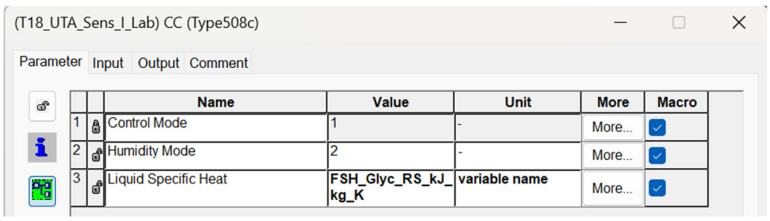

Figure 10. Parameters of CC Type.

The liquid specific heat is a parameter recalled from the calculator named "Water_Glycol_Properties" where fluid specific heat of the glycol mixture is defined according to the manufacturers' data.
Table 16a and b illustrate the inputs and outputs of the cooling coil type, respectively.

Table 16a. Inputs of CC Type.

INPUTS	
LIST OF INPUTS	INPUTS USED
Fluid Inlet Temperature	Experimental Fluid Temperature - T_F_in_CC
Fluid Flowrate	Experimental Fluid mass flowrate - m_F_in_CC
Air Inlet Temperature	Mixed Air Temperature - T_MA (output FSA Calculator)
Air Humidity Ratio	-
Air % Relative Humidity	Mixed Air Relative Humidity - RH_MA (output FSA Calculator)
Air Flowrate	Mixed Air mass flowrate - m_MA (output FSA Calculator)
Air Pressure	Mixed air pressure outlet the Supply air filter - p_A_out_FSA
Air-Side Pressure Drop	0.0001756 atm (constant value)

Finanziato dall'Unione europea NextGenerationEU | Ministero dell'Università e della Ricerca | Italiadomani PIANO NAZIONALE DI RIPRESA E RESILIENZA

Coil Bypass Fraction	Cooling Coil Bypass Fraction BF_CC (output CC_BFactor Calculator)
Setpoint: Outlet Air Temperature	0 °C (constant value)

Table 16b. Outputs of CC Type.

OUTPUTS	
LIST OF OUTPUTS	OUTPUTS USED
Fluid Outlet Temperature	Fluid Outlet Temperature - T_F_out_CC
Outlet Fluid Flowrate	Experimental Fluid mass flowrate - m_F_in_CC
Outlet Air Temperature	Outlet Air Temperature - T_A_out_CC
Outlet Air % Relative Humidity	Outlet Air Relative Humidity - RH_A_out_CC
Outlet Air Pressure	Air pressure outlet the CC - p_A_out_CC

The cooling coil bypass fraction is calculated according to the following Eq. 5, as function of return and supply air fan operating conditions:

$$BF\_CC = 0.330*(eql(Set\_OL\_SAF,5)*eql(Set\_OL\_RAF,5))+ 0.268*(eql(Set\_OL\_SAF,5)*eql(Set\_OL\_RAF,0))+ 0.34*(eql(Set\_OL\_SAF,0)*eql(Set\_OL\_RAF,5)) \quad (5)$$

Where:

- The constant value 0.330 is the experimental cooling coil bypass fraction when the return air fan velocity and the supply air fan velocity is equal to 50% (fault-free scenario);
- Set_OL_SAF is the experimental supply air fan velocity;
- Set_OL_RAF is the experimental return air fan velocity;
- The constant value 0.268 is the experimental cooling coil bypass fraction when the return air fan velocity is equal to 0% (faulty scenario) and the supply air fan velocity is equal to 50% (fault-free scenario);
- The constant value 0.34 is the experimental cooling coil bypass fraction when the return air fan velocity is equal to 50% (fault-free scenario) and the supply air fan velocity is equal to 0% (faulty scenario).

1.16 Three-way mixing valve Cooling Coil to Refrigerating System (CC to RS) - Type 649

The three-way mixing valve CC to RS is modelled by the Type 649. Fig. 11 reports the parameters of the three-way valve CC to RS.

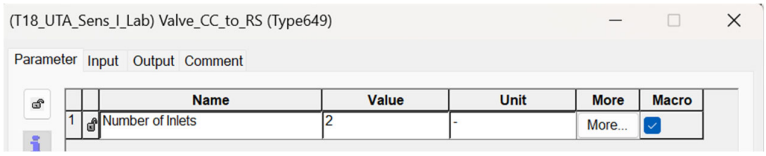

Figure 11. Parameters of Three-way mixing valve CC to RS.

Tables 17a and b illustrate the inputs and outputs of the three-way valve CC to RS, respectively.

Table 17a. Inputs of Three-way mixing valve CC to RS Type.

INPUTS	
LIST OF INPUTS	INPUTS USED
Temperature at Inlet-1	Fluid Outlet Temperature - T_F_out_CC
Flowrate at Inlet-1	Experimental Fluid mass flowrate - m_F_in_CC
Temperature at Inlet-2_CC	Fluid Temperature to RS (output Type 647)

Finanziato dall'Unione europea NextGenerationEU | Ministero dell'Università e della Ricerca | Italiadomani PIANO NAZIONALE DI RIPRESA E RESILIENZA

Flowrate at Inlet-2_CC	Fluid Flowrate to RS (output Type 647)

Table 17b. Outputs of Three-way mixing valve CC to RS Type.

OUTPUTS	
LIST OF OUTPUTS	OUTPUTS USED
Outlet Temperature	Outlet Fluid Temperature
Outlet Flowrate	Outlet Fluid Flowrate

The inputs Fluid Temperature to RS and Fluid Flowrate to RS are the outputs of the three-way flow diverter valve CC.

1.17 Pipe Cooling Coil to Refrigerating System (CC to RS) - Type 31

The Pipe CC to RS is modelled by using the Type 31. Fig. 12 reports the parameters of the pipe type.

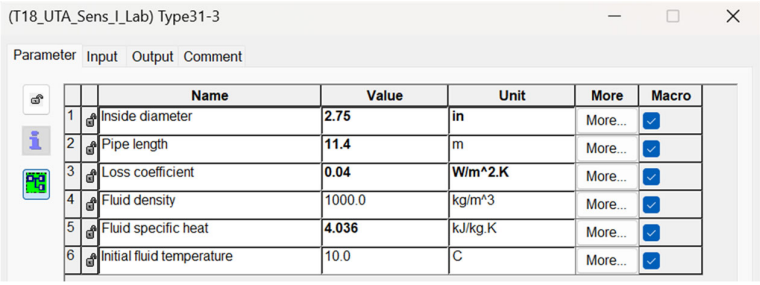

Figure 12. Parameters of Pipe CC to RS.

Tables 18a and b illustrate the inputs and outputs of the pipe CC to RS type.

Table 18a. Inputs of Pipe CC to RS Type.

INPUTS	
LIST OF INPUTS	INPUTS USED
Inlet temperature	Inlet Fluid Temperature (output Type 649)
Inlet flow rate	Inlet Fluid Flowrate (output Type 649)
Environment temperature	Experimental Outdoor Air Temperature - T_OA

Table 18b. Outputs of Pipe CC to RS Type.

OUTPUTS	
LIST OF OUTPUTS	OUTPUTS USED
Outlet Temperature	Outlet Fluid Temperature

The Inlet Fluid Temperature and Inlet Fluid Flowrate are the outputs of the three-way mixing valve CC to RS.

1.18 Heat Pump (HP) -Type 941

The Heat Pump (HP) is modelled by using the Type 941. Fig. 13 reports the parameters of HP type.

Finanziato dall'Unione europea NextGenerationEU
Ministero dell'Università e della Ricerca
Italiadomani PIANO NAZIONALE DI RIPRESA E RESILIENZA

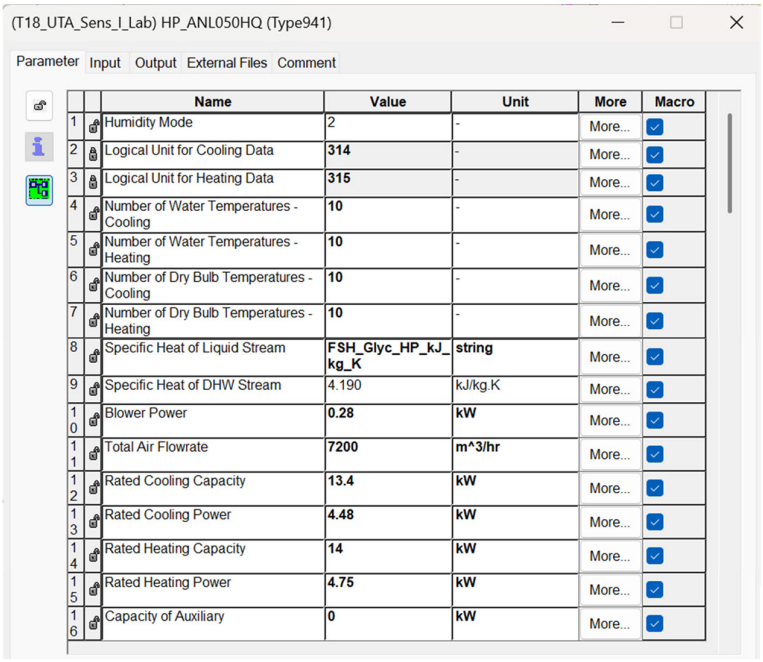

	Name	Value	Unit	More	Macro
1	Humidity Mode	2	-	More...	☑
2	Logical Unit for Cooling Data	314	-	More...	☑
3	Logical Unit for Heating Data	315	-	More...	☑
4	Number of Water Temperatures - Cooling	10	-	More...	☑
5	Number of Water Temperatures - Heating	10	-	More...	☑
6	Number of Dry Bulb Temperatures - Cooling	10	-	More...	☑
7	Number of Dry Bulb Temperatures - Heating	10	-	More...	☑
8	Specific Heat of Liquid Stream	FSH_Glyc_HP_kJ_kg_K	string	More...	☑
9	Specific Heat of DHW Stream	4.190	kJ/kg.K	More...	☑
10	Blower Power	0.28	kW	More...	☑
11	Total Air Flowrate	7200	m^3/hr	More...	☑
12	Rated Cooling Capacity	13.4	kW	More...	☑
13	Rated Cooling Power	4.48	kW	More...	☑
14	Rated Heating Capacity	14	kW	More...	☑
15	Rated Heating Power	4.75	kW	More...	☑
16	Capacity of Auxiliary	0	kW	More...	☑

Figure 13. Parameters of HP Type.

Tables 19a and b illustrates the inputs and outputs of heat pump type, respectively.

Table 19a. Inputs of HP Type.

INPUTS	
LIST OF INPUTS	INPUTS USED
Inlet Liquid Temperature	Experimental Inlet Fluid Temperature - T_F_in_HP
Inlet Liquid Flowrate	Experimental Fluid mass flowrate - m_PHP
Inlet Air Temperature	Experiemental Outdoor Air Temperature - T_OA
Inlet Air Humidity Ratio	-
Inlet Air % Relative Humidity	Experimental Outdoor Air Relative Humidity - RH_OA
Inlet Air Pressure	Outdoor air pressure (output Type 15-3)
Air pressure rise across heat pump	2 atm (constant value)
Cooling Control Signal	0 (constant value)
Heating Control Signal	1 - Ctrl_HP_sign_ON_OFF (output Ctrl_HP Calculator)
Auxiliary Signal	0 (constant value)
Inlet DHW Temperature	20 °C (constant value)
DHW Flowrate	0 kJ/h (constant value)
Desuperheater Temperature - Cooling Mode	20 °C (constant value)
Desuperheater Temperature - Heating Mode	20 °C (constant value)
Desuperheater UA - Cooling Mode	0 kJ/hK (constant value)
Desuperheater UA - Heating Mode	0 kJ/hK (constant value)
Compressor Loss Fraction	0.1 (constant value)

Table 19b. Outputs of HP Type.

OUTPUTS	
LIST OF OUTPUTS	OUTPUTS USED

Finanziato dall'Unione europea NextGenerationEU
Ministero dell'Università e della Ricerca
Italiadomani PIANO NAZIONALE DI RIPRESA E RESILIENZA

Exiting Fluid Temperature	Experimental Outlet Fluid Temperature - T_F_out_HP
Exiting Fluid Flowrate	Experimental Fluid mass flowrate - m_PHP
Heat Pump Power	Electric Power EP_HP

Outdoor Air pressure is derived from the Type 15-3 taking into account the Energy+ weather data of Naples city.
This type required as an external file the performance map of the refrigerating systems. This map, derived from the manufacturers' manual, has been changed according to the real performance of the experimental set-up.

1.19 Heat Pump Tank (HP Tank) - Type 1534

The Heat Pump Tank (HP Tank) is modelled by using the Type 1534. Fig. 14 reports the parameters of HP Tank type defined in the required external file.

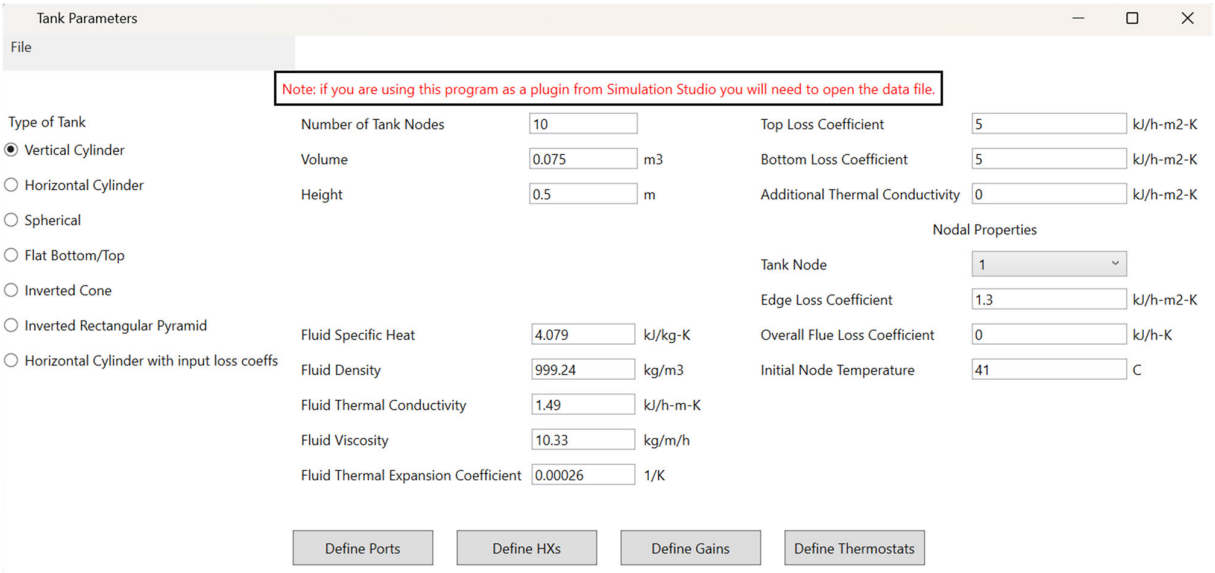

Figure 14 . Parameters of HP Tank Type.

Tables 20a and b illustrate the inputs and outputs of heat pump tank type, respectively.

Table 20a. Inputs of HP Tank Type.

INPUTS	
LIST OF INPUTS	INPUTS USED
Inlet Temperature for Port	Experimental Outlet Fluid Temperature - T_F_out_HP
Inlet Flowrate for Port	Experimental Fluid mass flowrate - m_P HP
Top Loss Temperature	Experimental Outdoor Air Temperature - T_OA
Edge Loss Temperature for Node-1	Experimental Outdoor Air Temperature - T_OA
Edge Loss Temperature for Node-2	Experimental Outdoor Air Temperature - T_OA
Edge Loss Temperature for Node-3	Experimental Outdoor Air Temperature - T_OA
Edge Loss Temperature for Node-4	Experimental Outdoor Air Temperature - T_OA
Edge Loss Temperature for Node-5	Experimental Outdoor Air Temperature - T_OA
Edge Loss Temperature for Node-6	Experimental Outdoor Air Temperature - T_OA
Edge Loss Temperature for Node-7	Experimental Outdoor Air Temperature - T_OA
Edge Loss Temperature for Node-8	Experimental Outdoor Air Temperature - T_OA
Edge Loss Temperature for Node-9	Experimental Outdoor Air Temperature - T_OA
Edge Loss Temperature for Node-10	Experimental Outdoor Air Temperature - T_OA

Finanziato dall'Unione europea NextGenerationEU | Ministero dell'Università e della Ricerca | Italiadomani PIANO NAZIONALE DI RIPRESA E RESILIENZA

Bottom Loss Temperature	Experimental Outdoor Air Temperature - T_OA
Gas Flue Temperature	20 °C (constant value)
Inversion Mixing Flowrate	-100 kJ/hK (constant value)
Auxiliary Heat Input for Node-1	0 kJ/h (constant value)
Auxiliary Heat Input for Node-2	0 kJ/h (constant value)
Auxiliary Heat Input for Node-3	0 kJ/h (constant value)
Auxiliary Heat Input for Node-4	0 kJ/h (constant value)
Auxiliary Heat Input for Node-5	0 kJ/h (constant value)
Auxiliary Heat Input for Node-6	0 kJ/h (constant value)
Auxiliary Heat Input for Node-7	0 kJ/h (constant value)
Auxiliary Heat Input for Node-8	0 kJ/h (constant value)
Auxiliary Heat Input for Node-9	0 kJ/h (constant value)
Auxiliary Heat Input for Node-10	0 kJ/h (constant value)

Table 20b. Outputs of HP Tank Type.

OUTPUTS	
LIST OF OUTPUTS	OUTPUTS USED
Temperature at Outlet	Experimental Outlet Fluid Temperature - T_F_out_HP
Flowrate at Outlet	Experimental Fluid mass flowrate - m_P HP

1.20 Heat Pump Recirculation Pump (Pump HP) - Type 742

The Heat Pump Recirculation Pump (Pump HP) is modelled by using the Type 742. Fig. 15 reports the parameters of Pump HP type.

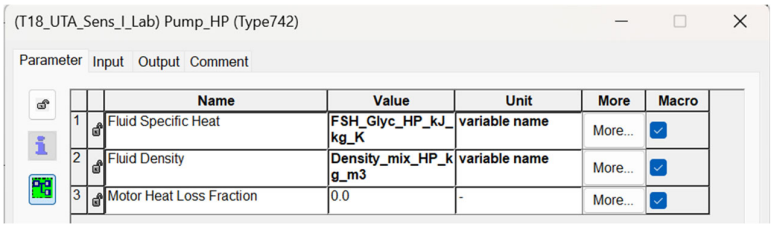

Figure 15. Parameters of Pump HP Type.

The fluid specific heat and the fluid density are parameters recalled from the calculator named "Water_Glycol_Properties" where are defined the fluid specific heat and the fluid density of the glycol mixture according to the manufacturers' data.

Tables 21a and b illustrate the inputs and outputs of heat pump recirculation pump type, respectively.

Table 21a. Inputs of Pump HP Type.

INPUTS	
LIST OF INPUTS	INPUTS USED
Inlet Fluid Temperature	Inlet Fluid Temperature (output Type 31)
Inlet Fluid Flowrate	Experimental Fluid mass flowrate - m_PHP
Overall Pump Efficiency	0.0277 (constant value)
Motor Efficiency	1 (constant value)
Pressure Drop	10 kPa (constant value)

Table 21b. Outputs of Pump HP Type.

Finanziato dall'Unione europea NextGenerationEU
Ministero dell'Università e della Ricerca
Italiadomani PIANO NAZIONALE DI RIPRESA E RESILIENZA

OUTPUTS	
LIST OF OUTPUTS	OUTPUTS USED
Outlet Fluid Flowrate	Experimental Fluid mass flowrate - m_PHP

The inlet fluid temperature input of the Pump HP is the output of a pipe modelled by the Type 31, that connect the three-way mixing valve at the outlet of the PostHC to the HP.
The electric power consumption of the recirculation pump is equal to 0.780 kW defined according to the experimental data.

1.21 Pipe Heat Pump to Post-Heating Coil (HP to PostHC) - Type 31

The Pipe HP to PostHC is modelled by using the Type 31. Fig. 16 reports parameters of the pipe type.

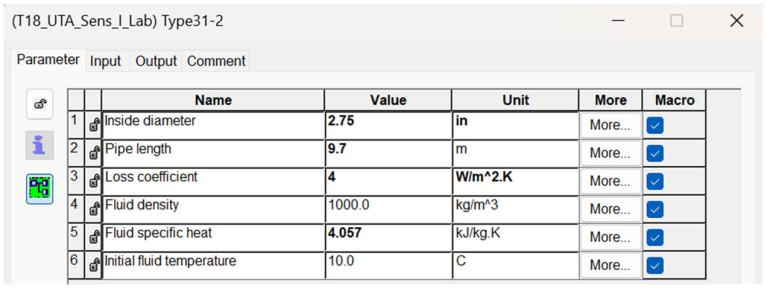

Figure 16. Parameters of Pipe HP to PostHC Type.

Table 22a and b illustrate the inputs and outputs of the pipe HP to PostHC type, respectively.

Table 22a. Inputs of Pipe HP to PostHC Type.

INPUTS	
LIST OF INPUTS	INPUTS USED
Inlet temperature	Inlet Fluid Temperature - T_F_out_HP
Inlet flow rate	Experimental Fluid mass flowrate - m_PHP
Environment temperature	Experimental Outdoor Air Temperature - T_OA

Table 22b. Outputs of Pipe HP to PostHC Type.

OUTPUTS	
LIST OF OUTPUTS	OUTPUTS USED
Outlet Temperature	Outlet Fluid Temperature - T_F_out_HP
Outlet Flowrate	Experimental Fluid mass flowrate - m_PHP

1.22 Three-way flow diverter valve Post-Heating Coil (PostHC) - Type 647

The three-way flow diverter valve PostHC is modelled by the Type 647. Fig. 17 reports the parameters of the three-way valve type.

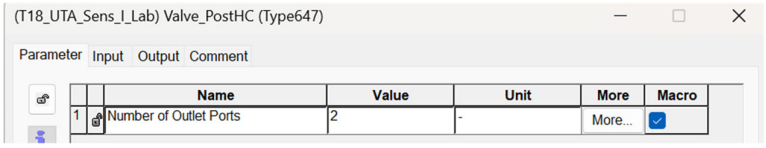

Figure 17. Parameters of Three-way flow diverter valve PostHC.

Tables 23a and b illustrate the inputs and outputs of the three-way flow diverter valve type, respectively.

Finanziato dall'Unione europea NextGenerationEU
Ministero dell'Università e della Ricerca
Italiadomani PIANO NAZIONALE DI RIPRESA E RESILIENZA

Table 23a. Inputs of Three-way flow diverter valve PostHC Type.

INPUTS	
LIST OF INPUTS	INPUTS USED
Inlet Temperature	Experimental Fluid Temperature - T_F_in_PostHC
Inlet Flowrate	Experimental Fluid mass flowrate - m_F_in_PostHC
Fraction of Flow to Outlet -1	Fraction of Flow to PostHC (output HP_Operation Calculator)
Fraction of Flow to Outlet -2_CC	Fraction of Flow to HP (output HP_Operation Calculator)

Table 23b. Outputs of Three-way flow diverter valve PostHC Type.

OUTPUTS	
LIST OF OUTPUTS	OUTPUTS USED
Outlet Temperature-1	Experimental Fluid Temperature - T_F_in_PostHC
Outlet Flowrate-1	Experimental Fluid mass flowrate - m_F_in_PostHC
Outlet Temperature-2	Outlet Fluid Temperature to HP
Outlet Flowrate-2	Outlet Fluid mass flowrate to HP

The inputs Fraction of Flow to PostHC and Fraction of Flow to HP are defined as function of the opening percentage of Post-Heating coil valve, in the calculator named “HP_Operation”.

1.23 Post-Heating Coil (CC) - Type 753b

The Cooling Coil CC is modelled by the Type 753b. Fig. 18 reports the parameters of pre-heating coil type.

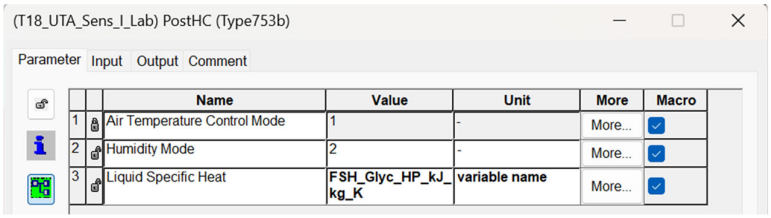

Figure 18. Parameters of PostHC Type.

Table 24a and b illustrate the inputs and outputs of the post-heating coil type, respectively.

Table 24a. Inputs of PostHC Type.

INPUTS	
LIST OF INPUTS	INPUTS USED
Fluid Inlet Temperature	Experimental Fluid Temperature - T_F_in_PostHC
Fluid Flowrate	Experimental Fluid mass flowrate - m_F_in_PostHC
Air Inlet Temperature	Experimental Air Temperature - T_A_out_CC
Air Humidity Ratio	-
Air % Relative Humidity	Experimental Air Relative Humidity - RH_A_out_CC
Air Flowrate	Mixed Air mass flowrate - m_A_out_HUM (output HUM Calculator)
Air Pressure	Air pressure outlet the CC - p_A_out_CC (output HUM Calculator)
Air-Side Pressure Drop	0.00004905 atm (constant value)
Coil Bypass Fraction	Post-Heating Coil Bypass Fraction - BF_HC (output HC_BFactor Calculator)
Setpoint: Outlet Air Temperature	100 °C (constant value)

Finanziato dall'Unione europea NextGenerationEU
Ministero dell'Università e della Ricerca
Italiadomani PIANO NAZIONALE DI RIPRESA E RESILIENZA

Table 24b. Outputs of PostHC Type.

OUTPUTS	
LIST OF OUTPUTS	OUTPUTS USED
Fluid Outlet Temperature	Fluid Outlet Temperature - T_F_out_PostHC
Outlet Fluid Flowrate	Experimental Fluid mass flowrate - m_F_in_PostHC
Outlet Air Temperature	Outlet Air Temperature - T_A_out_PostHC
Outlet Air % Relative Humidity	Outlet Air Relative Humidity - RH_A_out_PostHC
Outlet Air Pressure	Air pressure outlet the PostHC - p_A_out_PostHC

The post-heating coil bypass fraction is calculated according to the following Eq. 6, as function of return and supply air fan operating conditions:

$$BF\_HC = 0.415*(eql(Set\_OL\_SAF,5)*eql(Set\_OL\_RAF,5))+ 0.46*(eql(Set\_OL\_SAF,5)*eql(Set\_OL\_RAF,0))+ 0.03*(eql(Set\_OL\_SAF,0)*eql(Set\_OL\_RAF,5)) \quad (6)$$

Where:

- The constant value 0.415 is the experimental cooling coil bypass fraction when the return air fan velocity and the supply air fan velocity is equal to 50% (fault-free scenario);
- Set_OL_SAF is the experimental supply air fan velocity;
- Set_OL_RAF is the experimental return air fan velocity;
- The constant value 0.46 is the experimental cooling coil bypass fraction when the return air fan velocity is equal to 0% (faulty scenario) and the supply air fan velocity is equal to 50% (fault-free scenario);
- The constant value 0.03 is the experimental cooling coil bypass fraction when the return air fan velocity is equal to 50% (fault-free scenario) and the supply air fan velocity is equal to 0% (faulty scenario).

1.24 Three-way mixing valve Post-Heating Coil to Heat Pump (PostHC to HP) - Type 649

The three-way mixing valve PostHC to HP is modelled by the Type 649. Fig. 19 reports the parameters of the three-way valve type.

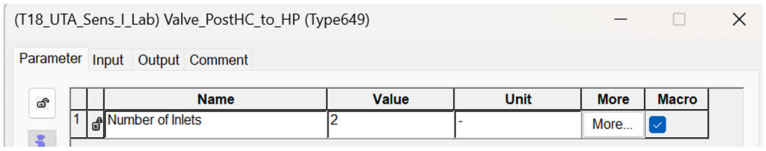

Figure 19. Three-way mixing valve PostHC to HP parameters.

Tables 25a and b illustrate the inputs and outputs of the three-way mixing valve PostHC to HP type.

Table 25a. Inputs of Three-way mixing valve PostHC to HP Type.

INPUTS	
LIST OF INPUTS	INPUTS USED
Temperature at Inlet-1	Fluid Outlet Temperature - T_F_out_PostHC
Flowrate at Inlet-1	Experimental Fluid mass flowrate - m_F_in_PostHC
Temperature at Inlet-2_CC	Fluid Temperature to HP (output Type 647)
Flowrate at Inlet-2_CC	Fluid Flowrate to HP (output Type 647)

Table 25b. Outputs of Three-way mixing valve PostHC to HP Type.

OUTPUTS

Finanziato dall'Unione europea NextGenerationEU
Ministero dell'Università e della Ricerca
Italiadomani PIANO NAZIONALE DI RIPRESA E RESILIENZA

LIST OF OUTPUTS	OUTPUTS USED
Outlet Temperature	Outlet Fluid Temperature
Outlet Flowrate	Outlet Fluid Flowrate

The inputs Fluid Temperature to HP and Fluid Flowrate to HP are the outputs of the three-way flow diverter valve PostHC.

1.25 Pipe Post-Heating Coil to Heat Pump (PostHC to HP) - Type 31

The Pipe PostHC to HP is modelled by using the Type 31. Fig. 20 reports the parameters of pipe type.

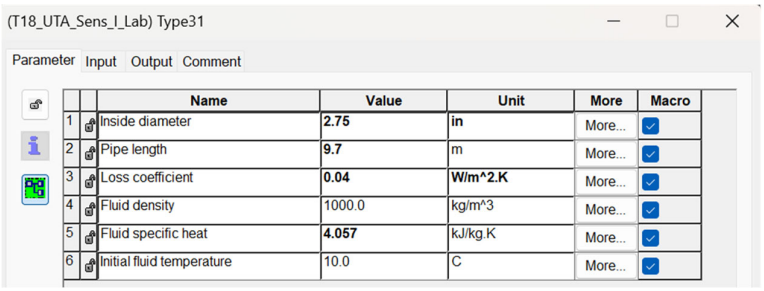

Figure 20. Parameters of Pipe PostHC to HP Type.

Tables 26a and b illustrate the inputs and outputs of the pipe PostHC to HP type, respectively.

Table 26a. Inputs of Pipe PostHC to HP Type.

INPUTS	
LIST OF INPUTS	INPUTS USED
Inlet temperature	Inlet Fluid Temperature (output Type 649)
Inlet flow rate	Inlet Fluid Flowrate (output Type 649)
Environment temperature	Experimental Outdoor Air Temperature - T_OA

Table 26b. Outputs of Pipe PostHC to HP Type.

OUTPUTS	
LIST OF OUTPUTS	OUTPUTS USED
Outlet Temperature	Outlet Fluid Temperature

The Inlet Fluid Temperature and Inlet Fluid Flowrate are the outputs of the three-way mixing valve PostHC to HP.

1.26 Humidifier (HUM) - Calculator

The Humidifier (HUM) is modelled by using a calculator and not a specific type. Table 27a and b illustrate the inputs and outputs of the humidifier calculator, respectively.

Table 27a. Inputs of HUM Calculator.

INPUTS	
LIST OF INPUTS	INPUTS USED
Inlet Air Temperature	Inlet Air Temperature - T_A_in_HUM (output Type 508c)
Inlet Air % Relative Humidity	Inlet Air Relative Humidity - RH_A_in_HUM (output Type 508c)
Inlet Air Specific Humidity	Inlet Air Specific Humidity - HR_A_in_HUM (output Type 508c)

Finanziato dall'Unione europea NextGenerationEU
Ministero dell'Università e della Ricerca
Italiadomani PIANO NAZIONALE DI RIPRESA E RESILIENZA

Inlet Air Flowrate	Inlet Air Flowrate - m_in_HUM (output Type 508c)
Inlet Air Pressure	Inlet Air Pressure - p_A_in_HUM (output Type 508c)
Control Signal	Ctrl_signal_HUM (output Type 23)

Table 27b. Outputs of HUM Calculator.

OUTPUTS	
LIST OF OUTPUTS	OUTPUTS USED
Outlet Air Temperature	Inlet Air Temperature - T_A_in_HUM
Outlet Air % Relative Humidity	Inlet Air Relative Humidity - RH_A_in_HUM
Outlet Air Specific Humidity	Outlet Air Specific Humidity - HR_A_out_HUM
Outlet Air Flowrate	Outlet Air mass flowrate - m_out_HUM
Outlet Vapour Flowrate	Outlet Vapour Flowrate - m_vapour_out_HUM
Outlet Air Pressure	Outlet Air Pressure - p_A_out_HUM
	Electric Power - EP_HUM

The vapour mass flowrate m_vapour_HUM is defined according to Eq. 7 according to the manufacturer's manual.

$$\begin{aligned} &\text{m\_in\_water\_HUM\_kg\_h} = 0*\text{lt}(\text{Ctrl\_HUM},0.05)+ \\ &1*(\text{ge}(\text{Ctrl\_HUM},0.05)*\text{lt}(\text{Ctrl\_HUM},0.1))+ \\ &5*\text{gt}(\text{Ctrl\_HUM},0.95)+ \\ &(4.70588235294118*(\text{Ctrl\_HUM}-0.1)+1)*(\text{ge}(\text{Ctrl\_HUM},0.1)*\text{le}(\text{Ctrl\_HUM},0.95)) \end{aligned} \quad (7)$$

Where:

- The constant value 0 represents the kg of steam produced when the humidifier valve is open at 5%;
- Ctrl_HUM is the output of PID type that regulate the opening percentage of humidifier valve;
- The constant value 1 represents the kg of steam produced when the humidifier valve is open between 5-10%;
- The constant value 5 represents the kg of steam produced when the humidifier valve is open at 100%;
- The portion of equation (4.70588235294118*(Ctrl_HUM–0.1)+1) represents the kg of steam produced when the humidifier valve is open between 10-95%;

The electric power EP_HUM is calculated according to the Eq.8, based on the manufacturer's manual as well as the experimental data.

$$\begin{aligned} &\text{SIM\_EP\_HUM\_kW} = ((\text{ge}(\text{Ctrl\_HUM},0)*\text{le}(\text{Ctrl\_HUM},0.05)*0)+ \\ &(\text{gt}(\text{Ctrl\_HUM},0.05)*\text{le}(\text{Ctrl\_HUM},0.1)*65.82)+ \\ &(\text{gt}(\text{Ctrl\_HUM},0.1)*\text{le}(\text{Ctrl\_HUM},0.95)*(380.49*\text{Ctrl\_HUM}-314.67))+ \\ &(\text{gt}(\text{Ctrl\_HUM},0.95)*\text{le}(\text{Ctrl\_HUM},1)*3300.00))/1000 \end{aligned} \quad (8)$$

Where:

- Ctrl_HUM is the output of PID type that regulate the opening percentage of humidifier valve;
- The constant value 65.82 is the experimental electric power demand of the humidifier when the opening percentage of its valve is between 5-10%;
- The portion of equation 380.49*Ctrl_HUM–314.67 is the experimental electric power demand of the humidifier when the opening percentage of its valve is between 10-95%;
- The constant value 3300.00 is the experimental electric power demand of the humidifier when the opening percentage of its valve is 100%.

Finanziato dall'Unione europea NextGenerationEU | Ministero dell'Università e della Ricerca | Italiadomani PIANO NAZIONALE DI RIPRESA E RESILIENZA

1.27 Supply Air Fan (SAF) - Calculator

The Supply Air Fan (SAF) is modelled by using a calculator and not a specific type. Tables 28a and b illustrate the inputs and outputs of supply air fan calculator, respectively.

Table 28a. Inputs of SAF Calculator.

INPUTS	
LIST OF INPUTS	INPUTS USED
Inlet Air Temperature	Experimental Supply Air Temperature - T_SA
Inlet Air % Relative Humidity	Experimental Supply Air Relative Humidity - RH_SA
Air Flowrate	Experimental Supply Air mass flowrate - m_SA
Inlet Air Pressure	Air pressure outlet the PostHC - p_A_out_PostHC (output Type 753b)

Table 28b. Outputs of SAF Calculator.

OUTPUTS	
LIST OF OUTPUTS	OUTPUTS USED
Outlet Air Temperature	Experimental Supply Air Temperature - T_SA
Outlet Air % Relative Humidity	Experimental Supply Air Relative Humidity - RH_SA
Outlet Air Flowrate	Experimental Supply Air mass flowrate - m_SA
Outlet Air Pressure	Air pressure outlet the SAF - p_A_out_SAF
	Electric power EP_SAF

The supply Air mass flowrate (m_SA) is calculated according to the Eq. 9, defined based on experimental data:

$$\begin{aligned} m\_SA = {} & (645.01*Density\_SA\_kg\_m3)*(eql(Set\_OL\_SAF,5)*eql(Set\_OL\_RAF,5))+ \\ & (611.43*Density\_SA\_kg\_m3)*(eql(Set\_OL\_SAF,5)*eql(Set\_OL\_RAF,0))+ \\ & (107.80*Density\_SA\_kg\_m3)*(eql(Set\_OL\_SAF,0)*eql(Set\_OL\_RAF,5))+ \\ & (1546.25*Density\_SA\_kg\_m3)*(eql(Set\_OL\_SAF,10)*eql(Set\_OL\_RAF,5))+ \\ & (673.28*Density\_SA\_kg\_m3)*(eql(Set\_OL\_SAF,5)*eql(Set\_OL\_RAF,10)) \end{aligned} \quad (9)$$

Where:

- The constant value 645.01 is the experimental supply air volumetric flowrate, when the return air fan velocity and the supply air fan velocity is equal to 50% (fault-free scenario);
- Density_SA_kg_m3 is the supply air density, calculated via the psychometric Type33e;
- Set_OL_SAF is the experimental supply air fan velocity;
- Set_OL_RAF is the experimental return air fan velocity;
- The constant value 611.43 is the experimental supply air volumetric flowrate when the return air fan velocity is equal to 50% (fault-free scenario) and the supply air fan velocity is equal to 0% (faulty scenario);
- The constant value 107.80 is the experimental supply volumetric air flowrate when the return air fan velocity is equal to 0% (faulty scenario) and the supply air fan velocity is equal to 50% (fault-free scenario);
- The constant value 1546.25 is the experimental supply volumetric air flowrate when the return air fan velocity is equal to 50% (fault-free scenario) and the supply air fan velocity is equal to 100% (faulty scenario);
- The constant value 673.28 is the experimental supply volumetric air flowrate when the return air fan velocity is equal to 100% (fauly scenario) and the supply air fan velocity is equal to 50% (fault-free scenario).

The electric power EP_SAF is defined according to Eq. 10. The equation is derived by interpolating the electrical power consumed by the supply air fan as a function of its velocity.

Finanziato dall'Unione europea NextGenerationEU | Ministero dell'Università e della Ricerca | Italiadomani PIANO NAZIONALE DI RIPRESA E RESILIENZA

$$SIM\_EP\_SAF\_kW = (0.117*Set\_OL\_SAF^4–0.545*Set\_OL\_SAF^3+11.949*Set\_OL\_SAF^2–8.949*Set\_OL\_SAF+89.712)/1000 \quad (10)$$

Where:

- Set_OL_SAF is the experimental supply air fan velocity.

1.28 External Supply Air Fan Duct (External SAD) - Type 607a

The External Supply Air Fan Duct is modelled by using the Type 607a. Fig. 21 reports the parameters of external supply air fan duct type.

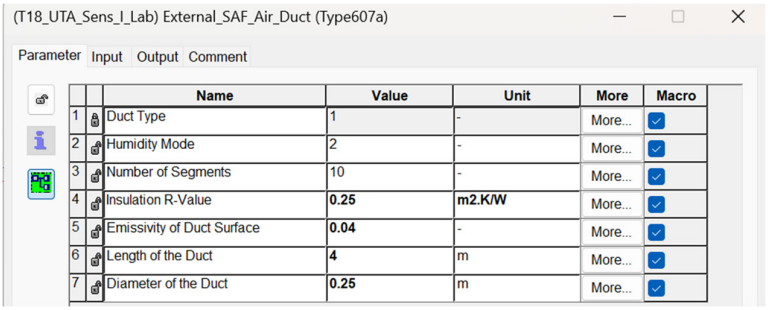

Figure 21. Parameters of External SAD Type.

Tables 29a and b illustrate the inputs and outputs of external supply air fan duct type, respectively.

Table 29a. Inputs of External SAD Type.

INPUTS	
LIST OF INPUTS	INPUTS USED
Inlet Air Temperature	Experimental Supply Air Temperature - T_SA
Inlet Air Humidity Ratio	-
Inlet Air % Relative Humidity	Experimental Supply Air Relative Humidity - RH_SA
Air Flowrate	Experimental Supply Air mass flowrate - m_SA
Inlet Air Pressure	Supply air pressure - p_SA (output SAF Calculator)
Environment Temperature	Experimental Outdoor Air Temperature - T_OA
Wind Velocity	Outdoor Air Velocity (output Type 15-3)

Table 29b. Outputs of External SAD Type.

OUTPUTS	
LIST OF OUTPUTS	OUTPUTS USED
Outlet Air Temperature	Experimental Supply Air Temperature - T_SA
Outlet Air % Relative Humidity	Experimental Supply Air Relative Humidity - RH_SA
Outlet Air Flowrate	Experimental Supply Air mass flowrate - m_SA
Outlet Air Pressure	Supply air pressure - p_SA

1.29 Internal Supply Air Fan Duct (Internal SAD) - Type 607a

The Internal Supply Air Fan Duct is modelled by using the Type 607a. Fig. 22 reports the parameters of the internal supply air fan duct.

Finanziato dall'Unione europea NextGenerationEU | Ministero dell'Università e della Ricerca | Italiadomani PIANO NAZIONALE DI RIPRESA E RESILIENZA

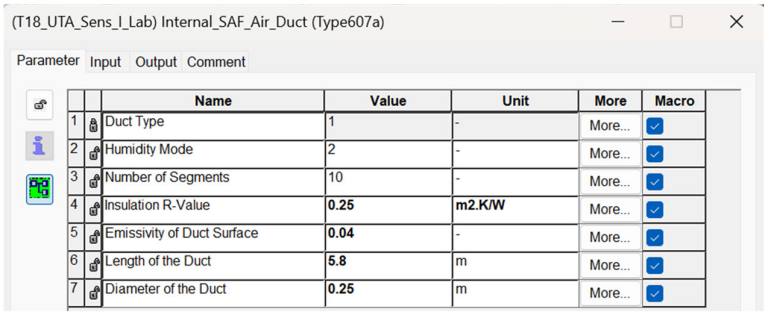

Figure 22. Parameters of Internal SAD Type.

Tables 30a and b illustrate the inputs and outputs of internal supply air fan duct type, respectively.

Table 30a. Inputs of Internal SAD Type.

INPUTS	
LIST OF INPUTS	INPUTS USED
Inlet Air Temperature	Experimental Supply Air Temperature - T_SA
Inlet Air Humidity Ratio	-
Inlet Air % Relative Humidity	Experimental Supply Air Relative Humidity - RH_SA
Air Flowrate	Experimental Supply Air mass flowrate - m_SA
Inlet Air Pressure	Supply air pressure - p_SA (output Type 607a)
Environment Temperature	Experimental Outdoor Air Temperature - T_OA

Table 30b. Outputs of Internal SAD Type.

OUTPUTS	
LIST OF OUTPUTS	OUTPUTS USED
Outlet Air Temperature	Experimental Supply Air Temperature - T_SA
Outlet Air % Relative Humidity	Experimental Supply Air Relative Humidity - RH_SA
Outlet Air Flowrate	Experimental Supply Air mass flowrate - m_SA
Outlet Air Pressure	Supply air pressure - p_SA

1.30 Controller Ctrl_RS - Type 2

The Controller Ctrl_RS is modelled by using the Type 2. Fig. 23 reports the parameters of the controller.

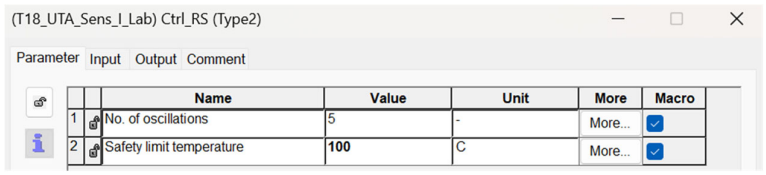

Figure 23. Parameters of Ctrl_RS Type.

Tables 31a and b illustrate the inputs and outputs of Ctrl_RS type, respectively.

Table 31a. Inputs of Ctrl_RS Type.

INPUTS	
LIST OF INPUTS	INPUTS USED
Temperature to watch	Experimental Outlet Fluid Temperature - T_F_out_RS
Setpoint temperature	Experimental RS_Set_Point

Finanziato dall'Unione europea NextGenerationEU | Ministero dell'Università e della Ricerca | Italiadomani PIANO NAZIONALE DI RIPRESA E RESILIENZA

High limit monitoring temperature	5 °C (constant value)
Input control function-->Connect from output control signal	0
Turn on temperature difference	1 - Experimental constant value
Turn off temperature difference	–1 - Experimental constant value

Table 31b. Outputs of Ctrl_RS Type.

OUTPUTS	
LIST OF OUTPUTS	OUTPUTS USED
Output control function	Ctrl_RS_sing

The output Ctrl_RS_sing is the input of the calculator named Ctrl_RS. This calculator, together with n. 1 Type 661, n. 4 Type 93 and with another calculator named Timer_RS, performs the function of delaying the turn on of the refrigerating system by 60 seconds, so as to make the behaviour of the RS simulated as close as possible to the behaviour of the RS in the experimental set-up.

1.31 Controller Ctrl_HP - Type 2

The Controller Ctrl_HP is modelled by using the Type 2. Fig. 24 reports the parameters of the controller.

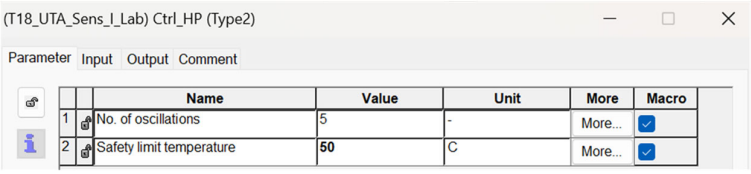

Figure 24. Parameters of Ctrl_HP Type.

Tables 32a and b illustrate the inputs and outputs of Ctrl_HP type, respectively.

Table 32a. Inputs of Ctrl_HP Type.

INPUTS	
LIST OF INPUTS	INPUTS USED
Temperature to watch	Experimental Outlet Fluid Temperature - T_F_out_HP
Setpoint temperature	Experimental HP_Set_Point
High limit monitoring temperature	5 °C (constant value)
Input control function-->Connect from output control signal	0
Turn on temperature difference	1 - Experimental constant value
Turn off temperature difference	–1 - Experimental constant value

Table 32b. Outputs of Ctrl_HP Type.

OUTPUTS	
LIST OF OUTPUTS	OUTPUTS USED
Output control function	Ctrl_HP_sing

The output Ctrl_HP_sing is the input of the calculator named Ctrl_HP. This calculator, together with n. 1 Type 661, n. 4 Type 93 and with another calculator named Timer_HP, performs the function of delaying the turn on of the heat pump by 60 seconds, so as to make the behaviour of the HP simulated as close as possible to the behaviour of the HP the experimental set-up.

Finanziato dall'Unione europea NextGenerationEU
Ministero dell'Università e della Ricerca
Italiadomani PIANO NAZIONALE DI RIPRESA E RESILIENZA

1.32 Controller Ctrl_HUM - Type 2

The Controller Ctrl_HUM is modelled by using the Type 2. Fig. 25 reports the parameters of the controller.

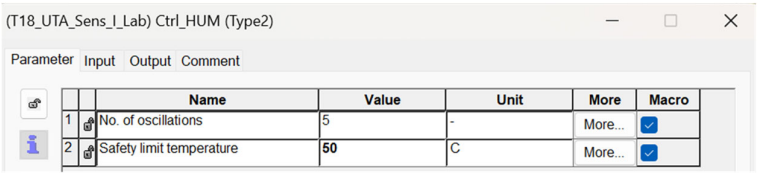

Figure 25. Parameters of Ctrl_HUM Type.

Tables 33a and b illustrate the inputs and outputs of Ctrl_HUM type, respectively.

Table 33a. Inputs of Ctrl_HUM Type.

INPUTS	
LIST OF INPUTS	INPUTS USED
Temperature to watch	Experimental Return Air Relative Humidity - RH_RA
Setpoint temperature	Experimental Return Air Relative Humidity Target Set_RH_target_RA
High limit monitoring temperature	5 °C (constant value)
Input control function-->Connect from output control signal	0
Turn on temperature difference	Experimental RH upper dead band - UDB_RH_target_RA
Turn off temperature difference	Experimental RH lower dead band - LDB_RH_target_RA

Table 33b. Outputs of Ctrl_HUM Type.

OUTPUTS	
LIST OF OUTPUTS	OUTPUTS USED
Output control function	Ctrl_Humid

1.33 Controller Ctrl_Dehum - Type 2

The Controller Ctrl_Dehum is modelled by using the Type 2. Fig. 26 reports the parameters of the controller.

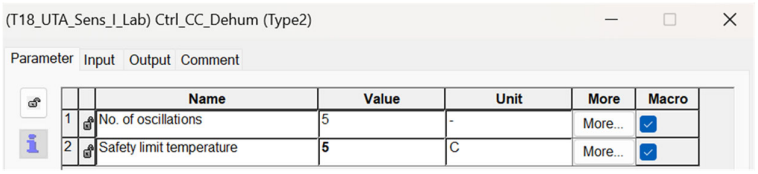

Figure 26. Parameters of Ctrl_Dehum Type.

Tables 34a and b illustrate the inputs and outputs of Ctrl_Dehum type, respectively.

Table 34a. Inputs of Ctrl_Dehum Type.

INPUTS	
LIST OF INPUTS	INPUTS USED
Temperature to watch	Experimental Return Air Relative Humidity - RH_RA
Setpoint temperature	Experimental Return Air Relative Humidity - Target Set_RH_target_RA
High limit monitoring temperature	5 °C (constant value)
Input control function-->Connect from output control signal	0

Finanziato dall'Unione europea NextGenerationEU
Ministero dell'Università e della Ricerca
Italiadomani PIANO NAZIONALE DI RIPRESA E RESILIENZA

Turn on temperature difference	Experimental RH upper dead band - UDB_RH_target_RA
Turn off temperature difference	Experimental RH lower dead band - LDB_RH_target_RA

Table 34b. Outputs of Ctrl_DehumType.

OUTPUTS	
LIST OF OUTPUTS	OUTPUTS USED
Output control function	Ctrl_CC_Dehum

1.34 Controller Ctrl_CC_Temp - Type 2

The Controller Ctrl_CC_Temp is modelled by using the Type 2. Fig. 27 reports the parameters of the controller.

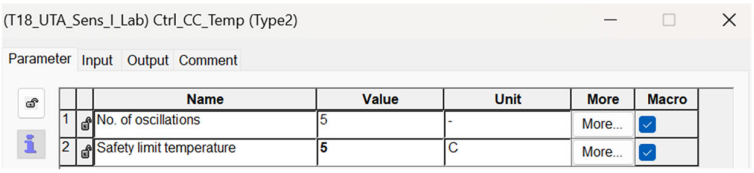

Figure 27. Parameters of Ctrl_CC_Temp Type.

Tables 35a and b illustrate the inputs and outputs of Ctrl_CC_Temp type, respectively.

Table 35a. Inputs of Ctrl_CC_Temp Type.

INPUTS	
LIST OF INPUTS	INPUTS USED
Temperature to watch	Experimental Return Air Temperature - T_RA
Setpoint temperature	Experimental Return Air Temperature - Target Set_T_target_RA
High limit monitoring temperature	7 °C (constant value)
Input control function-->Connect from output control signal	0
Turn on temperature difference	Experimental T upper dead band - UDB_T_target_RA
Turn off temperature difference	Experimental T lower dead band - LDB_T_target_RA

Table 35b. Outputs of Ctrl_CC_Temp Type.

OUTPUTS	
LIST OF OUTPUTS	OUTPUTS USED
Output control function	Ctrl_CC_temp

1.35 Controller Ctrl_PostHC_Temp - Type 2

The Controller Ctrl_PostHC_Temp is modelled by using the Type 2. Fig. 28 reports the parameters of the controller.

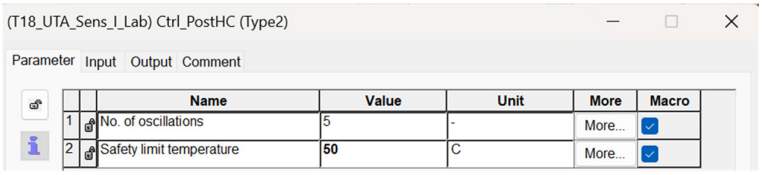

Figure 28. Parameters of Ctrl_PostHC_Temp Type.

Tables 36a and b illustrate the inputs and outputs of Ctrl_PostHC_Temp type, respectively.

Finanziato dall'Unione europea NextGenerationEU | Ministero dell'Università e della Ricerca | Italiadomani PIANO NAZIONALE DI RIPRESA E RESILIENZA

Table 36a. Inputs of Ctrl_PostHC_Temp Type.

INPUTS	
LIST OF INPUTS	INPUTS USED
Temperature to watch	Experimental Return Air Temperature - T_RA
Setpoint temperature	Experimental Return Air Temperature - Target Set_T_target_RA
High limit monitoring temperature	50 °C (constant value)
Input control function-->Connect from output control signal	0
Turn on temperature difference	Experimental T upper dead band - UDB_T_target_RA
Turn off temperature difference	Experimental T lower dead band - LDB_T_target_RA

Table 36b. Outputs of Ctrl_PostHC_Temp Type.

OUTPUTS	
LIST OF OUTPUTS	OUTPUTS USED
Output control function	Ctrl_PostHC

1.36 PID Controller CC_Temp - Type 23

The PID Controller CC_Temp is modelled by using the Type 23. Fig. 29 reports the parameters of the PID controller.

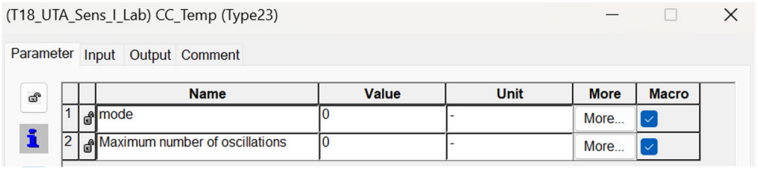

Figure 29. Parameters of PID Controller CC_Temp Type.

Tables 37a and b illustrate the inputs and outputs of PID Controller CC_Temp type, respectively.

Table 37a. Inputs of PID Controller CC_Temp Type.

INPUTS	
LIST OF INPUTS	INPUTS USED
Setpoint	Experimental Return Air Temperature - T_RA
Controlled variable	Experimental Return Air Temperature - Target Set_T_target_RA
On / Off signal	Ctrl_CC_temp (output Type 2)
Minimum control signal	0 (constant value)
Maximum control signal	1 (constant value)
Threshold for non-zero output	0 (constant value)
Gain constant	– 0.05 - Experimental constant value
Integral time	1 min - Experimental constant value
Derivative time	0.1 min - Experimental constant value
Tracking time for anti-windup	–1 (constant value)
Fraction of ySet for proportional effect	1 (constant value)
Fraction of ySet for derivative effect	1 (constant value)

Finanziato dall'Unione europea NextGenerationEU
Ministero dell'Università e della Ricerca
Italiadomani PIANO NAZIONALE DI RIPRESA E RESILIENZA

High-frequency limit on derivative	10 (constant value)

Table 37b. Outputs of PID Controller CC_Temp Type.

OUTPUTS	
LIST OF OUTPUTS	OUTPUTS USED
Control signal	Valve_CC_temp

1.37 PID Controller CC_Dehum - Type 23

The PID Controller CC_Dehum is modelled by using the Type 23. Fig. 30 reports the parameters of the PID controller.

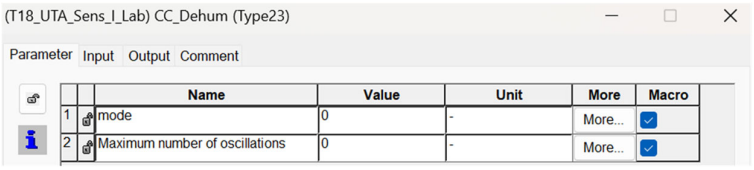

Figure 30. Parameters of PID Controller CC_Dehum Type.

Tables 38a and b illustrate the inputs and outputs of PID Controller CC_Dehum type, respectively.

Table 38a. Inputs of PID Controller CC_Dehum Type.

INPUTS	
LIST OF INPUTS	INPUTS USED
Setpoint	Experimental Return Air Relative Humidity - RH_RA
Controlled variable	Experimental Return Air Relative Humidity - Target Set_RH_target_RA
On / Off signal	Ctrl_CC_Dehum (output Type 2)
Minimum control signal	0 (constant value)
Maximum control signal	1 (constant value)
Threshold for non-zero output	0 (constant value)
Gain constant	– 0.1 - Experimental constant value
Integral time	1 min - Experimental constant value
Derivative time	0.1 min - Experimental constant value
Tracking time for anti-windup	–1 (constant value)
Fraction of ySet for proportional effect	1 (constant value)
Fraction of ySet for derivative effect	1 (constant value)
High-frequency limit on derivative	10 (constant value)

Table 38b. Outputs of PID Controller CC_Dehum Type.

OUTPUTS	
LIST OF OUTPUTS	OUTPUTS USED
Control signal	Valve_CC_dehum

1.38 PID Controller PostHC - Type 23

The PID Controller PostHC is modelled by using the Type 23. Fig. 31 reports the parameters of the PID controller.

Finanziato dall'Unione europea NextGenerationEU
Ministero dell'Università e della Ricerca
Italiadomani PIANO NAZIONALE DI RIPRESA E RESILIENZA

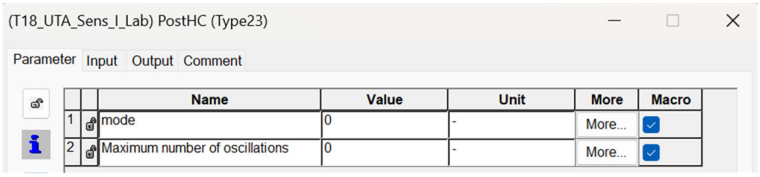

Figure 31. Parameters of PID Controller PostHC Type.

Tables 39a and b illustrate the inputs and outputs of PID Controller PostHC type, respectively.

Table 39a. Inputs of PID Controller PostHC Type.

INPUTS	
LIST OF INPUTS	INPUTS USED
Setpoint	Experimental Return Air Temperature - T_RA
Controlled variable	Experimental Return Air Temperature - Target Set_T_target_RA
On / Off signal	Ctrl_PostHC (output Type 2)
Minimum control signal	0 (constant value)
Maximum control signal	1 (constant value)
Threshold for non-zero output	0 (constant value)
Gain constant	– 0.1 - Experimental constant value
Integral time	1 min - Experimental constant value
Derivative time	0.1 min - Experimental constant value
Tracking time for anti-windup	– 1 (constant value)
Fraction of ySet for proportional effect	1 (constant value)
Fraction of ySet for derivative effect	1 (constant value)
High-frequency limit on derivative	10 (constant value)

Table 39b. Outputs of PID Controller PostHC Type.

OUTPUTS	
LIST OF OUTPUTS	OUTPUTS USED
Control signal	Valve_PostHC

1.39 PID Controller Humidifier - Type 23

The PID Controller Humidifier is modelled by using the Type 23. Fig. 32 reports the parameters of the PID controller.

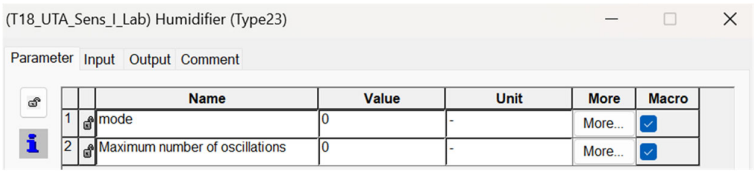

Figure 32. Parameters of PID Controller Humidifier Type.

Tables 40a and b illustrate the inputs and outputs of PID Controller Humidifier type, respectively.

Table 40a. Inputs of PID Controller Humidifier Type.

INPUTS	
LIST OF INPUTS	INPUTS USED

Finanziato dall'Unione europea NextGenerationEU
Ministero dell'Università e della Ricerca
Italiadomani PIANO NAZIONALE DI RIPRESA E RESILIENZA

Setpoint	Experimental Return Air Relative Humidity - RH_RA
Controlled variable	Experimental Return Air Relative Humidity - Target Set_RH_target_RA
On / Off signal	Ctrl_Humid (output Type 2)
Minimum control signal	0 (constant value)
Maximum control signal	1 (constant value)
Threshold for non-zero output	0 (constant value)
Gain constant	0.1 - Experimental constant value
Integral time	1 min - Experimental constant value
Derivative time	0.1 min - Experimental constant value
Tracking time for anti-windup	–1 (constant value)
Fraction of ySet for proportional effect	1 (constant value)
Fraction of ySet for derivative effect	1 (constant value)
High-frequency limit on derivative	10 (constant value)

Table 40b. Outputs of PID Controller Humidifier Type.

OUTPUTS	
LIST OF OUTPUTS	OUTPUTS USED
Control signal	Ctrl_HUM

1.40 Printer and Plotter - Type 25c and Type 65d

Finally, **Type 25c** and **Type 65d** model a printer and an online plotter, respectively, which were used to display in real time the trends of the variables to be analysed and to "print" them to an external file for subsequent processing.

2. Simulation Results

The validation of TRNSYS AHU model is carried out against the normal experimental data obtained from tests performed both in summer and in winter. Specifically, the comparison between experimental and simulated data is conducted component by component, in terms of electrical energy consumption (EE) of the RS, the HP, the SAF, the RAF, and the HUM, in terms of thermal energy (TP) dissipated by the HP and the PostHC, and in terms of cooling energy (CP) dissipated by the RS and the CC.

In the following tables, the percentage difference (%d) of the previous parameters between simulated and experimental data, calculated as follows (Eq. q), are reported.

$$\%d = \frac{(SIM - EXP)}{EXP} \cdot 100 \quad (1)$$

where:

- SIM are the values of EE, TP and CP associated to the simulated data;
- EXP are the values of EE, TP and CP associated to the experimental data.

A positive %d indicates that the EE/TP/CP value associated with the experimental data is lower than the corresponding value obtained from the simulation. This means that the simulation overestimates the performance of the AHU components.

Tables 41a and b report the %d in terms of EE of the return and supply air fan, during summer and winter, respectively.

Table 41a. Values of %d (calculated via Eq. 1) for RAF and SAF in terms of EE during summer.

Finanziato dall'Unione europea NextGenerationEU | Ministero dell'Università e della Ricerca | Italiadomani PIANO NAZIONALE DI RIPRESA E RESILIENZA

Test ID	RAF electric energy (kWh)		RAF electric energy percentage difference (%)	SAF electric energy (kWh)		SAF electric energy percentage difference (%)
	EXP	SIM	SIM-EXP	EXP		EXP
SN1	0.67	0.66	**-1.68%**	3.09	3.14	**1.45%**
SN2	0.67	0.66	**-0.81%**	3.04	3.14	**3.38%**
SN3	0.66	0.66	**-0.61%**	3.05	3.14	**3.02%**
SN4	0.66	0.66	**0.13%**	3.07	3.14	**2.13%**
SN5	0.66	0.66	**-0.52%**	3.10	3.14	**1.21%**
SN6	0.66	0.66	**-0.25%**	3.04	3.14	**3.26%**
SN7	0.65	0.66	**1.84%**	3.08	3.14	**1.98%**
SN8	0.65	0.66	**1.13%**	3.19	3.14	**-1.59%**
SN9	0.65	0.66	**1.74%**	3.17	3.14	**-1.10%**
SN10	0.65	0.66	**1.85%**	3.07	3.14	**2.09%**
SN11	0.65	0.66	**1.99%**	3.01	3.14	**4.42%**
SN12	0.66	0.66	**0.80%**	3.07	3.14	**2.16%**
SN13	0.67	0.66	**-0.78%**	3.02	3.14	**3.89%**
SN14	0.65	0.66	**1.11%**	2.96	3.14	**6.09%**
SN15	0.65	0.66	**1.65%**	2.90	3.14	**8.08%**
SN16	0.65	0.66	**1.29%**	3.14	3.14	**-0.01%**
SN17	0.65	0.66	**0.84%**	3.07	3.14	**2.14%**
SN18	0.66	0.66	**0.46%**	3.07	3.14	**2.34%**
SN19	0.65	0.66	**2.10%**	3.06	3.14	**2.52%**

Table 41b. Values of %d (calculated via Eq. 1) for RAF and SAF in terms of EE during winter.

Test ID	RAF electric energy (kWh)		RAF electric energy percentage difference (%)	SAF electric energy (kWh)		SAF electric energy percentage difference (%)
	EXP	SIM	SIM-EXP	EXP	SIM	EXP
WN1	0.68	0.66	**-2.28%**	3.08	3.14	**1.74%**
WN2	0.68	0.66	**-3.02%**	3.14	3.14	**-0.13%**
WN3	0.68	0.66	**-2.98%**	3.15	3.14	**-0.45%**
WN4	0.68	0.66	**-2.97%**	3.12	3.14	**0.64%**
WN5	0.68	0.66	**-3.39%**	3.19	3.14	**-1.66%**
WN6	0.68	0.66	**-2.98%**	3.18	3.14	**-1.26%**
WN7	0.68	0.66	**-3.05%**	3.22	3.14	**-2.58%**
WN8	0.68	0.66	**-2.58%**	3.23	3.14	**-2.77%**
WN9	0.68	0.66	**-2.80%**	3.24	3.14	**-3.16%**
WN10	0.67	0.66	**-1.59%**	3.12	3.14	**0.44%**
WN11	0.68	0.66	**-2.35%**	3.19	3.14	**-1.75%**
WN12	0.67	0.66	**-2.09%**	3.22	3.14	**-2.66%**
WN13	0.67	0.66	**-1.49%**	3.19	3.14	**-1.55%**
WN14	0.66	0.66	**-0.21%**	3.13	3.14	**0.24%**
WN15	0.67	0.66	**-1.97%**	3.16	3.14	**-0.64%**
WN16	0.67	0.66	**-1.73%**	3.21	3.14	**-2.25%**

Tables 42a and b illustrate the %d in terms of HUM electric energy consumption, during summer and winter, respectively.

Table 42a. Values of %d (calculated via Eq. 1) for HUM in terms of EE during summer.

Finanziato dall'Unione europea NextGenerationEU | Ministero dell'Università e della Ricerca | Italiadomani PIANO NAZIONALE DI RIPRESA E RESILIENZA

Test ID	HUM electric energy (kWh)		HUM electric energy percentage difference (%)
	EXP	SIM	SIM-EXP
SN1	5.34	4.73	**-11.35%**
SN2	5.07	4.62	**-8.81%**
SN3	4.41	4.38	**-0.60%**
SN4	4.27	4.35	**1.90%**
SN5	5.69	5.74	**0.87%**
SN6	0.00	0.00	**N.A.**
SN7	4.50	4.64	**3.25%**
SN8	4.91	5.00	**1.80%**
SN9	6.18	6.26	**1.24%**
SN10	5.49	5.50	**0.23%**
SN11	6.22	6.34	**2.05%**
SN12	7.08	7.08	**-0.05%**
SN13	0.92	0.85	**-8.20%**
SN14	3.03	2.85	**-5.84%**
SN15	3.38	3.34	**-1.19%**
SN16	2.54	2.21	**-12.84%**
SN17	1.91	1.803	**-5.43%**
SN18	1.92	1.797	**-6.56%**
SN19	2.29	2.13	**-6.92%**

Table 42b. Values of %d (calculated via Eq. 1) for HUM in terms of EE during winter.

Test ID	HUM electric energy (kWh)		HUM electric energy percentage difference (%)
	EXP	SIM	SIM-EXP
WN1	0.00	0.00	**0.00%**
WN2	0.42	0.49	**15.64%**
WN3	1.65	1.78	**8.34%**
WN4	0.00	0.00	**0.00%**
WN5	3.52	3.54	**0.51%**
WN6	4.09	4.18	**2.08%**
WN7	0.00	0.00	**0.00%**
WN8	2.69	2.75	**2.25%**
WN9	5.29	5.33	**0.84%**
WN10	0.00	0.00	**#DIV/0!**
WN11	0.00	0.00	**#DIV/0!**
WN12	0.00	0.00	**#DIV/0!**
WN13	0.00	0.00	**#DIV/0!**
WN14	0.00	0.00	**#DIV/0!**
WN15	0.00	0.00	**#DIV/0!**
WN16	0.53	0.57	**7.28%**

Tables 43a and b show the %d in terms of EE of refrigerating system and heat pump, during summer and winter, respectively.

Finanziato dall'Unione europea NextGenerationEU | Ministero dell'Università e della Ricerca | Italiadomani PIANO NAZIONALE DI RIPRESA E RESILIENZA

Table 43a. Values of %d (calculated via Eq. 1) for RS and HP in terms of EE during summer.

Test ID	RS electric energy (kWh)		RS electric energy percentage difference (%)	HP electric energy (kWh)		HP electric energy percentage difference (%)
	EXP	SIM	SIM-EXP	EXP	SIM	SIM-EXP
SN1	23.98	25.85	**7.81%**	12.28	12.35	**0.52%**
SN2	29.38	30.40	**3.48%**	12.05	12.72	**5.55%**
SN3	29.72	30.17	**1.52%**	12.46	13.03	**4.55%**
SN4	27.00	28.31	**4.86%**	12.77	13.16	**2.98%**
SN5	25.34	27.73	**9.41%**	11.80	12.53	**6.21%**
SN6	25.15	29.57	**17.59%**	13.20	13.58	**2.84%**
SN7	32.73	33.37	**1.94%**	13.91	14.94	**7.45%**
SN8	31.34	29.86	**-4.72%**	15.31	15.31	**0.02%**
SN9	31.32	30.33	**-3.16%**	14.51	14.92	**2.85%**
SN10	32.53	32.39	**-0.45%**	13.30	14.50	**8.99%**
SN11	27.96	28.36	**1.45%**	13.47	13.43	**-0.35%**
SN12	21.62	24.27	**12.26%**	16.05	14.57	**-9.21%**
SN13	33.74	34.72	**2.89%**	13.35	14.54	**8.91%**
SN14	24.00	29.05	**21.05%**	13.72	14.09	**2.76%**
SN15	25.88	31.14	**20.32%**	13.09	13.95	**6.53%**
SN16	29.59	31.43	**6.20%**	14.89	14.10	**-5.31%**
SN17	26.24	31.06	**18.40%**	15.58	18.06	**15.96%**
SN18	25.66	30.94	**20.56%**	15.75	17.49	**11.06%**
SN19	33.89	34.40	**1.50%**	13.87	15.64	**12.83%**

Table 43a. Values of %d (calculated via Eq. 1) for RS and HP in terms of EE during winter.

Test ID	RS electric energy (kWh)		RS electric energy percentage difference (%)	HP electric energy (kWh)		HP electric energy percentage difference (%)
	EXP	SIM	SIM-EXP	EXP	SIM	EXP
WN1	13.07	11.00	**-15.80%**	16.68	15.22	**-8.79%**
WN2	14.70	14.82	**0.82%**	13.97	13.83	**-1.01%**
WN3	13.17	11.78	**-10.56%**	15.98	14.72	**-7.87%**
WN4	16.49	16.89	**2.44%**	14.41	14.41	**-0.05%**
WN5	14.06	13.08	**-6.92%**	12.77	11.80	**-7.57%**
WN6	14.08	14.20	**0.89%**	12.17	12.78	**5.04%**
WN7	16.08	14.99	**-6.79%**	17.27	15.59	**-9.71%**
WN8	15.77	14.40	**-8.67%**	18.29	17.52	**-4.18%**
WN9	15.58	13.62	**-12.56%**	17.92	17.18	**-4.11%**
WN10	15.10	15.09	**-0.07%**	15.84	15.09	**-4.73%**
WN11	14.97	14.98	**0.10%**	14.54	15.80	**8.63%**
WN12	16.29	17.11	**5.06%**	16.80	16.91	**0.66%**
WN13	16.19	16.82	**3.91%**	16.07	15.88	**-1.17%**
WN14	18.27	19.96	**9.27%**	15.33	15.10	**-1.50%**
WN15	16.83	17.65	**4.88%**	17.20	16.52	**-3.97%**
WN16	17.42	19.21	**10.33%**	16.66	16.10	**-3.36%**

Tables 44a and b report the %d in terms of CP of refrigerating system and TP of heat pump, during summer and winter, respectively.

Finanziato dall'Unione europea NextGenerationEU | Ministero dell'Università e della Ricerca | Italiadomani PIANO NAZIONALE DI RIPRESA E RESILIENZA

Table 44a. Values of %d (calculated via Eq. 1) for RS and HP in terms of CP and TP during summer.

Test ID	RS cooling energy (kWh)		RS cooling energy percentage difference (%)	HP thermal energy (kWh)		HP thermal energy percentage difference (%)
	EXP	SIM	SIM-EXP	EXP	SIM	SIM-EXP
SN1	29.00	33.13	**14.22%**	16.16	16.35	**1.14%**
SN2	36.92	37.01	**0.25%**	16.33	18.39	**12.59%**
SN3	34.22	33.41	**-2.36%**	18.52	18.60	**0.43%**
SN4	34.47	36.33	**5.40%**	17.94	18.02	**0.45%**
SN5	30.87	34.61	**12.10%**	14.69	18.12	**23.34%**
SN6	30.59	35.91	**17.38%**	18.92	19.78	**4.51%**
SN7	41.23	38.80	**-5.89%**	18.92	21.73	**14.87%**
SN8	35.50	36.21	**2.00%**	18.69	22.97	**22.93%**
SN9	32.74	33.97	**3.74%**	17.79	22.90	**28.72%**
SN10	42.02	38.56	**-8.23%**	17.01	21.90	**28.69%**
SN11	34.10	35.07	**2.84%**	15.63	17.40	**11.37%**
SN12	24.73	29.24	**18.23%**	18.98	17.46	**-7.98%**
SN13	43.23	39.07	**-9.63%**	18.42	21.62	**17.39%**
SN14	30.96	37.07	**19.73%**	18.52	18.99	**2.54%**
SN15	35.29	37.51	**6.30%**	18.16	18.97	**4.48%**
SN16	35.00	38.71	**10.62%**	17.93	19.16	**6.85%**
SN17	33.43	38.21	**14.29%**	23.03	28.23	**22.59%**
SN18	33.65	38.82	**15.36%**	22.50	26.02	**15.64%**
SN19	41.66	39.92	**-4.20%**	20.77	24.85	**19.67%**

Test ID	RS cooling energy (kWh)		RS cooling energy percentage difference (%)	HP thermal energy (kWh)		HP thermal energy percentage difference (%)
	EXP	SIM	SIM-EXP	EXP	SIM	EXP
N1	8.85	8.53	**-3.65%**	19.73	17.22	**-12.74%**
N2	12.78	13.03	**1.95%**	15.47	15.82	**2.29%**
N3	9.63	9.64	**0.09%**	18.28	16.72	**-8.55%**
N4	15.08	15.05	**-0.19%**	17.22	16.91	**-1.76%**
N5	11.61	11.56	**-0.45%**	9.20	9.91	**7.75%**
N6	12.69	12.18	**-4.02%**	10.07	11.90	**18.22%**
N7	14.03	12.63	**-9.95%**	17.08	16.90	**-1.02%**
N8	12.82	12.62	**-1.53%**	18.89	20.44	**8.22%**
N9	12.37	11.78	**-4.75%**	17.48	19.76	**13.03%**
N10	13.01	14.40	**10.67%**	15.80	15.86	**0.39%**
N11	13.09	13.21	**0.91%**	13.16	17.33	**31.65%**
N12	13.93	16.59	**19.12%**	17.71	19.94	**12.55%**
N13	13.76	16.62	**20.79%**	16.33	17.69	**8.35%**
N14	16.45	20.09	**22.13%**	15.87	17.11	**7.84%**
N15	13.93	17.28	**24.09%**	18.54	18.78	**1.29%**
N16	15.25	18.30	**20.02%**	17.57	19.12	**8.83%**

Tables 45a and b illustate the %d in terms of CC cooling energy and PostHC thermal energy, during summer and winter, respectively.

Finanziato dall'Unione europea NextGenerationEU | Ministero dell'Università e della Ricerca | Italiadomani PIANO NAZIONALE DI RIPRESA E RESILIENZA

Table 45a. Values of %d (calculated via Eq. 1) for CC and PostHC in terms of CP and TP during summer.

Test ID	CC cooling energy (kWh)		CC cooling energy percentage difference (%)	PostHC thermal energy (kWh)		PostHC thermal energy percentage difference (%)
	EXP	SIM	SIM-EXP	EXP	SIM	SIM-EXP
SN1	32.4	30.6	**-5.60%**	18.34	19.09	**4.09%**
SN2	41.1	39.5	**-3.91%**	18.25	19.69	**7.90%**
SN3	38.3	36.3	**-5.42%**	20.58	22.87	**11.10%**
SN4	38.0	37.0	**-2.43%**	19.92	21.38	**7.31%**
SN5	34.7	33.0	**-4.92%**	16.61	17.47	**5.22%**
SN6	35.1	34.0	**-3.00%**	21.10	21.97	**4.13%**
SN7	46.3	47.5	**2.47%**	19.95	20.63	**3.39%**
SN8	40.0	40.6	**1.31%**	19.66	20.23	**2.88%**
SN9	37.4	37.0	**-1.05%**	19.28	20.08	**4.12%**
SN10	47.0	48.4	**2.86%**	18.92	19.19	**1.39%**
SN11	38.9	39.3	**0.99%**	17.78	17.45	**-1.86%**
SN12	27.9	28.2	**0.82%**	20.31	20.66	**1.73%**
SN13	47.4	49.9	**5.22%**	19.73	19.64	**-0.45%**
SN14	35.5	37.2	**4.65%**	19.23	19.16	**-0.34%**
SN15	38.8	40.3	**3.99%**	19.28	19.02	**-1.34%**
SN16	40.2	41.3	**2.75%**	18.82	18.92	**0.54%**
SN17	38.2	39.5	**3.49%**	21.98	22.34	**1.62%**
SN18	38.4	39.8	**3.60%**	22.15	22.16	**0.05%**
SN19	45.9	50.5	**10.03%**	20.14	20.44	**1.50%**

Table 45b. Values of %d (calculated via Eq. 1) for CC and PostHC in terms of CP and TP during winter.

Test ID	CC cooling energy (kWh)		CC cooling energy percentage difference (%)	PostHC thermal energy (kWh)		PostHC thermal energy percentage difference (%)
	EXP	SIM	SIM-EXP	EXP	SIM	SIM-EXP
WN1	12.63	14.07	**11.38%**	20.8	20.9	**0.48%**
WN2	16.41	16.19	**-1.34%**	16.6	16.0	**-3.93%**
WN3	13.26	13.07	**-1.40%**	19.9	18.9	**-4.79%**
WN4	18.87	19.89	**5.41%**	18.7	18.6	**-0.74%**
WN5	14.98	13.49	**-9.95%**	9.2	8.2	**-10.77%**
WN6	15.83	13.80	**-12.83%**	10.3	9.7	**-6.24%**
WN7	17.14	17.29	**0.89%**	17.9	17.5	**-2.12%**
WN8	16.12	15.19	**-5.77%**	20.2	19.4	**-3.92%**
WN9	15.39	14.03	**-8.83%**	19.0	17.9	**-5.86%**
WN10	16.30	18.24	**11.86%**	16.0	15.5	**-3.35%**
WN11	16.09	15.27	**-5.12%**	14.2	13.3	**-6.58%**
WN12	17.33	17.51	**1.04%**	16.4	15.3	**-6.82%**
WN13	17.35	19.14	**10.30%**	15.3	14.4	**-5.86%**
WN14	20.62	23.02	**11.65%**	14.1	14.0	**-1.06%**
WN15	17.73	19.48	**9.84%**	17.1	16.7	**-2.37%**
WN16	19.01	18.07	**-4.93%**	16.5	15.8	**-3.87%**

Finanziato dall'Unione europea NextGenerationEU | Ministero dell'Università e della Ricerca | Italiadomani PIANO NAZIONALE DI RIPRESA E RESILIENZA

3. Description of TRNSYS files of the digital twin

The TRNSYS files of the digital twin are represented by 34 files with the .xlsx extension, where each test is identified by a specific ID composed of:

- a first letter, S or W, indicating whether the test refers to summer (S) or winter (W) boundary conditions;
- a second letter, N, indicating that the test is a normal (N);
- a sequential number.

Each file is characterized by 18 columns, which report the simulated operational parameters with 1-second timestep:

- Column 1: Experimental Return Air Fan (RAF) Power (EP) consumption EXP_EP_RAF (kW);
- Column 2: Simulated Return Air Fan (RAF) Power (EP) consumption SIM_EP_RAF (kW);
- Column 3: Experimental Supply Air Fan (SAF) Power (EP) consumption EXP_EP_SAF (kW);
- Column 4: Simulated Supply Air Fan (SAF) Power (EP) consumption SIM_EP_SAF (kW);
- Column 5: Experimental Humidifier (HUM) Power (EP) consumption EXP_EP_HUM (kW);
- Column 6: Simulated Humidifier (HUM) Power (EP) consumption SIM_EP_HUM (kW);
- Column 7: Experimental Refrigerating System (RS) Power (EP) consumption EXP_EP_RS (kW);
- Column 8: Simulated Refrigerating System (RS) Power (EP) consumption SIM_EP_RS (kW);
- Column 9: Experimental Refrigerating System (RS) Cooling Power (CP) EXP_CP_RS (kW);
- Column 10: Simulated Refrigerating System (RS) Cooling Power (CP) SIM_CP_RS (kW);
- Column 11: Experimental Heat Pump (HP) Power (EP) consumption EXP_EP_HP (kW);
- Column 12: Simulated Heat Pump (HP) Power (EP) consumption SIM_EP_HP (kW);
- Column 13: Experimental Heat Pump (HP) Thermal Power (TP) EXP_TP_HP (kW);
- Column 14: Simulated Heat Pump (HP) Thermal Power (TP) SIM_EP_HP (kW);
- Column 15: Experimental Cooling Coil (CC) Cooling Power (CP) EXP_CP_CC (kW);
- Column 16: Simulated Cooling Coil (CC) Cooling Power (CP) SIM_CP_CC (kW);
- Column 17: Experimental Post-Heating Coil (PostHC) Thermal Power (TP) EXP_TP_PostHC (kW);
- Column 18: Simulated Post-Heating Coil (PostHC) Thermal Power (TP) SIM_EP_ PostHC (kW).

The TRNSYS files of the digital twin named “PRIN22_UTMOST FDD_Deliverable WP3_D2” is available at the following link: https://www.dropbox.com/scl/fo/tcxmoly5pfugbqh3cw9n8/APxMZeqsI0EeN3-LaXhsEPE?rlkey=l8aa1wcueows4usnzdfvs6z80&dl=0

Finanziato dall'Unione europea NextGenerationEU
Ministero dell'Università e della Ricerca
Italiadomani PIANO NAZIONALE DI RIPRESA E RESILIENZA

DELIVERABLE WP3_D3

DEVELOPMENT OF A SIMULATION DATASET WITH AHU OPERATIONAL FAULTY AND FAULT FREE DATA

EDIT BY UNICAMPANIA

PRIN 2022 - UTMOST FDD: AN AUTOMATED, OPEN, SCALABLE AND TRANSPARENT FAULT DETECTION AND DIAGNOSIS PROCESS FOR AIR-HANDLING UNITS BASED ON A HYBRID EXPERT AND ARTIFICIAL INTELLIGENCE APPROACH

Funded by the European Union - Next Generation EU within the "Piano Nazionale di Ripresa e Resilienza (PNRR), missione 4 componente 2 investimento 1.1 - fondo per il programma nazionale di ricerca e progetti di rilevante interesse nazionale (PRIN)"

Finanziato dall'Unione europea NextGenerationEU

Ministero dell'Università e della Ricerca

Italiadomani PIANO NAZIONALE DI RIPRESA E RESILIENZA

The UTMOST FDD Project is organised into the following 7 Work Packages (WPs):
WP0) PROJECT COORDINATION
WP1) EXPERIMENTAL ANALYSIS FOR THE CHARACTERIZATION OF FAULTY AND NORMAL OPERATION OF A TYPICAL AHU
WP2) KPIs IDENTIFICATION FOR ASSESSING FAULT IMPACT IN AHU OPERATION
WP3) AHU DIGITAL TWIN AND SIMULATION–BASED FAULT IMPACT SCENARIO ANALYSIS
WP4) DEFINITION OF HYBRID FDD STRATEGIES FOR AHUs
WP5) TRANSFERABILITY ANALYSIS OF THE FDD STRATEGIES
WP6) KNOWLEDGE TRANSFER AND DISSEMINATION

The WPs are organized into Tasks (T) ranging from 2 to 4 for each WP.

The WP3 aims at achieving the following main objectives: 1) analyse and categorize the scientific studies on digital twins of Air–Handling Units (AHUs) for Automated Fault Detection and Diagnosis (AFDD) purposes, 2) publicly provide a detailed digital twin of a typical AHU validated against measured data, 3) publicly provide labelled simulation data accurately representing the performance of a typical AHU under a wide range of fault free and faulty conditions, 4) perform an impact scenario analysis associated to faults' occurrence based on simulation results.

This WP3 will help in a) better understanding the current research gaps, b) address the lack of simulation tools of AHUs for impact scenario analyses, c) support the development of, and benchmark the performance accuracy of AFDD methods, d) recognize fault patterns of AHUs and rank the faults with most adverse impacts, e) assess the gap between AHU faulty operation and design expectations.

The WP3 will include the following 4 tasks (WP3_T1, WP3_T2, WP3_T3, WP3_T4):

– WP3_T1) this task provided a scientific written report (1st WP3 deliverable WP3_D1) carrying out a literature review of Air–Handling Unit (AHU) simulation studies for Automated Fault Detection and Diagnosis (AFDD).

– WP3_T2) this task developed a simulation model able to accurately predict the performance of the typical AHU set–up for AFDD purposes at the "SENS i–Lab". The digital twin will be developed by means of the commercial software "Transient System Simulation Tool (TRNSYS) 18" (https://www.trnsys.com/), worldwide used and well–established in the scientific community. A specific model of each system component will be conceived and characterized to capture its dynamic performance; dedicated features allowing to model the desired faults will be included. The digital twin will be calibrated and validated against the data measured in the WP1. The TRNSYS files of the digital twin, together with the related documentation, will be uploaded in a public repository as 2nd WP3 deliverable WP3_D2.

– WP3_T3) this task runs the validated AHU digital twin with reference to a working week by assuming a 1–minute simulation time–step to obtain a huge simulation dataset representing the performance of the AHU under a wide range of fault free and single/multiple faulty scenarios. The simulations will extend the experimental dataset obtained in the WP1 by considering the same faults' types with additional faults' intensities, faults' durations, operational/seasonal/weather conditions (at least one city for each Italian climatic zone will be analysed). The derived simulation dataset, together with its detailed description, will be uploaded in a public repository as 3rd WP3 deliverable WP3_D3.

– WP3_T4) this task will perform an impact scenario analysis by comparing the simulation outputs related to faulty scenarios with those associated to fault free conditions obtained under the same boundary conditions (simulation period/time–step, climatic zone, location, AHU configuration and control logics) by means of the KPIs selected in the WP2. A scientific written report illustrating the faults' symptoms on AHU performance derived from the simulation dataset will be uploaded in a public repository as 4th WP3 deliverable WP3_D4.

In this deliverable WP3_D3, the simulations extend the experimental dataset developed in WP1 by considering the same fault types while expanding the range of fault intensities, fault durations, and operational/seasonal/weather conditions. In particular, while the experimental campaign investigated only the occurrence of a fault related to humidifier valve stuck at 0% (because the valve stuck at maximum opening for 9 consecutive hours would have caused significant issues to the component of the experimental setup), the simulation analysis considers humidifier valve stuck at 100%. In addition, the duration of the fault occurrence is significantly extended compared to the experimental set-up; whereas the experimental tests considered a 9-hour fault occurrence, the simulations assume a continuous fault lasting a working week, with a 1-minute

Finanziato dall'Unione europea NextGenerationEU | Ministero dell'Università e della Ricerca | Italiadomani PIANO NAZIONALE DI RIPRESA E RESILIENZA

simulation time step, evaluated under both summer and winter operating conditions. The reference weeks selected for the analysis are July 14-18 for summer scenarios and January 12-16 for winter scenarios. Moreover, different weather conditions (in addition to those of Naples) are considered; in particular, the following representative cities are selected to cover the Italian climatic zones A, B, C, D, and E:

1. Pantelleria - Climatic zone A.
   This climatic zone is characterized by mild winters, hot dry summers, intense sunshine, and low rainfall.;
2. Palermo - Climatic zone B.
   This climatic zone is characterized by mild winters, hot dry summers, rare frost, and temperatures moderated;
3. Naples - Climatic zone C.
   This climatic zone is characterized by mild winters, warm to hot summers, moderate rainfall, and stable temperatures;
4. Rome - Climatic zone D.
   This climatic zone is characterized by mild winters, warm summers, and moderate rainfall.
5. Turin - Climatic zone E.
   This climatic characterized by cold foggy winters, hot humid summers, strong seasonal temperature contrasts, and moderate rainfall.

No simulations are performed for the climatic zone F as the database of weather files available in TRNSYS does not include any cities belonging to this climatic zone.

The simulation dataset consists of 20 files with the .xlsx extension, where each test is identified by a specific ID composed of:

- a first letter, S or W, indicating whether the test refers to summer (S) or winter (W) boundary conditions;
- a second letter, N or F, indicating whether the test is a normal (N) or faulty (F) condition;
- an acronym identifying the city selected to represent each Italian climatic zone, namely: PAN for Pantelleria, PA for Palermo, NA for Naples, RM for Rome, and TO for Turin.

Each file is characterized by 8 columns, which report the simulated operational parameters with 1-minute timestep:

- Column 1: Date&Time (gg/mm/aaa - hh:mm:ss);
- Column 2: Return Air Temperature T_RA (°C);
- Column 3: Return Air Relative Humidity RH_RA (%);
- Column 4: Refrigerating System (RS) Electric Power (EP) consumption EP_RS (W);
- Column 5: Heat Pump (HP) Electric Power (EP) consumption EP_HP (W);
- Column 6: Humidifier (HUM) Electric Power (EP) consumption EP_HUM (W);
- Column 7: Return Air Fan (RAF) Electric Power (EP) consumption EP_RAF (W);
- Column 8: Supply Air Fan (SAF) Electric Power (EP) consumption EP_SAF (W).

The simulation dataset named “PRIN22_UTMOST FDD_Deliverable WP3_D3” is available at the following link:
https://www.dropbox.com/scl/fo/ajjkhg768zt8hlik0ft2b/ACSwlQPTLvIKmeqitvIGOHM?rlkey=bq8xkft3adhcg9i0uboo1lf1s&dl=0

Finanziato dall'Unione europea NextGenerationEU
Ministero dell'Università e della Ricerca
Italiadomani PIANO NAZIONALE DI RIPRESA E RESILIENZA

MISSIONE 4
ISTRUZIONE RICERCA

DELIVERABLE WP3_D4

IMPACT SCENARIO ANALYSIS BASED ON SIMULATION AHU FAULTY AD FAULT FREE DATA

EDIT BY UNICAMPANIA

PRIN 2022 - UTMOST FDD: AN AUTOMATED, OPEN, SCALABLE AND TRANSPARENT FAULT DETECTION AND DIAGNOSIS PROCESS FOR AIR-HANDLING UNITS BASED ON A HYBRID EXPERT AND ARTIFICIAL INTELLIGENCE APPROACH

Funded by the European Union - Next Generation EU within the "Piano Nazionale di Ripresa e Resilienza (PNRR), missione 4 componente 2 investimento 1.1 - fondo per il programma nazionale di ricerca e progetti di rilevante interesse nazionale (PRIN)"

Finanziato dall'Unione europea NextGenerationEU
Ministero dell'Università e della Ricerca
Italiadomani PIANO NAZIONALE DI RIPRESA E RESILIENZA

The UTMOST FDD Project is organised into the following 7 Work Packages (WPs):
WP0) PROJECT COORDINATION
WP1) EXPERIMENTAL ANALYSIS FOR THE CHARACTERIZATION OF FAULTY AND NORMAL OPERATION OF A TYPICAL AHU
WP2) KPIs IDENTIFICATION FOR ASSESSING FAULT IMPACT IN AHU OPERATION
WP3) AHU DIGITAL TWIN AND SIMULATION–BASED FAULT IMPACT SCENARIO ANALYSIS
WP4) DEFINITION OF HYBRID FDD STRATEGIES FOR AHUs
WP5) TRANSFERABILITY ANALYSIS OF THE FDD STRATEGIES
WP6) KNOWLEDGE TRANSFER AND DISSEMINATION

The WPs are organized into Tasks (T) ranging from 2 to 4 for each WP.

The WP3 aims at achieving the following main objectives: 1) analyse and categorize the scientific studies on digital twins of Air–Handling Units (AHUs) for Automated Fault Detection and Diagnosis (AFDD) purposes, 2) publicly provide a detailed digital twin of a typical AHU validated against measured data, 3) publicly provide labelled simulation data accurately representing the performance of a typical AHU under a wide range of fault free and faulty conditions, 4) perform an impact scenario analysis associated to faults' occurrence based on simulation results.

This WP3 will help in a) better understanding the current research gaps, b) address the lack of simulation tools of AHUs for impact scenario analyses, c) support the development of, and benchmark the performance accuracy of AFDD methods, d) recognize fault patterns of AHUs and rank the faults with most adverse impacts, e) assess the gap between AHU faulty operation and design expectations.

The WP3 will include the following 4 tasks (WP3_T1, WP3_T2, WP3_T3, WP3_T4):

- WP3_T1) this task provided a scientific written report (1st WP3 deliverable WP3_D1) carrying out a literature review of Air-Handling Unit (AHU) simulation studies for Automated Fault Detection and Diagnosis (AFDD).
- WP3_T2) this task developed a simulation model able to accurately predict the performance of the typical AHU set-up for AFDD purposes at the "SENS i-Lab". The digital twin will be developed by means of the commercial software "Transient System Simulation Tool (TRNSYS) 18" (https://www.trnsys.com/), worldwide used and well-established in the scientific community. A specific model of each system component will be conceived and characterized to capture its dynamic performance; dedicated features allowing to model the desired faults will be included. The digital twin will be calibrated and validated against the data measured in the WP1. The TRNSYS files of the digital twin, together with the related documentation, will be uploaded in a public repository as 2nd WP3 deliverable WP3_D2.
- WP3_T3) this task will ran the validated AHU digital twin with reference to a working week by assuming a 1-minute simulation time-step to obtain a huge simulation dataset representing the performance of the AHU under a wide range of fault free and single/multiple faulty scenarios. The simulations will extend the experimental dataset obtained in the WP1 by considering the same faults' types with additional faults' intensities, faults' durations, operational/seasonal/weather conditions (at least one city for each Italian climatic zone will be analysed). The derived simulation dataset, together with its detailed description, will be uploaded in a public repository as 3rd WP3 deliverable WP3_D3.
- WP3_T4) this task performs an impact scenario analysis by comparing the simulation outputs related to faulty scenarios with those associated to fault free conditions obtained under the same boundary conditions (simulation period/time-step, climatic zone, location, AHU configuration and control logics) by means of the KPIs selected in the WP2. A scientific written report illustrating the faults' symptoms on AHU performance derived from the simulation dataset will be uploaded in a public repository as 4th WP3 deliverable WP3_D4.

Deliverable WP3_D4 provides an analysis of impact scenarios by evaluating the differences between simulation results for faulty and fault-free conditions, all obtained under the same boundary conditions (simulation period and time step, climatic zone, location, AHU configuration, and control logics). The comparison is performed specifically with reference to the percentages of time during which indoor air temperature and indoor air relative humidity are maintained within the specified deadbands as well as in terms of electrical energy demands component by component and total.

Finanziato dall'Unione europea NextGenerationEU | Ministero dell'Università e della Ricerca | Italiadomani PIANO NAZIONALE DI RIPRESA E RESILIENZA

20 simulations have been performed under varying summer and winter conditions. Notably, 10 simulations have been conducted under normal (N) conditions to assess fault-free operation; in more detail, 5 tests (SN_PAN, SN_PA, SN_NA, SN_RM and SN_TO) have been carried out during the summer (S), while the other 5 tests (WN_PAN, WN_PA, WN_NA, WN_RM and WN_TO) have been performed during the winter (W). The remaining 10 faulty (F) tests (SF_PAN, SF_PA, SF_NA, SF_RM, SF_TO, WF_PAN, WF_PA, WF_NA, WF_RM and WF_TO) have been conducted during both summer (S) and winter (W) with 1 faulty test per season. In particular, the opening percentage of the humidifier stuck at 100% (fully opened) has been simulated.
During the fault-free tests the following parameters are manually set: (i) the indoor air temperature setpoint (Set_T_target_RA) is 20 °C in winter and 26 °C in summer, with a deadband (UDB_T_target_RA/LDB_T_target_RA) of ±1 °C; (ii) the indoor air relative humidity setpoint (Set_RH_target_RA) is 50% during both seasons, with a deadband (UDB_RH_target_RA/ LDB_RH_target_RA) of ±5%; (iii) the supply and return air fans are set to operate with a percentage velocity (Set_OL_RAF, Set_OL_SAF) at 50% of their maximum velocities; (iv) the opening percentages of the cooling coil valve, the humidifier valve and the post-heating coil valve opening percentages can vary between 0÷100% according to the AHU control logic in order to keep the desired indoor conditions. The faulty simulations have been conducted using the same settings as the normal ones, except the opening percentage of the humidifier valve.

In the following, each test is identified by a specific ID composed of:

1. a first letter, S or W, indicating whether the test refers to summer (S) or winter (W) boundary conditions;
2. a second letter, N or F, indicating whether the test is a normal (N) or faulty (F) condition;
3. an acronym identifying the city selected to represent each Italian climatic zone, namely: PAN for Pantelleria (Climatic Zone A, very warm climate), PA for Palermo (Climatic Zone B, warm climate), NA for Naples (Climatic Zone C, mild temperate climate), RM for Rome (Climatic Zone D, temperate climate), and TO for Turin (Climatic Zone E, cold temperate climate).

In the next sections, the faults' impacts in terms of indoor thermo-hygrometric conditions (Section 1), and electrical energy demand (Section 2) are described.

1. Indoor thermo-hygrometric conditions

In this section the impacts of the investigated faults on indoor air temperature and relative humidity are analysed. In greater detail, the percentages of time during which indoor air temperature (TMR) or indoor air relative humidity (RHMR) is maintained within the specified deadbands for each normal and corresponding faulty test are calculated via the following formulas based on the measured data:

$$TMR = \frac{N_{in,DBT}}{N} \cdot 100 \quad (1)$$

$$RHMR = \frac{N_{in,DBRH}}{N} \cdot 100 \quad (2)$$

where:

- $N_{in,DBT}$ represents the number of experimental data points throughout the test duration when return air temperature T_{RA} falls within its corresponding deadbands;
- $N_{in,DBRH}$ represents the number of experimental data points throughout the test duration when return air relative humidity RH_{RA} falls within its corresponding deadbands;
- N denotes the total number of recorded data points per test (considering a 1-minute sampling rate and a working week operating period from January 12 at 00:00 a.m. to January 16 at 00:00 p.m., during winter and from July 14 at 00:00 a.m. to July 18 at 00:00 p.m., during summer, this leads to have 5761 simulated data points).

Tables 1a and 1b report the values of parameters calculated via Eqs. (1-2), during summer and winter, respectively.

Table 1a. Daily indoor air temperature/relative humidity met ratios during summer.

Finanziato dall'Unione europea NextGenerationEU | Ministero dell'Università e della Ricerca | Italiadomani PIANO NAZIONALE DI RIPRESA E RESILIENZA

Test ID	TMR (%)	RHMR (%)
SN_PAN	98.1%	97.3%
SF_PAN	99.6%	0.0%
SN_PA	99.7%	84.7%
SF_PA	99.6%	0.0%
SN_NA	99.7%	91.3%
SF_NA	99.6%	0.0%
SN_RM	99.7%	84.4%
SF_RM	99.6%	0.0%
SN_TO	99.8%	100.0%
SF_TO	99.6%	0.0%

Table 1b. Daily indoor air temperature/relative humidity met ratios during winter.

Test ID	TMR (%)	RHMR (%)
WN_PAN	99.8%	99.8%
WF_PAN	99.9%	0.0%
WN_PA	99.8%	99.7%
WF_PA	99.9%	0.0%
WN_NA	99.9%	99.1%
WF_NA	99.9%	0.0%
WN_RM	99.8%	95.6%
WF_RM	99.8%	0.0%
WN_TO	99.4%	99.6%
WF_TO	99.4%	0.0%

2. Effects of faults on daily electrical energy consumption

In this section the effects of the selected fault in terms of daily electric energy consumption are analysed. Tables 2a and b report the percentage difference %EE calculated as follows:

$$\%EE = \frac{\left(EE_{Faulty} - EE_{Baseline}\right)}{EE_{Baseline}} \cdot 100 \quad (3)$$

where EE_{Faulty} and $EE_{Baseline}$ are, respectively, the daily electric energy consumption during faulty and corresponding fault-free test. The cells in Tables 2a and b are filled in yellow if %EE is included in the range ±100%, in red if %EE is greater than 1000% or lower than –1000%, in orange in other cases (the symbol N.A. denotes that the AHU component has not been activated during both fault-free/faulty simulations and the calculation of %EE is not applicable, while the symbol '∞' indicates that the AHU component has not been activated only during the fault-free simulations).

Table 2a. Values of %Eel (calculated via Eq. 3) as function of both fault-free/faulty simulations and AHU component, during summer.

	SAF	RAF	RS	HP	HUM	TOTAL
EE of SN_PAN (kW/h)	33.5	7.0	18.9	52.7	3.4	115.6
EE of SF_PAN (kW/h)	33.5	7.0	202.5	138.8	316.9	698.6
%EE $_{SF\_PAN\ vs\ SN\_PAN}$ (%)	**N.A.**	**N.A.**	**968.4**	**163.0**	**9194.4**	**504.2**
EE of SN_PA (kW/h)	33.5	7.0	39.1	49.8	0.0	129.4
EE of SF_PA (kW/h)	33.5	7.0	201.1	124.9	316.9	683.4
%EE $_{SF\_PA\ vs\ SN\_PA}$ (%)	**N.A.**	**N.A.**	**414.2**	**151.0**	**886207.7**	**428.0**
EE of SN_NA (kW/h)	33.5	7.0	27.4	49.4	0.1	117.4

Finanziato dall'Unione europea NextGenerationEU | Ministero dell'Università e della Ricerca | Italiadomani PIANO NAZIONALE DI RIPRESA E RESILIENZA

EE of SF_NA (kW/h)	33.5	7.0	200.7	131.5	316.9	689.6
%EE $_{SF\_NA\ vs\ SN\_NA}$ (%)	**N.A.**	**N.A.**	**633.6**	**166.3**	**257855.2**	**487.4**
EE of SN_RM (kW/h)	33.5	7.0	40.5	69.3	0.0	150.3
EE of SF_RM (kW/h)	33.5	7.0	205.8	144.7	316.9	707.9
%EE $_{SF\_RM\ vs\ SN\_RM}$ (%)	**N.A.**	**N.A.**	**408.4**	**108.7**	**∞**	**370.9**
EE of SN_TO (kW/h)	33.5	7.0	11.6	67.5	12.2	131.9
EE of SF_TO (kW/h)	33.5	7.0	188.4	157.7	316.9	703.5
%EE $_{SF\_TO\ vs\ SN\_TO}$ (%)	**N.A.**	**N.A.**	**1518.5**	**133.5**	**2490.6**	**433.2**

Legend

–100% ≤ %EE ≤ +100%

+100% < %EE ≤ +1000% OR –1000% ≤ %EE < –100%

% EE > +1000% OR % EE < –1000%

Table 2b. Values of %Eel (calculated via Eq. 3) as function of both faut-free/faulty simulations and AHU component, during winter.

	SAF	**RAF**	**RS**	**HP**	**HUM**	**TOTAL**
EE of WN_TP (kW/h)	33.5	7.0	8.3	107.8	8.0	164.7
EE of WF_TP (kW/h)	33.5	7.0	67.7	164.4	316.9	589.5
%EE $_{WF\_PAN\ vs\ WN\_PAN}$ (%)	**N.A.**	**N.A.**	**714.1**	**52.5**	**3872.2**	**258.0**
EE of WN_PA (kW/h)	33.5	7.0	8.7	99.3	2.0	150.5
EE of WF_PA (kW/h)	33.5	7.0	76.7	157.3	316.9	591.4
%EE $_{WF\_PA\ vs\ WN\_PA}$ (%)	**N.A.**	**N.A.**	**781.3**	**58.5**	**15698.0**	**293.0**
EE of WN_NA (kW/h)	33.5	7.0	8.7	120.9	5.2	175.4
EE of WF_NA (kW/h)	33.5	7.0	69.8	178.6	316.9	605.8
%EE $_{WF\_NA\ vs\ WN\_NA}$ (%)	**N.A.**	**N.A.**	**699.2**	**47.7**	**6029.8**	**245.5**
EE of WN_RM (kW/h)	33.5	7.0	9.8	123.4	6.5	180.2
EE of WF_RM (kW/h)	33.5	7.0	64.4	176.8	316.9	598.6
%EE $_{WF\_RM\ vs\ WN\_RM}$ (%)	**N.A.**	**N.A.**	**554.2**	**43.3**	**4782.2**	**232.1**
EE of WN_TO (kW/h)	33.5	7.0	7.2	181.9	22.2	251.8
EE of WF_TO (kW/h)	33.5	7.0	48.3	238.1	316.9	643.9
%EE $_{WF\_TO\ vs\ WN\_TO}$ (%)	**N.A.**	**N.A.**	**573.5**	**30.9**	**1330.5**	**155.7**

Legend

–10% ≤ %EE ≤ +10%

+100% < %EE ≤ +1000% OR –1000% ≤ %EE < –100%

% EE > +1000% OR % EE < –1000%

Finanziato dall'Unione europea NextGenerationEU | Ministero dell'Università e della Ricerca | Italiadomani PIANO NAZIONALE DI RIPRESA E RESILIENZA

MISSIONE 4
ISTRUZIONE RICERCA

WP4 - *Definition of hybrid FDD strategies for AHUs*

Finanziato dall'Unione europea NextGenerationEU
Ministero dell'Università e della Ricerca
Italiadomani
PIANO NAZIONALE DI RIPRESA E RESILIENZA

MISSIONE 4
ISTRUZIONE RICERCA

DELIVERABLE WP4_D1

LITERATURE REVIEW ON THE MAIN APPROACHES EMPLOYED FOR CONDUCTING FDD WITH SPECIFIC REFERENCE TO AHUS

EDIT BY POLITO

PRIN 2022 - UTMOST FDD: AN AUTOMATED, OPEN, SCALABLE AND TRANSPARENT FAULT DETECTION AND DIAGNOSIS PROCESS FOR AIR-HANDLING UNITS BASED ON A HYBRID EXPERT AND ARTIFICIAL INTELLIGENCE APPROACH

Funded by the European Union - Next Generation EU within the "Piano Nazionale di Ripresa e Resilienza (PNRR), missione 4 componente 2 investimento 1.1 - fondo per il programma nazionale di ricerca e progetti di rilevante interesse nazionale (PRIN)"

Finanziato dall'Unione europea NextGenerationEU
Ministero dell'Università e della Ricerca
Italiadomani PIANO NAZIONALE DI RIPRESA E RESILIENZA

The UTMOST FDD Project is organised into the following 7 Work Packages (WPs):
WP0) PROJECT COORDINATION
WP1) EXPERIMENTAL ANALYSIS FOR THE CHARACTERIZATION OF FAULTY AND NORMAL OPERATION OF A TYPICAL AHU
WP2) KPIs IDENTIFICATION FOR ASSESSING FAULT IMPACT IN AHU OPERATION
WP3) AHU DIGITAL TWIN AND SIMULATION-BASED FAULT IMPACT SCENARIO ANALYSIS
WP4) DEFINITION OF HYBRID FDD STRATEGIES FOR AHUs
WP5) TRANSFERABILITY ANALYSIS OF THE FDD STRATEGIES
WP6) KNOWLEDGE TRANSFER AND DISSEMINATION

The WPs are organized into Tasks (T) ranging from 2 to 4 for each WP.

The aim of the WP4 is the definition of FDD strategies that can be exploited for detecting and diagnosing anomalies in AHUs during their operation. The definition of FDD logics will be based on a hybrid approach, considering both data-driven and knowledge-based strategies.

The WP4 will include the following 4 tasks (WP4_T1, WP4_T2, WP4_T3, WP4_T4):

- WP4_T1) the aim of this task is providing a scientific written report (1st WP4 deliverable WP4_D1) including a detailed categorization of the scientific studies on the main approaches employed for conducting FDD of AHUs. It will help in (a) better understanding the current research on knowledge-based and data-driven FDD strategies, and (b) define current gaps and opportunities in the definition of robust FDD strategies.
- WP4_T2) in this task, a special effort will be devoted to the study of possible configurations of strategies that leverage supervised and unsupervised AI techniques for detecting and diagnosing the main faults that can occur during AHUs operation. The results obtained in both WP1 and WP3 will be used as reference datasets. The algorithms that will be tested belong to the family of machine learning considering a multi-variate approach based on timeseries analytics. The FDD logics will be tested off-line, and their robustness assessed through different quality metrics (e.g., false negative and positive rates, true negative and positive rates, correct and misdiagnosis rates). A scientific written report (2nd WP4 deliverable WP4_D2), including the algorithms employed for defining the data-driven FDD strategies and the methodological processes followed for their training and testing on the reference dataset, will be delivered.
- WP4_T3) this task aims to identify knowledge-based FDD logics formulated as IF-THEN rules. The set of FDD rules will be defined starting from domain expertise and standards/handbooks/guidelines that represent a reference in this research field (e.g., ASHRAE guideline 36 [26], APAR rules [6]). Based on the results obtained from WP1, WP2 and WP3, it will be possible to exploit the main relationships that exist between faults and their effects on a single or group of operational variables for defining a typological fault-symptom library.
- WP4_T4) in this task, data-driven and expert-based logics will be combined defining hybrid FDD strategies taking advantages from both methods. The energy, environmental and economic performance of the AHU when the hybrid FDD methods are applied in the framework of a continuous commissioning process will be compared with the cases where a reactive or a preventive maintenance program is adopted. A scientific written report (3rd WP4 deliverable WP4_D3), including the data-driven algorithms and expert rules employed for defining the hybrid FDD strategies, the methodological processes followed for the training and testing of the developed strategies and the opportunities related to their deployment considering re-training logics and data-scarcity problems in the initialization phase of FDD tools, will be delivered.

1. Introduction

Heating, Ventilation, and Air-Conditioning (HVAC) systems typically contribute to 50-60% of a building's energy consumption and represent approximately 10-20% of global energy usage, highlighting their critical role in improving energy efficiency within the building sector [1]. In this context, Fault Detection and Diagnosis (FDD) methods are essential for identifying faults or anomalous operational patterns in HVAC system components and diagnosing their root causes [2]. A variety of FDD approaches have been proposed in the literature, which, as discussed in [3], can be categorized as illustrated in the following Fig. 1.

Finanziato dall'Unione europea NextGenerationEU | Ministero dell'Università e della Ricerca | Italiadomani PIANO NAZIONALE DI RIPRESA E RESILIENZA

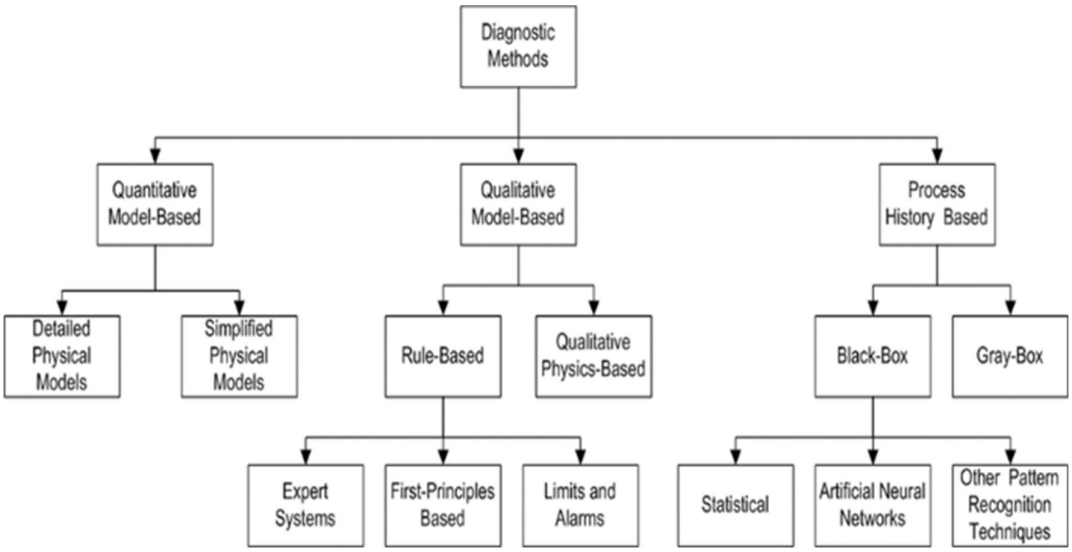

Figure 1. Classification of FDD methods [3].

2. Quantitative Model-Based methods (knowledge-driven)

Quantitative FDD approaches use physical principles, like mass and energy balance, to identify faults in HVAC systems. These methods involve creating a model that describes how the system should operate based on its physical behavior. Faults are detected by comparing measured values to those predicted by the model. If the difference, or residual, exceeds a set threshold, it signals a potential fault. Since these approaches don't rely on historical data for training, they are effective at identifying new or unseen faults.

The study by [4] presents a quantitative model-based FDD methodology for zone-level analysis in buildings. A foundational model was developed using MATLAB, enabling the identification of five zone-level inefficiencies. The severity of these inefficiencies was evaluated, revealing excessive energy consumption by the Air Handling Unit (AHU) fans. The recurrence of these faults across the building results in unnecessary energy expenditure, underscoring the critical role of FDD systems. Key benefits of this approach include the detection of pre-existing faults stemming from the initial design phase and the flexibility to apply the methodology to both new and existing buildings, provided sufficient sensing and metering infrastructure is in place. By addressing inefficiencies, this methodology contributes to improved building energy performance.

The authors in [5] emphasize the importance of correctly implementing sequences of operation for HVAC systems into BAS to ensure optimal building performance. Common errors arise when mechanical design sequences are misinterpreted, incorrectly translated into BAS programs, or when ad-hoc modifications are made in response to occupant complaints. The paper introduces an innovative inverse model-based FDD method aimed at identifying programming logic faults in Variable Air Volume (VAV) systems. This method leverages widely accessible BAS trend data to train inverse models that represent the heat and air mass balance across key components of a VAV-AHU system, including the mixing box, heating and cooling coils, VAV terminal units, and thermal zones. By referencing the ASHRAE Guideline 36 sequences of operation and the trained models, the method predicts the expected operational behavior of the system. Deviations from this expected behavior are interpreted as symptoms of programming logic faults. The approach is validated using BAS trend data from a 41-zone VAV-AHU system in Ottawa, Canada. The method successfully identified two faults related to supply air temperature and pressure reset programs, which had been contributing to excessive fan electricity consumption and increased heating energy use.

3. Qualitative Model-Based methods (knowledge-driven)

The qualitative approach to FDD, also known as the rule-based approach, relies on mass and energy balance equations to assess whether an HVAC system is functioning correctly. By translating in-depth knowledge of HVAC operation into IF-THEN rules, researchers in [6] developed a set of Performance Assessment Rules (APAR) specifically for FDD in Air Handling Units. They established 28 rules based on steady-state conditions to detect faults in AHUs equipped with hydronic heating and cooling coils. These rules use only sensor data and control signals and are tailored to different operational modes, including heating, free cooling, and mechanical cooling.

Finanziato dall'Unione europea NextGenerationEU | Ministero dell'Università e della Ricerca | Italiadomani PIANO NAZIONALE DI RIPRESA E RESILIENZA

In [7], the authors developed and validated a sequential rule-based FDD algorithm. This algorithm utilizes a set of expert rules to detect and diagnose faults in sensors. To test its effectiveness, experiments were conducted both on an AHU installed in a green building and on a small-scale AHU simulator. To simulate sensor faults, a variable resistance device was connected either in series or parallel to the temperature sensors, introducing artificial errors. The experiments demonstrated that the rule-based FDD algorithm was capable of successfully isolating faulty temperature sensors within the AHU.

While APAR provides a framework for detecting faults, it does not address all possible issues in AHU components, such as fans, filters, or simultaneous multiple faults, nor does it offer comprehensive fault isolation. To enhance fault isolation capabilities, [8] proposed a combined approach using CUSUM (Cumulative Sum) charts and expert rules for online FDD in VAV terminals. The CUSUM algorithm detects faults by accumulating the error between the measured value and the control variable set point. Fault diagnosis is then achieved through a rule-based fault classifier incorporating expert rules.

4. Process History-Based methods (data-driven)

Process History-Based methods, also known as data-driven methods, use machine learning (ML) or multivariate statistical techniques to develop models based on monitored data for fault detection and diagnosis in HVAC systems. This process typically follows several sequential steps. After operational data is collected from the Building Automation System (BAS), it is stored, cleansed, and pre-processed to enhance model training performance. Pre-processing tasks may include feature selection, data reduction, and scaling techniques to refine the representation of operational patterns. For real-time implementation, streaming data from the BAS is often compared with baseline data or models representing the system's normal operation. This comparison enables residual analysis to identify deviations from expected behavior. The final stages of the FDD process focus on fault detection and diagnosis, which may be conducted either independently or as a combined analysis. Fault diagnosis is typically framed as a classification problem. According to the literature [9,10,11,12], common data-driven methods for fault detection and diagnosis in HVAC systems include clustering, Principal Component Analysis (PCA), Decision Trees (DT), Support Vector Machines (SVM), Neural Networks (NN), Bayesian Networks (BN), and Ensemble Learning approaches.

To enhance energy efficiency and improve thermal comfort, the authors in [13] introduced a robust diagnostic tool aimed at identifying and mitigating various types of faults. The proposed method combines basic and auxiliary neural networks to create an advanced fault detection system, particularly targeting abnormalities in AHUs, which are commonly found in commercial buildings. Clustering analysis, an unsupervised data mining technique, is employed to categorize different faulty conditions adaptively. Specifically, subtractive clustering analysis is used to separate faults into distinct zones within the data space, allowing for the clear identification of different fault types. In addition to detect known faults stored in a fault library, the method is capable of recognizing previously unknown faults and dynamically adding them to the fault library. The system effectively identifies common issues such as fixed sensor biases, drifting biases, complete sensor failures, and chilled water valve malfunctions, validating its utility in real building environments.

The study by [14] proposes a data-driven FDD approach for AHUs that requires only normal operation data. The solution incorporates three fault detection levels based on data availability: daily energy benchmarking, control performance evaluation, and data-driven modeling of mechanical systems. The method was tested using experimental data from ASHRAE project 1312-RP and real-world data from a French office building. The results show that the system can isolate both control and mechanical faults at the component level using only normal operation data.

5. Hybrid approaches

How can it be deduced from what has been said so far, quantitative approaches are often computationally complex. They require specific definitions or adjustments of first principle equations for each system and assume fault-free sensors when applied to equipment malfunction FDD. In contrast, the performance of rule-based methods depends on various factors, including the components of the HVAC system, the sensors, control logic, available metadata, and fault tolerance thresholds. Additionally, the precision of expert rules in FDD is evidently lower than data-driven methods since the former is more generalized for different systems, whereas the latter is tailored on historical data. Furthermore, data-driven methods require a significant amount of both normal and faulty data, particularly for fault diagnosis, and collecting such data can be economically challenging in many cases. As a result, hybrid approaches are becoming increasingly valuable, as they combine

Finanziato dall'Unione europea NextGenerationEU | Ministero dell'Università e della Ricerca | Italiadomani PIANO NAZIONALE DI RIPRESA E RESILIENZA

the strengths of each method. The primary goal of hybrid approaches is to enhance the overall efficiency and reliability of fault diagnosis techniques.

Authors in [15] used a combination of first principle thermodynamic modeling and expert rules, resulting in faster fault detection with minimal non-intrusive measurements. This approach effectively detected certain faults, such as stuck or leaking dampers, by calculating the ideal damper positions and subsequently comparing the ideal Mixed Air Temperature (MAT) with the measured one.

The study by [16] introduces a hybrid modeling approach that combines first-principles knowledge with Principal Component Analysis (PCA) to detect faults in HVAC systems. The method uses residuals—discrepancies between expected and observed behaviors—and temperature measurements to develop multiple PCA models that describe the normal operation of AHUs in different states. To monitor the system and detect faults, Hotelling's T2 and Squared Prediction Error (SPE) statistics are calculated from the hybrid PCA model for new observations. The effectiveness of this approach is evaluated against two benchmark methods: (1) residual analysis based on first-principles models, and (2) a data-driven PCA method using raw temperature data. Simulation tests with common fault scenarios demonstrate that the hybrid method outperforms both benchmarks.

In [17], the authors proposed a Diagnostic Bayesian Network (DBN) focusing on FDD of AHU airside subsystems and coils/sensors. The structure of the DBN is based on first-principles and expert rules drawn from the literature, while certain parameters of the Building Management System (BMS) evidence nodes—such as fan power consumption and pressure drop across filters—are predicted using data-driven black-box approaches that rely on fault-free data. The method was evaluated using experimental data from the ASHRAE Project RP-1312. The results show that the DBN-based approach is effective in diagnosing faults, even when diagnostic information is uncertain or incomplete.

6. References

[1] Mirnaghi, M. S., and Haghighat, F.: Fault detection and diagnosis of large-scale HVAC systems in buildings using data-driven methods: A comprehensive review. Energy and Buildings. 229, 110492 (2020).
[2] Frank, S., et al.: A performance evaluation framework for building fault detection and diagnosis algorithms. Energy and Buildings. 192, pp.84-92 (2019).
[3] Katipamula, S. and Brambley, M.R.: Methods for fault detection, diagnostics, and prognostics for building systems - a review, part i. HVAC&R Research 11 (2005).
[4] Berquist, Justin David: A Quantitative Model-Based Fault Detection & Diagnostics (FDD) System for Zone-Level Inefficiencies. Master Thesis. Carleton University (2017).
[5] Gunay, B., et al.: Inverse model-based detection of programming logic faults in multiple zone vav ahu systems. Building and Environment 211, 108732 (2022).
[6] House, J.M., et al.: An Expert Rule Set for Fault Detection in Air-Handling Units. ASHRAE Transactions. Vol. 107, Pt. 1: pp. 858-871 (2001).
[7] Yang, H., et al.: Sequential rule based algorithms for temperature sensor fault detection in air handling units. Energy Conversion and Management 49(8), 2291–2306 (2008).
[8] Wang, H. et al.: An online fault diagnosis tool of VAV terminals for building management and control systems. Autom. Constr., 22, pp.203-211 (2012).
[9] Fan, C. et al.: Leveraging graph convolutional networks for semi-supervised fault diagnosis of HVAC systems in data-scarce contexts. Build. Simul., pp. 1-19 (2023).
[10] Chiosa, R. et al.: Towards a self-tuned data analytics-based process for an automatic context-aware detection and diagnosis of anomalies in building energy consumption timeseries. Energy Build, 270, 112302 (2022).
[11] Chen, Z et al.: A review of data-driven fault detection and diagnostics for building HVAC systems. Applied Energy, 339, 121030 (2023).
[12] Zhao D., et al.: Artificial intelligence-based fault detection and diagnosis methods for building energy systems: Advantages, challenges and the future. Renewable Sustainable Energy Rev., 109, pp.85-101 (2019).
[13] Du, Z., et al.: Fault detection and diagnosis for buildings and hvac systems using combined neural networks and subtractive clustering analysis. Building and Environment 73, 1–11 (2014).
[14] Gao, Tianyun, et al.: Data mining and data-driven modelling for air handling unit fault detection, E3S Web Conf. 111 (2019) 05009.
[15] Deshmukh, S. et al.: Fault detection in commercial building VAV AHU: A case study of an academic building. Energy Build., 201, pp.163-173 (2019).
[16] Hassanpour, H. et al.: A hybrid modeling approach integrating first-principles knowledge with statistical methods for fault detection in HVAC systems. Comput Chem Eng., 142, 107022 (2020).
[17] Zhao, Y., et al.: Diagnostic Bayesian networks for diagnosing air handling units faults–part I: Faults in dampers, fans, filters and sensors. Appl. Therm. Eng., 111, pp.1272-1286 (2017)

MISSIONE 4
ISTRUZIONE RICERCA

DELIVERABLE WP4_D2

DEFINITION OF DATA-DRIVEN FDD STRATEGIES FOR AHUS

EDIT BY POLITO

PRIN 2022 - UTMOST FDD: AN AUTOMATED, OPEN, SCALABLE AND TRANSPARENT FAULT DETECTION AND DIAGNOSIS PROCESS FOR AIR-HANDLING UNITS BASED ON A HYBRID EXPERT AND ARTIFICIAL INTELLIGENCE APPROACH

Funded by the European Union - Next Generation EU within the "Piano Nazionale di Ripresa e Resilienza (PNRR), missione 4 componente 2 investimento 1.1 - fondo per il programma nazionale di ricerca e progetti di rilevante interesse nazionale (PRIN)"

Finanziato dall'Unione europea NextGenerationEU
Ministero dell'Università e della Ricerca
Italiadomani PIANO NAZIONALE DI RIPRESA E RESILIENZA

The UTMOST FDD Project is organised into the following 7 Work Packages (WPs):
WP0) PROJECT COORDINATION
WP1) EXPERIMENTAL ANALYSIS FOR THE CHARACTERIZATION OF FAULTY AND NORMAL OPERATION OF A TYPICAL AHU
WP2) KPIs IDENTIFICATION FOR ASSESSING FAULT IMPACT IN AHU OPERATION
WP3) AHU DIGITAL TWIN AND SIMULATION-BASED FAULT IMPACT SCENARIO ANALYSIS
WP4) DEFINITION OF HYBRID FDD STRATEGIES FOR AHUs
WP5) TRANSFERABILITY ANALYSIS OF THE FDD STRATEGIES
WP6) KNOWLEDGE TRANSFER AND DISSEMINATION

The WPs are organized into Tasks (T) ranging from 2 to 4 for each WP.

The aim of the WP4 is the definition of FDD strategies that can be exploited for detecting and diagnosing anomalies in AHUs during their operation. The definition of FDD logics will be based on a hybrid approach, considering both data-driven and knowledge-based strategies.

The WP4 will include the following 4 tasks (WP4_T1, WP4_T2, WP4_T3, WP4_T4):

- WP4_T1) the aim of this task is providing a scientific written report (1st WP4 deliverable WP4_D1) including a detailed categorization of the scientific studies on the main approaches employed for conducting FDD of AHUs. It will help in (a) better understanding the current research on knowledge-based and data-driven FDD strategies, and (b) define current gaps and opportunities in the definition of robust FDD strategies.
- WP4_T2) in this task, a special effort will be devoted to the study of possible configurations of strategies that leverage supervised and unsupervised AI techniques for detecting and diagnosing the main faults that can occur during AHUs operation. The results obtained in both WP1 and WP3 will be used as reference datasets. The algorithms that will be tested belong to the family of machine learning considering a multi-variate approach based on timeseries analytics. The FDD logics will be tested off-line, and their robustness assessed through different quality metrics (e.g., false negative and positive rates, true negative and positive rates, correct and misdiagnosis rates). A scientific written report (2nd WP4 deliverable WP4_D2), including the algorithms employed for defining the data-driven FDD strategies and the methodological processes followed for their training and testing on the reference dataset, will be delivered.
- WP4_T3) this task aims to identify knowledge-based FDD logics formulated as IF-THEN rules. The set of FDD rules will be defined starting from domain expertise and standards/handbooks/guidelines that represent a reference in this research field (e.g., ASHRAE guideline 36 [26], APAR rules [6]). Based on the results obtained from WP1, WP2 and WP3, it will be possible to exploit the main relationships that exist between faults and their effects on a single or group of operational variables for defining a typological fault-symptom library.
- WP4_T4) in this task, data-driven and expert-based logics will be combined defining hybrid FDD strategies taking advantages from both methods. The energy, environmental and economic performance of the AHU when the hybrid FDD methods are applied in the framework of a continuous commissioning process will be compared with the cases where a reactive or a preventive maintenance program is adopted. A scientific written report (3rd WP4 deliverable WP4_D3), including the data-driven algorithms and expert rules employed for defining the hybrid FDD strategies, the methodological processes followed for the training and testing of the developed strategies and the opportunities related to their deployment considering re-training logics and data-scarcity problems in the initialization phase of FDD tools, will be delivered.

1. Introduction

In the field of Fault Detection and Diagnosis (FDD), AI has shifted toward data-driven approaches, leveraging machine learning and multivariate statistical techniques to build models based on monitored data. Bayesian Networks (BNs) are particularly valuable for HVAC FDD due to their ability to model complex dependencies and uncertainties [1]. BNs offer a probabilistic graphical representation of relationships between HVAC variables, helping to understand fault propagation. They integrate prior knowledge and monitored data, enabling continuous learning and adaptation. This allows BNs to update fault scenario probabilities over time, improving the accuracy and timeliness of fault detection and diagnosis. Additionally, BNs enhance diagnostic reasoning by clearly depicting causal relationships, aiding in fault detection and root cause identification.

Both discrete and continuous BNs are effective for FDD in building energy systems. Discrete BNs handle variables that are discretized into a finite set of categories, making them computationally efficient and easier

Finanziato dall'Unione europea NextGenerationEU | Ministero dell'Università e della Ricerca | Italiadomani PIANO NAZIONALE DI RIPRESA E RESILIENZA

to implement. A study [1] introduced a method using discrete BNs to diagnose and isolate cross-level faults in HVAC systems, significantly reducing the False Alarm Rate (FAR) and improving diagnostic accuracy compared to component-level FDD tools. The model correctly diagnosed 11 out of 14 fault cases, with the remaining three cases identifying the top three most likely faults. For chiller fault detection, [2] proposed a method incorporating discretization into BNs, using data from ASHRAE RP-1043. This approach demonstrated higher diagnostic accuracy than traditional methods.

On the other hand, continuous BNs, which model variables with continuous probability distributions, offer a more precise representation of data trends crucial for HVAC systems. However, they can be computationally intensive. A study [3] introduced an FDD methodology for chillers that integrates probabilistic boundaries within a Bayesian network classifier to reduce FAR and missed detection rates (MDR). This approach, applied to a 90-ton water-cooled centrifugal chiller, decreased FAR from 22.7% to 4.4% and lowered the MDR for refrigerant overcharge and leakage. Moreover, [4] proposed a Bayesian network model with a distance rejection technique and multi-source non-sensor data, enhancing diagnostic accuracy and enabling the identification of new fault types in chiller systems. The method showed high accuracy, with results ranging from 56.8% to 100% for different new fault types.

2. Definition of data-driven FDD strategies for AHUs

It is evident that BNs using both discrete and continuous input data exhibit high performances in terms of FDD accuracy. This report involves investigating and comparing discrete and continuous data-driven BNs, respectively Tree Augmented Naïve Bayes classifier (TAN) and Conditional Gaussian Network (CGN). The second contribution is the reduction for both BN models of the FAR using a cost-sensitive process. As a results four different BN models (i.e., TAN, CS-TAN, CGN and CS-CGN) are compared in terms of different FDD metrics (accuracy, MDR, FAR, FNR as reported in [5]) and benchmarked against a baseline ML model based on random forest. The models were trained to accomplish the detection and diagnosis task simultaneously as multi-class classifiers, separately for the winter and summer operation mode of the AHU. Specifically, the models were trained to classify winter and summer data into 12 different classes (11 fault classes and 1 normal class). The faults were artificially implemented from 9 a.m. until 6 p.m. (one day for each fault) at one second time steps while one-minute aggregation interval is used in this paper for conducting the FDD analysis. In addition, data pertaining fault-free operation of AHU were collected for 17 days that represent the normal condition. The experimental data include the following faults:

- DRA 0% - Return air damper kept always closed (stuck at 0%);
- DOA 0% - Outdoor air damper kept always closed (stuck at 0%);
- DOA 100% Outdoor air damper kept always open (stuck at 100%);
- DEA 0%/100% - Exhaust air damper kept always closed in summer (stuck at 0%) and always open in winter (stuck at 100%);
- HUM 0% - Complete failure of the Humidifier;
- SAF 0% - Complete failure of the Supply Air Fan;
- RAF 0% - Complete failure of the Return Air Fan;
- CCV 100% - Cooling Coil Valve kept always open (stuck 100%);
- CCV 0% - Cooling Coil Valve kept always closed (stuck 0%);
- HCV 100% - Post-Heating Coil Valve kept always open (stuck 100%);
- HCV 0% - Post-Heating Coil Valve kept always closed (stuck 0%).

To train the identified models and perform the FDD task, a pre-processing step is performed on the raw experimental data. Specifically, transient periods were removed from the dataset by eliminating the start-up phase of the plant (the first 15 minutes of each analyzed day). The EWMA method was then used to smooth the values of the collected variables. As a result, around 14.000 data points out of 15.120 initial datapoints are considered for both seasons. Among them 11.424 instances (80%) comprise the training set and 2859 instances (20%) belong to the test set. As a second step a feature selection was performed by using the Mutual Information (MI) score. This metric helps identify which features are most relevant to the target one. This process enhances model performance by reducing dimensionality, eliminating irrelevant features, and improving interpretability. High MI score indicates a strong dependency between the feature and the target, suggesting the feature relevance in the prediction problem. In this report, MI score was used to define different scenarios in which 5, 10 and 15 input variables were considered to address the classification task. According to the nature of the model, MI score was evaluated on discrete or continuous variables, as reported in the following tables.

Finanziato dall'Unione europea NextGenerationEU | Ministero dell'Università e della Ricerca | Italiadomani PIANO NAZIONALE DI RIPRESA E RESILIENZA

Table 1. Groups of relevant variables considered for developing the TAN and CS-TAN.

1st tier of relevant variables	2nd tier of relevant variables	3rd tier of relevant variables
- RAF power - Return air temperature - Air RH after CC - Air temperature after postHC - Mixing air RH	- Mixing air temperature - Air temperature after CC - Air RH after postHC - Supply air temperature - SAF power	- CC thermal power - RS and circulation pump electric power - Supply air RH - Return air RH - HP and circulation pump electric power

Table 2. Groups of relevant variables considered for developing the CGN, CS-CGN and RF

1st tier of relevant variables	2nd tier of relevant variables	3rd tier of relevant variables
- RAF power - Return air temperature - Air RH after CC - Air temperature after CC - SAF power	- Mixing air RH - Supply air temperature - Mixing air temperature - CC thermal power - Air temperature after postHC	- Air RH after postHC - RS and circulation pump electric power - Return air RH - HP and circulation pump electric power - Supply air RH

An explanation of each data-driven method used is provided below.

1. Tree Augmented Naïve Bayes classifier (TAN)

The Tree Augmented Naïve Bayes (TAN) classifier extends the Naïve Bayes classifier to improve performance by modeling dependencies between features with a tree structure [6]. Unlike Naïve Bayes, TAN constructs a tree where nodes represent features and edges represent dependencies. The tree is rooted at the class node, aiming to maximize data likelihood using a maximum weight spanning tree algorithm based on mutual information between features. TAN estimates the probabilities of each class, each feature given the class, and each feature given the class and its parent feature in the tree. In this work, probabilities were estimated from training data using Maximum Likelihood Estimation (MLE) after discretizing variables with an entropy-based method;

2. Cost-Sensitive Tree Augmented Naïve Bayes Classifier (CS-TAN)

Cost-sensitive Tree Augmented Naïve Bayes (CS-TAN) extends the TAN classifier by incorporating misclassification costs into the learning process [6]. While standard TAN aims to maximize overall accuracy, CS-TAN minimizes total misclassification cost by accounting for different error costs. The process starts by defining misclassification costs, then adjusts the learning process to minimize expected cost instead of maximizing accuracy. This involves altering the objective function to weight error probabilities by their relative costs and adjusting decision thresholds to minimize total expected misclassification cost;

3. Conditional Gaussian Network (CGN)

Conditional Gaussian Networks (CGNs) are Bayesian Networks designed for continuous variables, using conditional Gaussian distributions to model relationships directly [3]. This allows accurate representation of continuous data. In a CGN, variables are connected through linear Gaussian distributions and conditional dependencies, with each node representing a continuous variable and edges indicating probabilistic dependencies. The conditional distribution of each variable, given its parents, is Gaussian;

4. Cost-Sensitive Conditional Gaussian Network (CS-CGN)

A CGN is not inherently sensitive to misclassification of any specific class, such as the Normal Class (NC) in an FDD classification task. To ensure that the misclassification rate for a specific class like NC stays within acceptable limits, a new conditional rule is added to the maximum a posteriori formula of the CGN. Specifically, this rule states that if the probability of NC exceeds a certain limit Lp, then the classification decision is NC. In this study, the approach introduced in [3] was used. It associates Lp with the NC class by defining a Control Limit (CL). The CL is determined by the significance level (α), the number of feature variables, and the number of instances in the NC. In the context of CS-CGN, the CL serves as the boundary between faulty classes and the NC. The parameter α is a significance level between 0 and 1 that reflects the

Finanziato dall'Unione europea NextGenerationEU | Ministero dell'Università e della Ricerca | Italiadomani PIANO NAZIONALE DI RIPRESA E RESILIENZA

user tolerance for misclassification of the NC. As a result, in CS-CGN if the probability of NC exceeds *Lp*, NC is selected as the classification decision;

5. Random forest

Random Forest (RF) is an ensemble ML method that is widely used for classification and regression in FDD tasks [5]. It operates by constructing a set of decision trees during training and providing as output the class that is the mode of the classes or mean prediction of the individual trees. In this work a RF classifier is trained as a baseline FDD model and compared against the considered BNs models. The hyperparameters for the model were set with a maximum tree depth of 5 and a population of 100 trees.

A summary of the results obtained from this analysis is provided below.

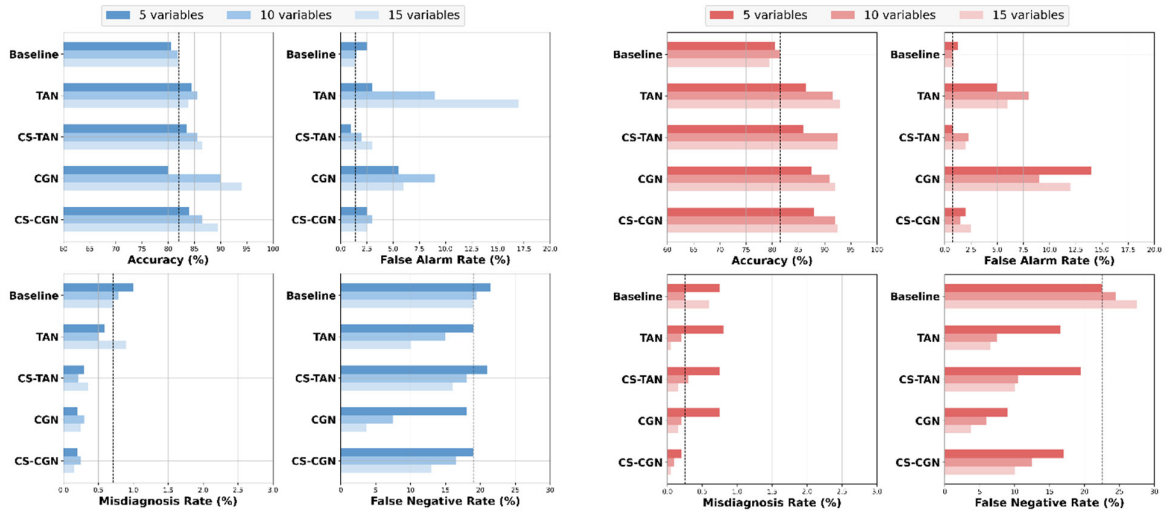

Figure 1. Performance metrics for each model considering summer (sx) and winter (dx) data.

In both seasons, the Baseline model shows moderate accuracy across all sets of input variables but does not achieve the highest levels. TAN demonstrates improved accuracy over the Baseline, while CS-TAN further enhances accuracy compared to TAN, indicating the benefit of cost-sensitive adjustments. CGN shows high accuracy, especially with 15 input variables, outperforming TAN and CS-TAN (especially in summer season). CS-CGN achieves the highest average accuracy (close to 85%) across all sets of input variables, with improvements as the number of variables increases, indicating its robustness and adaptability. For both seasons, the Baseline model exhibits a relatively low FAR (less than 2,5%). In contrast TAN and CGN are characterized by higher FAR compared to the Baseline during both summer and winter season. The benefit of cost sensitive analysis is then clear when the results of CS-TAN and CS-CGN are analyzed. For those models the achieved FAR is relatively low and comparable to the baseline model. In both seasons, the Baseline model is characterized by higher values of MDR. TAN improves on the Baseline but does not perform as well as CS-TAN, CGN or CS-CGN. CS-CGN achieves the lowest MDR (lower than 0.5%), outperforming all other models while, in general, all the models benefit from the inclusion of more input variables in the training step. For what is concerned the FNR, during summer season with 5 input variables all the models perform similarly. The best improvement is achieved for the BN models when exploiting 10 or 15 input variables. During both seasons the CGN achieved the best value of FNR close to 5%. More in general, both seasons show similar trends, with models generally performing better with more variables. In addition, based on the analysis across all metrics, CS-CGN stands out as the best model. It consistently achieves high values of accuracy and low values of FAR, MDR and FNR. The cost-sensitive approach of both CS-CGN and CS-TAN optimize the trade-offs between different types of errors, leading to overall superior performance further validating its effectiveness and adaptability in FDD problems.

3. References

[1] Chen, Y., et al: Using discrete Bayesian networks for diagnosing and isolating cross-level faults in HVAC systems. Appl. Energy, 327 (2022).
[2] Wang, Y., et al.: A practical chiller fault diagnosis method based on discrete Bayesian network. Int. J. Refrig., 102, pp.159-167 (2019).
[3] He, S., et al.: Fault detection and diagnosis of chiller using Bayesian network classifier with probabilistic boundary. Appl. Therm. Eng., 107, pp. 37-47 (2016).
[4] Wang, Z. et al.: Fault detection and diagnosis of chillers using Bayesian network merged distance rejection and multi-source non-sensor information.

Finanziato dall'Unione europea NextGenerationEU
Ministero dell'Università e della Ricerca
Italiadomani PIANO NAZIONALE DI RIPRESA E RESILIENZA

Appl. Energy, 188, pp. 200-214 (2017).
[5] Chen, Z. et al.: A review of data-driven fault detection and diagnostics for building HVAC systems. Appl. Energy, 339 (2023).
[6] Jiang, L. et al.: Cost-sensitive Bayesian network classifiers. Pattern Recognit. Lett., 45, pp. 211-216 (2014).

Finanziato dall'Unione europea NextGenerationEU
Ministero dell'Università e della Ricerca
Italiadomani PIANO NAZIONALE DI RIPRESA E RESILIENZA

DELIVERABLE WP4_D3

DEFINITION OF HYBRID FDD STRATEGIES THAT COMBINE DATA-DRIVEN AND KNOWLEDGE-BASED APPROACHES

EDIT BY POLITO

PRIN 2022 - UTMOST FDD: AN AUTOMATED, OPEN, SCALABLE AND TRANSPARENT FAULT DETECTION AND DIAGNOSIS PROCESS FOR AIR-HANDLING UNITS BASED ON A HYBRID EXPERT AND ARTIFICIAL INTELLIGENCE APPROACH

Funded by the European Union - Next Generation EU within the "Piano Nazionale di Ripresa e Resilienza (PNRR), missione 4 componente 2 investimento 1.1 - fondo per il programma nazionale di ricerca e progetti di rilevante interesse nazionale (PRIN)"

Finanziato dall'Unione europea NextGenerationEU

Ministero dell'Università e della Ricerca

Italiadomani PIANO NAZIONALE DI RIPRESA E RESILIENZA

The UTMOST FDD Project is organised into the following 7 Work Packages (WPs):
WP0) PROJECT COORDINATION
WP1) EXPERIMENTAL ANALYSIS FOR THE CHARACTERIZATION OF FAULTY AND NORMAL OPERATION OF A TYPICAL AHU
WP2) KPIs IDENTIFICATION FOR ASSESSING FAULT IMPACT IN AHU OPERATION
WP3) AHU DIGITAL TWIN AND SIMULATION-BASED FAULT IMPACT SCENARIO ANALYSIS
WP4) DEFINITION OF HYBRID FDD STRATEGIES FOR AHUs
WP5) TRANSFERABILITY ANALYSIS OF THE FDD STRATEGIES
WP6) KNOWLEDGE TRANSFER AND DISSEMINATION

The WPs are organized into Tasks (T) ranging from 2 to 4 for each WP.

The aim of the WP4 is the definition of FDD strategies that can be exploited for detecting and diagnosing anomalies in AHUs during their operation. The definition of FDD logics will be based on a hybrid approach, considering both data-driven and knowledge-based strategies.

The WP4 will include the following 4 tasks (WP4_T1, WP4_T2, WP4_T3, WP4_T4):

- WP4_T1) the aim of this task is providing a scientific written report (1st WP4 deliverable WP4_D1) including a detailed categorization of the scientific studies on the main approaches employed for conducting FDD of AHUs. It will help in (a) better understanding the current research on knowledge-based and data-driven FDD strategies, and (b) define current gaps and opportunities in the definition of robust FDD strategies.
- WP4_T2) in this task, a special effort will be devoted to the study of possible configurations of strategies that leverage supervised and unsupervised AI techniques for detecting and diagnosing the main faults that can occur during AHUs operation. The results obtained in both WP1 and WP3 will be used as reference datasets. The algorithms that will be tested belong to the family of machine learning considering a multi-variate approach based on timeseries analytics. The FDD logics will be tested off-line, and their robustness assessed through different quality metrics (e.g., false negative and positive rates, true negative and positive rates, correct and misdiagnosis rates). A scientific written report (2nd WP4 deliverable WP4_D2), including the algorithms employed for defining the data-driven FDD strategies and the methodological processes followed for their training and testing on the reference dataset, will be delivered.
- WP4_T3) this task aims to identify knowledge-based FDD logics formulated as IF-THEN rules. The set of FDD rules will be defined starting from domain expertise and standards/handbooks/guidelines that represent a reference in this research field (e.g., ASHRAE guideline 36 [26], APAR rules [6]). Based on the results obtained from WP1, WP2 and WP3, it will be possible to exploit the main relationships that exist between faults and their effects on a single or group of operational variables for defining a typological fault-symptom library.
- WP4_T4) in this task, data-driven and expert-based logics will be combined defining hybrid FDD strategies taking advantages from both methods. The energy, environmental and economic performance of the AHU when the hybrid FDD methods are applied in the framework of a continuous commissioning process will be compared with the cases where a reactive or a preventive maintenance program is adopted. A scientific written report (3rd WP4 deliverable WP4_D3), including the data-driven algorithms and expert rules employed for defining the hybrid FDD strategies, the methodological processes followed for the training and testing of the developed strategies and the opportunities related to their deployment considering re-training logics and data-scarcity problems in the initialization phase of FDD tools, will be delivered.

1. Introduction

Among the main approaches in the field of Fault Detection and Diagnosis (FDD), hybrid methods, defined as the combination of two or more techniques, aim to overcome the limitations of single-solution strategies, such as fully data-driven approaches or methods entirely based on expert rules. By leveraging domain knowledge, hybrid FDD approaches enhance robustness, transparency, and interpretability, particularly during the diagnostic phase, and are therefore well suited for replicating diagnostic reasoning across different systems [1].

Within the literature on FDD for HVAC systems, Bayesian Networks (BNs) have proven to be particularly effective in integrating expert knowledge with data-driven processes. This effectiveness is mainly due to their ability to model complex dependencies among variables, manage uncertainty, and incorporate prior information related to system configuration and operation [2].

Finanziato dall'Unione europea NextGenerationEU | Ministero dell'Università e della Ricerca | Italiadomani PIANO NAZIONALE DI RIPRESA E RESILIENZA

In this context, the present WP focuses on the development of a hybrid FDD methodology [3] applied to the HVAC system installed at the SENS i Lab of the University of Campania "Luigi Vanvitelli" [4]. The proposed approach adopts a Bayesian Network as the core probabilistic reasoning framework, integrating information derived from data-driven models, which are used to generate virtual evidence, with knowledge-based rules employed to define hard evidence. This combination enhances the robustness, interpretability, and practical applicability of the methodology in real HVAC applications.

To assess its performance, the proposed hybrid framework is compared with two fully data-driven approaches, namely a Random Forest classifier and a Conditional Gaussian Network (CGN), which are used as benchmarks and evaluated on the same real-world dataset. Overall, this work introduces a hybrid FDD framework specifically designed for real HVAC systems, capable of addressing common challenges reported in the literature, such as the scarcity of labeled fault data, while simultaneously improving diagnostic robustness, interpretability, and transparency.

1.1 Definition of hybrid FDD strategies that combine data-driven and knowledge-based approaches

The proposed methodology adopts a hybrid Fault Detection and Diagnosis (FDD) approach that combines data-driven and knowledge-based techniques through the use of Bayesian Networks (BN) [3]. The overall workflow of the process is illustrated in Figure 1 and consists of multiple sequential stages, ranging from data preprocessing to diagnostic inference. The methodology was tested using data collected from the experimental Air Handling Unit installed at the SENS i Lab of the University of Campania "Luigi Vanvitelli" [4]. The experimental activity included both normal operating conditions and artificially induced faults, each maintained for the entire duration of the test.

The faults introduced in the AHU were grouped into the following categories:

- Valve stuck faults, affecting the cooling coil (Fault CC) and the post-heating coil (Fault PostHC), with imposed valve positions equal to 0 %, 25 %, 50 %, 75 %, and 100 %;
- Fan faults, affecting the supply air fan (Fault SAF) and the return air fan (Fault RAF), with imposed speed levels equal to 0 %, 25 %, 75 %, and 100 %;
- Sensor bias faults, applied to return air temperature and humidity measurements, corresponding to temperature offsets of plus or minus 3 degrees Celsius and humidity offsets of plus or minus 15 % (Fault T_RA Sensor and Fault RH_RA Sensor);
- Damper stuck faults, involving the exhaust air, outdoor air, and return air dampers, which were grouped into a single fault class denoted as Fault AIR_DUCT.

Finanziato dall'Unione europea NextGenerationEU
Ministero dell'Università e della Ricerca
Italiadomani PIANO NAZIONALE DI RIPRESA E RESILIENZA

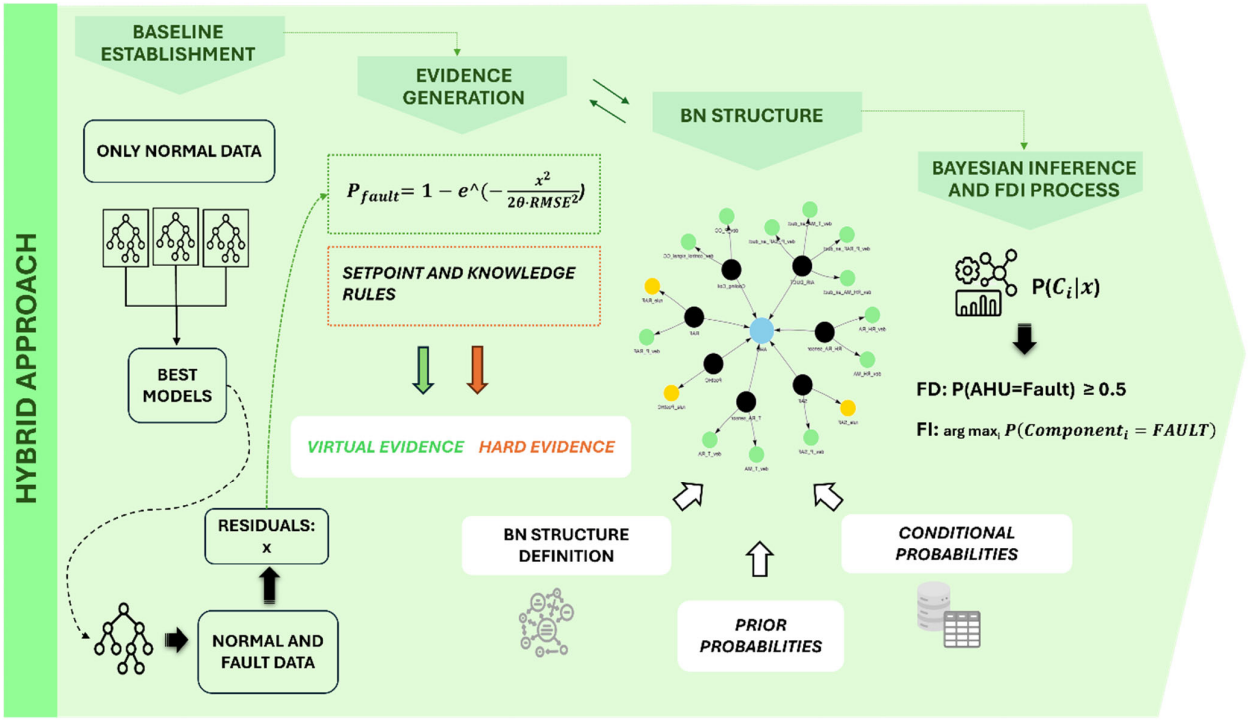

Figure 1. Schematic representation of the hybrid Fault Detection and Diagnosis approach.

The first stage of the methodology consists of defining a normal operating baseline for the HVAC system. This baseline is obtained using a set of Random Forest regression models trained exclusively on fault-free operating data, without requiring any fault-labeled samples. Each Random Forest model is trained to predict a specific target variable, selected based on physical knowledge of the system and on the availability of sensor measurements in real HVAC installations. The input variables include environmental conditions and upstream component parameters that influence the behavior of the target variable.

When applied to previously unseen test data, the Random Forest models produce residuals, defined as the difference between measured and predicted values. These residuals quantify the deviation of system behavior from the expected normal operating condition and constitute the basis for the generation of virtual evidence. The evidence generation phase and the construction of the Bayesian Network are closely interconnected, since the variables predicted in the first phase define the observable nodes of the network. Two types of evidence are considered in this work, namely virtual evidence and hard evidence.

Virtual evidence is derived from the residuals of the Random Forest models and enables the representation of non-deterministic system conditions. Since these residuals approximately follow a Gaussian distribution, they are transformed into fault probabilities ranging from zero to one using the following relation [5]:

$$P_{fault} = 1 - e^{-\frac{x^2}{2\theta\,\mathrm{RMSE}^2}} \quad (1)$$

where RMSE is the root mean square error of the regression model and θ is an empirical scaling coefficient used to control the sensitivity of the fault probability. The resulting fault probability values are used as virtual evidence within the Bayesian Network and are implemented as binary probability distributions, assigning to each observed node the likelihood of being in either the normal or faulty state.

In addition to virtual evidence, the Bayesian Network also incorporates hard evidences, defined through expert rules and operational thresholds derived from physical knowledge of the HVAC system and its control logic. Specifically, the following rules are implemented:

- Fan setpoint rules, where a fault is triggered if the speed setpoint of the supply or return fan deviates by more than 0.01 from its nominal value;
- Expert rule on return air temperature, where a fault condition associated with the post-heating coil is activated if the return air temperature deviates by more than 1.5 degrees Celsius from its nominal value while the cooling coil is operating;

Finanziato dall'Unione europea NextGenerationEU | Ministero dell'Università e della Ricerca | Italiadomani PIANO NAZIONALE DI RIPRESA E RESILIENZA

Since hard evidence is deterministic in nature, it is associated with a higher level of confidence and contributes to strengthening the reliability of the diagnostic inference.

The construction of the Bayesian Network represents the core of the hybrid diagnostic framework. The network architecture is initially guided by the semantic model of the HVAC system based on the Brick schema, which enables a hierarchical organization consisting of three levels, namely the system node, component nodes, and evidence nodes. This structure was subsequently refined using expert knowledge in order to remove redundant nodes, improve the representation of physical relationships among variables, and integrate system control logic. Some measured variables were used both as evidence nodes and as component fault nodes, enabling the identification of sensor bias faults. In addition to defining the network structure, the probabilistic parameters were specified, including prior probabilities and conditional probability distributions.

The Bayesian inference process is executed every 15 minutes, updating the posterior fault probabilities at both system and component levels. Fault Detection is performed based on the posterior probability of the system node representing the AHU. When this probability exceeds a threshold of 0.5, the system is classified as faulty. In the presence of an anomaly, Fault Isolation is carried out by identifying the component associated with the highest posterior fault probability. When ambiguous or conflicting symptoms are present, the Bayesian Network preserves a coherent representation of diagnostic uncertainty by distributing probabilities across multiple components rather than enforcing a deterministic decision.

2. Fully Data-Driven Approaches

In order to evaluate the effectiveness and advantages of the proposed hybrid approach, two additional fully data-driven Fault Detection and Diagnosis (FDD) methods were developed and tested in this work. These methods were used as benchmarks for the comparison of diagnostic performance. Both approaches rely exclusively on labeled historical data and do not require any physical knowledge or explicit modeling of the HVAC system.

The first approach employs a Random Forest (RF) classifier for the automatic identification of fault conditions. The model is trained through a hyperparameter optimization procedure based on grid search and cross-validation, and it directly provides the system operating state label for each time interval. This method represents a well-established reference in the FDD literature due to its simplicity of implementation and strong generalization capabilities.

The second approach is based on a Conditional Gaussian Network (CGN), which is a probabilistic model capable of handling continuous variables and estimating, for each time step, the posterior probabilities associated with the different fault classes. The CGN provides an explicit representation of diagnostic uncertainty and includes a decision rule based on statistical confidence thresholds to improve classification robustness, particularly in regions where normal and faulty conditions overlap.

Both fully data-driven approaches were applied to the same dataset used for the hybrid framework and were evaluated using standard classification metrics. Their inclusion enables a direct and consistent comparison, aimed at highlighting the benefits introduced by the integration of data-driven and knowledge-based methods in the proposed hybrid Bayesian Network-based approach.

3. Results

Table 1 reports the accuracy comparison among the three Fault Detection and Diagnosis (FDD) approaches developed in this work, namely two fully data-driven methods, the Random Forest classifier and the Conditional Gaussian Network, and the proposed hybrid approach. As shown in the table, the fully data-driven methods achieve higher accuracy values, equal to 0.91 for the Random Forest classifier and 0.86 for the Conditional Gaussian Network. In contrast, the hybrid approach achieves an overall accuracy of 0.80 in the Fault Isolation task, that is, in identifying the component responsible for the system fault.

Table 1. Accuracy comparison among the proposed FDD approaches.

Method	Accuracy
Hybrid Aprroach	0.80
Random Forest Classifier	0.91
Conditional Gaussian Network (CGN)	0.86

Finanziato dall'Unione europea NextGenerationEU | Ministero dell'Università e della Ricerca | Italiadomani PIANO NAZIONALE DI RIPRESA E RESILIENZA

This result is consistent with findings reported in the literature, where fully data-driven models trained directly on labeled fault data are able to learn dataset-specific patterns and maximize classification performance. However, these results must be interpreted in light of the different methodological assumptions underlying the compared approaches. In particular, both fully data-driven methods require the availability of labeled data for all fault conditions and rely on a relatively large set of input variables, requirements that are rarely met in real HVAC systems.

Figure 2. Confusion matrix for the hybrid approach.

Although the hybrid approach exhibits lower accuracy, it introduces a methodologically relevant trade-off among performance, interpretability, and practical applicability. Unlike fully data-driven methods, the hybrid framework does not require fault-labeled data for training the baseline models and exploits a probabilistic representation that is consistent with the physical structure of the HVAC system. As a result, the lower accuracy reflects increased robustness to previously unseen operating conditions and reduced dependence on the specific distribution of the training data.

To further analyze the diagnostic behavior of the hybrid approach and investigate the origin of classification errors, Figure 2 presents the confusion matrix corresponding to the Fault Isolation phase. This representation enables the evaluation of class-specific performance and the identification of systematic confusions among functionally related components. As discussed in the following section, the matrix highlights excellent performance for the most impactful faults, such as SAF, RAF, and PostHC, while the main limitations are associated with faults characterized by weak symptoms or partially compensated by the control logic, including those related to the AIR_DUCT subsystem and sensor bias conditions.

3.1 References

[1] Li, W., Li, H., Gu, S., & Chen, T. (2020). Process fault diagnosis with model-and knowledge-based approaches: Advances and opportunities. Control Engineering Practice, 105, 104637.

[2] Lampis, M., & Andrews, J. D. (2009). Bayesian belief networks for system fault diagnostics. Quality and Reliability Engineering International, 25(4), 409-426.

[3] Paolini, M., Piscitelli, M. S., & Capozzoli, A. (2025). A label-free hybrid fault detection and diagnosis approach for HVAC systems using bayesian networks. Energy and Buildings, 116658.

[4] Rosato, A., Guarino, F., Filomena, V., Sibilio, S., & Maffei, L. (2020). Experimental calibration and validation of a simulation model for fault detection of HVAC systems and application to a case study. Energies, 13(15), 3948.

[5] Gao, T., Marié, S., Béguery, P., Thebault, S., & Lecoeuche, S. (2024). Integrated building fault detection and diagnosis using data modeling and Bayesian networks. Energy and Buildings, 306, 113889.

Finanziato dall'Unione europea NextGenerationEU
Ministero dell'Università e della Ricerca
Italiadomani PIANO NAZIONALE DI RIPRESA E RESILIENZA

MISSIONE 4
ISTRUZIONE RICERCA

WP5 - *Transferability analysis of the FDD strategies*

Finanziato dall'Unione europea NextGenerationEU
Ministero dell'Università e della Ricerca
Italiadomani
PIANO NAZIONALE DI RIPRESA E RESILIENZA

MISSIONE 4
ISTRUZIONE RICERCA

DELIVERABLE WP5_D1

LITERATURE REVIEW ON THE MAIN APPROACHES EMPLOYED FOR TRANSFER LEARNING IN FDD AND IDENTIFICATION OF A TARGET AHU SYSTEM

EDIT BY POLITO

PRIN 2022 - UTMOST FDD: AN AUTOMATED, OPEN, SCALABLE AND TRANSPARENT FAULT DETECTION AND DIAGNOSIS PROCESS FOR AIR-HANDLING UNITS BASED ON A HYBRID EXPERT AND ARTIFICIAL INTELLIGENCE APPROACH

Funded by the European Union - Next Generation EU within the "Piano Nazionale di Ripresa e Resilienza (PNRR), missione 4 componente 2 investimento 1.1 - fondo per il programma nazionale di ricerca e progetti di rilevante interesse nazionale (PRIN)"

Finanziato dall'Unione europea NextGenerationEU
Ministero dell'Università e della Ricerca
Italiadomani PIANO NAZIONALE DI RIPRESA E RESILIENZA

The UTMOST FDD Project is organised into the following 7 Work Packages (WPs):
WP0) PROJECT COORDINATION
WP1) EXPERIMENTAL ANALYSIS FOR THE CHARACTERIZATION OF FAULTY AND NORMAL OPERATION OF A TYPICAL AHU
WP2) KPIs IDENTIFICATION FOR ASSESSING FAULT IMPACT IN AHU OPERATION
WP3) AHU DIGITAL TWIN AND SIMULATION-BASED FAULT IMPACT SCENARIO ANALYSIS
WP4) DEFINITION OF HYBRID FDD STRATEGIES FOR AHUs
WP5) TRANSFERABILITY ANALYSIS OF THE FDD STRATEGIES
WP6) KNOWLEDGE TRANSFER AND DISSEMINATION

The WP5 aims at assessing the transferability of the hybrid FDD strategies conceived in the WP4 for enhancing its penetration and adoption in buildings.

A variety of transfer learning methods, which differ in their transfer methods (i.e., instance-based, feature-based, parameter-based, and relational knowledge-based) and application natures (i.e., transductive, inductive and unsupervised), have been reviewed in the literature. The main aim of this WP is to transfer the FDD strategies, pre-trained on the existing labeled datasets derived from the WP1 and WP3, exploiting them with reference to an external target AHU for accomplishing the same task.

The WP5 will include the following 4 tasks (WP5_T1, WP5_T2, WP5_T3, WP5_T4):

- WP5_T1) the aim of this task was providing a scientific written report (1st WP5 deliverable WP5_D1) including a detailed categorization of the studies on the main approaches employed for conducting transfer learning of FDD strategies in AHUs. It will help in (a) better understanding the current research on transfer learning approaches, and (b) define current gaps and opportunities in the definition of transferability and scalability strategies for FDD in AHUs. In addition, among the publicly available tagged datasets of AHU faulty operations, the target AHU system for testing the transfer learning framework of the FDD strategy conceived in the WP4 will be identified;
- WP5_T2) this task aimed to address the issue of knowledge representation of the metering infrastructure of the considered experimental facility and the one of the target AHU identified in the WP5_T1 through the implementation of an ontology schema, enabling the i) interoperability and ii) transferability of the FDD logics conceived in the WP4. In the considered AHU systems, the ontology will be used to represent sensors, subsystems, and the relationships between them. A preliminary study of the state of the art of the ontology schema within the building energy field will be conducted. The identified ontology schema will address the system labelling problem by compiling a normalized list of domain terms (i.e., vocabulary) and a list of relationships capturing dependencies and connections in and between AHU sensors, actuators, commands, set-points and related equipment. Open standards, such as Semantic Web, RDF (Resource Description Framework), SPARQL query language, will be used to enable ontology interoperability;
- WP5_T3) the aim of this task is the development of a digital twin of the external AHU assumed as target (selected in the WP5_T1) by means of the software TRNSYS 18 (https://www.trnsys.com/) by including dedicated features to model the desired faults and validating the simulation outputs against the publicly available corresponding experimental data. The TRNSYS files of the digital twin, together with its documentation, will be uploaded in a public repository as 2nd WP5 deliverable WP5_D2. This will help in extending the operating ranges covered by the most used public FDD databases;
- WP5_T4) this task aims to define the methodology to be employed to transfer the FDD logic from the source AHU system to the target one. The transferability analysis of the FDD strategy will be performed especially considering the data-driven methods. Parameter-based transfer learning strategies which adopt either freezing or fine-tuning approaches for knowledge transfer will be applied on the pre-trained data-driven FDD models. Eventually, by evaluating the achieved performance in terms of detection and diagnosis rates on the target dataset, the transferability potential of the conceived FDD strategy will be assessed. A scientific written report (3rd WP5 deliverable: WP5_D3), including the transfer learning strategies, and the results obtained in terms of detection and diagnosis accuracy pertaining to the target AHU dataset, will be delivered.

1. Introduction

The use of data-driven models for FDD tasks in building energy systems has gained significant popularity due to their flexibility and high accuracy. However, a major challenge in this field is the limited availability of data for individual buildings or systems, which can compromise the effective deployment of robust data-driven FDD tools. The acquisition of comprehensive datasets that fully represent the normal and faulty conditions of

Finanziato dall'Unione europea NextGenerationEU | Ministero dell'Università e della Ricerca | Italiadomani PIANO NAZIONALE DI RIPRESA E RESILIENZA

a system is essential for a reliable data-driven FDD but remains laborious, time-consuming, and costly. Additionally, machine learning algorithms are highly sensitive to the extrapolation problem; discrepancies between training and testing datasets—arising from variations in load or operating modes—can severely impact their ability to detect and diagnose faults accurately during system operation. To overcome these challenges, researchers worldwide have identified Transfer Learning (TL) as a promising approach to enhance the applicability and effectiveness of data-driven FDD processes.

Transfer learning aims to leverage the data or knowledge learnt from source domains to facilitate data-driven tasks in target domains. Research efforts should be paid to address the following two technical issues. Firstly, existing studies mainly assumed that there is a common subset of data variables which can be applied as inputs for classification model development. In practice, different building systems or components may collect completely different data variables and therefore, advanced solutions are needed to tackle the heterogenous data challenge for source data integration and unification. Secondly, there is a lack of studies to systematically assess the value of transfer learning in fighting against insufficient and imbalanced data scenarios for cross-domain FDD applications.

2. Related works

Currently, research on the application of TL for FDD tasks in building energy systems is limited. This section reviews the most relevant studies in this area, with a particular focus on the methodologies employed, the metrics used to evaluate the similarity between source and target system, and the criteria applied to assess TL performance.

2.1 Chillers, Refrigeration Systems, and Heat Pumps

Liu et al. introduced two TL scenarios to evaluate the effectiveness of TL in performing FDD on centrifugal chillers [2]. These scenarios were designed to simulate situations with insufficient data in the source domain for knowledge learning. Specifically, the first scenario assumed that complete chiller operation data was available in the source domain, while the second scenario considered varying levels of data availability in the source domain. Four different TL strategies, incorporating various combinations of weight initialization, fine-tuning, and feature extraction, were tested. The results revealed that the fault diagnosis accuracies in the two learning tasks were 5.71% and 3.44%, respectively, when no transfer learning was applied. This highlights the difficulty of directly using models trained on source data in another domain without a TL approach. In the first learning scenario, the accuracies of the transferred models exceeded the benchmarks in most training cases. In the second scenario, the maximum accuracy improvement due to TL was substantial, showcasing significant performance enhancements achieved through TL.

The authors in [3] proposed a general framework for transferring prior knowledge from a data-rich source chiller to develop a diagnostic model for a new target chiller. The process begins with heterogeneous data standardization, which harmonizes the original datasets from various chillers. Next, domain adaptation is applied to address the domain shift caused by differences in feature distributions between chillers. A Domain Adversarial Neural Network (DANN) is then employed to generate the diagnostic model for the target chiller, utilizing only easily obtainable normal operation data from the target chiller alongside prior knowledge from the source chiller (normal and faulty data) during training. To validate the proposed TL approach, two screw chillers with different capacities were used as the source and target chillers. The results demonstrated that the transferred diagnostic model achieved good performance, with accuracies of approximately 81% and 75% for the first and second refrigeration cycles, respectively. In comparison, five conventional machine learning models trained on target domain data achieved accuracies below 55%. These findings underscore the significant performance advantages and practical potential of the proposed TL approach.

In their paper, Li et al. [4] proposed highly adaptable fault diagnosis models for building energy systems using three deep TL strategies: network-based fine-tuning, mapping-based domain adaptive neural network, and adversarial-based domain adversarial neural network. The effectiveness of these TL-based fault diagnosis approaches was validated using fault datasets from a 703 kW screw chiller and a 316 kW centrifugal chiller, both generated under the ASHRAE project RP-1043 framework. The study explored two distinct TL scenarios: cross-operation-condition fault diagnosis and cross-system fault diagnosis. In the first case, the fault diagnosis task is performed on a single chiller by investigating the deep TL strategies trained on limited data from known operation conditions for diagnosis unknown ones that are not covered in the training dataset. In the second case, one of the two chillers is chosen as the target domain for fault diagnosis and the other as the source domain for knowledge transfer. The results demonstrated that network-based fine-tuning achieved an average

Finanziato dall'Unione europea NextGenerationEU | Ministero dell'Università e della Ricerca | Italiadomani PIANO NAZIONALE DI RIPRESA E RESILIENZA

fault diagnosis accuracy of 93% across both scenarios, representing an average accuracy improvement of 55% compared to a non-transfer benchmark model based on CNN.

In [5] the authors investigated the benefits of TL for implementing FDD strategies on refrigeration systems. In particular, they introduced an auto-scale transfer learning methodology starting from the publicly available data on water chiller faults included in the ASHRAE RP-1043 dataset. The trained FDD strategy was based on the use of five ML classifiers and was then transferred to 100 refrigeration systems in 39 different locations, ranging in power from 1/4 to 10 hp (horsepower). The introduced TL approach was defined as a Transitive Transfer Learning problem that leverages the use of an intermediate domain selection component to transfer knowledge. The practical case studies demonstrated that the TL-based FDD strategy can lead to energy savings in refrigeration systems in the range from 13% to 27%. Furthermore the total return on investment, considering the annual cost of the cloud platform for running the FDD strategy and the installation cost related to the IoT sensors required, was about 41%.

Guo et al. [8] proposed four feature transformation-based transfer learning FDD methods for carbon dioxide heat pump systems, including transfer component analysis (TCA), joint distribution adaptation (JDA), balanced distribution adaptation (BDA), and correlation alignment (CORAL). They optimized the models through feature parameter screening, classifier tuning, and adjusting the training set proportion. The study found that the MMD-based method outperformed geometric feature transformation methods with or without parameter optimization. With parameter optimization, the TCA, JDA, and BDA methods saw accuracy rise from 97.79% to 98.89%, while CORAL benefited significantly from optimization, with accuracy jumped from 15.67% to 74.23%. They also noted that the training set proportion had the most significant impact on diagnostic accuracy.

2.2 Air Handling Units

The study by [1] proposes an image-based transfer learning framework, enabling the integration of multi-source data and cross-domain knowledge sharing in the building sector. The image transformation method involves the following steps: data preprocessing (normalization and matrix transposition), application of the t-distributed stochastic neighbor embedding (t-SNE) algorithm to reduce the number of columns in the transposed matrix from n to 2, and defining image dimensions to calculate the size of each pixel along both the x- and y-axes. Convolutional neural networks (CNNs) were utilized for image-based fault diagnosis. Experiments were conducted to evaluate the benefits of transfer learning under various conditions, such as data quantity, imbalance ratios, and parameter-based learning strategies (freezing and fine-tuning). The results confirm the effectiveness of image-based transfer learning for HVAC FDD tasks, providing valuable insights into combining operational data from different sources and enhancing cross-domain applications.

Authors in [6] proposed a methodology that addresses the discrepancy between the source and target domains and incorporates a dissimilarity filter. This filter selectively rejects samples that may result in negative knowledge transfer during the training process of the chosen algorithm. The inclusion of this filter is combined with a classical neural network architecture to perform a parameter-based transfer learning (fine-tuning). In particular the TL strategy was tested using the ASHRAE RP-1312 dataset as a source domain and an experimental dataset obtained from a single-zone VAV-AHU located at the Lawrence Berkeley National Laboratory (FLEXLAB) as target domain. The FDD task consisted in the detection and diagnosis of three major faults (outdoor air damper stuck at the fully closed position, heating coil valve leak and cooling coil valve stuck). Results emphasize the potential of the proposed domain dissimilarity analysis reaching a classification accuracy in the FDD task of 92% under a TL framework, with a significant increase in comparison to other TL classical approaches (feature-based and instance-based).

In [7] Feng et al. developed a multi-attention mechanism that operates across channel, spatial, and temporal dimensions, significantly improving the model's ability to discriminate sensor fault features. Additionally, they introduced an innovative alignment method that combines Loss of Maximum Mean Discrepancy, Cross-entropy, and Discriminator Classification to address the misalignment issues in feature mapping between source and target domains. The results demonstrate that this new method, i.e., Multi-Attention based Transfer Learning (MATL), outperforms traditional transfer learning techniques like TCA, Joint Adaptation Network (JAN), and Deep Domain Confusion (DDC), achieving a fault diagnosis accuracy of 93%. Furthermore, ablation studies confirm the robustness and effectiveness of the method under various settings, including different attention modules, fault types, and data volumes.

In the study by [9], a novel transfer learning approach for AHU FDD is proposed. The transformer model is modified to include one encoder and two decoders, enabling dual outputs. The first decoder determines the HVAC system's fault type or confirm normal operation, while the second decoder, taking the output of the

Finanziato dall'Unione europea NextGenerationEU | Ministero dell'Università e della Ricerca | Italiadomani PIANO NAZIONALE DI RIPRESA E RESILIENZA

first decoder as its input, evaluates the fault's severity level. The modified transformer model allows to handle missing features in the target domain, providing a robust foundation for transfer learning. The data utilized in this study are sourced from the LBNL fault detection and diagnostics data sets (dual-duct AHU and single-duct AHU). The modified transformer demonstrates effective performance in complex systems (dual-duct AHU as source system), achieving an accuracy of 91.38% in a system with 16 faults and multiple fault severity levels. Two typical scenarios are designed to assess the transfer performance. The first scenario involves a cross-system transfer (both simulated datasets). The second scenario involves a simulation-to-reality transfer. An adapter-based parameter-efficient transfer learning method is investigated, enabling the transfer of pretrained models by integrating small adapter modules. This approach achieves performance comparable to full fine-tuning while requiring fewer trainable parameters and proves effective even with limited data in the target domain.

3. References

[1] C. Fan, et al.: A novel image-based transfer learning framework for cross-domain hvac fault diagnosis: From multi-source data integration to knowledge sharing strategies. Energy and Buildings 262 (2022) 111995.
[2] J. Liu, et al.: Transfer learning-based strategies for fault diagnosis in building energy systems. Energy and Buildings 250 (2021) 111256.
[3] X. Zhu, et al.: Transfer learning based methodology for migration and application of fault detection and diagnosis between building chillers for improving energy efficiency. Building and Environment 200 (2021) 107957.
[4] G. Li, et al.: Comparative study on deep transfer learning strategies for cross-system and cross-operation-condition building energy systems fault diagnosis. Energy 263 (2023) 125943.
[5] D. Lee, et al.: Achieving energy savings through artificial-intelligence-assisted fault detection and diagnosis: Case study on refrigeration systems. Case Studies in Thermal Engineering 40 (2022) 102499.
[6] V. Martinez-Viol, et al.: Semi-supervised transfer learning methodology for fault detection and diagnosis in air-handling units. Applied Sciences 12 (17) (2022).
[7] B. Feng, et al.: Attention-empowered transfer learning method for hvac sensor fault diagnosis in dynamic building environments. Building and Environment 250 (2024) 111148.
[8] Y. Guo, et al.: Research on fault detection and diagnosis of carbon dioxide heat pump systems in buildings based on transfer learning. Journal of Building Engineering 85 (2024) 108774.
[9] Zi-Cheng Wang, et al.: A modified transformer and adapter-based transfer learning for fault detection and diagnosis in HVAC systems. Energy Storage and Saving 3 (2024) 96–105.

DELIVERABLE WP5_D2

DEVELOPMENT OF A CALIBRATED DIGITAL TWIN FOR THE AHU IDENTIFIED AS TARGET

EDIT BY UNICAMPANIA

PRIN 2022 - UTMOST FDD: AN AUTOMATED, OPEN, SCALABLE AND TRANSPARENT FAULT DETECTION AND DIAGNOSIS PROCESS FOR AIR-HANDLING UNITS BASED ON A HYBRID EXPERT AND ARTIFICIAL INTELLIGENCE APPROACH

Funded by the European Union - Next Generation EU within the "Piano Nazionale di Ripresa e Resilienza (PNRR), missione 4 componente 2 investimento 1.1 - fondo per il programma nazionale di ricerca e progetti di rilevante interesse nazionale (PRIN)"

Finanziato dall'Unione europea NextGenerationEU

Ministero dell'Università e della Ricerca

Italiadomani PIANO NAZIONALE DI RIPRESA E RESILIENZA

The UTMOST FDD Project is organised into the following 7 Work Packages (WPs):
WP0) PROJECT COORDINATION
WP1) EXPERIMENTAL ANALYSIS FOR THE CHARACTERIZATION OF FAULTY AND NORMAL OPERATION OF A TYPICAL AHU
WP2) KPIs IDENTIFICATION FOR ASSESSING FAULT IMPACT IN AHU OPERATION
WP3) AHU DIGITAL TWIN AND SIMULATION-BASED FAULT IMPACT SCENARIO ANALYSIS
WP4) DEFINITION OF HYBRID FDD STRATEGIES FOR AHUs
WP5) TRANSFERABILITY ANALYSIS OF THE FDD STRATEGIES
WP6) KNOWLEDGE TRANSFER AND DISSEMINATION

The WP5 aims at assessing the transferability of the hybrid FDD strategies conceived in the WP4 for enhancing its penetration and adoption in buildings.

A variety of transfer learning methods, which differ in their transfer methods (i.e., instance-based, feature-based, parameter-based, and relational knowledge-based) and application natures (i.e., transductive, inductive and unsupervised), have been reviewed in the literature. The main aim of this WP is to transfer the FDD strategies, pre-trained on the existing labeled datasets derived from the WP1 and WP3, exploiting them with reference to an external target AHU for accomplishing the same task.

The WP5 will include the following 4 tasks (WP5_T1, WP5_T2, WP5_T3, WP5_T4):

- WP5_T1) the aim of this task was providing a scientific written report (1st WP5 deliverable WP5_D1) including a detailed categorization of the studies on the main approaches employed for conducting transfer learning of FDD strategies in AHUs. It will help in (a) better understanding the current research on transfer learning approaches, and (b) define current gaps and opportunities in the definition of transferability and scalability strategies for FDD in AHUs. In addition, among the publicly available tagged datasets of AHU faulty operations, the target AHU system for testing the transfer learning framework of the FDD strategy conceived in the WP4 will be identified;
- WP5_T2) this task aimed to address the issue of knowledge representation of the metering infrastructure of the considered experimental facility and the one of the target AHU identified in the WP5_T1 through the implementation of an ontology schema, enabling the i) interoperability and ii) transferability of the FDD logics conceived in the WP4. In the considered AHU systems, the ontology will be used to represent sensors, subsystems, and the relationships between them. A preliminary study of the state of the art of the ontology schema within the building energy field will be conducted. The identified ontology schema will address the system labelling problem by compiling a normalized list of domain terms (i.e., vocabulary) and a list of relationships capturing dependencies and connections in and between AHU sensors, actuators, commands, set-points and related equipment. Open standards, such as Semantic Web, RDF (Resource Description Framework), SPARQL query language, will be used to enable ontology interoperability;
- WP5_T3) the aim of this task is the development of a digital twin of the external AHU assumed as target (selected in the WP5_T1) by means of the software TRNSYS 18 (https://www.trnsys.com/) by including dedicated features to model the desired faults and validating the simulation outputs against the publicly available corresponding experimental data. The TRNSYS files of the digital twin, together with its documentation, will be uploaded in a public repository as 2nd WP5 deliverable WP5_D2. This will help in extending the operating ranges covered by the most used public FDD databases;
- WP5_T4) this task aims to define the methodology to be employed to transfer the FDD logic from the source AHU system to the target one. The transferability analysis of the FDD strategy will be performed especially considering the data-driven methods. Parameter-based transfer learning strategies which adopt either freezing or fine-tuning approaches for knowledge transfer will be applied on the pre-trained data-driven FDD models. Eventually, by evaluating the achieved performance in terms of detection and diagnosis rates on the target dataset, the transferability potential of the conceived FDD strategy will be assessed. A scientific written report (3rd WP5 deliverable: WP5_D3), including the transfer learning strategies, and the results obtained in terms of detection and diagnosis accuracy pertaining to the target AHU dataset, will be delivered.

This Deliverable WP5_D2 describes the digital twin of the external AHU assumed as target developed in TRNSYS.

1. Description of TRNSYS AHU model

Fig.1 reports a schematic of the AHU as modelled in TRNSYS.

Finanziato dall'Unione europea NextGenerationEU | Ministero dell'Università e della Ricerca | Italiadomani PIANO NAZIONALE DI RIPRESA E RESILIENZA

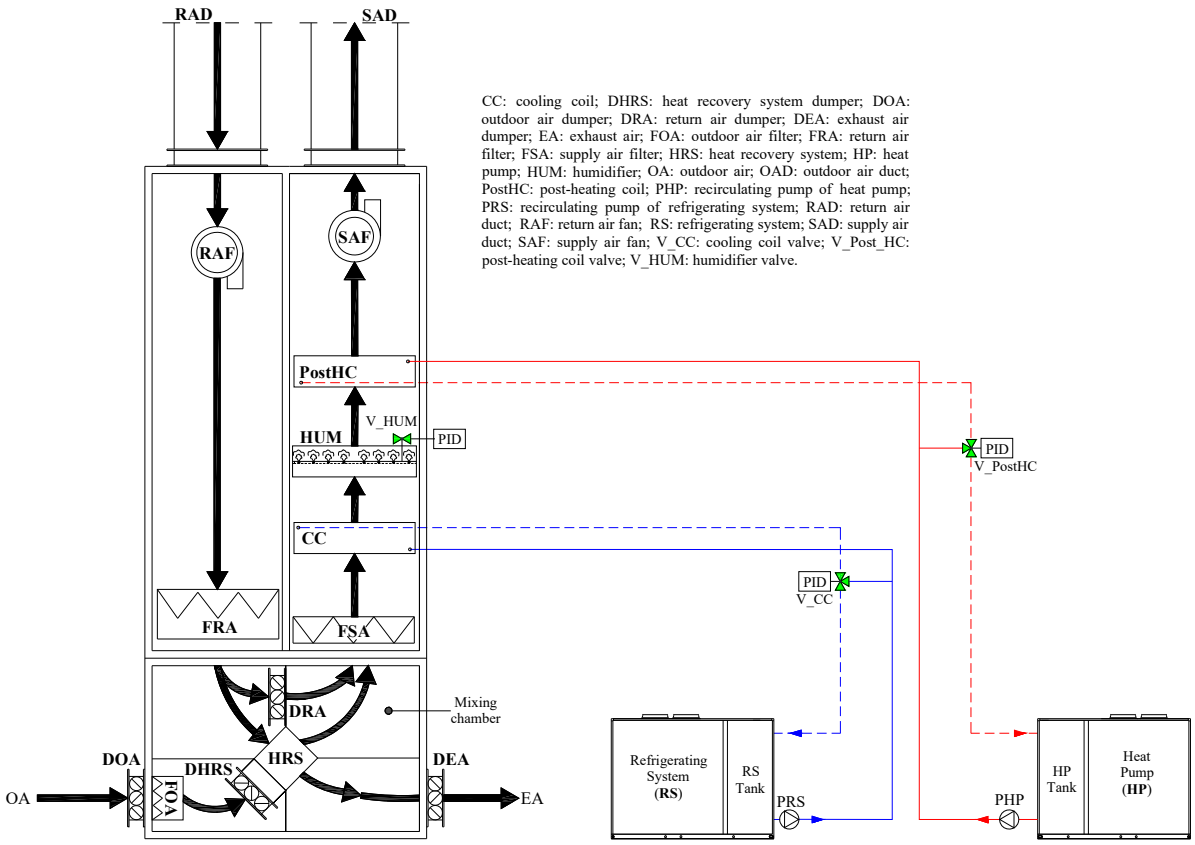

Figure 1. AHU TRNSYS model scheme.

Table 1 reports the TRNSYS Types used to model each AHU component.

Table 1. TRNSYS Model Types.

LIST OF TYPES	MODEL COMPONENTS
56	Building
Calculator	Input
607a	Return Air Fan Duct (RAD)
Calculator	Return Air Fan (RAF)
Calculator	Return Air Filter (FRA)
Calculator	Exhaust and Return Air Dampers (DEA, DRA)
Calculator	Outdoor Air Damper (DOA)
Calculator	Outdoor Air Filter (FOA)
Type 667b	Heat Recovery System (HRS)
Type 648	Mixing Chamber
Calculator	Supply Air Filter (FSA)
Type 941	Refrigerating System (RS)
Type 1534	Refrigerating System Tank (RS Tank)
Type 742	Refrigerating System Recirculation Pump (Pump RS)
Type 31	Pipe Refrigerating System to Cooling Coil (RS to CC)

Finanziato dall'Unione europea NextGenerationEU
Ministero dell'Università e della Ricerca
Italiadomani PIANO NAZIONALE DI RIPRESA E RESILIENZA

Type 647	Three-way flow diverter valve Cooling Coil (CC)
Type 508c	Cooling Coil (CC)
Type 649	Three-way mixing valve Cooling Coil to Refrigerating System (CC to RS)
Type 31	Pipe Cooling Coil to Refrigerating System (CC to RS)
Type 941	Heat Pump (HP)
Type 1534	Heat Pump Tank (HP Tank)
Type 742	Heat Pump Recirculation Pump (Pump HP)
Type 31	Pipe Heat Pump to Post-Heating Coil (HP to PostHC)
Type 647	Three-way flow diverter valve Post-Heating Coil (PostHC)
Type 753b	Post-Heating Coil (CC)
Type 649	Three-way mixing valve Post-Heating Coil to Heat Pump (PostHC to HP)
Type 31	Pipe Post-Heating Coil to Heat Pump (PostHC to HP)
Calculator	Humidifier (HUM)
Calculator	Supply Air Fan (SAF)
Type 607a	External Supply Air Fan Duct (External SAD)
Type 607a	Internal Supply Air Fan Duct (Internal SAD)
Type 2	Controller Ctrl_RS
Type 2	Controller Ctrl_HP
Type 2	Controller Ctrl_HUM
Type 2	Controller Ctrl_Dehum
Type 2	Controller Ctrl_CC_Temp
Type 2	Controller Ctrl_PostHC_Temp
Type 23	PID Controller CC_Temp
Type 23	PID Controller CC_Dehum
Type 23	PID Controller PostHC
Type 23	PID Controller Humidifier
Type 33e	Psychrometrics
Type 25c	Printer
Type 65d	Online plotter

In the following subsections, the above-mentioned TRNSYS Types, used to model each AHU component, are detailed.

1.1 Building - Type 56

The building is modelled in TRNBuild and then the output file with extension .bui is used as external file for the Type 56. The parameters of the Building type are reported in Fig. 2.

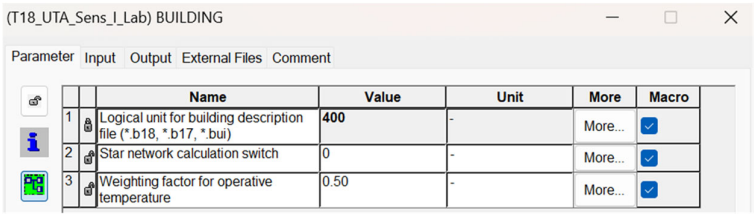

Figure 2. Parameters of Building Type.

Finanziato dall'Unione europea NextGenerationEU
Ministero dell'Università e della Ricerca
Italiadomani PIANO NAZIONALE DI RIPRESA E RESILIENZA

Tables 2a and b illustrate the inputs and outputs of return air fan duct, respectively.

Table 2a. Inputs of Building Type.

INPUTS	
LIST OF INPUTS	INPUTS USED
1- TAMB	Return Air Temperature - T_RA
2- RELHUMAMB	Return Air Relative Humidity - RH_RA
3- TSKY	Effective sky temperature
4- TSGRD	Effective ground temperature (0 °C)
5- AZEN	Solar zenith angle
6- AAZM	Solar azimuth angle
7- GRDREF	Ground reflectance
8- SUPPLY_AIR_FLOWRATE	Supply Air Temperature - T_SA
9- SUPPLY_AIR_TEMPERATURE	Supply Air Relative Humidity - RH_SA
10- SUPPY_AIR_RH	Supply Air mass flowrate - m_SA

Table 2b. Outputs of Building Type.

OUTPUTS	
LIST OF OUTPUTS	OUTPUTS USED
1- TAIR_BUILDING	Return Air Temperature - T_RA
2- RELHUM_BUILDING	Return Air Relative Humidity - RH_RA

1.2 Input - Calculator

In the Input calculator, all the parameters that can be set by the end-user are included. Tables 3 illustrates the outputs of input calculator.

Table 3. Outputs of Input Calculator.

OUTPUTS	
LIST OF OUTPUTS	OUTPUTS USED
Set_OL_RAF	Return Air Fan velocity
Set_OL_SAF	Supply Air Fan velocity
Set_OP_DHRS	Opening percentage of Heat Recovery System Damper
Set_T_target_RA	Return Air Temperature Target
UDB_T_target_RA	Upper deadband of Return Air Temperature Target
LDB_T_target_RA	Lower deadband of Return Air Temperature Target
Set_RH_target_RA	Return Air Relative Humidity Target
UDB_RH_target_RA	Upper deadband of Return Air Relative Humidity Target
LDB_RH_target_RA	Lower deadband of Return Air Relative Humidity Target

1.3 Return Air Fan Duct (RAD) - Type 607a

The return Air Fan Duct (RAD) is modelled by the Type 607a. The parameters of the Return Air Fan Duct (RAD) type are reported in Fig. 3.

Finanziato dall'Unione europea NextGenerationEU | Ministero dell'Università e della Ricerca | Italiadomani PIANO NAZIONALE DI RIPRESA E RESILIENZA

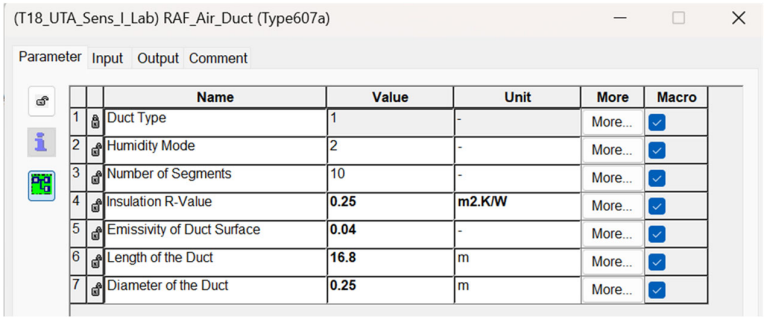

Figure 3. Parameters of RAD Types.

Tables 4a and b illustrate the inputs and outputs of return air fan duct, respectively.

Table 4a. Inputs of RAD Type.

INPUTS	
LIST OF INPUTS	INPUTS USED
Inlet Air Temperature	Return Air Temperature - T_RA (output Type 56)
Inlet Air Humidity Ratio	-
Inlet Air % Relative Humidity	Return Air Relative Humidity - RH_RA (output Type 56)
Air Flowrate	Return Air mass flowrate - m_RA
Inlet Air Pressure	1 atm (constant value) - p_RA
Environment Temperature	Outdoor Air Temperature - T_OA (output Type 15-3)
Wind Velocity	Outdoor Air Velocity (output Type 15-3)

Table 4b. Outputs of RAD Type.

OUTPUTS	
LIST OF OUTPUTS	OUTPUTS USED
Outlet Air Temperature	Return Air Temperature - T_RA
Outlet Air % Relative Humidity	Return Air Relative Humidity - RH_RA
Outlet Air Flowrate	Return Air mass flowrate - m_RA
Outlet Air Pressure	Return Air Pressure - p_RA

The return air mass flowrate is defined according to Eq. 1 defined based on experimental data:

$$\begin{aligned} m\_RA = {} & (751.04*Density\_RA\_kg\_m3)*(eql(Set\_OL\_SAF,5)*eql(Set\_OL\_RAF,5)) \\ & +((611.43*Density\_SA\_kg\_m3+0*Density\_EA\_kg\_m3)- \\ & 252.69*Density\_OA\_kg\_m3)*(eql(Set\_OL\_SAF,5)*eql(Set\_OL\_RAF,0)) \\ & +(311.90*Density\_RA\_kg\_m3)*(eql(Set\_OL\_SAF,0)*eql(Set\_OL\_RAF,5)) \\ & +(682.12*Density\_RA\_kg\_m3)*(eql(Set\_OL\_SAF,10)*eql(Set\_OL\_RAF,5)) \\ & +(1149.68*Density\_RA\_kg\_m3)*(eql(Set\_OL\_SAF,5)*eql(Set\_OL\_RAF,10)) \end{aligned} \quad (1)$$

Where:

- The constant value 751.04 is the experimental return air volumetric flowrate, when the return air fan velocity and the supply air fan velocity is equal to 50% (fault-free scenario);
- Density_RA_kh_m3 is the return air density, calculated via the psychometric Type33e;
- Set_OL_SAF is the experimental supply air fan velocity;
- Set_OL_RAF is the experimental return air fan velocity;

Finanziato dall'Unione europea NextGenerationEU
Ministero dell'Università e della Ricerca
Italiadomani PIANO NAZIONALE DI RIPRESA E RESILIENZA

- The constant value 611.43 is the experimental supply air volumetric flowrate when the return air fan velocity is equal to 0% (faulty scenario) and the supply air fan velocity is equal to 50% (fault-free scenario);
- Density_SA_kg_m3 is the supply air density, calculated via the psychometric Type33e;
- The constant value 0 is the experimental exhaust volumetric air flowrate when the return air fan velocity is equal to 0% (faulty scenario) and the supply air fan velocity is equal to 50% (fault-free scenario);
- Density_EA_kg_m3 is the exhaust air density, calculated via the psychometric Type33e;
- The constant value 252.69 is the experimental outdoor air volumetric flowrate when the return air fan velocity is equal to 0% (faulty scenario) and the supply air fan velocity is equal to 50% (fault-free scenario);
- Density_OA_kg_m3 is the outdoor air density, calculated via the psychometric Type33e;
- The constant value 311.90 is the experimental return air volumetric flowrate, when the return air fan velocity is equal to 50% (fault-free scenario) and the supply air fan velocity is equal to 0% (faulty scenario);
- The constant value 682.12 is the experimental return air volumetric flowrate, when the return air fan velocity is equal to 50% (fault-free scenario) and the supply air fan velocity is equal to 100% (faulty scenario);
- The constant value 1149.68 is the experimental return air volumetric flowrate, when the return air fan velocity is equal to 100% (faulty scenario) and the supply air fan velocity is equal to 50% (fault-free scenario).

1.4 Return Air Fan (RAF) - Calculator

The Return Air Fan (RAF) is modelled by using a calculator and not a specific type. Tables 5a and b illustrate the inputs and outputs of return air fan calculator, respectively.

Table 5a. Inputs of RAF Calculator.

INPUTS	
LIST OF INPUTS	INPUTS USED
Inlet Air Temperature	Return Air Temperature - T_RA (output Type 607a)
Inlet Air % Relative Humidity	Return Air Relative Humidity - RH_RA (output Type 607a)
Air Flowrate	Return Air mass flowrate - m_RA (output Type 607a)
Inlet Air Pressure	Return Air Pressure inlet the RAF - p_A_in_RAF

Table 5b. Outputs of RAF Calculator.

OUTPUTS	
LIST OF OUTPUTS	OUTPUTS USED
Outlet Air Temperature	Return Air Temperature - T_RA
Outlet Air % Relative Humidity	Return Air Relative Humidity - RH_RA
Outlet Air Flowrate	Return Air mass flowrate - m_RA
Outlet Air Pressure	Return Air Pressure outlet the RAF - p_A_out_RAF
	Electric power EP_RAF

The Electric power EP_{RAF} is defined according to Eq. 2. The equation is derived by interpolating the electrical power consumed by the return air fan as a function of its velocity.

$$EP\_RAF = (-0.0142*Set\_OL\_RAF^5+0.2882*Set\_OL\_RAF^4-1.3779*Set\_OL\_RAF^3+4.0138*Set\_OL\_RAF^2-1.5187*Set\_OL\_RAF+17.101)/1000 \quad (2)$$

Where:

- Set_OL_RAF is the return air fan velocity.

Finanziato dall'Unione europea NextGenerationEU | Ministero dell'Università e della Ricerca | Italiadomani PIANO NAZIONALE DI RIPRESA E RESILIENZA

1.5 Return Air Filter (FRA) - Calculator

The Return Air Filter (FRA) is modelled by using a calculator and not a specific type. Tables 6a and 6b illustrates the inputs and outputs of return air filter calculator, respectively.

Table 6a. Inputs of FRA Calculator.

INPUTS	
LIST OF INPUTS	INPUTS USED
Inlet Air Temperature	Return Air Temperature - T_RA (output RAF Calculator)
Inlet Air % Relative Humidity	Return Air Relative Humidity - RH_RA (output RAF Calculator)
Air Flowrate	Return Air mass flowrate - m_RA (output RAF Calculator)
Inlet Air Pressure	Return Air Pressure inlet the FRA - p_A_in_FRA (output RAF Calculator)

Table 6b. Outputs of FRA Calculator.

OUTPUTS	
LIST OF OUTPUTS	OUTPUTS USED
Outlet Air Temperature	Return Air Temperature - T_RA
Outlet Air % Relative Humidity	Return Air Relative Humidity - RH_RA
Outlet Air Flowrate	Return Air mass flowrate - m_RA
Outlet Air Pressure	Return Air Pressure outlet the FRA - p_A_out_FRA
Outlet Air Pressure Drop	Return air pressure difference outlet the FRA - Dp_A_FRA

1.6 Exhaust and Return Air Dampers (DEA, DRA) - Calculator

The Exhaust and Return Air Dampers (DEA, DRA) are modelled by using a calculator and not a specific type. Tables 7a and b illustrate the inputs and outputs of exhaust and return air dampers calculator, respectively.

Table 7a. Inputs of DEA and DRA Calculator.

INPUTS	
LIST OF INPUTS	INPUTS USED
Inlet Air Temperature	Return Air Temperature - T_RA (output FRA Calculator)
Inlet Air % Relative Humidity	Return Air Relative Humidity - RH_RA (output FRA Calculator)
Inlet Air Pressure	Return Air Pressure intlet the DRA - p_A_in_DRA (output FRA Calculator)
Air Density	Exhaust Air Density (output Type33e)

Table 7b. Outputs of DEA and DRA Calculator.

OUTPUTS	
LIST OF OUTPUTS	OUTPUTS USED
Outlet Air Temperature	Return Air Temperature - T_RA
Outlet Air % Relative Humidity	Return Air Relative Humidity - RH_RA
Outlet Air Flowrate -1	Exhaust Air mass flowrate - m_EA
Outlet Air Pressure	Return air pressure outlet the DRA - p_A_out_DRA
Outlet Air Pressure Drop	Return air pressure difference outlet the DRA - Dp_A_DRA
Outlet Air Flowrate -2	Recirculation Air mass flowrate - m_Recirc

Exhaust Air mass flowrate (m_EA) is defined according to Eq. 3, based on experimental data:

Finanziato dall'Unione europea NextGenerationEU | Ministero dell'Università e della Ricerca | Italiadomani PIANO NAZIONALE DI RIPRESA E RESILIENZA

$$\begin{aligned} m\_EA = {} & (155.70*Density\_EA\_kg\_m3)*(eql(Set\_OL\_SAF,5)*eql(Set\_OL\_RAF,5)) \\ & +(0*Density\_EA\_kg\_m3)*(eql(Set\_OL\_SAF,5)*eql(Set\_OL\_RAF,0)) \\ & +((311.90*Density\_RA\_kg\_m3+252.69*Density\_OA\_kg\_m3)- \\ & 107.80*Density\_SA\_kg\_m3)*(eql(Set\_OL\_SAF,0)*eql(Set\_OL\_RAF,5)) \\ & +(18.20*Density\_EA\_kg\_m3)*(eql(Set\_OL\_SAF,10)*eql(Set\_OL\_RAF,5)) \\ & +((1149.68*Density\_RA\_kg\_m3+0*Density\_OA\_kg\_m3)- \\ & 673.28*Density\_SA\_kg\_m3)*(eql(Set\_OL\_SAF,5)*eql(Set\_OL\_RAF,10)) \end{aligned} \quad (3)$$

Where:

- The constant value 155.70 is the experimental exhaust air volumetric flowrate, when the return air fan velocity and the supply air fan velocity is equal to 50% (fault-free scenario);
- Density_EA_kg_m3 is the exhaust air density, calculated via the psychometric Type33e;
- Set_OL_SAF is the supply air fan velocity;
- Set_OL_RAF is the return air fan velocity;
- The constant value 0 is the experimental exhaust air volumetric flowrate when the return air fan velocity is equal to 0% (faulty scenario) and the supply air fan velocity is equal to 50% (fault-free scenario);
- The constant value 311.90 is the experimental return air volumetric flowrate when the return air fan velocity is equal to 50% (fault-free scenario) and the supply air fan velocity is equal to 0% (faulty scenario);
- Density_RA_kh_m3 is the return air density, calculated via the psychometric Type33e;
- The constant value 252.69 is the experimental outdoor air volumetric flowrate when the return air fan velocity is equal to 50% (fault-free scenario) and the supply air fan velocity is equal to 0% (faulty scenario);
- Density_OA_kg_m3 is the outdoor air density, calculated via the psychometric Type33e;
- The constant value 107.80 is the experimental supply air volumetric flowrate when the return air fan velocity is equal to 50% (fault-free scenario) and the supply air fan velocity is equal to 0% (faulty scenario);
- Density_SA_kg_m3 is the supply air density, calculated via the psychometric Type33e;
- The constant value 18.20 is the experimental exhaust air volumetric flowrate when the return air fan velocity is equal to 50% (fault-free scenario) and the supply air fan velocity is equal to 100% (faulty scenario);
- The constant value 1149.68 is the experimental return air volumetric flowrate when the return air fan velocity is equal to 100% (faulty scenario) and the supply air fan velocity is equal to 50% (fault-free scenario);
- The constant value 0 is the experimental outdoor air volumetric flowrate when the return air fan velocity is equal to 100% (faulty scenario) and the supply air fan velocity is equal to 50% (fault-free scenario);
- The constant value 673.28 is the experimental supply air volumetric flowrate when the return air fan velocity is equal to 100% (faulty scenario) and the supply air fan velocity is equal to 50% (fault-free scenario).

The Recirculation Air mass flowrate (m_Recirc) is calculated as the difference between m_RA and m_EA.

1.7 Outdoor Air Damper (DOA) - Calculator

Outdoor Air Damper (DOA) is modelled by using a calculator and not a specific type. Tables 8a and b illustrate the inputs and outputs of outdoor air damper calculator, respectively.

Table 8a. Inputs of DOA Calculator.

INPUTS	
LIST OF INPUTS	INPUTS USED
Inlet Air Temperature	Outdoor Air Temperature - T_OA (output Type 15-3)
Inlet Air % Relative Humidity	Outdoor Air Relative Humidity - RH_OA (output Type 15-3)
Inlet Flowrate	Outdoor Air mass flowrate - m_OA

Finanziato dall'Unione europea NextGenerationEU | Ministero dell'Università e della Ricerca | Italiadomani PIANO NAZIONALE DI RIPRESA E RESILIENZA

Inlet Air Pressure	Outdoor Air Pressure inlet the DOA - p_A_in_DOA (output Type 15-3)
Air Density	Outdoor Air Density (output Type 33e)

Table 8b. Outputs of DOA Calculator.

OUTPUTS	
LIST OF OUTPUTS	OUTPUTS USED
Outlet Air Temperature	Outdoor Air Temperature - T_OA
Outlet Air % Relative Humidity	Outdoor Air Relative Humidity - RH_OA
Outlet Air Flowrate	Outdoor Air mass flowrate - m_OA
Outlet Air Pressure	Outdoor Air Pressure outlet the DOA - p_A_out_DOA
Outlet Air Pressure Drop	Outdoor air pressure difference outlet the DOA - Dp_A_DOA

The Outdoor Air mass flowrate (m_OA) is defined according to Eq. 4, based on experimental data.

$$\begin{aligned} m\_OA = &((645.01*Density\_SA\_kg\_m3+155.70*Density\_EA\_kg\_m3)– \\ &751.04*Density\_RA\_kg\_m3)*(eql(Set\_OL\_SAF,5)*eql(Set\_OL\_RAF,5)) \\ &+(252.69*Density\_OA\_kg\_m3)*(eql(Set\_OL\_SAF,5)*eql(Set\_OL\_RAF,0)) \\ &+(0*Density\_OA\_kg\_m3)*(eql(Set\_OL\_SAF,0)*eql(Set\_OL\_RAF,5)) \\ &+((1546.25*Density\_SA\_kg\_m3+18.20*Density\_EA\_kg\_m3)– \\ &682.12*Density\_RA\_kg\_m3)*(eql(Set\_OL\_SAF,10)*eql(Set\_OL\_RAF,5)) \\ &+(0*Density\_OA\_kg\_m3)*(eql(Set\_OL\_SAF,5)*eql(Set\_OL\_RAF,10)) \end{aligned} \quad (4)$$

Where:

- The constant value 645.01 is the experimental supply air volumetric flowrate, when the return air fan velocity and the supply air fan velocity is equal to 50% (fault-free scenario);
- Density_SA_kg_m3 is the supply air density, calculated via the psychometric Type33e;
- The constant value 155.70is the experimental exhaust air volumetric flowrate, when the return air fan velocity and the supply air fan velocity is equal to 50% (fault-free scenario);
- Density_EA_kg_m3 is the exhaust air density, calculated via the psychometric Type33e;
- The constant value 751.04 is the experimental return air volumetric flowrate, when the return air fan velocity and the supply air fan velocity is equal to 50% (fault-free scenario);
- Density_RA_kh_m3 is the return air density, calculated via the psychometric Type33e;
- Set_OL_SAF is the supply air fan velocity;
- Set_OL_RAF is the return air fan velocity;
- The constant value 252.69 is the experimental outdoor air volumetric flowrate when the return air fan velocity is equal to 0% (faulty scenario) and the supply air fan velocity is equal to 50% (fault-free scenario);
- Density_OA_kg_m3 is the outdoor air density, calculated via the psychometric Type33e;
- The constant value 0 is the experimental outdoor air volumetric flowrate when the return air fan velocity is equal to 50% (fault-free scenario) and the supply air fan velocity is equal to 0% (faulty scenario);
- The constant value 1546.25 is the experimental supply air volumetric flowrate when the return air fan velocity is equal to 50% (fault-free scenario) and the supply air fan velocity is equal to 100% (faulty scenario);
- The constant value 18.20 is the experimental exhaust air volumetric flowrate when the return air fan velocity is equal to 50% (fault-free scenario) and the supply air fan velocity is equal to 100% (faulty scenario);
- The constant value 682.12 is the experimental return air volumetric flowrate when the return air fan velocity is equal to 50% (fault-free scenario) and the supply air fan velocity is equal to 100% (faulty scenario);

Finanziato dall'Unione europea NextGenerationEU | Ministero dell'Università e della Ricerca | Italiadomani PIANO NAZIONALE DI RIPRESA E RESILIENZA

- The constant value 0 is the experimental outdoor air volumetric flowrate when the return air fan velocity is equal to 100% (faulty scenario) and the supply air fan velocity is equal to 50% (fault-free scenario).

1.8 Outdoor Air Filter (FOA) - Calculator

Outdoor Air Filter (FOA) is modelled by using a calculator and not a specific type. Tables 9a and b illustrate the inputs and outputs of outdoor ai filter calculator, respectively.

Table 9a. Inputs of FOA Calculator.

INPUTS	
LIST OF INPUTS	INPUTS USED
Inlet Air Temperature	Outdoor Air Temperature - T_OA (output DOA Calculator)
Inlet Air % Relative Humidity	Outdoor Air Relative Humidity - RH_OA (output DOA Calculator)
Inlet Flowrate	Outdoor Air mass flowrate - m_OA (output DOA Calculator)
Inlet Air Pressure	Outdoor Air Pressure inlet the FOA - p_A_in_FOA

Table 9b. Outputs of FOA Calculator.

OUTPUTS	
LIST OF OUTPUTS	OUTPUTS USED
Outlet Air Temperature	Outdoor Air Temperature - T_OA
Outlet Air % Relative Humidity	Outdoor Air Relative Humidity - RH_OA
Outlet Air Flowrate	Outdoor Air mass flowrate - m_OA
Outlet Air Pressure	Outdoor Air Pressure outlet the FOA - p_A_out_FOA
Outlet Air Pressure Drop	Outdoor air pressure difference outlet the FOA - Dp_A_FOA

1.9 Heat Recovery System (HRS) - Type 667b

The Heat Recovery System (HRS) is modelled by the Type 667b. Fig. 3 reports the HRS type parameters.

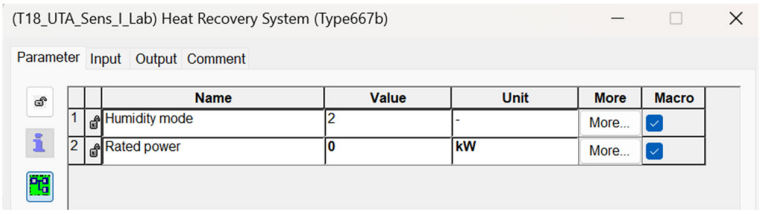

Figure 3. Parameters of HRS Type.

This component is disabled, therefore the Rated power parameter is set equal to 0.
Table 8a and b illustrate the inputs and outputs of heat recovery system type, respectively.

Table 8a. Inputs of HRS Type.

INPUTS	
LIST OF INPUTS	INPUTS USED
Exhaust air temperature	Return Air Temperature - T_RA (output FRA Calculator)
Exhaust Air Humidity Ratio	-
Exhaust air %RH	Return Air Relative Humidity - RH_RA (output FRA Calculator)
Exhaust air flow rate	Return Air mass flowrate - m_RA (output FRA Calculator)

Finanziato dall'Unione europea NextGenerationEU
Ministero dell'Università e della Ricerca
Italiadomani PIANO NAZIONALE DI RIPRESA E RESILIENZA

Exhaust air pressure	Return Air Pressure outlet the DRA - p_A_out_DRA (output DRA, DEA Calculator)
Exhaust air pressure drop	0.000474 (constant value)
Fresh air temperature	Outdoor Air Temperature - T_OA (output FOA Calculator)
Fresh Air Humidity Ratio	-
Fresh air %RH	Outdoor Air Relative Humidity - RH_OA (output FOA Calculator)
Fresh air flow rate	Outdoor Air mass flowrate - m_OA (output FOA Calculator)
Fresh air pressure	Outdoor Air Pressure outlet the FOA - p_A_out_FOA (output FOA Calculator)
Fresh air pressure drop	0.000464 (constant value)
Sensible effectiveness	0.7481 (constant value)
Latent effectiveness	0.794 (constant value)
On/Off Control Signal	Opening percentage of HRS damper - Set_OP_DHRS

Table 8b. Outputs of HRS Type.

OUTPUTS	
LIST OF OUTPUTS	OUTPUTS USED
Fresh air temperature	Outdoor Air Temperature - T_OA
Fresh air %RH	Outdoor Air Relative Humidity - RH_OA
Fresh air flow rate	Outdoor Air mass flowrate - m_OA
Fresh air pressure	Outdoor Air Pressure outlet the FOA - p_A_out_FOA

1.10 Mixing Chamber - Type 648

The mixing chamber is modelled by the Type 648. Fig. 4 illustrates the mixing chamber parameters.

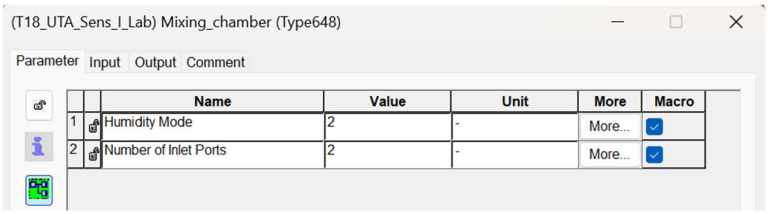

Figure 4. Parameters of Mixing Chamber Type.

Tables 9a and b illustrate the inputs and outputs of mixing chamber type, respectively.

Table 9a. Inputs of Mixing Chamber Type.

INPUTS	
LIST OF INPUTS	INPUTS USED
Inlet Air Temperature-1	Outdoor Air Temperature - T_OA (output Type 667b)
Inlet Air Humidity Ratio-1	-
Inlet Air % Relative Humidity-1	Outdoor Air Relative Humidity - RH_OA (output Type 667b)
Inlet Air Flowrate-1	Outdoor Air mass flowrate - m_OA (output Type 667b)
Inlet Air Pressure-1	Outdoor air pressure outlet the FOA - p_A_out_FOA (output Type 667b)
Inlet Air Temperature-2	Return Air Temperature - T_RA (output DEA, DRA Calculator)
Inlet Air Humidity Ratio-2	-

Finanziato dall'Unione europea NextGenerationEU
Ministero dell'Università e della Ricerca
Italiadomani PIANO NAZIONALE DI RIPRESA E RESILIENZA

Inlet Air % Relative Humidity-2	Return Air Relative Humidity - RH_RA (output DEA, DRA Calculator)
Inlet Air Flowrate-2	Return Air mass flowrate - m_RA (output DEA, DRA Calculator)
Inlet Air Pressure-2	Return Air pressure outlet the DRA - p_A_out_DRA (output DEA, DRA Calculator)
Air-Side Pressure Drop	0 atm (constant value)

Table 9b. Outputs of Mixing Chamber Type.

OUTPUTS	
LIST OF OUTPUTS	OUTPUTS USED
Outlet Air Temperature	Mixed Air Temperature - T_MA
Outlet Air % Relative Humidity	Mixed Air Relative Humidity - RH_MA
Outlet Air Flowrate	Mixed Air mass flowrate - m_MA
Outlet Air Pressure	Mixed air pressure - p_A_out_MA

1.11 Supply Air Filter (FSA) - Calculator

The Supply Air Filter (FSA) is modelled by using a calculator and not a specific type. Tables 10a and b illustrate the inputs and outputs of supply air filter calculator, respectively.

Table 10a. Inputs of FSA Calculator.

INPUTS	
LIST OF INPUTS	INPUTS USED
Inlet Air Temperature	Mixed Air Temperature - T_MA (output Type 648)
Inlet Air % Relative Humidity	Mixed Air Relative Humidity - RH_MA (output Type 648)
Inlet Air Flowrate	Mixed Air mass flowrate - m_MA (output Type 648)
Inlet Air Pressure	Mixed air pressure - p_A_in_FSA (output Type 648)

Table 10b. Outputs of FSA Calculator.

OUTPUTS	
LIST OF OUTPUTS	OUTPUTS USED
Outlet Air Temperature	Mixed Air Temperature - T_MA
Outlet Air % Relative Humidity	Mixed Air Relative Humidity - RH_MA
Outlet Air Flowrate	Mixed Air mass flowrate - m_MA
Outlet Air Pressure	Mixed air pressure - p_A_out_FSA
Outlet Air Pressure Drop	Mixed air pressure difference outlet the FSA - Dp_A_FSA

1.12 Refrigerating System (RS) - Type 941

The Refrigerating System (RS) is modelled by using the Type 941. Fig. 5 reports parameters of refrigerating system type.

Finanziato dall'Unione europea NextGenerationEU | Ministero dell'Università e della Ricerca | Italiadomani PIANO NAZIONALE DI RIPRESA E RESILIENZA

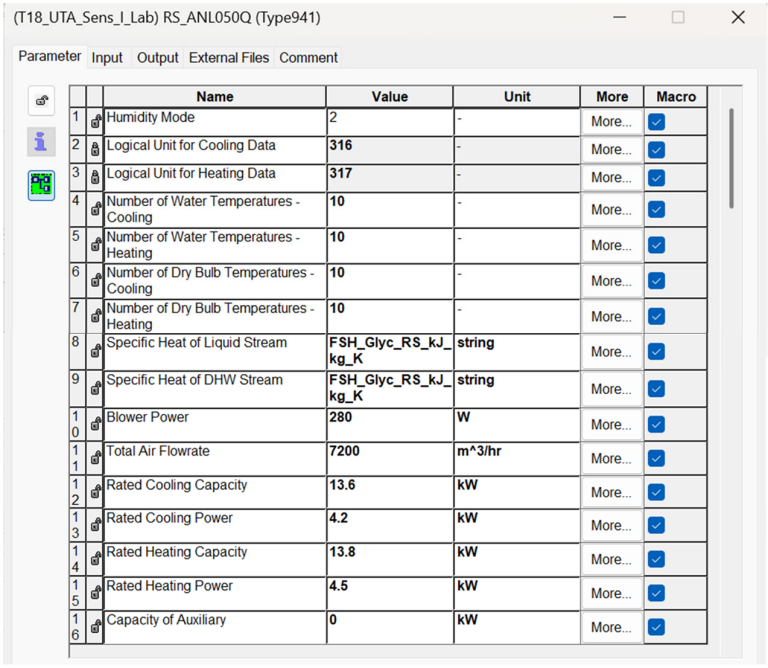

	Name	Value	Unit	More	Macro
1	Humidity Mode	2	-	More...	☑
2	Logical Unit for Cooling Data	316	-	More...	☑
3	Logical Unit for Heating Data	317	-	More...	☑
4	Number of Water Temperatures - Cooling	10	-	More...	☑
5	Number of Water Temperatures - Heating	10	-	More...	☑
6	Number of Dry Bulb Temperatures - Cooling	10	-	More...	☑
7	Number of Dry Bulb Temperatures - Heating	10	-	More...	☑
8	Specific Heat of Liquid Stream	FSH_Glyc_RS_kJ_kg_K	string	More...	☑
9	Specific Heat of DHW Stream	FSH_Glyc_RS_kJ_kg_K	string	More...	☑
10	Blower Power	280	W	More...	☑
11	Total Air Flowrate	7200	m^3/hr	More...	☑
12	Rated Cooling Capacity	13.6	kW	More...	☑
13	Rated Cooling Power	4.2	kW	More...	☑
14	Rated Heating Capacity	13.8	kW	More...	☑
15	Rated Heating Power	4.5	kW	More...	☑
16	Capacity of Auxiliary	0	kW	More...	☑

Figure 5 . Parameters of RS Type.

Tables 11a and b illustrate the inputs and outputs of refrigerating system type, respectively.

Table 11a. Inputs of RS Type.

INPUTS	
LIST OF INPUTS	INPUTS USED
Inlet Liquid Temperature	Inlet Fluid Temperature - T_F_in_RS (output Type 742)
Inlet Liquid Flowrate	Fluid mass flowrate - m_PRS (output Type 742)
Inlet Air Temperature	Outdoor Air Temperature - T_OA (output Type 15-3)
Inlet Air Humidity Ratio	-
Inlet Air % Relative Humidity	Outdoor Air Relative Humidity - RH_OA (output Type 15-3)
Inlet Air Pressure	Outdoor air pressure (output Type 15-3)
Air pressure rise across heat pump	2 atm (constant value)
Cooling Control Signal	1 - Ctrl_RS_sign_ON_OFF (output Ctrl_RS Calculator)
Heating Control Signal	0 (constant value)
Auxiliary Signal	0 (constant value)
Inlet DHW Temperature	20 °C (constant value)
DHW Flowrate	0 kJ/h (constant value)
Desuperheater Temperature - Cooling Mode	20 °C (constant value)
Desuperheater Temperature - Heating Mode	20 °C (constant value)
Desuperheater UA - Cooling Mode	0 kJ/hK (constant value)
Desuperheater UA - Heating Mode	0 kJ/hK (constant value)
Compressor Loss Fraction	0.1 (constant value)

Table 11b. Outputs of RS Type.

OUTPUTS	
LIST OF OUTPUTS	OUTPUTS USED

Finanziato dall'Unione europea NextGenerationEU
Ministero dell'Università e della Ricerca
Italiadomani PIANO NAZIONALE DI RIPRESA E RESILIENZA

Exiting Fluid Temperature	Outlet Fluid Temperature - T_F_out_RS
Exiting Fluid Flowrate	Fluid mass flowrate - m_PRS
Heat Pump Power	Electric Power EP_RS

This type required as an external file the performance map of the refrigerating systems. This map, derived from the manufacturers' manual, has been changed according to the real performance of the experimental set-up.

1.13 Refrigerating System Tank (RS Tank) - Type 1534

The Refrigerating System Tank (RS Tank) is modelled by using the Type 1534. Fig. 6 reports the parameters of RS Tank type defined in the required external file.

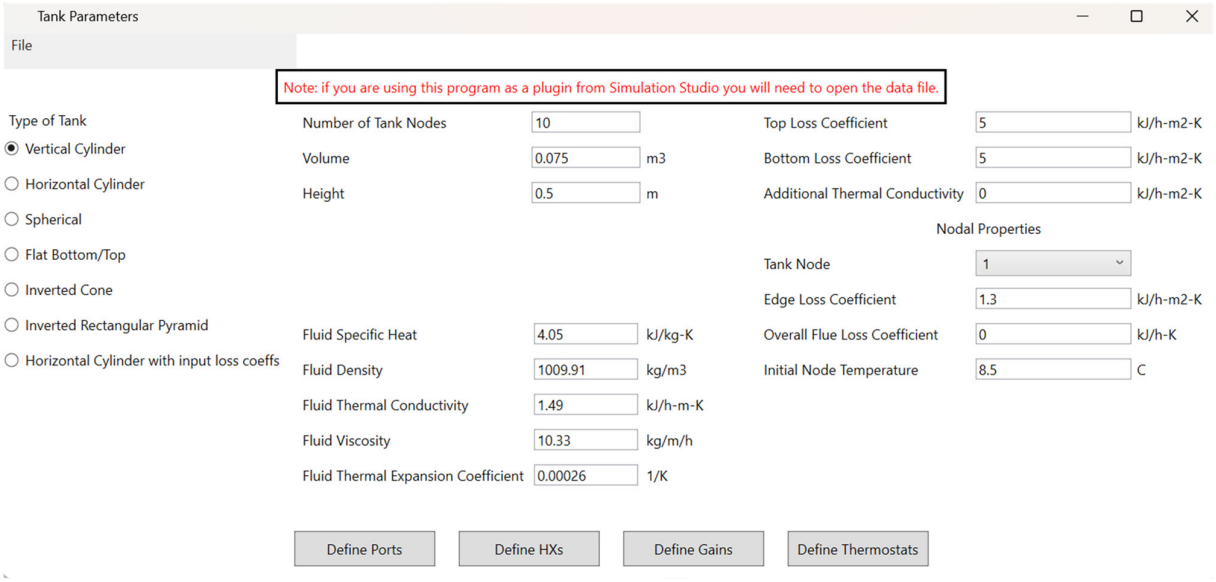

Figure 6 . RS Tank parameters.

Table 12a and b illustrate the inputs and outputs of refrigerating system's tank type, respectively.

Table 12a. Inputs of RS Tank Type.

INPUTS	
LIST OF INPUTS	INPUTS USED
Inlet Temperature for Port	Outlet Fluid Temperature - T_F_out_RS (output Type 941)
Inlet Flowrate for Port	Fluid mass flowrate - m_PRS (output Type 941)
Top Loss Temperature	Outdoor Air Temperature - T_OA (output Type 15-3)
Edge Loss Temperature for Node-1	Outdoor Air Temperature - T_OA (output Type 15-3)
Edge Loss Temperature for Node-2	Outdoor Air Temperature - T_OA (output Type 15-3)
Edge Loss Temperature for Node-3	Outdoor Air Temperature - T_OA (output Type 15-3)
Edge Loss Temperature for Node-4	Outdoor Air Temperature - T_OA (output Type 15-3)
Edge Loss Temperature for Node-5	Outdoor Air Temperature - T_OA (output Type 15-3)
Edge Loss Temperature for Node-6	Outdoor Air Temperature - T_OA (output Type 15-3)
Edge Loss Temperature for Node-7	Outdoor Air Temperature - T_OA (output Type 15-3)
Edge Loss Temperature for Node-8	Outdoor Air Temperature - T_OA (output Type 15-3)
Edge Loss Temperature for Node-9	Outdoor Air Temperature - T_OA (output Type 15-3)
Edge Loss Temperature for Node-10	Outdoor Air Temperature - T_OA (output Type 15-3)
Bottom Loss Temperature	Outdoor Air Temperature - T_OA (output Type 15-3)

Finanziato dall'Unione europea NextGenerationEU
Ministero dell'Università e della Ricerca
Italiadomani PIANO NAZIONALE DI RIPRESA E RESILIENZA

Gas Flue Temperature	20 °C (constant value)
Inversion Mixing Flowrate	-100 kJ/hK (constant value)
Auxiliary Heat Input for Node-1	0 kJ/h (constant value)
Auxiliary Heat Input for Node-2	0 kJ/h (constant value)
Auxiliary Heat Input for Node-3	0 kJ/h (constant value)
Auxiliary Heat Input for Node-4	0 kJ/h (constant value)
Auxiliary Heat Input for Node-5	0 kJ/h (constant value)
Auxiliary Heat Input for Node-6	0 kJ/h (constant value)
Auxiliary Heat Input for Node-7	0 kJ/h (constant value)
Auxiliary Heat Input for Node-8	0 kJ/h (constant value)
Auxiliary Heat Input for Node-9	0 kJ/h (constant value)
Auxiliary Heat Input for Node-10	0 kJ/h (constant value)

Table 12b. Outputs of RS Tank Type.

OUTPUTS	
LIST OF OUTPUTS	OUTPUTS USED
Temperature at Outlet	Outlet Fluid Temperature - T_F_out_RS
Flowrate at Outlet	Fluid mass flowrate - m_PRS

1.14 Refrigerating System Recirculation Pump (Pump RS) - Type 742

The Refrigerating System Recirculation Pump (Pump RS) is modelled by using the Type 742. Fig. 7 reports the parameters of Pump RS type.

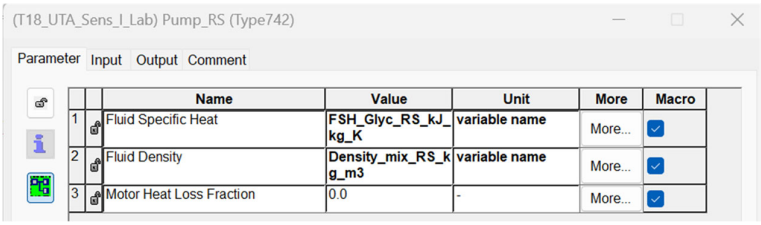

Figure 7. Parameters of Pump RS Type.

The fluid specific heat and the fluid density are parameters recalled from the calculator named "Water_Glycol_Properties" where are defined the fluid specific heat and the fluid density of the glycol mixture according to the manufacturers' data.

Tables 13a and b illustrate the inputs and outputs of refrigerating system's recirculation pump type, respectively.

Table 13a. Inputs of Pump RS Type.

INPUTS	
LIST OF INPUTS	INPUTS USED
Inlet Fluid Temperature	Inlet Fluid Temperature (output Type 31)
Inlet Fluid Flowrate	Fluid mass flowrate - m_PRS (constant value)
Overall Pump Efficiency	0.0277 (constant value)
Motor Efficiency	1 (constant value)
Pressure Drop	10 kPa (constant value)

Table 13b. Outputs of Pump RS Type.

Finanziato dall'Unione europea NextGenerationEU | Ministero dell'Università e della Ricerca | Italiadomani PIANO NAZIONALE DI RIPRESA E RESILIENZA

OUTPUTS	
LIST OF OUTPUTS	OUTPUTS USED
Outlet Fluid Flowrate	Fluid mass flowrate - m_PRS (constant value)

The electric power consumption of the recirculation pump is equal to 0.780 kW defined according to the experimental data.

1.15 Pipe Refrigerating System to Cooling Coil (RS to CC) - Type 31

The Pipe RS to CC is modelled by using the Type 31. Fig. 8 reports parameters of pipe type.

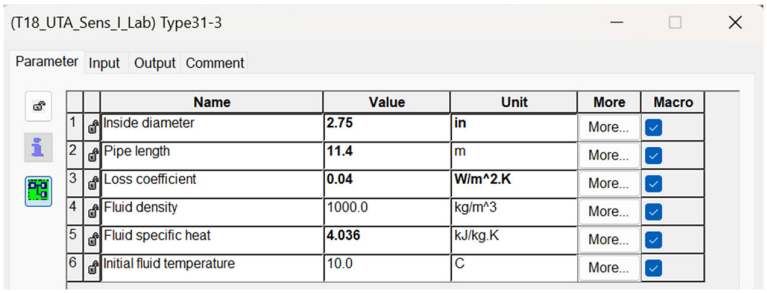

Figure 8. Parameters of Pipe RS to CC.

Table 14a and b illustrate the inputs and outputs of the pipe type, respectively.

Table 14a. Inputs of Pipe RS to CC Type.

INPUTS	
LIST OF INPUTS	INPUTS USED
Inlet temperature	Inlet Fluid Temperature - T_F_out_RS (output Type 1534)
Inlet flow rate	Fluid mass flowrate - m_PRS (output Type 1534)
Environment temperature	Outdoor Air Temperature - T_OA (output Type 15-3)

Table 14b. Outputs of Pipe RS to CC Type.

OUTPUTS	
LIST OF OUTPUTS	OUTPUTS USED
Outlet temperature	Outlet Fluid Temperature - T_F_out_RS
Outlet flow rate	Experimental Fluid mass flowrate - m_PRS

1.16 Three-way flow diverter valve Cooling Coil (CC) - Type 647

The three-way flow diverter valve CC is modelled by the Type 647. Fig. 9 reports the parameters of the three-way valve type.

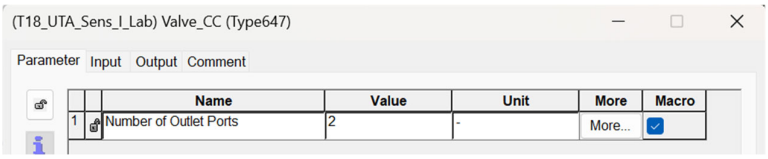

Figure 9. Three-way flow diverter valve CC parameters.

Table 15a and b illustrate the inputs and outputs of the three-way flow diverter valve CC type.

Table 15a. Inputs of Three-way flow diverter valve CC Type.

INPUTS

Finanziato dall'Unione europea NextGenerationEU
Ministero dell'Università e della Ricerca
Italiadomani PIANO NAZIONALE DI RIPRESA E RESILIENZA

LIST OF INPUTS	INPUTS USED
Inlet Temperature	Fluid Temperature - T_F_in_CC (output Type 31)
Inlet Flowrate	Fluid mass flowrate - m_F_in_CC (output Type 31)
Fraction of Flow to Outlet -1	Fraction of Flow to CC (output CC_Operation Calculator)
Fraction of Flow to Outlet -2_CC	Fraction of Flow to RS (output CC_Operation Calculator)

Table 15b. Outputs of Three-way flow diverter valve CC Type.

OUTPUTS	
LIST OF OUTPUTS	OUTPUTS USED
Outlet Temperature-1	Fluid Temperature - T_F_in_CC
Outlet Flowrate-1	Fluid mass flowrate - m_F_in_CC
Outlet Temperature-2	Outlet Fluid Temperature to RS
Outlet Flowrate-2	Outlet Fluid mass flowrate to RS

The inputs Fraction of Flow to CC and Fraction of Flow to RS are defined as function of the opening percentage of Cooling coil valve, in the calculator named "CC_Operation".

1.17 Cooling Coil (CC) - Type 508c

The Cooling Coil CC is modelled by the Type 508c. Fig. 10 reports the parameters of cooling coil type.

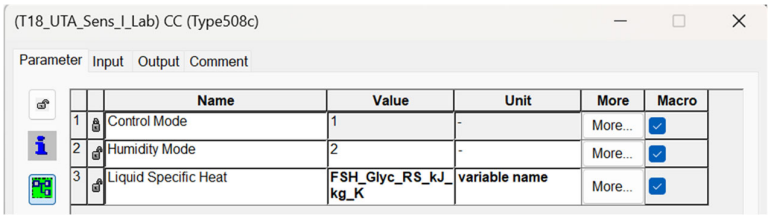

Figure 10. Parameters of CC Type.

The liquid specific heat is a parameter recalled from the calculator named "Water_Glycol_Properties" where fluid specific heat of the glycol mixture is defined according to the manufacturers' data.
Table 16a and b illustrate the inputs and outputs of the cooling coil type, respectively.

Table 16a. Inputs of CC Type.

INPUTS	
LIST OF INPUTS	INPUTS USED
Fluid Inlet Temperature	Fluid Temperature - T_F_in_CC (output Type 647)
Fluid Flowrate	Fluid mass flowrate - m_F_in_CC (output Type 647)
Air Inlet Temperature	Mixed Air Temperature - T_MA (output FSA Calculator)
Air Humidity Ratio	-
Air % Relative Humidity	Mixed Air Relative Humidity - RH_MA (output FSA Calculator)
Air Flowrate	Mixed Air mass flowrate - m_MA (output FSA Calculator)
Air Pressure	Mixed air pressure outlet the SAF - p_A_out_FSA (output FSA Calculator)
Air-Side Pressure Drop	0.0001756 atm (constant value)
Coil Bypass Fraction	Cooling Coil Bypass Fraction BF_CC (output CC_BFactor Calculator)
Setpoint: Outlet Air Temperature	0 °C (constant value)

Finanziato dall'Unione europea NextGenerationEU
Ministero dell'Università e della Ricerca
Italiadomani PIANO NAZIONALE DI RIPRESA E RESILIENZA

Table 16b. Outputs of CC Type.

OUTPUTS	
LIST OF OUTPUTS	OUTPUTS USED
Fluid Outlet Temperature	Fluid Outlet Temperature - T_F_out_CC
Outlet Fluid Flowrate	Fluid mass flowrate - m_F_in_CC
Outlet Air Temperature	Outlet Air Temperature - T_A_out_CC
Outlet Air % Relative Humidity	Outlet Air Relative Humidity - RH_A_out_CC
Outlet Air Pressure	Air pressure outlet the CC - p_A_out_CC

The cooling coil bypass fraction is calculated according to the following Eq. 5, as function of return and supply air fan operating conditions:

$$BF\_CC = 0.330*(eql(Set\_OL\_SAF,5)*eql(Set\_OL\_RAF,5))+ 0.268*(eql(Set\_OL\_SAF,5)*eql(Set\_OL\_RAF,0))+ 0.34*(eql(Set\_OL\_SAF,0)*eql(Set\_OL\_RAF,5)) \quad (5)$$

Where:

- The constant value 0.330 is the experimental cooling coil bypass fraction when the return air fan velocity and the supply air fan velocity is equal to 50% (fault-free scenario);
- Set_OL_SAF is the experimental supply air fan velocity;
- Set_OL_RAF is the experimental return air fan velocity;
- The constant value 0.268 is the experimental cooling coil bypass fraction when the return air fan velocity is equal to 0% (faulty scenario) and the supply air fan velocity is equal to 50% (fault-free scenario);
- The constant value 0.34 is the experimental cooling coil bypass fraction when the return air fan velocity is equal to 50% (fault-free scenario) and the supply air fan velocity is equal to 0% (faulty scenario).

1.18 Three-way mixing valve Cooling Coil to Refrigerating System (CC to RS) - Type 649

The three-way mixing valve CC to RS is modelled by the Type 649. Fig. 11 reports the parameters of the three-way valve CC to RS.

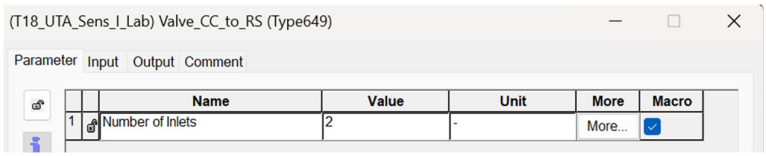

Figure 11. Parameters of Three-way mixing valve CC to RS.

Tables 17a and b illustrate the inputs and outputs of the three-way valve CC to RS, respectively.

Table 17a. Inputs of Three-way mixing valve CC to RS Type.

INPUTS	
LIST OF INPUTS	INPUTS USED
Temperature at Inlet-1	Fluid Outlet Temperature - T_F_out_CC (output Type 508c)
Flowrate at Inlet-1	Experimental Fluid mass flowrate - m_F_in_CC (output Type 508c)
Temperature at Inlet-2_CC	Fluid Temperature to RS (output Type 647)
Flowrate at Inlet-2_CC	Fluid Flowrate to RS (output Type 647)

Table 17b. Outputs of Three-way mixing valve CC to RS Type.

Finanziato dall'Unione europea NextGenerationEU
Ministero dell'Università e della Ricerca
Italiadomani PIANO NAZIONALE DI RIPRESA E RESILIENZA

OUTPUTS	
LIST OF OUTPUTS	OUTPUTS USED
Outlet Temperature	Outlet Fluid Temperature
Outlet Flowrate	Outlet Fluid Flowrate

1.19 Pipe Cooling Coil to Refrigerating System (CC to RS) - Type 31

The Pipe CC to RS is modelled by using the Type 31. Fig. 12 reports the parameters of the pipe type.

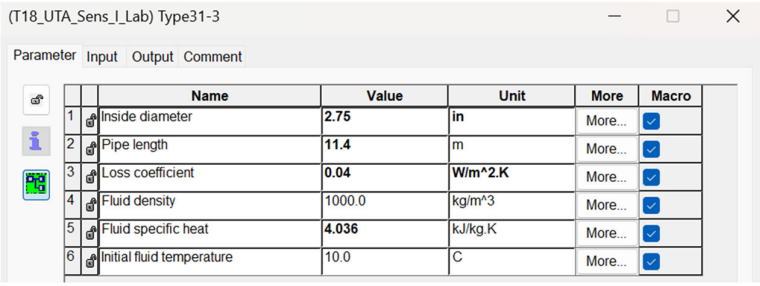

Figure 12. Parameters of Pipe CC to RS.

Tables 18a and b illustrate the inputs and outputs of the pipe CC to RS type.

Table 18a. Inputs of Pipe CC to RS Type.

INPUTS	
LIST OF INPUTS	INPUTS USED
Inlet temperature	Inlet Fluid Temperature (output Type 649)
Inlet flow rate	Inlet Fluid Flowrate (output Type 649)
Environment temperature	Outdoor Air Temperature - T_OA (output Type 15-3)

Table 18b. Outputs of Pipe CC to RS Type.

OUTPUTS	
LIST OF OUTPUTS	OUTPUTS USED
Outlet Temperature	Outlet Fluid Temperature

1.20 Heat Pump (HP) -Type 941

The Heat Pump (HP) is modelled by using the Type 941. Fig. 13 reports the parameters of HP type.

Finanziato dall'Unione europea NextGenerationEU
Ministero dell'Università e della Ricerca
Italiadomani PIANO NAZIONALE DI RIPRESA E RESILIENZA

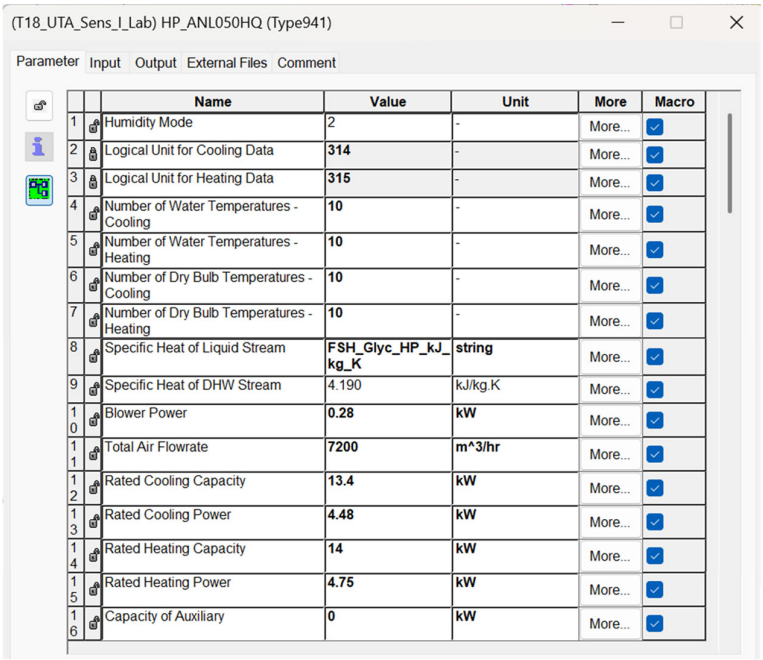

	Name	Value	Unit	More	Macro
1	Humidity Mode	2	-	More...	☑
2	Logical Unit for Cooling Data	314	-	More...	☑
3	Logical Unit for Heating Data	315	-	More...	☑
4	Number of Water Temperatures - Cooling	10	-	More...	☑
5	Number of Water Temperatures - Heating	10	-	More...	☑
6	Number of Dry Bulb Temperatures - Cooling	10	-	More...	☑
7	Number of Dry Bulb Temperatures - Heating	10	-	More...	☑
8	Specific Heat of Liquid Stream	FSH_Glyc_HP_kJ_kg_K	string	More...	☑
9	Specific Heat of DHW Stream	4.190	kJ/kg.K	More...	☑
10	Blower Power	0.28	kW	More...	☑
11	Total Air Flowrate	7200	m^3/hr	More...	☑
12	Rated Cooling Capacity	13.4	kW	More...	☑
13	Rated Cooling Power	4.48	kW	More...	☑
14	Rated Heating Capacity	14	kW	More...	☑
15	Rated Heating Power	4.75	kW	More...	☑
16	Capacity of Auxiliary	0	kW	More...	☑

Figure 13. Parameters of HP Type.

Tables 19a and b illustrates the inputs and outputs of heat pump type, respectively.

Table 19a. Inputs of HP Type.

INPUTS	
LIST OF INPUTS	INPUTS USED
Inlet Liquid Temperature	Inlet Fluid Temperature - T_F_in_HP (output Type 742)
Inlet Liquid Flowrate	Fluid mass flowrate - m_PHP (output Type 742)
Inlet Air Temperature	Outdoor Air Temperature - T_OA (output Type 15-3)
Inlet Air Humidity Ratio	-
Inlet Air % Relative Humidity	Outdoor Air Relative Humidity - RH_OA (output Type 15-3)
Inlet Air Pressure	Outdoor air pressure (output Type 15-3)
Air pressure rise across heat pump	2 atm (constant value)
Cooling Control Signal	0 (constant value)
Heating Control Signal	1 - Ctrl_HP_sign_ON_OFF (output Ctrl_HP Calculator)
Auxiliary Signal	0 (constant value)
Inlet DHW Temperature	20 °C (constant value)
DHW Flowrate	0 kJ/h (constant value)
Desuperheater Temperature - Cooling Mode	20 °C (constant value)
Desuperheater Temperature - Heating Mode	20 °C (constant value)
Desuperheater UA - Cooling Mode	0 kJ/hK (constant value)
Desuperheater UA - Heating Mode	0 kJ/hK (constant value)
Compressor Loss Fraction	0.1 (constant value)

Table 19b. Outputs of HP Type.

OUTPUTS	
LIST OF OUTPUTS	OUTPUTS USED

Finanziato dall'Unione europea NextGenerationEU
Ministero dell'Università e della Ricerca
Italiadomani PIANO NAZIONALE DI RIPRESA E RESILIENZA

Exiting Fluid Temperature	Outlet Fluid Temperature - T_F_out_HP
Exiting Fluid Flowrate	Fluid mass flowrate - m_PHP
Heat Pump Power	Electric Power EP_HP

Outdoor Air pressure is derived from the Type 15-3 taking into account the Energy+ weather data of Naples city.
This type required as an external file the performance map of the refrigerating systems. This map, derived from the manufacturers' manual, has been changed according to the real performance of the experimental set-up.

1.21 Heat Pump Tank (HP Tank) - Type 1534

The Heat Pump Tank (HP Tank) is modelled by using the Type 1534. Fig. 14 reports the parameters of HP Tank type defined in the required external file.

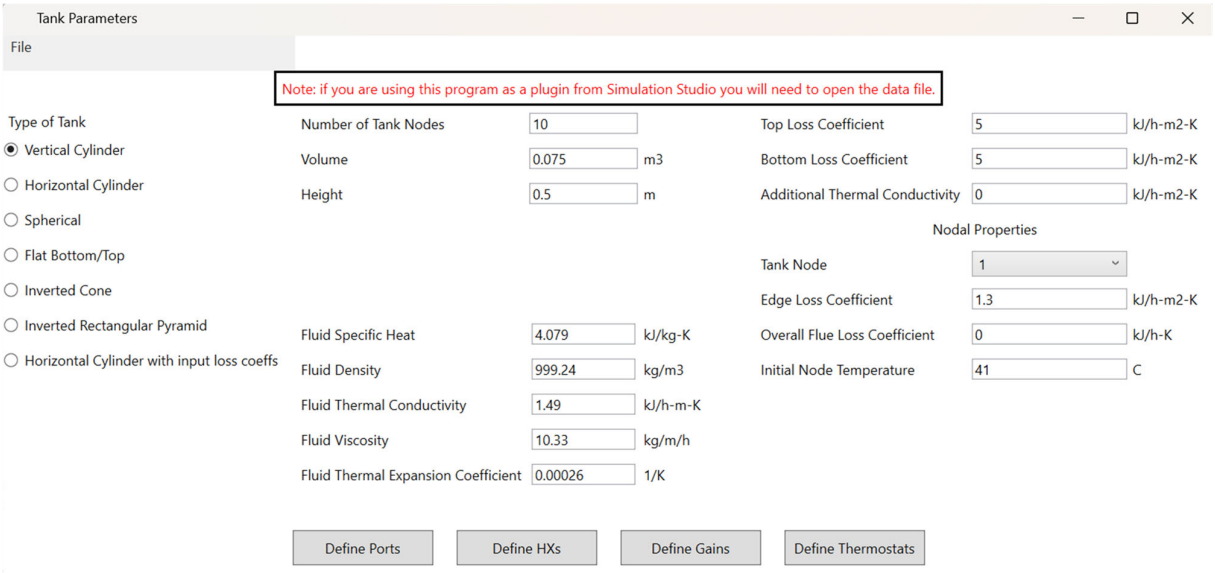

Figure 14 . Parameters of HP Tank Type.

Tables 20a and b illustrate the inputs and outputs of heat pump tank type, respectively.

Table 20a. Inputs of HP Tank Type.

INPUTS	
LIST OF INPUTS	INPUTS USED
Inlet Temperature for Port	Outlet Fluid Temperature - T_F_out_HP (output Type 941)
Inlet Flowrate for Port	Fluid mass flowrate - m_PHP (output Type 941)
Top Loss Temperature	Outdoor Air Temperature - T_OA (output Type 15-3)
Edge Loss Temperature for Node-1	Outdoor Air Temperature - T_OA (output Type 15-3)
Edge Loss Temperature for Node-2	Outdoor Air Temperature - T_OA (output Type 15-3)
Edge Loss Temperature for Node-3	Outdoor Air Temperature - T_OA (output Type 15-3)
Edge Loss Temperature for Node-4	Outdoor Air Temperature - T_OA (output Type 15-3)
Edge Loss Temperature for Node-5	Outdoor Air Temperature - T_OA (output Type 15-3)
Edge Loss Temperature for Node-6	Outdoor Air Temperature - T_OA (output Type 15-3)
Edge Loss Temperature for Node-7	Outdoor Air Temperature - T_OA (output Type 15-3)
Edge Loss Temperature for Node-8	Outdoor Air Temperature - T_OA (output Type 15-3)
Edge Loss Temperature for Node-9	Outdoor Air Temperature - T_OA (output Type 15-3)
Edge Loss Temperature for Node-10	Outdoor Air Temperature - T_OA (output Type 15-3)

Finanziato dall'Unione europea NextGenerationEU
Ministero dell'Università e della Ricerca
Italiadomani PIANO NAZIONALE DI RIPRESA E RESILIENZA

Bottom Loss Temperature	Outdoor Air Temperature - T_OA (output Type 15-3)
Gas Flue Temperature	20 °C (constant value)
Inversion Mixing Flowrate	-100 kJ/hK (constant value)
Auxiliary Heat Input for Node-1	0 kJ/h (constant value)
Auxiliary Heat Input for Node-2	0 kJ/h (constant value)
Auxiliary Heat Input for Node-3	0 kJ/h (constant value)
Auxiliary Heat Input for Node-4	0 kJ/h (constant value)
Auxiliary Heat Input for Node-5	0 kJ/h (constant value)
Auxiliary Heat Input for Node-6	0 kJ/h (constant value)
Auxiliary Heat Input for Node-7	0 kJ/h (constant value)
Auxiliary Heat Input for Node-8	0 kJ/h (constant value)
Auxiliary Heat Input for Node-9	0 kJ/h (constant value)
Auxiliary Heat Input for Node-10	0 kJ/h (constant value)

Table 20b. Outputs of HP Tank Type.

OUTPUTS	
LIST OF OUTPUTS	OUTPUTS USED
Temperature at Outlet	Outlet Fluid Temperature - T_F_out_HP
Flowrate at Outlet	Fluid mass flowrate - m_P HP

1.22 Heat Pump Recirculation Pump (Pump HP) - Type 742

The Heat Pump Recirculation Pump (Pump HP) is modelled by using the Type 742. Fig. 15 reports the parameters of Pump HP type.

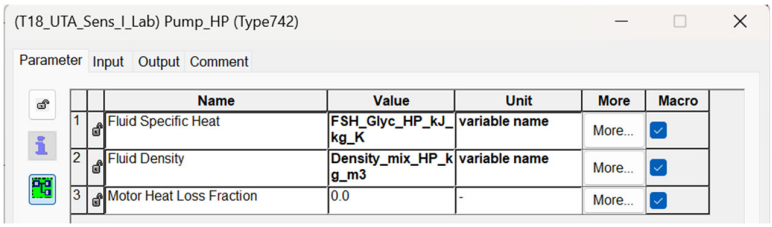

Figure 15. Parameters of Pump HP Type.

The fluid specific heat and the fluid density are parameters recalled from the calculator named "Water_Glycol_Properties" where are defined the fluid specific heat and the fluid density of the glycol mixture according to the manufacturers' data.

Tables 21a and b illustrate the inputs and outputs of heat pump recirculation pump type, respectively.

Table 21a. Inputs of Pump HP Type.

INPUTS	
LIST OF INPUTS	INPUTS USED
Inlet Fluid Temperature	Inlet Fluid Temperature (output Type 31)
Inlet Fluid Flowrate	Fluid mass flowrate - m_PHP (constant value)
Overall Pump Efficiency	0.0277 (constant value)
Motor Efficiency	1 (constant value)
Pressure Drop	10 kPa (constant value)

Table 21b. Outputs of Pump HP Type.

Finanziato dall'Unione europea NextGenerationEU | Ministero dell'Università e della Ricerca | Italiadomani PIANO NAZIONALE DI RIPRESA E RESILIENZA

OUTPUTS	
LIST OF OUTPUTS	OUTPUTS USED
Outlet Fluid Flowrate	Fluid mass flowrate - m_PHP (constant value)

The electric power consumption of the recirculation pump is equal to 0.780 kW defined according to the experimental data.

1.23 Pipe Heat Pump to Post-Heating Coil (HP to PostHC) - Type 31

The Pipe HP to PostHC is modelled by using the Type 31. Fig. 16 reports parameters of the pipe type.

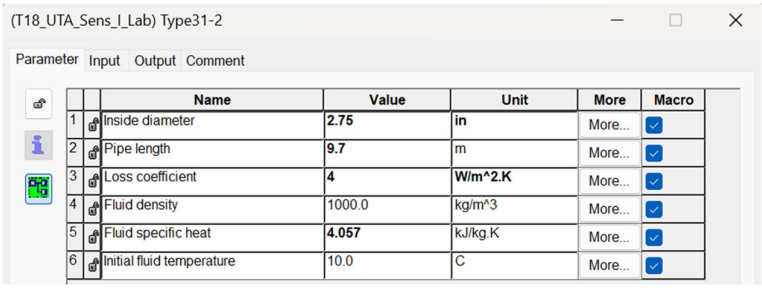

Figure 16. Parameters of Pipe HP to PostHC Type.

Table 22a and b illustrate the inputs and outputs of the pipe HP to PostHC type, respectively.

Table 22a. Inputs of Pipe HP to PostHC Type.

INPUTS	
LIST OF INPUTS	INPUTS USED
Inlet temperature	Inlet Fluid Temperature - T_F_out_HP (output Type 1534)
Inlet flow rate	Fluid mass flowrate - m_PHP (output Type 1534)
Environment temperature	Outdoor Air Temperature - T_OA (output Type 15-3)

Table 22b. Outputs of Pipe HP to PostHC Type.

OUTPUTS	
LIST OF OUTPUTS	OUTPUTS USED
Outlet Temperature	Outlet Fluid Temperature - T_F_out_HP
Outlet Flowrate	Fluid mass flowrate - m_PHP

1.24 Three-way flow diverter valve Post-Heating Coil (PostHC) - Type 647

The three-way flow diverter valve PostHC is modelled by the Type 647. Fig. 17 reports the parameters of the three-way valve type.

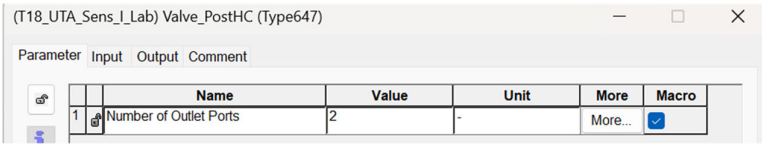

Figure 17. Parameters of Three-way flow diverter valve PostHC.

Tables 23a and b illustrate the inputs and outputs of the three-way flow diverter valve type, respectively.

Table 23a. Inputs of Three-way flow diverter valve PostHC Type.

INPUTS

Finanziato dall'Unione europea NextGenerationEU
Ministero dell'Università e della Ricerca
Italiadomani PIANO NAZIONALE DI RIPRESA E RESILIENZA

LIST OF INPUTS	INPUTS USED
Inlet Temperature	Fluid Temperature - T_F_in_PostHC (output Type 31)
Inlet Flowrate	Fluid mass flowrate - m_F_in_PostHC (output Type 31)
Fraction of Flow to Outlet -1	Fraction of Flow to PostHC (output HC_Operation Calculator)
Fraction of Flow to Outlet -2_CC	Fraction of Flow to HP

Table 23b. Outputs of Three-way flow diverter valve PostHC Type.

OUTPUTS	
LIST OF OUTPUTS	OUTPUTS USED
Outlet Temperature-1	Fluid Temperature - T_F_in_PostHC
Outlet Flowrate-1	Fluid mass flowrate - m_F_in_PostHC
Outlet Temperature-2	Outlet Fluid Temperature to HP
Outlet Flowrate-2	Outlet Fluid mass flowrate to HP

The inputs Fraction of Flow to PostHC and Fraction of Flow to HP are defined as function of the opening percentage of Post-Heating coil valve, in the calculator named "HP_Operation".

1.25 Post-Heating Coil (CC) - Type 753b

The Cooling Coil CC is modelled by the Type 753b. Fig. 18 reports the parameters of pre-heating coil type.

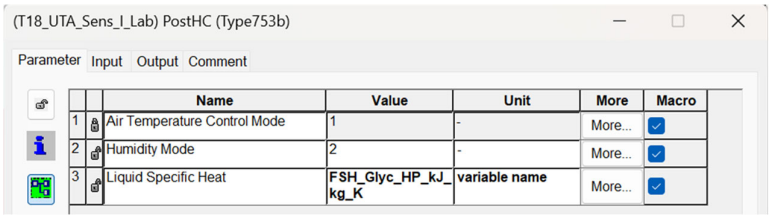

Figure 18. Parameters of PostHC Type.

Table 24a and b illustrate the inputs and outputs of the post-heating coil type, respectively.

Table 24a. Inputs of PostHC Type.

INPUTS	
LIST OF INPUTS	INPUTS USED
Fluid Inlet Temperature	Fluid Temperature - T_F_in_PostHC (output Type 647)
Fluid Flowrate	Fluid mass flowrate - m_F_in_PostHC (output Type 647)
Air Inlet Temperature	Air Temperature - T_A_out_CC (output Type 508c)
Air Humidity Ratio	-
Air % Relative Humidity	Air Relative Humidity - RH_A_out_CC (output Type 508c)
Air Flowrate	Mixed Air mass flowrate - m_A_out_HUM (output HUM Calculator)
Air Pressure	Air pressure outlet the CC - p_A_out_CC (output Type 508c)
Air-Side Pressure Drop	0.00004905 atm (constant value)
Coil Bypass Fraction	Post-Heating Coil Bypass Fraction - BF_HC (output HC_BFactor)
Setpoint: Outlet Air Temperature	100 °C (constant value)

Table 24b. Outputs of PostHC Type.

OUTPUTS

Finanziato dall'Unione europea NextGenerationEU
Ministero dell'Università e della Ricerca
Italiadomani PIANO NAZIONALE DI RIPRESA E RESILIENZA

LIST OF OUTPUTS	OUTPUTS USED
Fluid Outlet Temperature	Fluid Outlet Temperature - T_F_out_PostHC
Outlet Fluid Flowrate	Experimental Fluid mass flowrate - m_F_in_PostHC
Outlet Air Temperature	Outlet Air Temperature - T_A_out_PostHC
Outlet Air % Relative Humidity	Outlet Air Relative Humidity - RH_A_out_PostHC
Outlet Air Pressure	Air pressure outlet the PostHC - p_A_out_PostHC

The post-heating coil bypass fraction is calculated according to the following Eq. 6, as function of return and supply air fan operating conditions:

$$BF\_HC = 0.415*(eql(Set\_OL\_SAF,5)*eql(Set\_OL\_RAF,5))+ 0.46*(eql(Set\_OL\_SAF,5)*eql(Set\_OL\_RAF,0))+ 0.03*(eql(Set\_OL\_SAF,0)*eql(Set\_OL\_RAF,5)) \quad (6)$$

Where:

- The constant value 0.415 is the experimental cooling coil bypass fraction when the return air fan velocity and the supply air fan velocity is equal to 50% (fault-free scenario);
- Set_OL_SAF is the supply air fan velocity;
- Set_OL_RAF is the return air fan velocity;
- The constant value 0.46 is the experimental cooling coil bypass fraction when the return air fan velocity is equal to 0% (faulty scenario) and the supply air fan velocity is equal to 50% (fault-free scenario);
- The constant value 0.03 is the experimental cooling coil bypass fraction when the return air fan velocity is equal to 50% (fault-free scenario) and the supply air fan velocity is equal to 0% (faulty scenario).

1.26 Three-way mixing valve Post-Heating Coil to Heat Pump (PostHC to HP) - Type 649

The three-way mixing valve PostHC to HP is modelled by the Type 649. Fig. 19 reports the parameters of the three-way valve type.

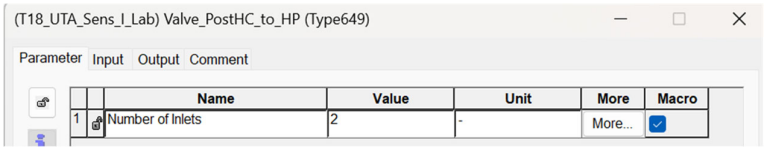

Figure 19. Three-way mixing valve PostHC to HP parameters.

Tables 25a and b illustrate the inputs and outputs of the three-way mixing valve PostHC to HP type.

Table 25a. Inputs of Three-way mixing valve PostHC to HP Type.

INPUTS	
LIST OF INPUTS	INPUTS USED
Temperature at Inlet-1	Fluid Outlet Temperature - T_F_out_PostHC (output Type 753b)
Flowrate at Inlet-1	Fluid mass flowrate - m_F_in_PostHC (output Type 753b)
Temperature at Inlet-2_CC	Fluid Temperature to HP (output Type 647)
Flowrate at Inlet-2_CC	Fluid Flowrate to HP (output Type 647)

Table 25b. Outputs of Three-way mixing valve PostHC to HP Type.

OUTPUTS	
LIST OF OUTPUTS	OUTPUTS USED
Outlet Temperature	Outlet Fluid Temperature

Finanziato dall'Unione europea NextGenerationEU | Ministero dell'Università e della Ricerca | Italiadomani PIANO NAZIONALE DI RIPRESA E RESILIENZA

Outlet Flowrate	Outlet Fluid Flowrate

1.27 Pipe Post-Heating Coil to Heat Pump (PostHC to HP) - Type 31

The Pipe PostHC to HP is modelled by using the Type 31. Fig. 20 reports the parameters of pipe type.

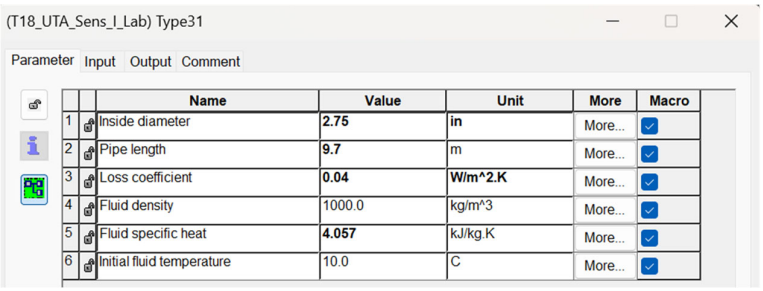

Figure 20. Parameters of Pipe PostHC to HP Type.

Tables 26a and b illustrate the inputs and outputs of the pipe PostHC to HP type, respectively.

Table 26a. Inputs of Pipe PostHC to HP Type.

INPUTS	
LIST OF INPUTS	INPUTS USED
Inlet temperature	Inlet Fluid Temperature (output Type 649)
Inlet flow rate	Inlet Fluid Flowrate (output Type 649)
Environment temperature	Outdoor Air Temperature - T_OA (output Type 15-3)

Table 26b. Outputs of Pipe PostHC to HP Type.

OUTPUTS	
LIST OF OUTPUTS	OUTPUTS USED
Outlet Temperature	Outlet Fluid Temperature

1.28 Humidifier (HUM) - Calculator

The Humidifier (HUM) is modelled by using a calculator and not a specific type. Table 27a and b illustrate the inputs and outputs of the humidifier calculator, respectively.

Table 27a. Inputs of HUM Calculator.

INPUTS	
LIST OF INPUTS	INPUTS USED
Inlet Air Temperature	Inlet Air Temperature - T_A_in_HUM (output Type 508c)
Inlet Air % Relative Humidity	Inlet Air Relative Humidity - RH_A_in_HUM (output Type 508c)
Inlet Air Specific Humidity	Inlet Air Specific Humidity - HR_A_in_HUM (output Type 508c)
Inlet Air Flowrate	Inlet Air Flowrate - m_in_HUM (output Type 508c)
Inlet Air Pressure	Inlet Air Pressure - p_A_in_HUM (output Type 508c)
Control Signal	Ctrl_signal_HUM (output Type 23)

Table 27b. Outputs of HUM Calculator.

OUTPUTS	
LIST OF OUTPUTS	OUTPUTS USED
Outlet Air Temperature	Inlet Air Temperature - T_A_in_HUM

Finanziato dall'Unione europea NextGenerationEU | Ministero dell'Università e della Ricerca | Italiadomani PIANO NAZIONALE DI RIPRESA E RESILIENZA

Outlet Air % Relative Humidity	Inlet Air Relative Humidity - RH_A_in_HUM
Outlet Air Specific Humidity	Outlet Air Specific Humidity - HR_A_out_HUM
Outlet Air Flowrate	Outlet Air mass flowrate - m_out_HUM
Outlet Vapour Flowrate	Outlet Vapour Flowrate - m_vapour_out_HUM
Outlet Air Pressure	Outlet Air Pressure - p_A_out_HUM
	Electric Power - EP_HUM

The vapour mass flowrate m_vapour_HUM is defined according to Eq. 7 according to the manufacturer's manual.

$$\begin{gathered}\text{m\_in\_water\_HUM\_kg\_h} = 0*\text{lt(Ctrl\_HUM,0.05)}+ \\ 1*(\text{ge(Ctrl\_HUM,0.05)}*\text{lt(Ctrl\_HUM,0.1)})+ \\ 5*\text{gt(Ctrl\_HUM,0.95)}+ \\ (4.70588235294118*(\text{Ctrl\_HUM}–0.1)+1)*(\text{ge(Ctrl\_HUM,0.1)}*\text{le(Ctrl\_HUM,0.95)})\end{gathered} \quad (7)$$

Where:

- The constant value 0 represents the kg of steam produced when the humidifier valve is open at 5%;
- Ctrl_HUM is the output of PID type that regulate the opening percentage of humidifier valve;
- The constant value 1 represents the kg of steam produced when the humidifier valve is open between 5-10%;
- The constant value 5 represents the kg of steam produced when the humidifier valve is open at 100%;

The portion of equation (4.70588235294118*(Ctrl_HUM–0.1)+1) represents the kg of steam produced when the humidifier valve is open between 10-95%;

The electric power EP_HUM is calculated according to the Eq.8, based on the manufacturer's manual as well as the experimental data.

$$\begin{gathered}\text{SIM\_EP\_HUM\_kW} = ((\text{ge(Ctrl\_HUM,0)}*\text{le(Ctrl\_HUM,0.05)}*0)+ \\ (\text{gt(Ctrl\_HUM,0.05)}*\text{le(Ctrl\_HUM,0.1)}*65.82)+ \\ (\text{gt(Ctrl\_HUM,0.1)}*\text{le(Ctrl\_HUM,0.95)}*(380.49*\text{Ctrl\_HUM}–314.67))+ \\ (\text{gt(Ctrl\_HUM,0.95)}*\text{le(Ctrl\_HUM,1)}*3300.00))/1000\end{gathered} \quad (8)$$

Where:

- Ctrl_HUM is the output of PID type that regulate the opening percentage of humidifier valve;
- The constant value 65.82 is the experimental electric power demand of the humidifier when the opening percentage of its valve is between 5-10%;
- The portion of equation 380.49*Ctrl_HUM–314.67 is the experimental electric power demand of the humidifier when the opening percentage of its valve is between 10-95%;
- The constant value 3300.00 is the experimental electric power demand of the humidifier when the opening percentage of its valve is 100%.

1.29 Supply Air Fan (SAF) - Calculator

The Supply Air Fan (SAF) is modelled by using a calculator and not a specific type. Tables 28a and b illustrate the inputs and outputs of supply air fan calculator, respectively.

Table 28a. Inputs of SAF Calculator.

INPUTS	
LIST OF INPUTS	INPUTS USED
Inlet Air Temperature	Supply Air Temperature - T_SA (output Type 753b)
Inlet Air % Relative Humidity	Supply Air Relative Humidity - RH_SA (output Type 753b)
Air Flowrate	Supply Air mass flowrate - m_SA (output Type 753b)
Inlet Air Pressure	Air pressure outlet the PostHC - p_A_out_PostHC (output Type 753b)

Finanziato dall'Unione europea NextGenerationEU | Ministero dell'Università e della Ricerca | Italiadomani PIANO NAZIONALE DI RIPRESA E RESILIENZA

Table 28b. Outputs of SAF Calculator.

OUTPUTS	
LIST OF OUTPUTS	OUTPUTS USED
Outlet Air Temperature	Supply Air Temperature - T_SA
Outlet Air % Relative Humidity	Supply Air Relative Humidity - RH_SA
Outlet Air Flowrate	Supply Air mass flowrate - m_SA
Outlet Air Pressure	Air pressure outlet the SAF - p_A_out_SAF
	Electric power EP_SAF

The supply Air mass flowrate (m_SA) is calculated according to the Eq. 9, defined based on experimental data:

$$\begin{aligned} m\_SA = {} & (645.01*Density\_SA\_kg\_m3)*(eql(Set\_OL\_SAF,5)*eql(Set\_OL\_RAF,5))+ \\ & (611.43*Density\_SA\_kg\_m3)*(eql(Set\_OL\_SAF,5)*eql(Set\_OL\_RAF,0))+ \\ & (107.80*Density\_SA\_kg\_m3)*(eql(Set\_OL\_SAF,0)*eql(Set\_OL\_RAF,5))+ \\ & (1546.25*Density\_SA\_kg\_m3)*(eql(Set\_OL\_SAF,10)*eql(Set\_OL\_RAF,5))+ \\ & (673.28*Density\_SA\_kg\_m3)*(eql(Set\_OL\_SAF,5)*eql(Set\_OL\_RAF,10)) \end{aligned} \quad (9)$$

Where:

- The constant value 645.01 is the experimental supply air volumetric flowrate, when the return air fan velocity and the supply air fan velocity is equal to 50% (fault-free scenario);
- Density_SA_kg_m3 is the supply air density, calculated via the psychometric Type33e;
- Set_OL_SAF is the supply air fan velocity;
- Set_OL_RAF is the return air fan velocity;
- The constant value 611.43 is the experimental supply air volumetric flowrate when the return air fan velocity is equal to 50% (fault-free scenario) and the supply air fan velocity is equal to 0% (faulty scenario);
- The constant value 107.80 is the experimental supply volumetric air flowrate when the return air fan velocity is equal to 0% (faulty scenario) and the supply air fan velocity is equal to 50% (fault-free scenario);
- The constant value 1546.25 is the experimental supply volumetric air flowrate when the return air fan velocity is equal to 50% (fault-free scenario) and the supply air fan velocity is equal to 100% (faulty scenario);
- The constant value 673.28 is the experimental supply volumetric air flowrate when the return air fan velocity is equal to 100% (fauly scenario) and the supply air fan velocity is equal to 50% (fault-free scenario).

The electric power EP_SAF is defined according to Eq. 10. The equation is derived by interpolating the electrical power consumed by the return air fan as a function of its velocity.

$$\begin{aligned} SIM\_EP\_SAF\_kW = {} & (0.117*Set\_OL\_SAF\text{^}4 - 0.545*Set\_OL\_SAF\text{^}3 + 11.949*Set\_OL\_SAF\text{^}2 - \\ & 8.949*Set\_OL\_SAF + 89.712)/1000 \end{aligned} \quad (10)$$

Where:

- Set_OL_SAF is the supply air fan velocity.

1.30 External Supply Air Fan Duct (External SAD) - Type 607a

The External Supply Air Fan Duct is modelled by using the Type 607a. Fig. 21 reports the parameters of external supply air fan duct type.

Finanziato dall'Unione europea NextGenerationEU | Ministero dell'Università e della Ricerca | Italiadomani PIANO NAZIONALE DI RIPRESA E RESILIENZA

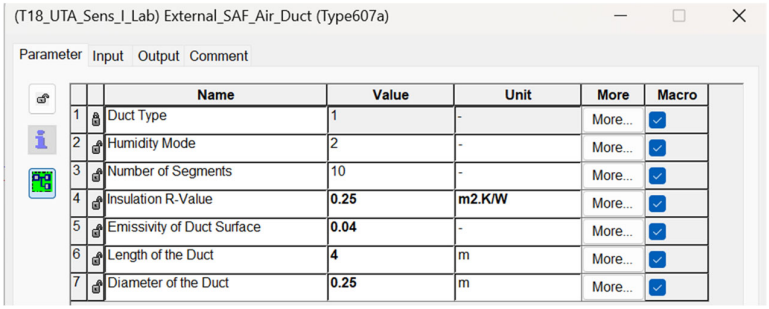

Figure 21. Parameters of External SAD Type.

Tables 29a and b illustrate the inputs and outputs of external supply air fan duct type, respectively.

Table 29a. Inputs of External SAD Type.

INPUTS	
LIST OF INPUTS	INPUTS USED
Inlet Air Temperature	Supply Air Temperature - T_SA (output SAF Calculator)
Inlet Air Humidity Ratio	-
Inlet Air % Relative Humidity	Supply Air Relative Humidity - RH_SA T_SA (output SAF Calculator)
Air Flowrate	Supply Air mass flowrate - m_SA T_SA (output SAF Calculator)
Inlet Air Pressure	Supply air pressure - p_SA T_SA (output SAF Calculator)
Environment Temperature	Outdoor Air Temperature - T_OA (output Type 15-3)
Wind Velocity	Outdoor Air Velocity (output Type 15-3)

Table 29b. Outputs of External SAD Type.

OUTPUTS	
LIST OF OUTPUTS	OUTPUTS USED
Outlet Air Temperature	Supply Air Temperature - T_SA
Outlet Air % Relative Humidity	Supply Air Relative Humidity - RH_SA
Outlet Air Flowrate	Supply Air mass flowrate - m_SA
Outlet Air Pressure	Supply air pressure - p_SA

1.31 Internal Supply Air Fan Duct (Internal SAD) - Type 607a

The Internal Supply Air Fan Duct is modelled by using the Type 607a. Fig. 22 reports the parameters of the internal supply air fan duct.

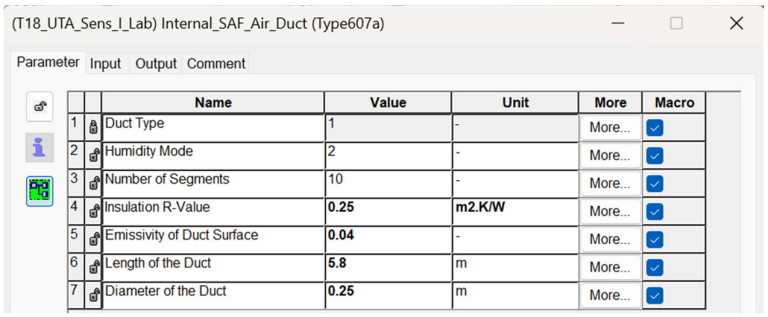

Figure 22. Parameters of Internal SAD Type.

Tables 30a and b illustrate the inputs and outputs of internal supply air fan duct type, respectively.

Finanziato dall'Unione europea NextGenerationEU
Ministero dell'Università e della Ricerca
Italiadomani PIANO NAZIONALE DI RIPRESA E RESILIENZA

Table 30a. Inputs of Internal SAD Type.

INPUTS	
LIST OF INPUTS	INPUTS USED
Inlet Air Temperature	Supply Air Temperature - T_SA (output Type 607a)
Inlet Air Humidity Ratio	-
Inlet Air % Relative Humidity	Supply Air Relative Humidity - RH_SA (output Type 607a)
Air Flowrate	Supply Air mass flowrate - m_SA (output Type 607a)
Inlet Air Pressure	Supply air pressure - p_SA (output Type 607a)
Environment Temperature	Outdoor Air Temperature - T_OA (output Type 15-3)

Table 30b. Outputs of Internal SAD Type.

OUTPUTS	
LIST OF OUTPUTS	OUTPUTS USED
Outlet Air Temperature	Supply Air Temperature - T_SA
Outlet Air % Relative Humidity	Supply Air Relative Humidity - RH_SA
Outlet Air Flowrate	Supply Air mass flowrate - m_SA
Outlet Air Pressure	Supply air pressure - p_SA

1.32 Controller Ctrl_RS - Type 2

The Controller Ctrl_RS is modelled by using the Type 2. Fig. 23 reports the parameters of the controller.

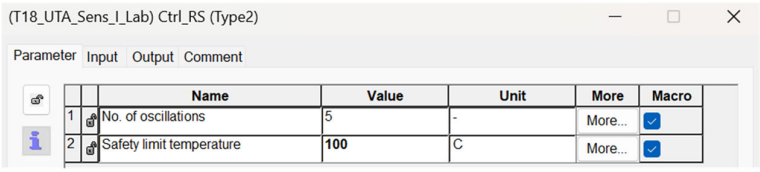

Figure 23. Parameters of Ctrl_RS Type.

Tables 31a and b illustrate the inputs and outputs of Ctrl_RS type, respectively.

Table 31a. Inputs of Ctrl_RS Type.

INPUTS	
LIST OF INPUTS	INPUTS USED
Temperature to watch	Outlet Fluid Temperature - T_F_out_RS (output Type 1534)
Setpoint temperature	8.4 °C (constant value)
High limit monitoring temperature	5 °C (constant value)
Input control function-->Connect from output control signal	0
Turn on temperature difference	1 (constant value)
Turn off temperature difference	–1 (constant value)

Table 31b. Outputs of Ctrl_RS Type.

OUTPUTS	
LIST OF OUTPUTS	OUTPUTS USED
Output control function	Ctrl_RS_sing

Finanziato dall'Unione europea NextGenerationEU
Ministero dell'Università e della Ricerca
Italiadomani PIANO NAZIONALE DI RIPRESA E RESILIENZA

The output Ctrl_RS_sing is the input of the calculator named Ctrl_RS. This calculator, together with n. 1 Type 661, n. 4 Type 93 and with another calculator named Timer_RS, performs the function of delaying the turn on of the refrigerating system by 60 seconds, so as to make the behaviour of the RS simulated as close as possible to the behaviour of the RS in the experimental set-up.

1.33 Controller Ctrl_HP - Type 2

The Controller Ctrl_HP is modelled by using the Type 2. Fig. 24 reports the parameters of the controller.

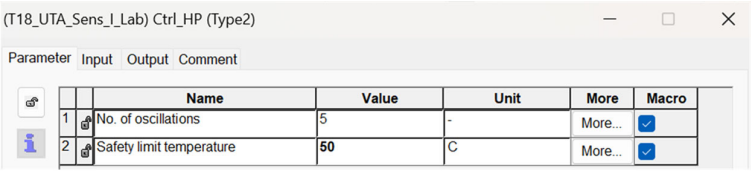

Figure 24. Parameters of Ctrl_HP Type.

Tables 32a and b illustrate the inputs and outputs of Ctrl_HP type, respectively.

Table 32a. Inputs of Ctrl_HP Type.

INPUTS	
LIST OF INPUTS	INPUTS USED
Temperature to watch	Outlet Fluid Temperature - T_F_out_HP (output Type 1534)
Setpoint temperature	48 °C (constant value)
High limit monitoring temperature	5 °C (constant value)
Input control function-->Connect from output control signal	0
Turn on temperature difference	1 (constant value)
Turn off temperature difference	–1 (constant value)

Table 32b. Outputs of Ctrl_HP Type.

OUTPUTS	
LIST OF OUTPUTS	OUTPUTS USED
Output control function	Ctrl_HP_sing

The output Ctrl_HP_sing is the input of the calculator named Ctrl_HP. This calculator, together with n. 1 Type 661, n. 4 Type 93 and with another calculator named Timer_HP, performs the function of delaying the turn on of the heat pump by 60 seconds, so as to make the behaviour of the HP simulated as close as possible to the behaviour of the HP the experimental set-up.

1.34 Controller Ctrl_HUM - Type 2

The Controller Ctrl_HUM is modelled by using the Type 2. Fig. 25 reports the parameters of the controller.

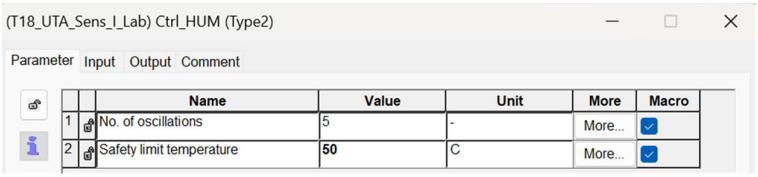

Figure 25. Parameters of Ctrl_HUM Type.

Tables 33a and b illustrate the inputs and outputs of Ctrl_HUM type, respectively.

Finanziato dall'Unione europea NextGenerationEU
Ministero dell'Università e della Ricerca
Italiadomani PIANO NAZIONALE DI RIPRESA E RESILIENZA

Table 33a. Inputs of Ctrl_HUM Type.

INPUTS	
LIST OF INPUTS	INPUTS USED
Temperature to watch	Return Air Relative Humidity - RH_RA (output Type 56)
Setpoint temperature	Return Air Relative Humidity Target Set_RH_target_RA (output Input Calculator)
High limit monitoring temperature	5 °C (constant value)
Input control function-->Connect from output control signal	0
Turn on temperature difference	RH upper dead band - UDB_RH_target_RA (output Input Calculator)
Turn off temperature difference	RH lower dead band - LDB_RH_target_RA (output Input Calculator)

Table 33b. Outputs of Ctrl_HUM Type.

OUTPUTS	
LIST OF OUTPUTS	OUTPUTS USED
Output control function	Ctrl_Humid

1.35 Controller Ctrl_Dehum - Type 2

The Controller Ctrl_Dehum is modelled by using the Type 2. Fig. 26 reports the parameters of the controller.

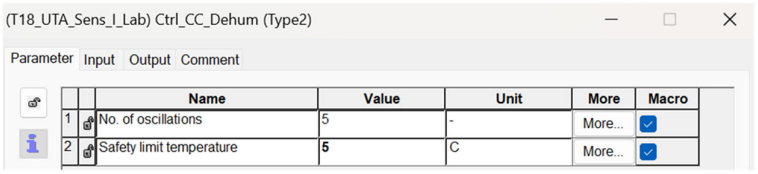

Figure 26. Parameters of Ctrl_Dehum Type.

Tables 34a and b illustrate the inputs and outputs of Ctrl_Dehum type, respectively.

Table 34a. Inputs of Ctrl_Dehum Type.

INPUTS	
LIST OF INPUTS	INPUTS USED
Temperature to watch	Return Air Relative Humidity - RH_RA (output Type 56)
Setpoint temperature	Return Air Relative Humidity - Target Set_RH_target_RA (output Input Calculator)
High limit monitoring temperature	5 °C (constant value)
Input control function-->Connect from output control signal	0
Turn on temperature difference	RH upper dead band - UDB_RH_target_RA (output Input Calculator)
Turn off temperature difference	RH lower dead band - LDB_RH_target_RA (output Input Calculator)

Table 34b. Outputs of Ctrl_DehumType.

OUTPUTS	
LIST OF OUTPUTS	OUTPUTS USED
Output control function	Ctrl_CC_Dehum

Finanziato dall'Unione europea NextGenerationEU
Ministero dell'Università e della Ricerca
Italiadomani PIANO NAZIONALE DI RIPRESA E RESILIENZA

1.36 Controller Ctrl_CC_Temp - Type 2

The Controller Ctrl_CC_Temp is modelled by using the Type 2. Fig. 27 reports the parameters of the controller.

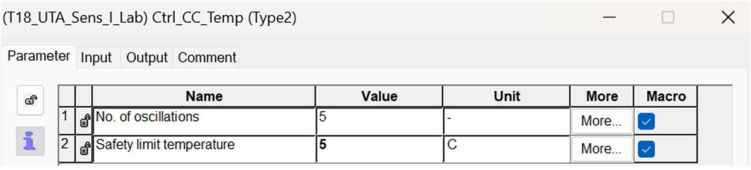

Figure 27. Parameters of Ctrl_CC_Temp Type.

Tables 35a and b illustrate the inputs and outputs of Ctrl_CC_Temp type, respectively.

Table 35a. Inputs of Ctrl_CC_Temp Type.

INPUTS	
LIST OF INPUTS	INPUTS USED
Temperature to watch	Return Air Temperature - T_RA (output Type 56)
Setpoint temperature	Return Air Temperature - Target Set_T_target_RA (output Input Calculator)
High limit monitoring temperature	7 °C (constant value)
Input control function-->Connect from output control signal	0
Turn on temperature difference	T upper dead band - UDB_T_target_RA (output Input Calculator)
Turn off temperature difference	T lower dead band - LDB_T_target_RA (output Input Calculator)

Table 35b. Outputs of Ctrl_CC_Temp Type.

OUTPUTS	
LIST OF OUTPUTS	OUTPUTS USED
Output control function	Ctrl_CC_temp

1.37 Controller Ctrl_PostHC_Temp - Type 2

The Controller Ctrl_PostHC_Temp is modelled by using the Type 2. Fig. 28 reports the parameters of the controller.

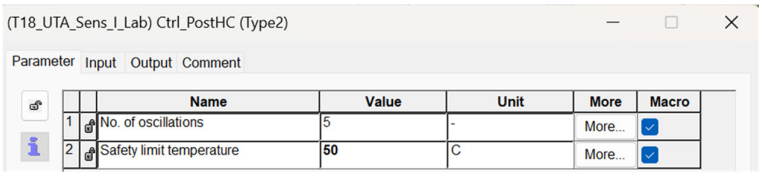

Figure 28. Parameters of Ctrl_PostHC_Temp Type.

Tables 36a and b illustrate the inputs and outputs of Ctrl_PostHC_Temp type, respectively.

Table 36a. Inputs of Ctrl_PostHC_Temp Type.

INPUTS	
LIST OF INPUTS	INPUTS USED
Temperature to watch	Return Air Temperature - T_RA (output Type 56)
Setpoint temperature	Return Air Temperature - Target Set_T_target_RA (output Input Calculator)

Finanziato dall'Unione europea NextGenerationEU
Ministero dell'Università e della Ricerca
Italiadomani PIANO NAZIONALE DI RIPRESA E RESILIENZA

High limit monitoring temperature	50 °C (constant value)
Input control function-->Connect from output control signal	0
Turn on temperature difference	T upper dead band - UDB_T_target_RA (output Input Calculator)
Turn off temperature difference	T lower dead band - LDB_T_target_RA (output Input Calculator)

Table 36b. Outputs of Ctrl_PostHC_Temp Type.

OUTPUTS	
LIST OF OUTPUTS	OUTPUTS USED
Output control function	Ctrl_PostHC

1.38 PID Controller CC_Temp - Type 23

The PID Controller CC_Temp is modelled by using the Type 23. Fig. 29 reports the parameters of the PID controller.

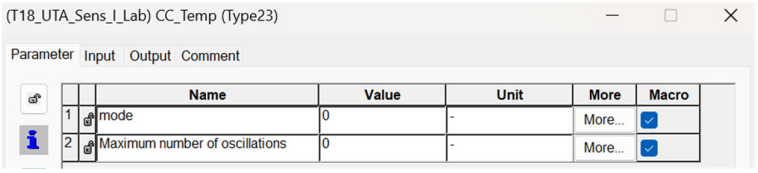

Figure 29. Parameters of PID Controller CC_Temp Type.

Tables 37a and b illustrate the inputs and outputs of PID Controller CC_Temp type, respectively.

Table 37a. Inputs of PID Controller CC_Temp Type.

INPUTS	
LIST OF INPUTS	INPUTS USED
Setpoint	Return Air Temperature - T_RA (output Type 56)
Controlled variable	Return Air Temperature - Target Set_T_target_RA (output Input Calculator)
On / Off signal	Ctrl_CC_temp ((output Type 2)
Minimum control signal	0 (constant value)
Maximum control signal	1 (constant value)
Threshold for non-zero output	0 (constant value)
Gain constant	– 0.05 (constant value)
Integral time	1 min (constant value)
Derivative time	0.1 min (constant value)
Tracking time for anti-windup	–1 (constant value)
Fraction of ySet for proportional effect	1 (constant value)
Fraction of ySet for derivative effect	1 (constant value)
High-frequency limit on derivative	10 (constant value)

Table 37b. Outputs of PID Controller CC_Temp Type.

OUTPUTS	
LIST OF OUTPUTS	OUTPUTS USED

Finanziato dall'Unione europea NextGenerationEU
Ministero dell'Università e della Ricerca
Italiadomani PIANO NAZIONALE DI RIPRESA E RESILIENZA

Control signal	Valve_CC_temp

1.39 PID Controller CC_Dehum - Type 23

The PID Controller CC_Dehum is modelled by using the Type 23. Fig. 30 reports the parameters of the PID controller.

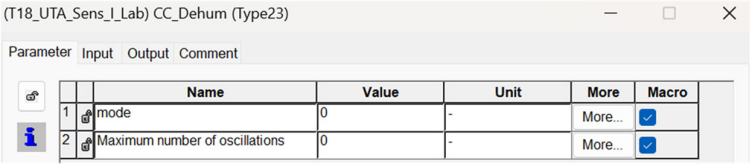

Figure 30. Parameters of PID Controller CC_Dehum Type.

Tables 38a and b illustrate the inputs and outputs of PID Controller CC_Dehum type, respectively.

Table 38a. Inputs of PID Controller CC_Dehum Type.

INPUTS	
LIST OF INPUTS	INPUTS USED
Setpoint	Return Air Relative Humidity - RH_RA (output Type 56)
Controlled variable	Return Air Relative Humidity - Target Set_RH_target_RA (output Input Calculator)
On / Off signal	Ctrl_CC_Dehum (output Type 2)
Minimum control signal	0 (constant value)
Maximum control signal	1 (constant value)
Threshold for non-zero output	0 (constant value)
Gain constant	– 0.1 (constant value)
Integral time	1 min (constant value)
Derivative time	0.1 min (constant value)
Tracking time for anti-windup	–1 (constant value)
Fraction of ySet for proportional effect	1 (constant value)
Fraction of ySet for derivative effect	1 (constant value)
High-frequency limit on derivative	10 (constant value)

Table 38b. Outputs of PID Controller CC_Dehum Type.

OUTPUTS	
LIST OF OUTPUTS	OUTPUTS USED
Control signal	Valve_CC_dehum

1.40 PID Controller PostHC - Type 23

The PID Controller PostHC is modelled by using the Type 23. Fig. 31 reports the parameters of the PID controller.

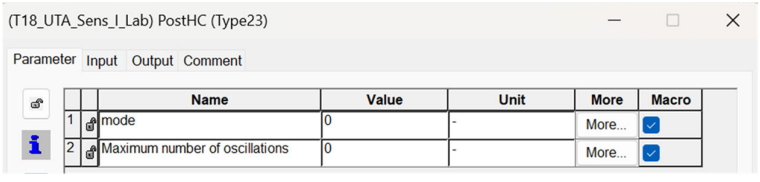

Finanziato dall'Unione europea NextGenerationEU
Ministero dell'Università e della Ricerca
Italiadomani PIANO NAZIONALE DI RIPRESA E RESILIENZA

Figure 31. Parameters of PID Controller PostHC Type.

Tables 39a and b illustrate the inputs and outputs of PID Controller PostHC type, respectively.

Table 39a. Inputs of PID Controller PostHC Type.

INPUTS	
LIST OF INPUTS	INPUTS USED
Setpoint	Return Air Temperature - T_RA (output Type 56)
Controlled variable	Return Air Temperature - Target Set_T_target_RA (output Input Calculator)
On / Off signal	Ctrl_PostHC (output Type 2)
Minimum control signal	0 (constant value)
Maximum control signal	1 (constant value)
Threshold for non-zero output	0 (constant value)
Gain constant	– 0.1 (constant value)
Integral time	1 min (constant value)
Derivative time	0.1 min (constant value)
Tracking time for anti-windup	– 1 (constant value)
Fraction of ySet for proportional effect	1 (constant value)
Fraction of ySet for derivative effect	1 (constant value)
High-frequency limit on derivative	10 (constant value)

Table 39b. Outputs of PID Controller PostHC Type.

OUTPUTS	
LIST OF OUTPUTS	OUTPUTS USED
Control signal	Valve_PostHC

1.41 PID Controller Humidifier - Type 23

The PID Controller Humidifier is modelled by using the Type 23. Fig. 32 reports the parameters of the PID controller.

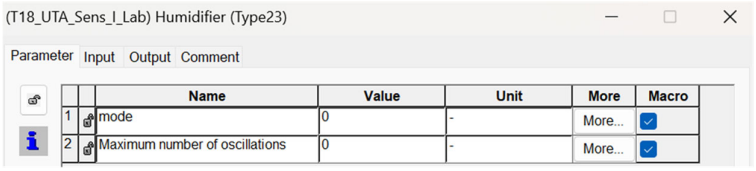

Figure 32. Parameters of PID Controller Humidifier Type.

Tables 40a and b illustrate the inputs and outputs of PID Controller Humidifier type, respectively.

Table 40a. Inputs of PID Controller Humidifier Type.

INPUTS	
LIST OF INPUTS	INPUTS USED
Setpoint	Return Air Relative Humidity - RH_RA (output Type 56)
Controlled variable	Return Air Relative Humidity - Target Set_RH_target_RA (output Input Calculator)
On / Off signal	Ctrl_Humid (output Type 2)

Finanziato dall'Unione europea NextGenerationEU
Ministero dell'Università e della Ricerca
Italiadomani PIANO NAZIONALE DI RIPRESA E RESILIENZA

Minimum control signal	0 (constant value)
Maximum control signal	1 (constant value)
Threshold for non-zero output	0 (constant value)
Gain constant	0.1 (constant value)
Integral time	1 min (constant value)
Derivative time	0.1 min (constant value)
Tracking time for anti-windup	–1 (constant value)
Fraction of ySet for proportional effect	1 (constant value)
Fraction of ySet for derivative effect	1 (constant value)
High-frequency limit on derivative	10 (constant value)

Table 40b. Outputs of PID Controller Humidifier Type.

OUTPUTS	
LIST OF OUTPUTS	OUTPUTS USED
Control signal	Ctrl_HUM

1.42 Printer and Plotter - Type 25c and Type 65d

Finally, **Type 25c** and **Type 65d** model a printer and an online plotter, respectively, which were used to display in real time the trends of the variables to be analysed and to "print" them to an external file for subsequent processing.

Finanziato dall'Unione europea NextGenerationEU | Ministero dell'Università e della Ricerca | Italiadomani PIANO NAZIONALE DI RIPRESA E RESILIENZA

DELIVERABLE WP5_D3

DEFINITION AND TESTING OF THE METHODOLOGY TO TRANSFER THE FDD STRATEGIES FROM THE SOURCE AHU SYSTEM TO THE TARGET ONE

EDIT BY POLITO

PRIN 2022 - UTMOST FDD: AN AUTOMATED, OPEN, SCALABLE AND TRANSPARENT FAULT DETECTION AND DIAGNOSIS PROCESS FOR AIR-HANDLING UNITS BASED ON A HYBRID EXPERT AND ARTIFICIAL INTELLIGENCE APPROACH

Funded by the European Union - Next Generation EU within the "Piano Nazionale di Ripresa e Resilienza (PNRR), missione 4 componente 2 investimento 1.1 - fondo per il programma nazionale di ricerca e progetti di rilevante interesse nazionale (PRIN)"

Finanziato dall'Unione europea NextGenerationEU

Ministero dell'Università e della Ricerca

Italiadomani PIANO NAZIONALE DI RIPRESA E RESILIENZA

The UTMOST FDD Project is organised into the following 7 Work Packages (WPs):
WP0) PROJECT COORDINATION
WP1) EXPERIMENTAL ANALYSIS FOR THE CHARACTERIZATION OF FAULTY AND NORMAL OPERATION OF A TYPICAL AHU
WP2) KPIs IDENTIFICATION FOR ASSESSING FAULT IMPACT IN AHU OPERATION
WP3) AHU DIGITAL TWIN AND SIMULATION-BASED FAULT IMPACT SCENARIO ANALYSIS
WP4) DEFINITION OF HYBRID FDD STRATEGIES FOR AHUs
WP5) TRANSFERABILITY ANALYSIS OF THE FDD STRATEGIES
WP6) KNOWLEDGE TRANSFER AND DISSEMINATION

The WP5 aims at assessing the transferability of the hybrid FDD strategies conceived in the WP4 for enhancing its penetration and adoption in buildings.

A variety of transfer learning methods, which differ in their transfer methods (i.e., instance-based, feature-based, parameter-based, and relational knowledge-based) and application natures (i.e., transductive, inductive and unsupervised), have been reviewed in the literature. The main aim of this WP is to transfer the FDD strategies, pre-trained on the existing labeled datasets derived from the WP1 and WP3, exploiting them with reference to an external target AHU for accomplishing the same task.

The WP5 will include the following 4 tasks (WP5_T1, WP5_T2, WP5_T3, WP5_T4):

- WP5_T1) the aim of this task was providing a scientific written report (1st WP5 deliverable WP5_D1) including a detailed categorization of the studies on the main approaches employed for conducting transfer learning of FDD strategies in AHUs. It will help in (a) better understanding the current research on transfer learning approaches, and (b) define current gaps and opportunities in the definition of transferability and scalability strategies for FDD in AHUs. In addition, among the publicly available tagged datasets of AHU faulty operations, the target AHU system for testing the transfer learning framework of the FDD strategy conceived in the WP4 will be identified;
- WP5_T2) this task aimed to address the issue of knowledge representation of the metering infrastructure of the considered experimental facility and the one of the target AHU identified in the WP5_T1 through the implementation of an ontology schema, enabling the i) interoperability and ii) transferability of the FDD logics conceived in the WP4. In the considered AHU systems, the ontology will be used to represent sensors, subsystems, and the relationships between them. A preliminary study of the state of the art of the ontology schema within the building energy field will be conducted. The identified ontology schema will address the system labelling problem by compiling a normalized list of domain terms (i.e., vocabulary) and a list of relationships capturing dependencies and connections in and between AHU sensors, actuators, commands, set-points and related equipment. Open standards, such as Semantic Web, RDF (Resource Description Framework), SPARQL query language, will be used to enable ontology interoperability;
- WP5_T3) the aim of this task is the development of a digital twin of the external AHU assumed as target (selected in the WP5_T1) by means of the software TRNSYS 18 (https://www.trnsys.com/) by including dedicated features to model the desired faults and validating the simulation outputs against the publicly available corresponding experimental data. The TRNSYS files of the digital twin, together with its documentation, will be uploaded in a public repository as 2nd WP5 deliverable WP5_D2. This will help in extending the operating ranges covered by the most used public FDD databases;
- WP5_T4) this task aims to define the methodology to be employed to transfer the FDD logic from the source AHU system to the target one. The transferability analysis of the FDD strategy will be performed especially considering the data-driven methods. Parameter-based transfer learning strategies which adopt either freezing or fine-tuning approaches for knowledge transfer will be applied on the pre-trained data-driven FDD models. Eventually, by evaluating the achieved performance in terms of detection and diagnosis rates on the target dataset, the transferability potential of the conceived FDD strategy will be assessed. A scientific written report (3rd WP5 deliverable: WP5_D3), including the transfer learning strategies, and the results obtained in terms of detection and diagnosis accuracy pertaining to the target AHU dataset, will be delivered.

1. Introduction

This deliverable presents a comprehensive study on the application of transfer learning methodologies for Fault Detection and Diagnosis (FDD) in Heating, Ventilation, and Air Conditioning (HVAC) systems. The core of the proposed approach involves transferring regression models trained on a source domain to predict

Finanziato dall'Unione europea NextGenerationEU | Ministero dell'Università e della Ricerca | Italiadomani PIANO NAZIONALE DI RIPRESA E RESILIENZA

operational variables in a target domain, where the predictive accuracy of these models critically determines the effectiveness of the subsequent fault isolation process [1,2].

The study evaluates and compares three distinct transfer strategies for regression model deployment: direct deployment of source-domain trained models to the target domain without adaptation, transfer learning employing the ADAPT library with the TrAdaBoostR2 algorithm [3] to adapt source models using limited target data, and model training from scratch using exclusively target-domain data. The methodology employs an ensemble of Random Forest regressors, each trained to predict specific operational variables including sensor measurements, actuator outputs, and control signals. The quality of these regression predictions is paramount, as prediction residuals constitute the primary evidence utilized by the Bayesian Network for probabilistic fault isolation (WP4_D3).

The integrated architecture operates in two sequential stages: first, regression models generate predictions for operational variables; second, a Bayesian Network analyzes the discrepancies between predicted and measured values to perform fault detection and component-level isolation. Consequently, the effectiveness of transfer learning at the regression stage directly impacts the diagnostic capability of the overall FDD system. The performance of each transfer strategy is assessed using operational data from the Air Handling Units (AHU) at the SENS i-Lab at the Department of Architecture and Industrial Design of the University of Campania Luigi Vanvitelli under both summer and winter conditions. Additionally, a sensitivity analysis is conducted to determine the minimum number of target-domain fine-tuning samples required for the from-scratch training approach to achieve performance levels comparable to those obtained through transfer learning, thereby providing quantitative guidelines for practical deployment scenarios.

1.1 Challenges in FDD Implementation

The implementation of FDD systems in HVAC operations is challenged by multiple interrelated factors. A primary limitation is data scarcity, as the collection of sufficiently labeled fault data from operational buildings is both costly and time intensive. This often results in the "cold start" problem, where newly deployed systems lack the historical data necessary for effective initial model training.

Even when data are available, models frequently encounter domain shift issues. Algorithms trained on simulation data or specific buildings often exhibit degraded performance when deployed in new environments due to distributional mismatches. Seasonal variations exacerbate this problem, as operational conditions differ significantly between summer and winter, necessitating model adaptation. Transfer learning offers a solution by enabling models to leverage knowledge from a source domain, such as prior seasons, simulations, or analogous buildings, to improve predictive performance in target domains characterized by limited data.

1.2 Research Objectives discussed in the Deliverable WP5_D3

This deliverable addresses three principal objectives within the framework of WP5, building upon the experimental foundation established in WP4.

The first objective concerns a systematic comparative evaluation of transfer learning via domain adaptation against two baseline strategies: direct model deployment (zero-shot transfer) and target-domain training from scratch. This comparison is conducted across both fault detection accuracy and fault isolation accuracy, using the identical held-out test set employed in WP4_D3 to ensure consistency and reproducibility of results. By benchmarking against these two contrasting baselines, the analysis isolates the specific contribution of domain adaptation, distinguishing gains attributable to source-domain knowledge from those achievable through target-domain data alone.

The second objective investigates data efficiency, with the aim of identifying the minimum volume of labeled target-domain samples required for a from-scratch training approach to achieve performance parity with transfer learning. This threshold analysis provides a practical quantification of the annotation cost savings that domain adaptation offers, and informs decisions around data collection strategy in deployment scenarios where labeling resources are constrained.

The third objective evaluates the robustness and generalizability of all three modeling approaches across varying fault types and operational conditions. In particular, the analysis contrasts model behavior under summer and winter operating regimes, which are characterized by substantially different ambient temperatures, load profiles, and system dynamics. This seasonal comparison serves to expose potential performance degradation or behavioral inconsistencies that may not be apparent under uniform test conditions, and provides evidence as to which modeling paradigm offers the most stable and reliable fault diagnosis across the full operational envelope.

Finanziato dall'Unione europea NextGenerationEU | Ministero dell'Università e della Ricerca | Italiadomani PIANO NAZIONALE DI RIPRESA E RESILIENZA

2. Methodology

The proposed framework integrates data-driven regression modeling with probabilistic reasoning engines to perform hierarchical fault diagnosis in a unified and interpretable pipeline. The architecture is designed to decompose the diagnostic problem into two complementary stages, each targeting a distinct aspect of the overall inference task. Within the context of WP5, this framework serves as the common diagnostic backbone across all experimental conditions, providing the structure within which transfer learning strategies are evaluated and compared.

In the first stage, ensemble regression models are trained to predict key system state variables from available sensor measurements and operational inputs. By leveraging the variance-reducing properties of ensemble methods, these models produce stable and accurate estimates of the expected system behavior under nominal conditions. The deviation between predicted and observed values, that is the prediction residual, serves as a structured and informative signal encoding the degree to which the system has departed from its expected operating point. In the transfer learning setting investigated in WP5, the source domain consists of synthetic data generated by a calibrated digital twin of the AHU, which was used to simulate normal operating conditions across representative summer and winter seasons. The target domain consists of real experimental monitoring data collected from the physical AHU installation at the SENS i-Lab. This source-to-target configuration reflects a practically relevant and challenging transfer scenario, as the statistical properties of simulated and real operational data inevitably differ due to modeling approximations, sensor noise, unmodeled disturbances, and the inherent gap between idealized simulation conditions and actual system behavior. The regression models constitute the primary locus of this domain shift: rather than training these models from scratch on target-domain data, domain adaptation techniques are applied to transfer knowledge acquired on the source domain, thereby reducing the dependence on large volumes of real experimental observations. The sensitivity of the residual signals to this simulation-to-real gap, and the extent to which it can be mitigated through adaptation, is therefore a central quantity of interest throughout the experimental analysis.

In the second stage, these residuals are passed to a Bayesian Network, which aggregates probabilistic evidence across multiple system components to perform fault inference. The Bayesian Network encodes the conditional dependencies between residual signals and underlying fault hypotheses, enabling the framework to reason jointly over multiple potential fault sources rather than treating each component in isolation. This probabilistic formulation allows uncertainty to be propagated and represented explicitly throughout the diagnostic chain, yielding posterior fault probabilities that reflect both the strength of the residual evidence and the prior likelihood of each fault condition. Because the Bayesian Network structure and its associated conditional probability tables are grounded in physical knowledge of the system rather than fitted purely from data, this stage is expected to exhibit greater stability across the simulation-to-real domain gap, making the regression stage the primary focus of the adaptation effort in WP5.

This layered design makes the framework particularly well suited to the cross-domain evaluation pursued in WP5, where the simulation-to-real gap may cause fault symptoms to manifest with different magnitudes or statistical characteristics, operating conditions vary substantially between seasons, and the available volume of real labeled target-domain data may be severely limited.

2.1 Domain Adaptation Problem Formulation

The domain adaptation problem addressed in this study is formulated as follows: given a source domain:

$$DS = \{(x_i^S, y_i^S)\}_{\{i=1\}}^{nS} \quad (1)$$

with abundant labeled samples and a target domain:

$$DT = \{(x_i^T, y_i^T)\}_{\{i=1\}}^{nT} \quad (2)$$

with limited labeled samples, where $nT \ll nS$, the objective is to train a model $fT: XT \rightarrow YT$ that achieves optimal performance on the target domain distribution [4-6]. The domains share similar feature spaces ($XS = XT$) and label spaces ($YS = YT$), but exhibit distribution shift: $P(XS, YS) \neq P(XT, YT)$.

In this specific context, the domain adaptation challenge consists of transferring regression models trained from a source domain generated through TRNSYS 18 simulation to a target domain comprising real experimental operational data from operational AHU systems.

Finanziato dall'Unione europea NextGenerationEU | Ministero dell'Università e della Ricerca | Italiadomani PIANO NAZIONALE DI RIPRESA E RESILIENZA

The source domain is characterized by physics-based simulation data providing comprehensive coverage of normal operating conditions within a controlled environment featuring idealized sensor characteristics. This domain offers substantial data availability with sample sizes of approximately 8,000-9,000 timesteps per seasonal configuration (summer and winter operational regimes), enabling thorough model training under well-characterized conditions.

Conversely, the target domain consists of real experimental data reflecting practical operational constraints, including realistic sensor noise, measurement uncertainties, and authentic system dynamics. The target domain is characterized by significantly limited labeled samples. Each day of simulation cover 9 hours of system operation, having 36 timesteps with 15 min granularity. This substantial disparity in sample availability constitutes the fundamental challenge necessitating effective transfer learning strategies.

The domain shift, formally denoted as $P(XS, YS) \neq P(XT, YT)$, manifests through a confluence of interrelated mechanisms. Measurement discrepancies emerge from the inherent contrast between idealized simulation sensors and physical instrumentation, the latter of which is subject to noise, signal drift, and calibration biases. Concurrently, system dynamics exhibit substantial divergence driven by variations in thermodynamic response characteristics and thermal inertia.

As established in WP4_D3, the FDD system is built upon an ensemble of Random Forest regression models, each trained to predict a specific system variable from a set of physically meaningful inputs. This modular structure reflects the hierarchical organization of the AHU and ensures that the residual signals generated by each model carry localized diagnostic information attributable to a well-defined component or subsystem. The selection of both target and input variables was guided by the physical relationships among system components and the practical constraints of real installations, prioritizing measurements that are commonly available in building monitoring systems and that exhibit sensitivity to the fault conditions of interest. Separate model instances were trained for the summer and winter operating modes, reflecting the distinct thermodynamic and control behaviors of the AHU across the two seasons.

The predicted variables are organized into the following functional groups, each capturing a distinct aspect of AHU behavior:

- **Sensor measurements** include return air temperature (T_RA) and return air relative humidity (RH_RA). The T_RA model takes as inputs the outdoor air temperature, supply air temperature, mixed air temperature, post-heating coil thermal power, and cooling coil thermal power, capturing the combined thermal influence of upstream components and external conditions on the return air state. The RH_RA model takes as inputs the outdoor, supply, and mixed air relative humidity values, alongside the post-heating coil and cooling coil thermal powers and the humidifier;
- **Heat exchange variables** include the cooling power of the cooling coil (P_CC), whose model takes as inputs the outdoor air temperature, the fluid inlet and outlet temperatures of the cooling coil circuit, the fluid volumetric flow rate, and the mixed air temperature. This variable encodes the effective thermal exchange capacity of the cooling coil and provides a direct indicator of anomalous energy demand or loss of controllability characteristic of valve stuck faults;
- **Control signals** include the cooling coil control signal (control_signal_CC), predicted from the supply air temperature, outdoor air temperature, return air temperature, post-heating coil control signal, and humidifier control signal;
- **Mixed air conditions** are represented by two models covering both the thermal and hygroscopic state of the air at the mixing point. The mixed air temperature (T_MA) is predicted from the return and outdoor air temperatures and relative humidities, and from the mixed air relative humidity, capturing the blending dynamics between recirculated and fresh air streams. The mixed air relative humidity (RH_MA) is predicted from the return and outdoor air relative humidities and temperatures, and from the mixed air temperature, completing the characterization of the mixed air state,
- **Fan parameters** include the supply air fan power (P_SAF) and return air fan power (P_RAF), each predicted from the corresponding air velocity measurement, the power of the other fan, and the outdoor and supply air relative humidity values.

Together, these eight variable-specific models ensure broad observability of the AHU across its main functional subsystems, enabling the ensemble to generate a rich and spatially distributed set of residual signals. This multi-variable residual structure is what ultimately allows the Bayesian Network to perform reliable fault isolation across the diverse fault taxonomy defined in WP4_D3, by cross-referencing evidence from multiple components simultaneously rather than relying on any single diagnostic channel.

Finanziato dall'Unione europea NextGenerationEU | Ministero dell'Università e della Ricerca | Italiadomani PIANO NAZIONALE DI RIPRESA E RESILIENZA

2.2 Approach 1: Direct Model Deployment

The first approach establishes a performance baseline representing conventional model deployment without domain adaptation. Models are trained exclusively on source domain data and deployed directly to target domain conditions.

Training Protocol:

1. Data Preparation: Source domain dataset DS undergoes preprocessing to remove non-physical operating points (simultaneous zero states across multiple actuators indicating system shutdown periods).
2. Model Training: For each variable *m*, a Random Forest regressor is trained:

$$y_m = RandomForest(DS_m, \Theta_m^*) \quad (3)$$

where Θ_m^* represents optimal hyperparameters determined through temporal cross-validation.

3. Hyperparameter Optimization: Grid search is conducted over hyperparameter space:
   - Number of trees: $n$trees$\in\{100,200\}$;
   - Maximum tree depth: $d$max$\in\{5,10,\text{None}\}$;
   - Minimum samples for splitting: $n$split$\in\{2,5\}$;
   - Minimum samples per leaf: $n$leaf$\in\{1,2\}$.
4. Temporal Validation: TimeSeriesSplit cross-validation with k=5k=5 folds ensures temporal ordering preservation, preventing information leakage from future to past data.

Trained models are applied to target domain test data without modification. Prediction residuals are computed and forwarded to the probabilistic inference stage. This approach quantifies the magnitude of performance degradation attributable to domain shift, serving as a critical baseline for evaluating adaptation strategies.

2.3 Approach 2: Adaptive Transfer Learning via Instance Weighting

The second approach adopts an instance-based transfer learning strategy through the TrAdaBoostR2 algorithm, with the objective of improving predictive performance on a target domain characterized by limited data availability. The central premise of this method is that not all source domain samples contribute positively to target domain performance. Consequently, the algorithm introduces an adaptive weighting mechanism that progressively discriminates between transferable and non-transferable source instances.

TrAdaBoostR2 operates through an iterative boosting procedure in which a base estimator is trained on the combined source and target dataset. After each iteration, the model's performance is evaluated exclusively on the target domain, and sample weights are updated accordingly. Source samples associated with large prediction errors are down-weighted, reflecting their limited compatibility with the target distribution, whereas target samples with large errors are up-weighted, thereby increasing their influence in subsequent iterations. This process of differential reweighting gradually suppresses misleading information from sources, amplifying informative contributions and emphasizing more complex target observations.

As iterations progress, the learning process shifts from an initial reliance on the full source dataset toward a more target-oriented representation. The final prediction is obtained by aggregating only the estimators produced in the latter half of the boosting sequence, thereby reducing residual source-domain bias and enhancing robustness.

From an implementation perspective, hyperparameter optimization of the Random Forest base estimator is conducted exclusively on target domain data prior to transfer learning, using the same Grid Search optimization presented for the Approach 1. This ensures that the model architecture is aligned with target-specific characteristics before incorporating source information. The optimized estimator is subsequently embedded within the TrAdaBoostR2 framework and trained over ten boosting iterations, providing a balance between computational efficiency and adaptation effectiveness.

Overall, this approach exploits the complementary strengths of abundant source data and scarce target data. By dynamically adjusting sample importance, TrAdaBoostR2 seeks to regularize the learning process through transferable knowledge while preserving sensitivity to target-domain specific patterns, thereby mitigating negative transfer and enhancing predictive performance under data scarcity conditions.

2.4 Approach 3: Target-Domain Exclusive Training

Finanziato dall'Unione europea NextGenerationEU | Ministero dell'Università e della Ricerca | Italiadomani PIANO NAZIONALE DI RIPRESA E RESILIENZA

The third approach trains models exclusively on target domain data, disregarding source domain information entirely.

Training Protocol:

1. Data Aggregation: all available target domain normal operation data are consolidated. The same real data used for the fine tuning of the approach 2 are here used as training dataset;
2. Hyperparameter Optimization: a comprehensive grid search utilizing Time Series Split validation was implemented to determine the optimal configuration tailored to the specific characteristics of the target domain. This rigorous optimization procedure was executed exclusively after a sufficient volume of training data had been accumulated. Consequently, during the initial computational iteration, a smaller regression tree estimator was employed to accommodate the preliminary data limitations;
3. Model Training: Random Forest regressors are trained as in Approach 1;
4. Model Validation: performance assessment uses temporally separated validation fold from cross-validation procedure.

When sufficient target data exist, training directly on target distribution theoretically eliminates domain shift artifacts present in cross-domain approaches. This paradigm tests whether the computational overhead of transfer learning is justified when target data abundance permits domain-specific training.

3. Comparative Evaluation of Domain Adaptation Algorithms

To identify the optimal strategy for mitigating the domain shift between simulation data and operational reality, a systematic benchmarking study was conducted on 3 distinct domain adaptation architectures. This comparative analysis seeks to establish an evidence-based selection of the most effective algorithmic approach for HVAC fault detection.

The investigation encompasses a diverse array of adaptation methodologies, categorized as follows:

- **Baseline (No Adaptation)**. A Random Forest model trained exclusively on the source domain and deployed directly to the test set of the target domain. This establishes the performance floor attributable to domain shift.
- **Boosting-Based Methods.** TrAdaBoostR2 and TwoStageTrAdaBoostR2 are employed to utilize adaptive boosting, differentially weighting source and target samples to prioritize instances most relevant to the target distribution.
- **Instance Reweighting.** KMM (Kernel Mean Matching) is utilized to align source and target distributions by reweighting source instances in the reproducing kernel Hilbert space. Additionally, NearestNeighborsWeighting assigns importance based on proximity to target instances.

To ensure rigorous comparability, all algorithms were trained on identical source-target data pairs. The training configuration utilized a comprehensive simulation dataset as the source domain, with a set of real operational data in normal condition (14 files, corresponding to 14 daily data) reserved for fine-tuning.

Subsequent evaluation was conducted on a strictly held out test set, which consisted of two isolated days representing normal operational states. Predictive performance was then quantified by calculating the Root Mean Square Error for each targeted variable. Ultimately, this rigorous assessment serves to identify the most accurate predictive model, establishing a crucial prerequisite for the subsequent integration of the Bayesian network within the proposed methodology.

3.1 Adapt algorithms comparison

The comparative evaluation of the four domain adaptation algorithms, summarized in the Table 1, reveals a clear performance divide between boosting based algorithms and instance reweighting methods.

The two instance reweighting approaches, Kernel Mean Matching (KMM) and Nearest Neighbors Weighting (NNW), proved largely ineffective at mitigating covariate shift. Their results closely mirrored the Baseline scenario, in which the source domain model is applied directly to the target domain without any adaptation. For the primary variable of interest, cooling coil power, KMM and NNW yielded RMSE values of 3836 W and 3406 W respectively, compared to the Baseline value of 3922 W, representing negligible improvement. This pattern held consistently across all evaluated variables, suggesting that these methods are unable to adequately align the high dimensional distributions of the source and target domains exploiting such a small portion of targed domain data for fine tuning.

Finanziato dall'Unione europea NextGenerationEU | Ministero dell'Università e della Ricerca | Italiadomani PIANO NAZIONALE DI RIPRESA E RESILIENZA

In contrast, both boosting-based methods demonstrated a strong capacity to bridge the domain gap, particularly for continuous regression tasks. Cooling coil power RMSE dropped from 3922 W at baseline to 215 W for TrAdaBoostR2 and 230 W for TwoStageTrAdaBoostR2, corresponding to a reduction of approximately 94%. This performance trend remained consistent across all evaluated systemic variables. The RMSE for Return air Fan Power P_{RAF} diminished from 0.98 W to approximately 0.78 W, while the Supply air Fan Power P_{SAF} error declined from 12.89 W to a bounded range of 5.13 W to 5.22 W. Furthermore, the RMSE metrics, quantified in °C for Mixing air Temperature T_{MA} and Return Air Temperature T_{RA}, registered substantial corresponding reductions.

While TrAdaBoostR2 achieved lower RMSE on most energetic and thermal features, TwoStageTrAdaBoostR2 performed marginally better on the cooling coil control signal, with an error of 0.06 versus 0.07 considering that the control signal is bounded in the range [0,1]. Overall, the two algorithms deliver comparable predictive accuracy across all tested variables. However, TrAdaBoostR2 was selected for the subsequent stages of the proposed methodology, as it offers equivalent predictive performance with lower computational overhead.

Table 1. Comparison of the domain adaptation algorithms against the baseline approach in terms of RMSE evaluated on the testing set for each regression model.

Algorithm	P_{CC} W	P_{RAF} W	P_{SAF} W	RH_{MA} %	RH_{RA} %	T_{MA} °C	T_{RA} °C	Control $Signal_{CC}$ -
Baseline	3922.26	0.97	12.893	4.406	2.822	3.206	0.619	0.873
KMM	3835.88	0.97	12.893	4.537	2.888	2.978	0.623	0.837
NNW	3406.37	0.97	12.893	4.43	5.307	2.976	0.654	0.834
TrAdaBoostR2	214.67	0.79	5.128	1.695	1.158	0.458	0.25	0.072
TwoStageTrAdaBoostR2	229.99	0.79	5.22	1.705	1.13	0.47	0.219	0.063

4. Sensitivity Analysis Methodology

A systematic sensitivity analysis was conducted to determine the critical data threshold (n_min) required for the target-only training strategy (Approach 3) to achieve performance parity with the transfer learning method (Approach 2). This analysis addresses a fundamental resource allocation question: at what point does the investment in collecting additional target domain data yield a model that matches or exceeds the performance gained through knowledge transfer?

Formally, the analysis identifies the minimum sample size n_min satisfying the condition:

$$\Phi\_3\ (n\_min\ ) \geq \Phi\_2\ (n\_min) \tag{4}$$

where Φ_3 (n) denotes the performance of the target-only model trained on n files, and Φ_2 (n)represents the fixed performance of the transfer learning model using the same set of files, used for the fine-tuning.

To locate this threshold an incremental evaluation framework was employed. The number of files used as target domain for Approach 2 and ad training dataset for Approach 3 was systematically varied.

The protocol proceeds through the following stages:

1. **Initialization**. The analysis begins with a baseline sample size of n=2 files (i.e., two days of normal operation), increasing by an increment of Δn=2 files per iteration, up to a maximum of 14 files for the summer case and 10 files for the winter case (i.e., the size of the training set used in WP4_D3 to train the regression models);
2. **Cumulative Training** (Approach 3). At each iteration, for the Approach 3, the baseline regression models (i.e., Random Forests) are trained on a cumulative dataset D_train pertaining

Finanziato dall'Unione europea NextGenerationEU | Ministero dell'Università e della Ricerca | Italiadomani PIANO NAZIONALE DI RIPRESA E RESILIENZA

the source domain reflecting the normal operation of the AHU. No source-domain data are used at this stage. This progressive retraining reflects the realistic scenario in which a practitioner builds a purely data-driven baseline using all real operational data collected up to the current point in time, without access to any simulation-derived knowledge.

3. **Cumulative Fine-Tuning** (Approach 2). In parallel, the transfer learning model based on TrAdaBoostR2 is applied using a fixed source domain consisting of the digital twin simulation data, combined with a cumulative set of n target-domain files used for adaptation. The source-domain component remains constant across iterations, ensuring that observed performance differences across iterations are attributable solely to the increasing availability of target-domain observations rather than to any change in the transferred knowledge base;
4. **Evaluation protocol.** To isolate the effect of domain adaptation and ensure comparability across all tests, both approaches are evaluated at each iteration on the same held-out test set used in WP4_D3, which comprises all normal operation files not included in the current training set, specifically two normal operation days, together with the complete fault library covering all fault types and severity levels defined in the experimental campaign. This fixed test set guarantees that performance estimates reflect generalization to the full operational and fault space of the AHU, rather than being influenced by the composition of the training data. Performance differentials $\Delta_{Detection}$ and $\Delta_{Isolation}$ are calculated at each step.

The iterative process terminates when Approach 3 demonstrates superior or equivalent performance to Approach 2 across both detection and isolation metrics simultaneously, or when the maximum data limit of 14 files is reached without parity being achieved, in which case the transfer learning advantage is considered persistent across the entire feasible data range.

This methodology enables the characterization of learning curves for both approaches as a function of available target-domain data, and supports the quantification of marginal performance gains per additional day of collected observations. The resulting evidence are provided and discussed for both the summer and winter condition.

5. Sensitivity Analysis Results

5.1 Summer Season

The sensitivity analysis conducted for the summer season reveals a clear and consistent pattern in the relative performance of Approach 2 (Domain adaptation) and Approach 3 (cumulative training in target domain) as a function of the number of available target-domain files. The results are summarized in the performance differential plot and the isolation accuracy comparison shown in Figure 1.

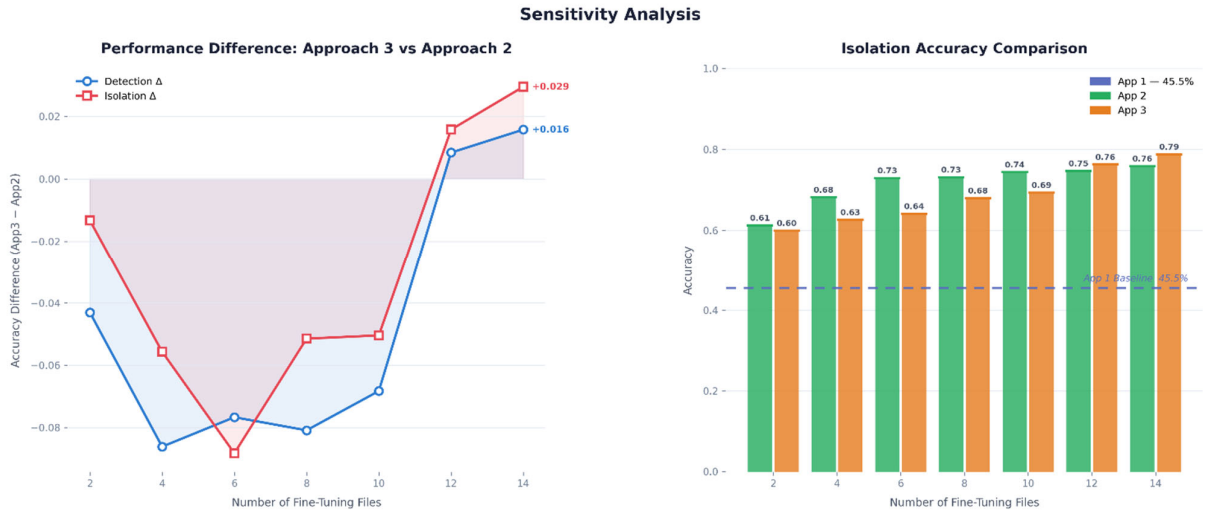

Figure 1. Performance gap in fault detection and isolation accuracy between Domain Adaptation (Approach 2) and Cumulative Training (Approach 3) as a function of the available fine-tuning data volume, evaluated under summer operating conditions.

Finanziato dall'Unione europea NextGenerationEU
Ministero dell'Università e della Ricerca
Italiadomani PIANO NAZIONALE DI RIPRESA E RESILIENZA

At the lowest data availability level of n = 2 files, Approach 2 already demonstrates a meaningful advantage over Approach 3, with a fault isolation accuracy (evaluated as reported in WP4_D3) values of 61% and 60% respectively, and a negative fault detection differential of approximately 4%. This initial gap confirms that, when target-domain data are severely limited, the knowledge transferred from the digital twin source domain provides a benefit that target-only training cannot replicate with so few observations.

As the number of files increases from n = 2 to n = 6, the advantage of Approach 2 widens considerably rather than narrowing. The detection differential reaches its most negative value at n = 6, dropping to approximately 8%, while the isolation differential simultaneously reaches its minimum of approximately 9%. This counterintuitive widening of the gap in the intermediate data range suggests that Approach 3, when trained on a small but non-trivial number of files, undergoes a phase of unstable learning in which the accumulated data are sufficient to overfit local patterns but insufficient to capture the full variability of normal AHU operation. Approach 2, by contrast, benefits from the regularizing effect of the source-domain simulation data throughout this phase, maintaining more stable regression residuals and therefore more reliable virtual evidence for the Bayesian Network. The corresponding isolation accuracy values at n = 6 are 73% for Approach 2 and 64% for Approach 3.

From n = 6 onward, the performance differential begins to recover monotonically and consistently for both detection and isolation metrics. At n = 8 the isolation accuracy of Approach 3 reaches 68% against 73% for Approach 2, and at n = 10 the values stand at 69% and 74% respectively, indicating a steady but gradual convergence. The recovery is driven by the progressive enrichment of the target-domain training set, which allows the from-scratch Random Forest regressors to build an increasingly representative baseline of normal system behavior.

The crossover point, that is the threshold n* at which Approach 3 achieves performance parity with Approach 2, is reached at n = 12 files for the isolation metric and consolidates at n = 14 files (this is the same setup of the experiments reported in WP4_D3) for both metrics simultaneously. At n = 14, the isolation accuracy of Approach 3 reaches 79%, surpassing Approach 2 which stabilizes at 76%, yielding a positive isolation differential of 2%. The detection differential at the same point is 1%, confirming that Approach 3 has crossed the parity threshold on both diagnostic stages. Notably, both approaches substantially and consistently outperform the Approach 1 zero-shot baseline of 45.5% isolation accuracy across the entire range of data availability, confirming that any form of target-domain adaptation, whether through transfer learning or direct training, is necessary for reliable diagnostic performance on the real experimental data.

In summary, for the summer season the data efficiency threshold lies at n* = 12 files for isolation and n* = 14 files for the simultaneous satisfaction of both detection and isolation parity conditions. This finding implies that transfer learning via TrAdaBoostR2 provides a sustained and practically significant advantage over target-only training for up to approximately ten days of available target-domain data, beyond which the from-scratch approach becomes competitive and eventually superior.

5.2 Winter Season

The sensitivity analysis for the winter season (Figure 2) exhibits a broadly similar trend to the summer case but with two important differences: the advantage of Approach 2 in the low-data regime is less pronounced, and the crossover threshold is reached earlier, requiring fewer target-domain files for Approach 3 to achieve performance parity. The results are summarized in the performance differential plot and the isolation accuracy comparison shown in Figure 2.

Finanziato dall'Unione europea NextGenerationEU
Ministero dell'Università e della Ricerca
Italiadomani PIANO NAZIONALE DI RIPRESA E RESILIENZA

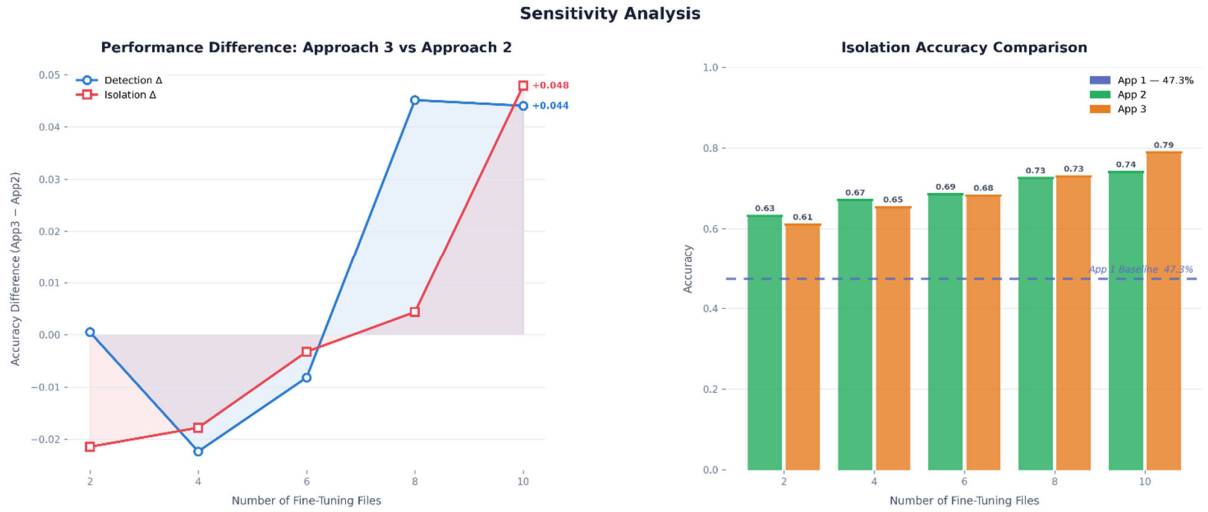

Figure 2. Performance gap in fault detection and isolation accuracy between Domain Adaptation (Approach 2) and Cumulative Training (Approach 3) as a function of the available fine-tuning data volume, evaluated under winter operating conditions.

At n = 2 files, the two approaches perform nearly identically in terms of fault detection, with a detection differential of approximately 0%, while the isolation differential is mildly negative at approximately 2%. The isolation accuracy values at this point are 63.% for Approach 2 and 61.% for Approach 3. This near-equivalence at the lowest data level suggests that, in the winter operating regime, the simulation-to-real domain gap may be somewhat smaller than in summer, possibly due to the more stable and less variable conditions characteristic of winter AHU operation, which make the digital twin a marginally more representative source of transferred knowledge.

As the number of files increases to n = 4, a modest negative divergence emerges, with the detection differential dropping to approximately 2% and the isolation differential reaching approximately 2% percentage points. The corresponding isolation accuracy values are 67% for Approach 2 and 65% for Approach 3. While this widening mirrors the pattern observed in summer, its magnitude is substantially smaller, indicating that the instability phase of Approach 3 is less severe in the winter season.

The recovery phase begins at n = 6 and proceeds steeply. Between n = 6 and n = 8, both differentials increase sharply, with the detection differential rising from approximately 0.9% to 4% and the isolation differential from approximately 0.3% to 0.4%. This abrupt transition indicates that in the winter case, the acquisition of eight days of target-domain normal operation data is sufficient to substantially close the gap with transfer learning, and that the learning curve of Approach 3 is steeper than in summer once a moderate data volume is available.

The crossover point is reached at n = 8 files for fault detection, making this the earliest threshold observed across both seasons and both metrics. By n = 10 files, Approach 3 achieves an isolation accuracy of 79 %, surpassing Approach 2 which stands at 74%, and yielding a positive isolation differential of 4.8% and a detection differential of 4.4%. These are the largest positive differentials recorded across the entire sensitivity analysis, indicating that in the winter season and with sufficient data, the from-scratch approach not only achieves parity but substantially outperforms transfer learning. As in summer, both approaches consistently exceed the Approach 1 zero-shot baseline of 47.3% throughout the analysis, reinforcing the conclusion that target-domain adaptation is essential regardless of the strategy adopted.

In summary, for the winter season the data efficiency threshold lies at n* = 8 files for fault detection and n* = 10 files for simultaneous satisfaction of both metrics, representing a materially lower data requirement than the summer case. This seasonal difference suggests that the winter simulation data from the digital twin are more readily transferable to the real system, reducing but not eliminating the data efficiency advantage of domain adaptation in the low-data regime.

6. Discussion

The results of the sensitivity analysis across both seasons yield several findings of practical and methodological relevance, which collectively characterize the conditions under which transfer learning offers a meaningful advantage and the point at which direct target-domain training becomes the preferred strategy.

Finanziato dall'Unione europea NextGenerationEU
Ministero dell'Università e della Ricerca
Italiadomani PIANO NAZIONALE DI RIPRESA E RESILIENZA

The most consistent finding across both seasons is the existence of a distinct low-data regime in which Approach 2 outperforms Approach 3 by a non-trivial margin, followed by a convergence and eventual crossover as more target-domain files are accumulated. This pattern is physically interpretable: when only a handful of real operational days are available, the from-scratch Random Forest regressors lack the statistical coverage to characterize the full range of normal AHU behavior, and the resulting residual signals are noisy and poorly calibrated as virtual evidence inputs to the Bayesian Network. Transfer learning mitigates this problem by anchoring the regression models in the simulation-derived source domain, which, despite its imperfect representation of the real system, provides a structurally sound and sufficiently rich baseline from which fine-tuning can proceed. The practical implication is that in early deployment scenarios, where only a few days of monitored normal operation are available, domain adaptation via TrAdaBoostR2 is the preferable strategy and delivers meaningfully superior diagnostic accuracy.

However, the analysis also reveals an important caveat to the transfer learning advantage: in both seasons, the performance gap between Approach 2 and Approach 3 widens before it narrows, reaching its maximum divergence at n = 6 files in summer and n = 4 files in winter. This transient degradation of Approach 3 in the intermediate data range reflects the well-documented instability of ensemble regression models when trained on datasets that are large enough to introduce variance but too small to adequately cover the operating space. Practitioners deploying Approach 3 in this intermediate range should therefore be aware that performance may temporarily deteriorate relative to the two-file baseline before recovering, a phenomenon that could lead to premature conclusions about the adequacy of the from-scratch approach if evaluation is conducted at a single data point rather than across the full learning curve.

The seasonal comparison reveals structurally important asymmetry. In summer, the transfer learning advantage persists over a wider data range, with parity only achieved at n = 12 to 14 files, while in winter the crossover occurs as early as n = 8 files.

Further observation concerns the absolute performance levels achieved by both approaches across the data range. Neither Approach 2 nor Approach 3 reaches the 80.0% isolation accuracy benchmark established by the hybrid framework in WP4_D3 until n = 14 files in summer and n = 10 files in winter, underscoring that a minimum volume of real operational data is necessary regardless of the modeling strategy adopted. The zero-shot baseline of Approach 1, which achieves only 45.5% in summer and 47.3% in winter, confirms that deploying the simulation-trained model directly without any form of adaptation is insufficient for reliable fault isolation on real experimental data, and should not be considered a viable operational strategy.

Taken together, these findings support a data-aware deployment protocol for the hybrid FDD framework in new target installations. In the earliest phase of deployment, when fewer than approximately six to eight days of normal operation data are available, transfer learning via domain adaptation is strongly recommended as it delivers superior and more stable diagnostic performance. As operational data accumulate beyond the seasonal crossover threshold, the from-scratch approach becomes equally or more effective and avoids the added algorithmic complexity of the adaptation procedure.

7. References

[1] De Mathelin, F. Deheeger, G. Richard, M. Mougeot e N. Vayatis, “ADAPT: Awesome Domain Adaptation Python Toolbox,” arXiv preprint arXiv:2107.03049, 2021.

[2] Gao, Y., Ruan, Y., Fang, C., & Yin, S. (2020). Deep learning and transfer learning models of energy consumption forecasting for a building with poor information data. Energy and Buildings, 223, 110156.

[3] Miyata, S., Kuwahara, Y., Tsunemoto, S., Tanaka, K., & Akashi, Y. (2023). Improving training efficiency for scalable automated fault detection and diagnosis in chilled water plants by transfer learning. Energy and buildings, 285, 112877.

[4] Pan, S. J., & Yang, Q. (2009). A survey on transfer learning. IEEE Transactions on knowledge and data engineering, 22(10), 1345-1359.

[5] Peng, Z., Zhang, W., Han, N., Fang, X., Kang, P., & Teng, L. (2019). Active transfer learning. IEEE Transactions on Circuits and Systems for Video Technology, 30(4), 1022-1036.

[5] Ruder, S., Peters, M. E., Swayamdipta, S., & Wolf, T. (2019). Transfer learning in natural language processing. In Proceedings of the 2019 conference of the North American chapter of the association for computational linguistics: Tutorials (pp. 15-18).

Finanziato dall'Unione europea NextGenerationEU
Ministero dell'Università e della Ricerca
Italiadomani PIANO NAZIONALE DI RIPRESA E RESILIENZA